UNIVERSITY OF CALIFORNIA, SAN DIEGO

Antimicrobial mechanism of action determination via cytological profiling in *Bacillus subtilis*

A dissertation submitted in partial satisfaction of the

requirements for the degree of Doctor of Philosophy

in

Biology

by

Anne M Lamsa

Committee in charge:

Professor Kit Pogliano, Chair
Professor Michael Burkart
Professor Pieter Dorrestein
Professor Susan Golden
Professor Maho Niwa Rosen

2012

The dissertation of Anne M Lamsa is approved,

and it is acceptable in quality and form for publication on

microfilm and electronically:

_____

_____

_____

_____

_____

Chair

University of California, San Diego

2012

DEDICATION

To my parents, who have been the most supportive parents anyone could ever ask for, and Caprica and Starbuck, the cutest guinea pigs on the planet.

TABLE OF CONTENTS

LIST OF ABBREVIATIONS

ΔpH……	Proton gradient across the membrane
ΔΨ……..	Membrane potential
CCCP…….	carbonyl cyanide-m-chlorophenylhydrazone
CFU……...	Colony forming units
DAPI……..	4',6-diamidino-2-phenylindole, a blue fluorescent DNA stain
$DiBAC_4$5……	Bis - (1,3 - dibutylbarbituric acid)pentamethine oxonol
$DiSC_3$5……...	3,3' - Dipropylthiadicarbocyanine iodide
DMSO……	Dimethyl sulfoxide
DNA……...	Deoxyribonucleic acid
DNP……...	2,4-dinitrophenol
FM 4-64…….	A red fluorescent membrane stain
LB……...	Luria-Bertani medium
MALDI IMS……..	Matrix-assisted laser desorption/ionization imaging mass spectrometry
MBC……...	Minimum bactericidal concentration
MIC……	Minimum inhibitory concentration
MOA……...	Mechanism of action
MRSA…….	Methicillin-resistant *Staphylococcus aureus*
MS……...	Mass spectrometry
MS/MS……	Tandem mass spectrometry
nanoDESI……	Nano-spray desorption electrospray ionization
NRPS……...	Non-ribosomal peptide synthase
PCA…….	Principle component analysis
PKS…….	Polyketide synthase
PMF…….	Proton motive force
RNA……	Ribonucleic acid
SDP…….	Sporulation delaying protein
SKF…….	Sporulation killing factor
SYTOX green…….	A green fluorescent DNA stain

LIST OF FIGURES

LIST OF TABLES

ACKNOWLEDGEMENTS

I'd like to thank all of the members of the Pogliano labs for providing such a great environment for me to learn in. Thank you to Shinobu Chiba for teaching me all about *Bacillus* when I first joined the lab, Alan Derman for countless conversations (sometimes about science), and Rachelle Trial for being with me every step of the way. My biggest thanks go out to Kit for her guidance and support throughout this process. I don't think anyone could ask for a more supportive advisor.

Chapter 2, in full, is a reprint of the material as it appears in *Proceedings of the National Academy of Sciences* 2010 (Vol.107(37) pp. 16286-16290). I was a secondary author and developed the microculture techniques required for the fluorescence microscopy and performed the experiments for the cell biology work displayed in Figures 3, 4, and 5B.

Chapter 3, in full, is a reprint of the material as it appears in *Molecular Microbiology* 2012 (Vol. 84(3) pp. 486-500) and in the online supplement. I was the primary author of this work, conducted all the experiments and made all of the figures.

The bromoalterochromide used in chapter 4 was purified in Pieter Dorrestein's lab by Don Nguyen, Xiling Zhao, and Wilna Moree. Stenothricin was purified in Pieter Dorrestein's lab by Wei-Ting Liu. Spirohexenolide A was provided by Mike Burkhart's lab. Poochit Nonejuie provided the *E. coli* cytological profiling data.

Chapter 5, in full, is a reprint of the material as it appears in *The European Molecular Biology Organization* 209 (Vol. 28 pp. 3461-3475). I was a secondary author and isolated and identified mutants from the random mutagenesis screen

important for confirming the *mifM* regulation by the *mifM* stemloop, MifM transmembrane domain and *spoIIIJ*.

VITA

2007 Bachelors of Science with honors, Biochemistry and Molecular Biology, University of California, Irvine

2012 Doctor of Philosophy, Biology, University of California, San Diego

PUBLICATIONS

Lamsa, A., W. T. Liu, P. C. Dorrestein & K. Pogliano, (2012) The Bacillus subtilis cannibalism toxin SDP collapses the proton motive force and induces autolysis. *Mol Microbiol*.

Liu, W. T., Y. L. Yang, Y. Xu, A. Lamsa, N. M. Haste, J. Y. Yang, J. Ng, D. Gonzalez, C. D. Ellermeier, P. D. Straight, P. A. Pevzner, J. Pogliano, V. Nizet, K. Pogliano & P. C. Dorrestein, (2010) Imaging mass spectrometry of intraspecies metabolic exchange revealed the cannibalistic factors of Bacillus subtilis. *Proc Natl Acad Sci U S A* **107**: 16286-16290.

Chiba, S., A. Lamsa & K. Pogliano, (2009) A ribosome-nascent chain sensor of membrane protein biogenesis in Bacillus subtilis. *EMBO J* **28**: 3461-3475.

Larsen, L. S., N. Beliakova-Bethell, V. Bilanchone, M. Zhang, A. Lamsa, R. Dasilva, G. W. Hatfield, K. Nagashima & S. Sandmeyer, (2008) Ty3 nucleocapsid controls localization of particle assembly. *J Virol* **82**: 2501-2514.

Larsen, L. S., M. Zhang, N. Beliakova-Bethell, V. Bilanchone, A. Lamsa, K. Nagashima, R. Najdi, K. Kosaka, V. Kovacevic, J. Cheng, P. Baldi, G. W. Hatfield & S. Sandmeyer, (2007) Ty3 capsid mutations reveal early and late functions of the amino-terminal domain. *J Virol* **81**: 6957-6972.

ABSTRACT OF THE DISSERTATION

Antimicrobial mechanism of action determination via cytological profiling in *Bacillus subtilis*

by

Anne M Lamsa

Doctor of Philosophy in Biology

University of California, San Diego, 2012

Professor Kit Pogliano, Chair

The appearance of multi-drug resistant microbes and the decrease in the number of new antibiotics to treat them coming through the clinical pipeline has created a great need for development of novel antibiotics. Although breakthroughs in sequencing technologies, mass spectrometry, and bioinformatics have revealed an almost unlimited potential for new compounds with antibiotic activity, there still remains a major bottleneck in the determination of mechanism of action (MOA) for these potential antibiotics. Thus although many new antimicrobial compounds are being isolated and structurally characterized, we lack MOA information for most. Determining the MOA is critical for understanding which new molecules will have the greatest potential as an antibiotic safe for clinical use. Current techniques to identify

MOA are lengthy, low-throughput and require a large amount of compound. We have developed a rapid and precise method to determine the MOA of compounds in *Bacillus subtilis* utilizing fluorescence microscopy and viability data, termed cytological profiling. We also developed microculture techniques that allow testing of compounds utilizing less than a microgram of material. This method was used to demonstrate that the cannibalistic toxin sporulation delaying protein (SDP) kills the cell via PMF collapse, which was confirmed by PMF assays, and we have applied the technique to other natural products. All natural products and control antibiotics have shown a distinctive pattern in cell architecture that is unique to their MOA. Further development of cytological profiling by screening of a large library of control compounds, complemented by cytological profiling data obtained from *E. coli,* and paired with development of automated image analysis and microscopy technologies will make cytological profiling a high-throughput and accurate method of MOA determination sensitive enough to be used at sub-MIC levels and to identify the MOA of natural products prior to purification through screening of crude extracts.

Chapter 1

Introduction

A. A brief history of antibiotic discovery: the Golden Era

Antibiotics have been at the forefront of medicine since the implementation of penicillin as a treatment for infections in the 1940s. The success of penicillin in fighting infections revolutionized treatment of infectious disease and led scientists to look for more of these miracle drugs. Screening for fermentation broths and cell extracts that affect cell growth, an approach termed empirical screening, yielded many of our commonly utilized antibiotics, including streptomycin, chloramphenicol, erythromycin and vancomycin (1-3). Members of the bacterial kingdom *Actinobacteria,* frequently isolated from the soil, provided an especially rich source of antibiotics (4). This rapid discovery of new antibiotics lasted until the early 1960s, when efforts began to be plagued by rediscovery of identical antibiotics (called replication) and ultimately returns of new potential therapeutics diminished almost completely (5-7). This led scientists to believe that the antibiotic capacity of known microbes was close to being reached. A turn toward more sophisticated means of screening and new sources of both natural products and synthetic alternatives were required if new antibiotics were to be discovered to combat the increasing prevalence of multidrug resistant bacteria (7).

B. Antibiotic discovery v 2.0

The early days of antibiotic screening focused on empirical screening to search for natural products with antibiotic activity, but the returns with this method had greatly diminished, and new methods were required to maximize discovery rates. Rapid rediscovery of antibiotics led scientists to search for dereplication methods to

avoid this issue (7). Additionally, pathogens resistant to commonly used antibiotics had appeared, creating the need for novel antibiotics that could be added to a doctor's arsenal (5, 8, 9). Scientists need to stay ahead of the ability of microbes to adapt to the new treatments, or risk falling back into the position of the pre-antibiotic era.

The first step in the effort for dereplication was the shift from empirical screening to target based screening (5, 10). The rational was to look for antibiotics targeting a specific pre-defined pathway or enzyme, which would then only require comparison of the lead to a subset of antibiotics to determine if rediscovery had occurred. This would allow more time and energy to be focused on discovery of new antibiotics. Target based screening also took advantage of the fact that some pathways, such as cell wall synthesis and protein synthesis, seemed to be common targets for antibiotics. Theoretically, choosing an essential and widely distributed pathway as an antibiotic target would result in a higher hit rate than screens based on other targets. Target based screening frequently involved using strains that were either genetically sensitized (11-13), or had reporters designed for activation under specific conditions induced by antibiotics (14-16). These screens were effective for dereplication but, other than cell wall active screens (10, 17), they have not fared well as a means of discovering novel antibiotics (5, 10, 18). The biggest issue is that by definition, screening for molecules that targets a specific pathway greatly narrows the range of activities and molecules that can be discovered. Screens for different targets can be run, but the antibiotics discovered will still be limited to the targets selected for the screens. The most effective arsenal of antibiotics is a diverse one, and target based screening stifles diversity and innovation.

As target based screening rose in popularity, the advent of new technologies for increased ease of protein production and purification made it suddenly possible to screen for inhibitors of a specific enzyme *in vitro*. This greatly opened up the number of targets that could be tested, and many inhibitors were discovered, but in general they were not viable as antibiotics (5, 6). Many inhibitors of essential enzymes were described in the literature (5, 11, 19), but a lack of follow up publications suggests that most likely were not viable as antibiotic leads once tested further. This is likely because *in vitro* screens against an enzyme target do not take into account what will happen in the context of a cell. Difficulties with permeability or the cell's capacity for efflux of the compound are not controlled for in an *in vitro* screen, and many promising inhibitors had no antibiotic activity when whole cell activity was tested (5, 6). Furthermore, inhibitors that showed potential antibacterial activity, many inhibitors displayed cytotoxicity for eukaryotic cells or they had secondary targets or interactions, such as a high affinity for serum albumin (20), that made them unsuitable for use as an antibiotic (5).

Recognizing that screening of natural products was bringing diminishing returns in term of novel antibiotics, pharmaceutical companies turned to growing chemical libraries to look for novel functions and structural classes (5, 6). Since these compounds could be easily synthesized in sufficient quantities for testing and did not required lengthy extractions from organisms, these libraries were an attractive source for antibiotics. So far though, chemical libraries have not lived up to expectations. The libraries produced are not nearly diverse enough, leading to a much lower hit rate than in natural products (5, 6, 21). Additionally, molecules from these libraries have

demonstrated a high occurrence of cytotoxic, non-specific membrane effects, and there is a high occurrence of false positives due to aggregates non-specifically inhibiting enzymes (5, 21, 22), suggesting that natural products are still the most attractive source of antibiotics. Indeed, the vast majority of antibiotics currently in the clinical trial phase are natural products or are based on natural product scaffolds (23-25). Microbes have the ability to synthesize a greater diversity of molecules than synthetic chemists and we still have only explored a fraction of the diversity they can provide. Furthermore, these molecules have been subject to natural selection to have the ability to penetrate cells, an essential trait for a successful antibiotic, and to induce an effect beneficial to the producing organism.

Although target based screening is very popular and an attractive model by which to obtain lead molecules, it still has not been nearly as successful as empirical screening (5, 6, 21). The decline in empirical screening of extracts containing natural products was firstly due to high rediscovery rates, and secondly due to the time and effort required to create these extracts. Lengthy culturing and isolation procedures made it difficult to produce large quantities of many extracts for use in high-throughput screening, as it is difficult to obtain the large number of samples required for high-throughput screening. Determining the best culture and extraction conditions requires a significant amount of time and is expensive. Large companies are not interested in anything small scale, and so are reluctant to use a tool unless it is easily adaptable to the high-throughput methods they wish to utilize.

The industry for drugs, including antibacterials, is driven by profit, and as the search for new antibiotics has become more difficult, the costs of development have

skyrocketed and profits have decreased (18). A recent article in Forbes magazine estimates that it requires at least $4 billion in research money per new drug introduced (26). This number takes into account any type of drug introduced, and it is likely that the cost for development of each new antibacterial compound is higher. Furthermore, the focus at large companies has turned to therapeutics for chronic, life-long diseases, which hold much more potential profit than drugs used to treat acute infections (5, 6, 8, 14). The useful life of an antibiotic is very short, especially with rising rates of resistance, compared to the amount of effort and time needed for development and approval. The time required for the development of an antibiotic is estimated to be almost 14 years from discovery to approval, and the average time before resistance appears in the population is only eight years (21, 27). This has resulted in less money being spent on antibiotic research and has left the burden of discovery on small specialized companies and academics with smaller pools of resources and thus longer timelines for development. Additionally, a review of the funding distribution of the National Institutes of Health and found that more than ten times the amount of research dollars are being granted per HIV death than per *Staphylococcus aureus* and *Clostridium difficile* related death, demonstrating that research efforts to develop novel antibacterial drugs are severely underfunded (28).

The race to develop of novel antibiotics to stay ahead of rising resistance is not going well. More than 70% of pathogenic bacteria are resistant to most antibiotics, and patients colonized with multi-drug resistant microbes have a higher chance of death when compared to patients infected with susceptible microbes (29). Almost 100,000 people a year die in the US due to hospital-acquired infections and there are over two

million deaths worldwide every year due to bacterial infection (6, 28). Of the greater than two million hospital-acquired infections in the US every year, 50-60% involves bacteria resistant to an antibiotic (30). Beyond the death toll, the cost to the healthcare system associated with each hospital acquired infection is anywhere from $1,200 for a catheter-associated urinary tract infection to $22,875 for ventilator-associated pneumonia (31). The increase of travel makes the spread of multi-drug resistant bacteria world-wide easy. Travelers can become colonized by pathogens during a stay in another country and spread them to new areas (32). Colonization by foreign bacteria during travel is common enough that screening travelers coming back from third world countries has been proposed as a way to track the emergence of new pathogens in those countries (33).

Clearly, novel antibiotics are sorely needed and the current strategies have not provided satisfactory results (8). The most recently discovered antibiotic with a novel scaffold to be approved for human therapy is daptomycin, which was discovered in 1987 (5). Modification of current scaffolds has yielded a multitude of antibiotics (25, 34), but there is a limit to how many effect antibiotics can be built on the same scaffold and new scaffolds must be discovered if we are to stay ahead of the microbes. This will require innovative new methods of antibiotic discovery and characterization.

C. Emerging methods in natural product discovery

New mass spectrometry (MS), sequencing, gene synthesis, and bioinformatics technologies in recent years have revolutionized the field of natural product discovery. These methods simplify the identification process for natural products and the search

for their synthetic machinery, and represent a method of dereplication that is compatible with empirical screening.

Two exciting new MS technologies are MALDI (matrix assisted laser desorption ionization) imaging mass spectrometry (IMS) and nanoDESI (nano-spray desorption electrospray ionization) (35, 36). In MALDI IMS, colonies of microbes (36), or even sections of an organism (37), are covered in matrix, dried down, and MALDI can be performed directly off the colonies/tissue section. A raster can be defined and spectra obtained from a grid of points spanning the sample. The spectra from each raster point can then be assembled to form a two dimensional visualization of the location of each major molecule within the sample (36). The ability to see the position of a natural product in a colony or interaction can sometimes lead to a clue as to the function of the molecule. For example, a molecule seen in a zone of clearing/inhibition might have antimicrobial properties as was shown to be the case for chalcomycin A, produced by *Streptomyces sp.* Mg1, and arylomycin, produced by *Streptomyces roseosporus* (38, 39).

Similar to MALDI IMS, nanoDESI mass spectrometry allows for sampling to occur directly from a colony or tissue section. Data is collected through analysis of a constant flow of solvent that is in contact with the sample. The solvent is flowed through capillary tubes so that a small exposed droplet of flowing solvent can be lowered onto the sample. This both eliminates sample prep and allows analysis of the same sample over multiple timepoints and with multiple solvents, because the sample is not destroyed during data collection (35). An advantage of nanoDESI over MALDI

IMS is that a matrix is not required for ionization; matrix signals can obscure molecules in the low molecular weight range from the sample.

Both MS techniques are ideal for natural product discovery for several reasons. MS is very sensitive, and so molecules can be detected that would otherwise be missed by other methods. Both of these techniques allow for direct sampling of a colony or an interaction and give differing amounts of spatial information for the natural products. MALDI IMS provides a greater range of spatial information, while nanoDESI provides more flexibility and the ability to see molecules that would be obscured by matrix in MALDI IMS. Both techniques allow sampling of microbes growing on solid surfaces, which is usually better for natural product production, and that allow biofilm formation and cell differentiation, maximizing metabolic output (35, 36). MS data can also be easily utilized to identify known antibiotics in the sample if MS/MS data is available, making it useful in dereplication (35, 39-43). MALDI IMS can generate MS/MS data, but only if the target ions have been identified prior to ionization, a disadvantage compared to nanoDESI, where MS/MS data can be collected without prior knowledge of the ions to be fragmented. To identify the molecules present, MS and MS/MS data can be paired with several new bioinformatics techniques that allow easy identification of molecules and that connect the products with their biosynthetic machinery and genes.

An exciting new bioinformatic technique that pairs well with MS data is molecular networking. This technique takes the MS/MS data collected from a sample, compares each spectra, gives each a relatedness score, and the resulting relatedness scored data is visualized using Cytoscape (41, 44). The result is clusters of related

spectra that represent different adducts of a molecule or, in the case of lipopeptides, different chain lengths of the same natural product. These spectra can be compared to known molecules or they can be identified through sequence tags if they include amino acids as do the ribosomally encoded antimicrobial peptides and the non-ribosomally encoded polypeptide synthases. The networks of two different species, conditions, or timepoints can be compared and represented on a single network using color coding to see differences between the samples (35). This approach has been used to identify molecules with antibacterial properties that are specifically induced during coculture with another bacterial species as has been shown for several molecules produced by *Streptomyces coelicolor* (35). One clear strength of this approach is that a variety of conditions can easily be screened and compared to look for production of a previously silent natural product.

A major breakthrough in natural product discovery came with the rise in power and accessibility of high-throughput sequencing technology. As sequencing whole genomes became possible and more popular, a wealth of genetic information became available. Examining the genomes of laboratory species (genome mining) revealed that we had grossly underestimated their metabolic potential (45, 46). Laboratory conditions are not designed to induce natural product production in most cases, and a multitude of conditions or competing organisms could be required to induce an organism to produce all of the natural products it is capable of producing (45). The NRPS/PKS cluster prediction program AntiSMASH allows easy prediction of the synthetic machinery for natural products hidden in an organism's genome and even the product of that machinery (46, 47), making genome mining accessible to a much

wider audience. The constant supply of genome sequences becoming available means that a vast array of natural products are just waiting for characterization. Excitingly, with all of the metagenomics surveys, these studies are not even limited to culturable organisms, and identification of an interesting cluster might in the future be used to justify additional effort culturing the organism or achieving expression of the gene cluster. The problem now lies not in discovery of natural products, but in identifying those that have the greatest potential as antibacterial drugs.

For natural products that are made under laboratory conditions, there still remains the problem of connecting the product to the gene or synthetic machinery. The integration of MS data and genome mining is perfect for this challenge. MS data can also include MS/MS spectra, fragmentation data from a single product, which can be used to generate a sequence tag. This tag can then be used to find the gene/machinery responsible. For ribosomally synthesized natural products, the tag can be directly linked to the gene product and has been done with a sequence tag of only five amino acids (40). The linking of a sequence tag from a NRPS or PKS natural product is not as straightforward, but can be done through matching of the sequence tag to the predicted natural product of a NRPS or PKS cluster (39).

The natural product synthesis machinery found by genome mining is often "silent", meaning the product has not been detected in culture, but the hope is to use other methods to induce production of these products. One way to induce these silent genes is to use coculture techniques. Spotting the producer species side by side with other species often results in production of natural produces that would not be made under other circumstances. This has proven successful in the discovery of several

previously silent natural products (48-51). Other ways of inducing silent gene expression involve genetic manipulation. Many of these clusters have regulatory proteins, and engineering a positive transcriptional regulator to be overexpressed or elimination of a repressor will result in the natural product being made (46, 52, 53). This is the simplest method, but if the organism is not genetically tractable, more complex methods are required. The entire gene cluster can be added to a plasmid or artificial chromosome and expressed in a different, more genetically tractable organism. This requires a lot of effort, but has proven successful in several cases (54, 55). With current technology, a site that is difficult to clone or a site from an uncultured organism can be utilized by DNA synthesis of the entire region and subsequent cloning into an appropriate vector, further expanding the diversity of products we can obtain.

The discovery of silent gene clusters has greatly expanded the diversity of the biosynthetic machinery for secreted metabolites at our disposal. An attractive way to manufacture new "unnatural" natural produces is by utilizing the modular nature of the machinery for producing polyketides (PKS) and non-ribosomally encoded polypeptides (NRPS), which are so far the most structurally diverse and successful scaffolds in the bacterial toolkit for making bioactive molecules. Different modules from the PKS and NRPS proteins can be swapped, shuffled, deleted, and modules from different organisms can be combined to make an organism that will manufacture the newly designed natural product for us (56-59). Creating new products through manipulation of domains could potentially lead to more diversity and more efficient synthesis of the end product than could the synthetic manipulation of a scaffold.

In recent years, the pool of natural products from which we can pull therapeutic lead compounds has expanded exponentially. In addition to genome mining, there is an influx of natural products from culturing of new organisms, especially those from marine environments. Soil organisms have been the most prevalent organisms screened for natural product production so far due to the ease of obtaining and culturing many of them. Now with improved culture techniques and metagenomic data, marine organisms are attractive as a divergent source of novel antibiotic natural products (60, 61). The amount of information at our disposal continues to grow as more organisms are available to work with. It is the utilization of this information that will provide the next breakthroughs in drug discovery. Thus, the major challenge in identifying new antibacterial compounds of potential therapeutic use no longer remains in discovery of more natural products, but in better methods to test these products for antibacterial abilities and to then develop them into useable drugs.

D. Natural products: more than just microbe killers

Humans have effectively coopted natural products to use as antibiotics in our fight against infectious disease, but what is the purpose of these natural products in the environment? As the techniques to monitor interspecies interactions, such as MS technologies, and to gain information directly from the environment, such as metagenomics, have improved, there has been an increased interest in the parvome, which is made up of all the secreted metabolites made by a cell. Antibiotics were assumed to be primarily used for bacterial defense in the environment as species battle

it out to create their own niche, but experiments that deal with this subject are performed under controlled laboratory conditions and thus there is little direct evidence from environmental sources to support this (62). Even if some of these molecules are used for this purpose, it is not likely they all are. It is more likely that at least some are used as signaling molecules at the low concentrations they might be present at in the environment. One study found that the expression of up to 5% of all promoters respond to sub-MIC levels of antibiotics (63), and another found that sub-MIC levels of tobramycin or tetracycline stimulate biofilm formation in *Pseudomonas aeruginosa* (64). A direct biofilm to biofilm signaling event occurs when *B. subtilis* biofilms produce surfactin, which represses the formation of aerial hyphae in a neighboring *Streptomyces coelicolor* biofilm (65). Numerous studies, such as those mentioned above, support the idea that molecules sometimes thought of only for antimicrobial purposes might serve multiple functions in the environment (62, 64, 66, 67).

Although it might seem that studying the purpose of natural products in the environment is not relevant to medicine, the opposite is true. Analyzing the purpose of natural products in the environment and in interspecies interactions could provide information of great importance to medicine. As microbes find more ways to combat antibiotics, we must look for all alternative therapeutic approaches that might harness other, non-lethal roles of natural products. For example, up to 65% of hospital-acquired infections involve biofilms (68), and in many cases these biofilms are more resistant to antibiotics than their non-biofilm counterparts (69-72). Biofilms frequently occur in the hospital setting, in patients, sometimes on medical implants, and on

catheters, endoscopes and any surface that can be colonized (73). Bacteria in a biofilm can sometimes even survive sanitization of equipment (74-76). Thus, infections caused by bacteria in biofilms are difficult to treat, and if the bacteria survive initial treatment, treatment becomes even more difficult (77). Dispersal of bacterial biofilms would therefore improve the chances of successful antibiotic treatment (78-81). Indeed, azithromycin is already being used in this capacity to treat *P. aeruginosa* infections in the lungs of cystic fibrosis patients: although azithromycin does not kill *P. aeruginosa*, it disperses the biofilms and increases the effectiveness of subsequent antibiotic treatment (82, 83). Thus, understanding molecules that promote biofilm formation and dispersal could lead to the discovery of new treatments that could be used in combination with current antibiotics to more effectively control infections that involve biofilms.

Many bacteria can also be beneficial to humans, in large part due to interspecies interactions that help keep humans healthy and infection free. The normal inhabitants of the human microbiome have colonized us and can ward off attempts at colonization from less friendly species (72, 84). Treatment with a probiotic that outcompetes an invading species is an attractive treatment option and could reduce the number of patients who require antibiotics (85, 86). Understanding the interactions of these microbes, which likely involves natural product signaling, is of great importance to the war on multi-drug resistant super bugs.

E. Determining the mechanism of action of natural products: How do they work?

A critical factor to consider when evaluating the potential of a new antibiotic is its mechanism of action (MOA). A good antibiotic must selectively target an essential process in the cell, but without having a target with structural homology to anything in eukaryotes or there is a risk of cytotoxic effects. Now that such a multitude of natural products have been discovered, the question remains, what are their MOAs? Most research has been targeted towards identifying and then structurally characterizing natural products, while approaches for MOA determination have not benefited from the rise of high-throughput screening. Screens designed to look for molecules that affect a specific target or pathway would seem to make MOA determination simple, however most targeted screens are performed *in vitro* and only test the ability to inhibit an enzyme under non-physiological conditions. Molecules often have secondary targets or non-specific effects that can only be detected when non-sensitized, whole cells are treated, and so experiments must still be performed to correlate the predicted MOA with a specific effect in whole cells.

There are several general methods that can be employed when there is not a concrete hypothesis for MOA. Measuring the effect of a compound on macromolecular synthesis monitored by radioactive labeling experiments has long been employed as a method of general MOA determination. By measuring the effect of treatment on DNA, RNA, protein, cell wall, and fatty acid or lipid biosynthesis, the pathway acted on by the compound can be determined. If a specific pathway is inhibited, then the compound has a MOA directed at a part of that pathway, but if all pathways are affected, then a non-specific MOA, such as lysis or membrane

depolarization, is likely. A major disadvantage of this technique is the requirement for radioactive labeling. The process is expensive, and not high-throughput.

Another method for MOA determination that has been around for decades, and is still frequently used today, is the isolation and characterization of spontaneous resistance mutants. Mapping and sequencing of the gene responsible for the resistance can provide valuable clues as to the MOA. In the simplest case, the mutation will map directly to the gene that produces the target (87-91). This is the case for many mutants resistant to β-lactam antibiotics and can identify the specific penicillin binding protein each β-lactam binds (87). Target identification directly through mapping of spontaneous resistance mutants is also common with protein synthesis inhibitors, where mutations usually map to ribosomal genes (88). However, in other cases, the mutation will cause physiological changes that allow the cell to bypass the effect of the antibiotic, which provide varying degrees of clues as to the target. It is common to find mutations that result in decreased uptake of the antibiotics and thus higher resistance, especially when dealing with aminoglycoside antibiotics (92-94). Thus, mapping of resistance mutants can provide high resolution data as to the target of an antibiotic, but only if resistance mutations map directly to the target. The process of obtaining the mutant and subsequent identification of the affected gene is not always an easy process, and it does not guarantee target identification.

Many antibiotics induce specific cell stress pathways, and understanding which of these are induced can provide clues as to the MOA. These approaches typically use microarrays to measure the effect of antibiotics on transcription of treated cells (95). Microarrays from cells treated with compounds can then be compared to those of

control compounds to look for general patterns and stress responses. These results are very complicated, and require a great deal of effort to interpret, with many factors, such as the amount of antibiotic and length of time of treatment playing a major role in the outcome. Unfortunately, the majority of studies have been small scale and were done under a variety of conditions with different medias, times exposed to antibiotics, and levels of antibiotics used. This makes direct comparison of most studies impossible. Some of these small studies have, however, been used to tease apart the differences in MOA between closely related compounds, such as daptomycin and fruilimycin B (96).

Several large-scale studies have elucidated patterns of gene expression indicative of the MOA of major drug classes. Two of these studies were in *B. subtilis* and one was in *Mycobacterium tuberculosis.* The first study in *B. subtilis*, comprised of the profiles of 37 compounds, demonstrated that compounds with similar MOAs could be clustered, but that accurate identification of MOA depends on number of compounds tested for each MOA (97). Cell wall inhibitors were classified particularly well since there are a large number of characterized compounds that target this pathway, and all drugs targeting the cell wall were clustered by this approach (even if they block different steps). All other classes contained at least one mis- or unidentified outlier. They estimate that five to six compounds per class are required, which may not be possible for every class. A follow up study proposed an alternative way to increase classification accuracy by including profiles of conditional mutants (98). The profiles of each conditional mutant showed equivalent responses to those treated with drugs that inhibit the product of the gene and allows for classification of molecules

with an MOA that lack a sufficient number of control compounds. This method allowed for the characterization of two molecules with novel MOAs. The study emphasized the importance of optimizing the methods used to collect the data, especially the timing and number of samples to be collected. Later timepoints (40 min) provided the best data for broadly classifying MOA, but the specific MOA could not be identified until the earlier (10 min) timepoint was also analyzed.

A microarray study in *M. tuberculosis* was able to accurately classify a number of compounds without as many outliers as the *B. subtilis* studies. For each class of compound, a core set of genes was identified whose expression levels acted as a signature of a particular MOA, and the effect on the genes could be logically explained directly by the MOA. Each of the large scale studies was able to cluster the compounds by MOA to varying degrees, but MOA identification is still limited to known MOAs. A major advance allowed by these results is the construction of biosensor genes that are induced preferentially after treatment with compounds with a specific MOA. These genes can be fused to reporters and used in screening efforts, either for target-based screens, or for dereplication for hits from an empirical screen.

Proteomics has been used as a relatively new method of MOA determination. A library of compounds with known MOAs was evaluated using 2D gel analysis to create a control set. Overlay and matching of these 2D gels can give a MOA if a similar compound has been tested previously. A major downfall is any change in the pI of any of the proteins as a side effect of treatment greatly heightens the difficulty of matching the gels (99, 100). Like microarrays, these results are very complicated and

difficult to interpret, but proteins that show large changes might provide clues to the precise MOA.

Other screens for MOA identification use mutant strains that either overexpress or underexpress target proteins to search for increased or decreased resistance to antibiotics and molecules of interest. Testing hundreds of strains individually would be laborious and time-consuming, but pooling of different strains allows the process to be performed with much fewer samples. Pools of strains each containing an inducible antisense RNA for an essential gene that has been induced enough to sensitize the strains, but not prevent growth. These pools can be treated with the compound being tested, and strains that are downregulated for the target of the compound will be sensitized to the compound and be killed off by the compound at sub-MIC levels for the wildtype strain or out-competed by the other strains in the pool. This has been developed in *Staphylococcus aureus* with good results (101, 102). A similar assay in *E. coli* aims to look for the opposite effect by screening pools of mutants each overexpressing an essential protein and looking for increased MICs (103), but six years later has not made it past the initial proof of principle study.

Recently, a new high-throughput method of MOA determination was proposed using the output of growth of 15 different bacterial species and strains after antibiotic treatment (104). This method, called bioMAP, is effectively a growth assay using strains and species that differ in their specific and non-specific antibiotic resistance mechanisms, with a variety of Gram-negative and Gram-positive species tested, as well as multidrug resistant strains such as MRSA and *P. aeruginosa*. The bioMAP assay therefore assesses structural class rather than MOA, although many compounds

in the same structural class have the same MOA. BioMAP was able to predict the structural class of some compounds by clustering with a panel of known control compounds. However, not all of the control compounds cluster perfectly, meaning many compounds could remain unidentified if they are outliers. Of the 12 different structural classes tested, six clustered perfectly, two did not cluster at all, and the rest had at least one outlier. This is a fairly high occurrence of outliers, and thus the method may only be useful in testing for compounds that fall into the six structural classes that clustered perfectly. Many of the compounds tested were the only representative of their structural class and thus could not be clustered, leading to an inability for the method to identify likely the majority of new natural products being discovered. Further testing with this method using more compounds within each class could improve clustering and make identification of a wider variety of structural classes possible. The most pressing medical need is for novel compounds that do not belong to the same structural classes as existing antibiotics, so perhaps the best use of bioMAP clustering is as a preliminary screen for molecules that fail to cluster, which might therefore be structurally novel. .

MOA determination remains a large bottleneck for natural product discovery, and new methods must be developed to ease this burden. Many of the methods I have discussed are not viable for adaptation for high-throughput testing, which will become essential as the amount of natural products available continues to increase exponentially. Furthermore, a major drawback of natural product discovery is that isolation is often a laborious task that produces very small quantities of purified product. Current methods for MOA determination typically require that milliliters of

cells be treated for a single experiment, which is not compatible with the amount of natural product that is usually available. New methods need to be created that work on a very small scale to conserve the natural product. Approaches that conserve the product mean that less time has to be spent on isolation, and in turn, more products can be isolated. Once a natural product has shown promise of a desirable MOA, more can be isolated and precise tests run to identify and confirm the exact target.

An intriguing method for MOA determination that depends on fluorescent microscopy, termed cytological profiling, has previously been utilized in eukaryotes with some success (105, 106). Cells were treated with antibiotics, fixed, and then stained with a total of 11 probes to provide information on cell properties such as DNA replication, protein synthesis, actin, microtubules. Automated microscopy was used to capture images in a high-throughput manner, and automated image analysis provided measurements of cell and organelle shape, intensity of each probe, and other important parameters. All of these parameters could then be scored and compared to the results of other compounds or to controls. Drugs with similar targets clustered together when all the variables were taken into account, and they were able to use comparisons to identify potential mechanisms for two compounds with unidentified MOAs (105). A similar study looking at the effects of a panel of protein kinase inhibitors further reduced the data using principle component analysis, which takes correlated variables and combines them, resulting in a smaller number of outputs and simplifying data comparison (106).

Cytological profiling is an attractive method to adapt for bacteria. It would be high-throughput, and since it involves looking at individual cells, with the right culture

techniques, could utilize a minimal amount of compound. However, each of the published cytological profiling studies used high-throughput microscopy systems of low magnification and resolution that are not suitable for determining the MOA of antibacterial compounds. It therefore remains unclear if this method for MOA determination can be achieved in a much smaller organism with a limited number of variables to measure, and if treatment with compounds with different MOAs will provide enough information to allow differentiation between a large number of MOAs. In the next several chapters I will cover the development of cytological profiling for use in *B. subtilis*. Chapter 2 covers the development of microculture techniques that reduce the sample size to 15 µl, making it possible to conduct experiments with extremely limited amounts of compound. In chapter 3, I demonstrate that cytological profiling is a viable option for MOA determination by determining the MOA of the cannibalism factor sporulation delaying protein (SDP) produced by *B. subtilis* utilizing less than 80 µg of compound. In chapter 4, I expand the list of compounds that have been profiled and demonstrate that cytological profiling in bacteria is a viable option for MOA determination that is worth further development. Finally, in Chapter 6 I discuss the current state of the approach and future developments necessary to make it as broadly applicable as possible.

F. References

1. Schatz, A., E. Bugle, and S.A. Waksman, Streptomycin, a Substance Exhibiting Antibiotic Activity Against Gram-Positive and Gram-Negative Bacteria.∗†. Proceedings of the Society for Experimental Biology and Medicine. Society for Experimental Biology and Medicine (New York, N.Y.), 1944. **55**(1): p. 66-69.

2. Ehrlich, J., D. Gottlieb, P.R. Burkholder, L.E. Anderson, and T.G. Pridham, *Streptomyces venezuelae*, N. Sp., the Source of Chloromycetin. J Bacteriol, 1948. **56**(4): p. 467-77.

3. Anderson, R., H. Higgins Jr, and C. Pettinga, Symposium: how a drug is born. Cincinnati J Med, 1961. **42**: p. 49-60.

4. Mahajan, G.B. and L. Balachandran, Antibacterial agents from actinomycetes - a review. Front Biosci (Elite Ed), 2012. **4**: p. 240-53.

5. Silver, L.L., Challenges of antibacterial discovery. Clin Microbiol Rev, 2011. **24**(1): p. 71-109.

6. Berdy, J., Thoughts and facts about antibiotics: Where we are now and where we are heading. J Antibiot (Tokyo), 2012. **65**(8): p. 441.

7. Conover Lloyd, H., *Discovery of Drugs from Microbiological Sources*, in *Drug Discovery*. 1971, AMERICAN CHEMICAL SOCIETY. p. 33-80.

8. Boucher, H.W., G.H. Talbot, J.S. Bradley, J.E. Edwards, D. Gilbert, L.B. Rice, M. Scheld, B. Spellberg, and J. Bartlett, Bad Bugs, No Drugs: No ESKAPE! An Update from the Infectious Diseases Society of America. Clinical Infectious Diseases, 2009. **48**(1): p. 1-12.

9. Palumbi, S.R., Humans as the world's greatest evolutionary force. Science, 2001. **293**(5536): p. 1786-90.

10. Mills, S.D. and T.J. Dougherty, *Cell-Based Screening in Antibacterial Discovery Antibiotic Discovery and Development*, T.J. Dougherty and M.J. Pucci, Editors. 2012, Springer US. p. 901-929.

11. Young, K., H. Jayasuriya, J.G. Ondeyka, K. Herath, C. Zhang, S. Kodali, A. Galgoci, R. Painter, V. Brown-Driver, R. Yamamoto, L.L. Silver, Y. Zheng, J.I. Ventura, J. Sigmund, S. Ha, A. Basilio, F. Vicente, J.R. Tormo, F. Pelaez, P. Youngman, D. Cully, J.F. Barrett, D. Schmatz, S.B. Singh, and J. Wang, Discovery of FabH/FabF inhibitors from natural products. Antimicrob Agents Chemother, 2006. **50**(2): p. 519-26.

12. Kitano, K., K. Nara, and Y. Nakao, Screening for beta-lactam antibiotics using a mutant of *Pseudomonas aeruginosa.* Jpn J Antibiot, 1977. **30 Suppl**: p. 239-45.

13. Kamogashira, T. and S. Takegata, A screening method for cell wall inhibitors using a D-cycloserine hypersensitive mutant. J Antibiot (Tokyo), 1988. **41**(6): p. 803-6.

14. DeCenzo, M., M. Kuranda, S. Cohen, J. Babiak, Z.D. Jiang, D. Su, M. Hickey, P. Sancheti, P.A. Bradford, P. Youngman, S. Projan, and D.M. Rothstein, Identification of compounds that inhibit late steps of peptidoglycan synthesis in bacteria. J Antibiot (Tokyo), 2002. **55**(3): p. 288-95.

15. Oyamada, Y., H. Ito, M. Fujimoto-Nakamura, A. Tanitame, N. Iwai, K. Nagai, J. Yamagishi, and M. Wachi, Anucleate cell blue assay: a useful tool for identifying novel type II topoisomerase inhibitors. Antimicrob Agents Chemother, 2006. **50**(1): p. 348-50.

16. Urban, A., S. Eckermann, B. Fast, S. Metzger, M. Gehling, K. Ziegelbauer, H. Rubsamen-Waigmann, and C. Freiberg, Novel whole-cell antibiotic biosensors for compound discovery. Appl Environ Microbiol, 2007. **73**(20): p. 6436-43.

17. Gadebusch, H.H., E.O. Stapley, and S.B. Zimmerman, The discovery of cell wall active antibacterial antibiotics. Crit Rev Biotechnol, 1992. **12**(3): p. 225-43.

18. Projan, S.J., Why is big Pharma getting out of antibacterial drug discovery? Curr Opin Microbiol, 2003. **6**(5): p. 427-30.

19. Mansour, T.S., C.E. Caufield, B. Rasmussen, R. Chopra, G. Krishnamurthy, K.M. Morris, K. Svenson, J. Bard, C. Smeltzer, S. Naughton, S. Antane, Y. Yang, A. Severin, D. Quagliato, P.J. Petersen, and G. Singh, Naphthyl tetronic acids as multi-target inhibitors of bacterial peptidoglycan biosynthesis. ChemMedChem, 2007. **2**(10): p. 1414-7.

20. Ehmann, D.E., J.E. Demeritt, K.G. Hull, and S.L. Fisher, Biochemical characterization of an inhibitor of *Escherichia coli* UDP-N-acetylmuramyl-l-alanine ligase. Biochim Biophys Acta, 2004. **1698**(2): p. 167-74.

21. Payne, D.J., M.N. Gwynn, D.J. Holmes, and D.L. Pompliano, Drugs for bad bugs: confronting the challenges of antibacterial discovery. Nat Rev Drug Discov, 2007. **6**(1): p. 29-40.

22. Feng, B.Y., A. Simeonov, A. Jadhav, K. Babaoglu, J. Inglese, B.K. Shoichet, and C.P. Austin, A high-throughput screen for aggregation-based inhibition in a large compound library. J Med Chem, 2007. **50**(10): p. 2385-90.

23. Coates, A.R. and G. Halls, Antibiotics in Phase II and III Clinical Trials. Handb Exp Pharmacol, 2012(211): p. 167-83.

24. Jabes, D., The antibiotic R&D pipeline: an update. Curr Opin Microbiol, 2011. **14**(5): p. 564-9.

25. Butler, M.S. and M.A. Cooper, Antibiotics in the clinical pipeline in 2011. J Antibiot (Tokyo), 2011. **64**(6): p. 413-25.

26. Herper, M. (2012) The Truly Staggering Cost of Inventing New Drugs. Forbes.

27. Schmieder, R. and R. Edwards, Insights into antibiotic resistance through metagenomic approaches. Future Microbiol, 2012. **7**(1): p. 73-89.

28. Kwon, S., M.L. Schweizer, and E.N. Perencevich, National Institute of Allergy and Infectious Disease (NIAID) Funding for Studies of Hospital-Associated Bacterial Pathogens: Are Funds Proportionate to Burden of Disease? Antimicrob Resist Infect Control, 2012. **1**(1): p. 5.

29. Nemeth, J., B. Ledergerber, B. Preiswerk, A. Nobile, S. Karrer, C. Ruef, and S.P. Kuster, Multidrug-resistant bacteria in travellers hospitalized abroad: prevalence, characteristics, and influence on clinical outcome. J Hosp Infect, 2012.

30. Bereket, W., K. Hemalatha, B. Getenet, T. Wondwossen, A. Solomon, A. Zeynudin, and S. Kannan, Update on bacterial nosocomial infections. Eur Rev Med Pharmacol Sci, 2012. **16**(8): p. 1039-44.

31. Perencevich, E.N., P.W. Stone, S.B. Wright, Y. Carmeli, D.N. Fisman, and S.E. Cosgrove, Raising standards while watching the bottom line: making a business case for infection control. Infect Control Hosp Epidemiol, 2007. **28**(10): p. 1121-33.

32. Le Hello, S., R.S. Hendriksen, B. Doublet, I. Fisher, E.M. Nielsen, J.M. Whichard, B. Bouchrif, K. Fashae, S.A. Granier, N. Jourdan-Da Silva, A. Cloeckaert, E.J. Threlfall, F.J. Angulo, F.M. Aarestrup, J. Wain, and F.X. Weill, International spread of an epidemic population of *Salmonella enterica* serotype Kentucky ST198 resistant to ciprofloxacin. J Infect Dis, 2011. **204**(5): p. 675-84.

33. Guerin, P.J., R.F. Grais, J.A. Rottingen, and A.J. Valleron, Using European travellers as an early alert to detect emerging pathogens in countries with limited laboratory resources. BMC Public Health, 2007. **7**: p. 8.

34. Donadio, S., S. Maffioli, P. Monciardini, M. Sosio, and D. Jabes, Antibiotic discovery in the twenty-first century: current trends and future perspectives. J Antibiot, 2010. **63**(8): p. 423-430.

35. Watrous, J., P. Roach, T. Alexandrov, B.S. Heath, J.Y. Yang, R.D. Kersten, M. van der Voort, K. Pogliano, H. Gross, J.M. Raaijmakers, B.S. Moore, J. Laskin, N. Bandeira, and P.C. Dorrestein, Mass spectral molecular networking of living microbial colonies. Proc Natl Acad Sci U S A, 2012. **109**(26): p. E1743-52.

36. Yang, J.Y., V.V. Phelan, R. Simkovsky, J.D. Watrous, R.M. Trial, T.C. Fleming, R. Wenter, B.S. Moore, S.S. Golden, K. Pogliano, and P.C. Dorrestein, Primer on agar-based microbial imaging mass spectrometry. J Bacteriol, 2012. **194**(22): p. 6023-8.

37. Rath, C.M., T. Alexandrov, S.K. Higginbottom, J. Song, M.E. Milla, M.A. Fischbach, J.L. Sonnenburg, and P.C. Dorrestein, Molecular Analysis of Model Gut Microbiotas by Imaging Mass Spectrometry and Nanodesorption Electrospray Ionization Reveals Dietary Metabolite Transformations. Anal Chem, 2012.

38. Barger, S.R., B.C. Hoefler, A. Cubillos-Ruiz, W.K. Russell, D.H. Russell, and P.D. Straight, Imaging secondary metabolism of *Streptomyces sp.* Mg1 during cellular lysis and colony degradation of competing Bacillus subtilis. Antonie Van Leeuwenhoek, 2012. **102**(3): p. 435-45.

39. Liu, W.T., R.D. Kersten, Y.L. Yang, B.S. Moore, and P.C. Dorrestein, Imaging mass spectrometry and genome mining via short sequence tagging identified the anti-infective agent arylomycin in *Streptomyces roseosporus*. J Am Chem Soc, 2011. **133**(45): p. 18010-3.

40. Kersten, R.D., Y.L. Yang, Y. Xu, P. Cimermancic, S.J. Nam, W. Fenical, M.A. Fischbach, B.S. Moore, and P.C. Dorrestein, A mass spectrometry-guided genome mining approach for natural product peptidogenomics. Nat Chem Biol, 2011. **7**(11): p. 794-802.

41. Guthals, A., J.D. Watrous, P.C. Dorrestein, and N. Bandeira, The spectral networks paradigm in high throughput mass spectrometry. Mol Biosyst, 2012. **8**(10): p. 2535-44.

42. Mohimani, H., W.T. Liu, J.S. Mylne, A.G. Poth, M.L. Colgrave, D. Tran, M.E. Selsted, P.C. Dorrestein, and P.A. Pevzner, Cycloquest: identification of cyclopeptides via database search of their mass spectra against genome databases. J Proteome Res, 2011. **10**(10): p. 4505-12.

43. Mohimani, H., W.T. Liu, Y.L. Yang, S.P. Gaudencio, W. Fenical, P.C. Dorrestein, and P.A. Pevzner, Multiplex de novo sequencing of peptide antibiotics. J Comput Biol, 2011. **18**(11): p. 1371-81.

44. Shannon, P., A. Markiel, O. Ozier, N.S. Baliga, J.T. Wang, D. Ramage, N. Amin, B. Schwikowski, and T. Ideker, Cytoscape: a software environment for integrated models of biomolecular interaction networks. Genome Res, 2003. **13**(11): p. 2498-504.

45. Nett, M., H. Ikeda, and B.S. Moore, Genomic basis for natural product biosynthetic diversity in the actinomycetes. Nat Prod Rep, 2009. **26**(11): p. 1362-84.

46. Zotchev, S.B., O.N. Sekurova, and L. Katz, Genome-based bioprospecting of microbes for new therapeutics. Curr Opin Biotechnol, 2012.

47. Medema, M.H., K. Blin, P. Cimermancic, V. de Jager, P. Zakrzewski, M.A. Fischbach, T. Weber, E. Takano, and R. Breitling, antiSMASH: rapid identification, annotation and analysis of secondary metabolite biosynthesis gene clusters in bacterial and fungal genome sequences. Nucleic Acids Res, 2011. **39**(Web Server issue): p. W339-46.

48. Seyedsayamdost, M.R., M.F. Traxler, S.L. Zheng, R. Kolter, and J. Clardy, Structure and biosynthesis of amychelin, an unusual mixed-ligand siderophore from *Amycolatopsis sp*. AA4. J Am Chem Soc, 2011. **133**(30): p. 11434-7.

49. Oh, D.C., C.A. Kauffman, P.R. Jensen, and W. Fenical, Induced production of emericellamides A and B from the marine-derived fungus *Emericella sp.* in competing co-culture. J Nat Prod, 2007. **70**(4): p. 515-20.

50. Oh, D.C., P.R. Jensen, C.A. Kauffman, and W. Fenical, Libertellenones A-D: induction of cytotoxic diterpenoid biosynthesis by marine microbial competition. Bioorg Med Chem, 2005. **13**(17): p. 5267-73.

51. Gonzalez, D.J., Y. Xu, Y.L. Yang, E. Esquenazi, W.T. Liu, A. Edlund, T. Duong, L. Du, I. Molnar, W.H. Gerwick, P.R. Jensen, M. Fischbach, C.C. Liaw, P. Straight, V. Nizet, and P.C. Dorrestein, Observing the invisible through imaging mass spectrometry, a window into the metabolic exchange patterns of microbes. J Proteomics, 2012. **75**(16): p. 5069-76.

52. Gottelt, M., S. Kol, J.P. Gomez-Escribano, M. Bibb, and E. Takano, Deletion of a regulatory gene within the cpk gene cluster reveals novel antibacterial activity in *Streptomyces coelicolor* A3(2). Microbiology, 2010. **156**(Pt 8): p. 2343-53.

53. Laureti, L., L. Song, S. Huang, C. Corre, P. Leblond, G.L. Challis, and B. Aigle, Identification of a bioactive 51-membered macrolide complex by

activation of a silent polyketide synthase in *Streptomyces ambofaciens*. Proc Natl Acad Sci U S A, 2011. **108**(15): p. 6258-63.

54. Shao, Z., Y. Luo, and H. Zhao, Rapid characterization and engineering of natural product biosynthetic pathways via DNA assembler. Mol Biosyst, 2011. **7**(4): p. 1056-9.

55. Malpartida, F. and D.A. Hopwood, Molecular cloning of the whole biosynthetic pathway of a *Streptomyces* antibiotic and its expression in a heterologous host. Nature, 1984. **309**(5967): p. 462-4.

56. Scharf, D.H. and A.A. Brakhage, Engineering fungal secondary metabolism: A roadmap to novel compounds. J Biotechnol, 2012.

57. Condurso, H.L. and S.D. Bruner, Structure guided approaches toward exploiting and manipulating nonribosomal peptide and polyketide biosynthetic pathways. Curr Opin Chem Biol, 2012. **16**(1-2): p. 162-9.

58. Fisch, K.M., W. Bakeer, A.A. Yakasai, Z. Song, J. Pedrick, Z. Wasil, A.M. Bailey, C.M. Lazarus, T.J. Simpson, and R.J. Cox, Rational domain swaps decipher programming in fungal highly reducing polyketide synthases and resurrect an extinct metabolite. J Am Chem Soc, 2011. **133**(41): p. 16635-41.

59. Oliynyk, M., M.J. Brown, J. Cortes, J. Staunton, and P.F. Leadlay, A hybrid modular polyketide synthase obtained by domain swapping. Chem Biol, 1996. **3**(10): p. 833-9.

60. Zhao, X.Q., Genome-based studies of marine microorganisms to maximize the diversity of natural products discovery for medical treatments. Evid Based Complement Alternat Med, 2011. **2011**: p. 384572.

61. Dionisi, H.M., M. Lozada, and N.L. Olivera, Bioprospection of marine microorganisms: biotechnological applications and methods. Rev Argent Microbiol, 2012. **44**(1): p. 49-60.

62. Davies, J. and K.S. Ryan, Introducing the parvome: bioactive compounds in the microbial world. ACS Chem Biol, 2012. **7**(2): p. 252-9.

63. Goh, E.B., G. Yim, W. Tsui, J. McClure, M.G. Surette, and J. Davies, Transcriptional modulation of bacterial gene expression by subinhibitory concentrations of antibiotics. Proc Natl Acad Sci U S A, 2002. **99**(26): p. 17025-30.

64. Linares, J.F., I. Gustafsson, F. Baquero, and J.L. Martinez, Antibiotics as intermicrobial signaling agents instead of weapons. Proc Natl Acad Sci U S A, 2006. **103**(51): p. 19484-9.

65. Straight, P.D., J.M. Willey, and R. Kolter, Interactions between *Streptomyces coelicolor* and *Bacillus subtilis*: Role of surfactants in raising aerial structures. J Bacteriol, 2006. **188**(13): p. 4918-25.

66. Shank, E.A. and R. Kolter, New developments in microbial interspecies signaling. Curr Opin Microbiol, 2009. **12**(2): p. 205-14.

67. Straight, P.D. and R. Kolter, Interspecies chemical communication in bacterial development. Annu Rev Microbiol, 2009. **63**: p. 99-118.

68. Costerton, J.W., P.S. Stewart, and E.P. Greenberg, Bacterial biofilms: a common cause of persistent infections. Science, 1999. **284**(5418): p. 1318-22.

69. Haussler, S., Multicellular signalling and growth of *Pseudomonas aeruginosa.* Int J Med Microbiol, 2010. **300**(8): p. 544-8.

70. Hibbing, M.E., C. Fuqua, M.R. Parsek, and S.B. Peterson, Bacterial competition: surviving and thriving in the microbial jungle. Nat Rev Microbiol, 2010. **8**(1): p. 15-25.

71. Lopez, D., H. Vlamakis, and R. Kolter, Biofilms. Cold Spring Harb Perspect Biol, 2010. **2**(7): p. a000398.

72. Percival, S.L., C. Emanuel, K.F. Cutting, and D.W. Williams, Microbiology of the skin and the role of biofilms in infection. Int Wound J, 2012. **9**(1): p. 14-32.

73. Thomsen, T.R., L. Hall-Stoodley, C. Moser, and P. Stoodley, *The Role of Bacterial Biofilms in Infections of Catheters and Shunts Biofilm Infections*, T. Bjarnsholt, et al., Editors. 2011, Springer New York. p. 91-109.

74. Bridier, A., P. Sanchez-Vizuete Mdel, D. Le Coq, S. Aymerich, T. Meylheuc, J.Y. Maillard, V. Thomas, F. Dubois-Brissonnet, and R. Briandet, Biofilms of a *Bacillus subtilis* hospital isolate protect *Staphylococcus aureus* from biocide action. PLoS One, 2012. **7**(9): p. e44506.

75. Vickery, K., A. Deva, A. Jacombs, J. Allan, P. Valente, and I.B. Gosbell, Presence of biofilm containing viable multiresistant organisms despite terminal cleaning on clinical surfaces in an intensive care unit. J Hosp Infect, 2012. **80**(1): p. 52-5.

76. Smith, K. and I.S. Hunter, Efficacy of common hospital biocides with biofilms of multi-drug resistant clinical isolates. Journal of Medical Microbiology, 2008. **57**(8): p. 966-973.

77. Ciofu, O., L.F. Mandsberg, H. Wang, and N. Hoiby, Phenotypes selected during chronic lung infection in cystic fibrosis patients: implications for the treatment of *Pseudomonas aeruginosa* biofilm infections. FEMS Immunol Med Microbiol, 2012. **65**(2): p. 215-25.

78. Zoubos, A.B., S.P. Galanakos, and P.N. Soucacos, Orthopedics and biofilm--what do we know? A review. Med Sci Monit, 2012. **18**(6): p. RA89-96.

79. Kaplan, J.B., Biofilm Dispersal: Mechanisms, Clinical Implications, and Potential Therapeutic Uses. Journal of Dental Research, 2010. **89**(3): p. 205-218.

80. Bjarnsholt, T., T. Tolker-Nielsen, N. Hoiby, and M. Givskov, Interference of *Pseudomonas aeruginosa* signalling and biofilm formation for infection control. Expert Rev Mol Med, 2010. **12**: p. e11.

81. Landini, P., D. Antoniani, J. Burgess, and R. Nijland, Molecular mechanisms of compounds affecting bacterial biofilm formation and dispersal. Applied Microbiology and Biotechnology, 2010. **86**(3): p. 813-823.

82. Yousef, A.A. and A. Jaffe, The role of azithromycin in patients with cystic fibrosis. Paediatr Respir Rev, 2010. **11**(2): p. 108-14.

83. Gillis, R.J., K.G. White, K.H. Choi, V.E. Wagner, H.P. Schweizer, and B.H. Iglewski, Molecular basis of azithromycin-resistant *Pseudomonas aeruginosa* biofilms. Antimicrob Agents Chemother, 2005. **49**(9): p. 3858-67.

84. Cogen, A.L., V. Nizet, and R.L. Gallo, Skin microbiota: a source of disease or defence? Br J Dermatol, 2008. **158**(3): p. 442-55.

85. Rendueles, O. and J.M. Ghigo, Multi-species biofilms: how to avoid unfriendly neighbors. FEMS Microbiol Rev, 2012.

86. Wolvers, D., J.M. Antoine, E. Myllyluoma, J. Schrezenmeir, H. Szajewska, and G.T. Rijkers, Guidance for substantiating the evidence for beneficial effects of probiotics: prevention and management of infections by probiotics. J Nutr, 2010. **140**(3): p. 698S-712S.

87. Hakenbeck, R., C. Martin, C. Dowson, and T. Grebe, Penicillin-binding protein 2b of *Streptococcus pneumoniae* in piperacillin-resistant laboratory mutants. J Bacteriol, 1994. **176**(17): p. 5574-7.

88. Bazzicalupo, M., B. Parisi, G. Pirali, M. Polsinelli, and F. Sala, Genetic and biochemical characterization of a ribosomal mutant of *Bacillus subtilis* resistant to sporangiomycin. Antimicrob Agents Chemother, 1975. **8**(6): p. 651-6.

89. Vizan, J.L., C. Hernandez-Chico, I. del Castillo, and F. Moreno, The peptide antibiotic microcin B17 induces double-strand cleavage of DNA mediated by *E. coli* DNA gyrase. EMBO J, 1991. **10**(2): p. 467-76.

90. Miyoshi, Y. and H. Yamagata, Sucrose-dependent spectinomycin-resistant mutants of *Escherichia coli.* J Bacteriol, 1976. **125**(1): p. 142-8.

91. Mills, S.D., W. Yang, and K. MacCormack, Molecular characterization of benzimidazole resistance in *Helicobacter pylori.* Antimicrob Agents Chemother, 2004. **48**(7): p. 2524-30.

92. Bryan, L.E., T. Nicas, B.W. Holloway, and C. Crowther, Aminoglycoside-resistant mutation of *Pseudomonas aeruginosa* defective in cytochrome c552 and nitrate reductase. Antimicrob Agents Chemother, 1980. **17**(1): p. 71-9.

93. Obaseiki-Ebor, E.E. and A.S. Breeze, Gentamicin- and neomycin-resistant mutants of *Escherichia coli* K-12 cross-resistant to nitrofurans. J Antimicrob Chemother, 1984. **13**(6): p. 567-76.

94. Hirai, K., H. Aoyama, S. Suzue, T. Irikura, S. Iyobe, and S. Mitsuhashi, Isolation and characterization of norfloxacin-resistant mutants of *Escherichia coli* K-12. Antimicrob Agents Chemother, 1986. **30**(2): p. 248-53.

95. Wecke, T. and T. Mascher, Antibiotic research in the age of omics: from expression profiles to interspecies communication. J Antimicrob Chemother, 2011. **66**(12): p. 2689-704.

96. Wecke, T., D. Zuhlke, U. Mader, S. Jordan, B. Voigt, S. Pelzer, H. Labischinski, G. Homuth, M. Hecker, and T. Mascher, Daptomycin versus Friulimicin B: in-depth profiling of *Bacillus subtilis* cell envelope stress responses. Antimicrob Agents Chemother, 2009. **53**(4): p. 1619-23.

97. Hutter, B., C. Schaab, S. Albrecht, M. Borgmann, N.A. Brunner, C. Freiberg, K. Ziegelbauer, C.O. Rock, I. Ivanov, and H. Loferer, Prediction of mechanisms of action of antibacterial compounds by gene expression profiling. Antimicrob Agents Chemother, 2004. **48**(8): p. 2838-44.

98. Freiberg, C., H.P. Fischer, and N.A. Brunner, Discovering the mechanism of action of novel antibacterial agents through transcriptional profiling of conditional mutants. Antimicrob Agents Chemother, 2005. **49**(2): p. 749-59.

99. Bandow, J.E., H. Brotz, L.I. Leichert, H. Labischinski, and M. Hecker, Proteomic approach to understanding antibiotic action. Antimicrob Agents Chemother, 2003. **47**(3): p. 948-55.

100. Reiss, S., J. Pane-Farre, S. Fuchs, P. Francois, M. Liebeke, J. Schrenzel, U. Lindequist, M. Lalk, C. Wolz, M. Hecker, and S. Engelmann, Global analysis of the *Staphylococcus aureus* response to mupirocin. Antimicrob Agents Chemother, 2012. **56**(2): p. 787-804.

101. Donald, R.G., S. Skwish, R.A. Forsyth, J.W. Anderson, T. Zhong, C. Burns, S. Lee, X. Meng, L. LoCastro, L.W. Jarantow, J. Martin, S.H. Lee, I. Taylor, D. Robbins, C. Malone, L. Wang, C.S. Zamudio, P.J. Youngman, and J.W. Phillips, A *Staphylococcus aureus* fitness test platform for mechanism-based profiling of antibacterial compounds. Chem Biol, 2009. **16**(8): p. 826-36.

102. Xu, H.H., J.D. Trawick, R.J. Haselbeck, R.A. Forsyth, R.T. Yamamoto, R. Archer, J. Patterson, M. Allen, J.M. Froelich, I. Taylor, D. Nakaji, R. Maile, G.C. Kedar, M. Pilcher, V. Brown-Driver, M. McCarthy, A. Files, D. Robbins, P. King, S. Sillaots, C. Malone, C.S. Zamudio, T. Roemer, L. Wang, P.J. Youngman, and D. Wall, *Staphylococcus aureus* TargetArray: comprehensive differential essential gene expression as a mechanistic tool to profile antibacterials. Antimicrob Agents Chemother, 2010. **54**(9): p. 3659-70.

103. Xu, H.H., L. Real, and M.W. Bailey, An array of *Escherichia coli* clones over-expressing essential proteins: a new strategy of identifying cellular targets of potent antibacterial compounds. Biochem Biophys Res Commun, 2006. **349**(4): p. 1250-7.

104. Wong, Weng R., Allen G. Oliver, and Roger G. Linington, Development of Antibiotic Activity Profile Screening for the Classification and Discovery of Natural Product Antibiotics. Chemistry & biology, 2012. **19**(11): p. 1483-1495.

105. Perlman, Z.E., M.D. Slack, Y. Feng, T.J. Mitchison, L.F. Wu, and S.J. Altschuler, Multidimensional drug profiling by automated microscopy. Science, 2004. **306**(5699): p. 1194-8.

106. Tanaka, M., R. Bateman, D. Rauh, E. Vaisberg, S. Ramachandani, C. Zhang, K.C. Hansen, A.L. Burlingame, J.K. Trautman, K.M. Shokat, and C.L. Adams, An unbiased cell morphology-based screen for new, biologically active small molecules. PLoS Biol, 2005. **3**(5): p. e128.

Chapter 2

Imaging mass spectrometry of intraspecies metabolic exchange revealed the cannibalistic factors of *Bacillus subtilis*

Imaging mass spectrometry of intraspecies metabolic exchange revealed the cannibalistic factors of *Bacillus subtilis*

Wei-Ting Liu[a,1], Yu-Liang Yang[b,1], Yuquan Xu[b,1], Anne Lamsa[c], Nina M. Haste[b,d], Jane Y. Yang[a], Julio Ng[e], David Gonzalez[a], Craig D. Ellermeier[f], Paul D. Straight[g], Pavel A. Pevzner[e,h], Joe Pogliano[c], Victor Nizet[b,d,i], Kit Pogliano[c], and Pieter C. Dorrestein[a,b,d,2]

[a]Department of Chemistry and Biochemistry, [b]Skaggs School of Pharmacy and Pharmaceutical Sciences, [c]Division of Biological Sciences, [d]Center for Marine Biotechnology and Biomedicine, and [e]Department of Computer Science, University of California at San Diego, La Jolla, CA 92093; [f]Department of Microbiology, University of Iowa, Iowa City, IA 52242; [g]Department of Biochemistry and Biophysics, Texas A&M University, College Station, TX 77843; and [h]National Center for Research Resources (NCRR) Center for Computational Mass Spectrometry and [i]Department of Pediatrics, University of California at San Diego, La Jolla, CA 92093

Edited by Richard M. Losick, Harvard University, Cambridge, MA, and approved August 4, 2010 (received for review June 14, 2010)

During bacterial cannibalism, a differentiated subpopulation harvests nutrients from their genetically identical siblings to allow continued growth in nutrient-limited conditions. Hypothesis-driven imaging mass spectrometry (IMS) was used to identify metabolites active in a *Bacillus subtilis* cannibalism system in which sporulating cells lyse nonsporulating siblings. Two candidate molecules with sequences matching the products of *skfA* and *sdpC*, genes for the proposed cannibalistic factors sporulation killing factor (SKF) and sporulation delaying protein (SDP), respectively, were identified and the structures of the final products elucidated. SKF is a cyclic 26-amino acid (aa) peptide that is posttranslationally modified with one disulfide and one cysteine thioether bridged to the α-position of a methionine, a posttranslational modification not previously described in biology. SDP is a 42-residue peptide with one disulfide bridge. In spot test assays on solid medium, overproduced SKF and SDP enact a cannibalistic killing effect with SDP having higher potency. However, only purified SDP affected *B. subtilis* cells in liquid media in fluorescence microscopy and growth assays. Specifically, SDP treatment delayed growth in a concentration-dependent manner, caused increases in cell permeability, and ultimately caused cell lysis accompanied by the production of membrane tubules and spheres. Similarly, SDP but not SKF was able to inhibit the growth of the pathogens *Staphylococcus aureus* and *Staphylococcus epidermidis* with comparable IC_{50} to vancomycin. This investigation, with the identification of SKF and SDP structures, highlights the strength of IMS in investigations of metabolic exchange of microbial colonies and also demonstrates IMS as a promising approach to discover novel biologically active molecules.

cannibalism | bacterial communication | natural product | posttranslational modifications | thioether

Metabolic exchange describes the process of exchanging signals or nutrients between cells or populations and is a common feature of all living systems. Bacteria produce a wide array of signaling molecules to control metabolic as well as morphological and developmental changes in either an interspecies or intraspecies manner (1). *Bacillus subtilis*, for example, has a complex life cycle and thrives in diverse living conditions ranging from soil, contaminated wounds, and the intestinal tract (2–4). To accommodate this, *B. subtilis* dedicates ~10% of its genome to the production of specific molecules involved in intra- and interspecies metabolic exchange (5). Two of these molecules are sporulation delaying protein (SDP) and sporulation killing factor (SKF), which, based on genetic experiments, are proposed to lyse a subpopulation of *B. subtilis* cells to provide nutrients for the remaining cells, a process referred to as bacterial cannibalism (6–10). This behavior is dependent on Spo0A, a master transcriptional regulator that also controls biofilm formation and sporulation (6–13). We set out to characterize these cannibalistic compounds to establish their roles in the *B. subtilis* life cycle and to understand their structure and biosynthesis. In addition, previous reports have suggested that the *skf* and *sdp* gene clusters preferentially target non-*B. subtilis* cells, suggesting that the cannibalistic factors might represent promising new antibiotic leads (14, 15).

Before this study, SDP had been partially purified (6), whereas SKF had not been identified or structurally characterized, although *B. subtilis* is the model organism for Gram-positive bacteria and many laboratories had investigated its metabolic output. The difficulties of identifying these molecules could arise from the fact that the cannibalistic effect was observed only on solid media but not in liquid media (6). Therefore, we decided to use imaging mass spectrometry (IMS) to visualize the process by growing the domesticated strain PY79 directly on the MALDI target plate (16–18). With this approach, we were able to purify and determine the structure of mature SKF and SDP. In solid medium, both molecules act as cannibalistic killing factors, however, only SDP inhibited the growth of *B. subtilis* and the Gram-positive pathogens *Staphylococcus aureus* and *Staphylococcus epidermidis* in liquid medium. This investigation demonstrates that IMS is an effective tool to identify cell-to-cell interaction signals, and provides an approach to the discovery of bioactive molecules.

Results and Discussion

Identification of SKF and SDP via IMS. The *B. subtilis* cannibalistic phenotype presents itself only on solid media (6), yet there are very few tools that can spatially characterize metabolic output on solid surfaces. We therefore used thin-layer agar IMS, which is capable of capturing the spatial distribution of metabolites in growing colonies and can be used to understand microbial metabolic exchange, to visualize the cannibalistic factors SKF and SDP (18). In this IMS experiment, a growing culture of *B. subtilis* PY79, used in the original report on cannibalism (6), was cultured adjacent to a Δ*spo0A* strain (KP648) and its metabolic output was profiled by IMS (Fig. 1*A*). We anticipated that a zone of clearing on the Δ*spo0A* strain would be observed and that IMS could be used to

Author contributions: C.D.E., P.D.S., P.A.P., J.P., V.N., K.P., and P.C.D. designed research; W.-T.L., Y.-L.Y., Y.X., A.L., N.M.H., J.Y.Y., J.N., D.G., C.D.E., J.P., and K.P. performed research; W.-T.L., Y.-L.Y., Y.X., A.L., N.M.H., J.Y.Y., J.N., D.G., J.P., K.P., and P.C.D. analyzed data; and W.-T.L., Y.-L.Y., K.P., and P.C.D. wrote the paper.

The authors declare no conflict of interest.

This article is a PNAS Direct Submission.

Freely available online through the PNAS open access option.

[1]W.-T.L, Y.-L.Y, and Y.X. contributed equally to this work.

[2]To whom correspondence should be addressed. E-mail: pdorrest@ucsd.edu.

This article contains supporting information online at www.pnas.org/lookup/suppl/doi:10.1073/pnas.1008368107/-/DCSupplemental.

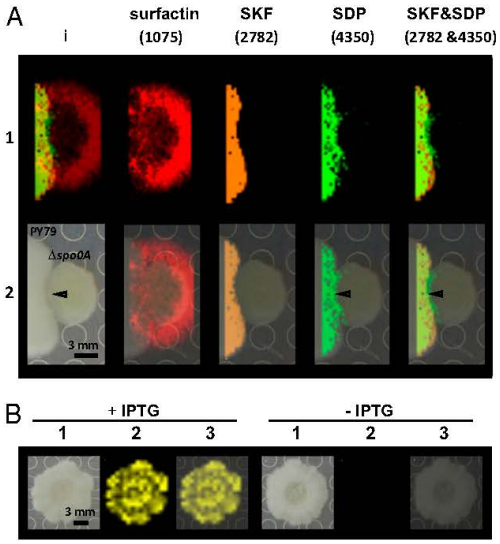

Fig. 1. IMS of intraspecies metabolic exchange. (*A*) IMS of PY79 and Δ*spo0A* (KP648) coculture. (*1*) Ion distributions observed for surfactin ($[M+K]^+$), SKF ($[M+H]^+$), and SDP ($[M+K]^+$). *1i* is a superimposition of all three ions. (*2*) Superimposition of the photograph and IMS data. Arrows point to glassy region of Δ*spo0A* and SDP overlap. (*B*) IMS of EG208 with or without IPTG. (*1*) Photographs of the colonies. (*2*) IMS pictures of ion 2782. (*3*) Superimposition of *1* and *2*.

identify candidate signals involved in the lysis of Δ*spo0A* cells. Indeed, we observed a decreased growth phenotype as well as a glassy appearance in the region of Δ*spo0A* adjacent to the cocultured PY79 cells (Fig. 1*A* and *SI Appendix*, Fig. S1).

Several ions were observed in the IMS data. First, KP648 (PY79, Δ*spo0A*) produced the nonribosomal peptide synthetase-derived lipopeptide antibiotic surfactin. This was unexpected, because PY79 has a frameshift mutation in the gene encoding for the phosphopantetheinyl transferase protein, Sfp (19), and we confirmed by DNA sequencing that this mutation is present in the Δ*spo0A* strain. This indicates that the surfactin nonribosomal peptide synthetases are activated via a lower efficiency phosphopantetheinylation pathway that is up-regulated in the absence of Spo0A. However, judging from their relative mass spectrometry (MS) intensities, the signal of surfactin at 96 h was at least 10-fold less than the amount produced by the nondomesticated *B. subtilis* strain 3610 (*SI Appendix*, Fig. S2), which has a functional *sfp* gene. Second, some signals produced by PY79 appeared to define a boundary between the PY79 and Δ*spo0A* colonies, including the ions at *m/z* 2782 and 4350 (Fig. 1*A*). Ion 2782 was associated with the border between the two cultures, and ion 4350 was found in the regions where the Δ*spo0A* strain was glassy and displayed reduced growth. Thus, the 4350 *m/z* ion was the favored candidate that caused the majority of the cannibalistic killing effect, because of the overlap with the zone of reduced growth on Δ*spo0A*, whereas the 2782 ion stopped at the interface of the two colonies.

After an 1-butanol extraction and a desalting step, the two uncharacterized ions were measured at *m/z* 2782 $[M+H]^+$ and 4312 $[M+H]^+$, suggesting that ion *m/z* 4350 is the potassium adduct form $[M+K]^+$ (*SI Appendix*, Fig. S3). These two ions were then subjected to fragmentation by MALDI-TOF tandem MS (TOF/TOF). The ion at *m/z* 4312 $[M+H]^+$ gave a long and unambiguous sequence tag corresponding to VAAGYLYVVGVNAVALQT-AAAVTTAVW and matched residues from Val^{148} to Trp^{174} of SdpC (*SI Appendix*, Figs. S4*A* and S5 and Table S1), whereas the TOF/TOF fragmentation of the 2782 ion gave a candidate sequence tag, LPHPA (*SI Appendix*, Fig. S4*B*). This sequence tag matched a sequence within SkfA, the proposed precursor for the mature form of SKF (6). However, the sequence tag was insufficient to positively identify SKF, because none of the ion masses could be directly matched with the linear sequence of SkfA, and many ions in the spectrum remained unexplained. To confirm the identity of this ion, strain EG208 with an IPTG inducible promoter in front of the *skf* gene cluster was subjected to IMS. If the ion with *m/z* of 2782 is SKF, it is expected to be present only when IPTG is added. Indeed, in the absence of IPTG, the ion at *m/z* 2782 is absent as judged by IMS (Fig. 1*B*). In addition, the production of this ion was abolished when the *skfA* gene was inactivated, solidifying that this 2782 ion is indeed the mature form of SKF (*SI Appendix*, Fig. S2, EG165). Similarly, the 4350 signal was not observed in an *sdpC* deletion strain, in agreement with the identification of this ion as SDP (*SI Appendix*, Fig. S2, EH273).

Isolation and Structural Elucidation of SDP and SKF. With the masses of SKF and SDP in hand, it became possible to use an MS-guided isolation for both molecules. Unlike the antibiotics surfactin and subtilosin, SDP and SKF did not readily diffuse into the solid media as judged by IMS (Fig. 1*A* and *B* and *SI Appendix*, Fig. S2). This implied that SDP and SKF are hydrophobic in nature, and thus we adapted our purification protocol accordingly (*SI Appendix, SI Methods*). The isolation and subsequent structural analysis using tandem MS and NMR enabled us to determine that SDP is a 42-aa peptide with a disulfide crosslink and that SKF is a 26-aa

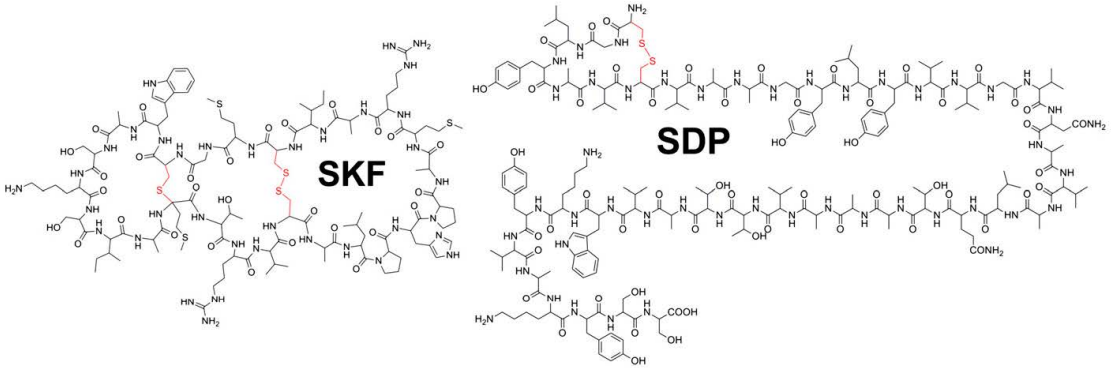

Fig. 2. Structures of SKF and SDP.

disulfide-containing cyclic peptide with a thioether crosslink of a cysteine to the α-carbon of a methionine (Fig. 2). This ribosomally encoded peptide is unusual in terms of structure but is consistent with the transport and biosynthetic enzymes found on the *skf* gene cluster as described in *SI Appendix, SI Text* (6). A full description of the data and methods that led us to the determination of these structures is provided in *SI Appendix, SI Text*.

Biological Effects of SDP and SKF. With the availability of microgram quantities of purified SKF and SDP, the biological effects of these compounds on *B. subtilis* growth in liquid and solid cultures and the effects on cell structure were evaluated. First, we added the purified compounds to liquid cultures of the undomesticated WT strain 3610, its domesticated laboratory descendent PY79, and a PY79 strain containing the Δ*spo0A* mutation (KP648). 3610 was included to verify the relevance of our findings to an undomesticated strain of *B. subtilis*. In rich media (ISP2 or LB media), 20 μg/mL purified SDP significantly and rapidly inhibited growth of 3610, PY79, and Δ*spo0A*, whereas 20 μg/mL SKF, surprisingly, had little observable effect on growth (*SI Appendix*, Fig. S6). PY79 was much less affected by the addition of SDP than the other strains, presumably because PY79 produces SKF and SDP during growth and likely expresses the resistance genes, whereas we were unable to detect the compounds in the Δ*spo0A* mutant under any conditions tested and 3610 produced low levels of the compounds only at late times on LB and DSM (*SI Appendix*, Figs. S2 and S7).

To determine the growth inhibitory activity of SDP in more detail, we investigated the effects of different concentrations of SDP on growth of the Δ*spo0A* strain KP648. A concentration-dependent growth effect was observed (Fig. 3*A*). Upon addition of 5–20 μg/mL SDP, growth was halted but was able to resume after several hours of continued incubation. The recovery represents survival of a subpopulation of SDP-resistant cells that are able to resume growth after a lag period (discussed below). The concentration of SDP significantly affected the degree to which growth was inhibited and the length of the growth lag. To evaluate how

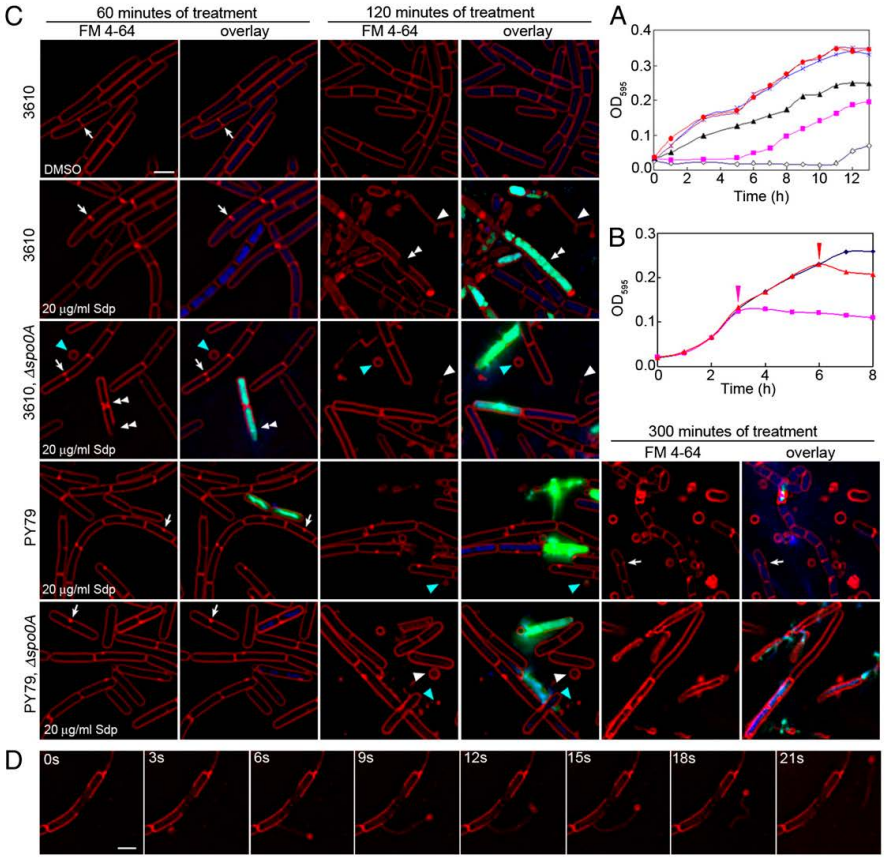

Fig. 3. Biological effects of SDP on *B. subtilis*. (*A*) Growth curves of KP648 (Δ*spo0A*) in ISP2 media with various concentration of SDP. SDP was added at 0 h. —◇—Indicates 20 μg/mL; —■—, 10 μg/mL; —▲—, 5 μg/mL; —✳—, 2 μg/mL; —✳—, 0.2 μg/mL; and —●—, DMSO control. (*B*) Growth curves of KP648 (Δ*spo0A*) in ISP2 media with 20 μg/mL SDP. SDP was added at 3 h (—■—) and 6 h (—▲—).—◆— Indicates DMSO control. (*C*) Fluorescence micrographs of growing cells of 3610, PY79, ALB1035 (3610, Δ*spo0A*), and KP648 (PY79, Δ*spo0A*) treated with DMSO or 20 μg/mL SDP for the time indicated. Red stain is FM 4–64, a fluorescent membrane stain; blue and green stains are DAPI and Sytox Green, two DNA stains that are membrane impermeable. Sytox Green is the least permeable and provides the greatest increase in fluorescence in permeabilized cells. White arrows point to dividing cells. In the DMSO control, the arrow points to a normal division, whereas in the other images the septa are asymmetric. Double arrowheads point to large gaps in membrane staining. Light blue triangles point to membrane spheres, whereas white triangles point to tubular membranes. After 300 min of treatment of PY79 with SDP, surviving cells are smaller, dividing, and impermeable to Sytox. (*D*) Time-lapse microscopy images collected at 110 min after SDP treatment. Still images from 0 to ~21 s are shown.

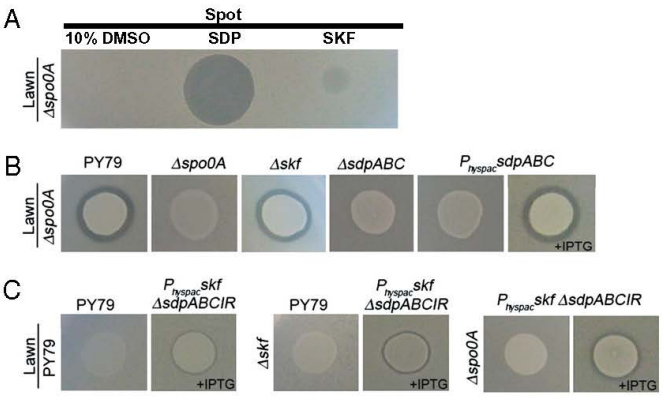

Fig. 4. Spot assays to compare the effect of exogenously supplied and endogenously produced SDP and SKF. Lawns of indicated strains were prepared in top agar. After solidification, the lawns were spotted with either (*A*) purified SDP, SKF, and DMSO or (*B*,*C*) the indicated strains that overexpress or lack SDP and SKF.

rapidly SDP inhibited growth, SDP was added to an exponentially growing culture. The addition of 20 μg/mL SDP at different time points rapidly caused growth to level off with very little decrease in optical density (Fig. 3*B*). These results demonstrate that purified SDP has rapid effects on growth of *B. subtilis* cells but that SKF does not at the highest concentration (20 μg/mL) that we tested.

We next performed fluorescence microscopy on living cells of 3610, PY79, and the Δ*spo0A* derivatives of these strains (ALB1035 and KP648, respectively) following treatment with 20 μg/mL SDP for various times in liquid culture. Cells were stained with FM 4–64, a fluorescent membrane stain that inserts into the outer leaflet of the bilayer, as well as Sytox Green and DAPI, two DNA stains that do not efficiently cross the bilayer unless the cells are permeabilized (Fig. 3*C*). The first effect was noted ≈60 min after the addition of SDP to 3610, when we observed that the cells often showed partial, asymmetric septa, and localized bright staining of membranes (arrows), suggesting the presence of deformations in the cytoplasmic membrane, particularly at division sites. Approximately 5% of the cells at this time also showed increased permeability to Sytox Green and DAPI, and a subset of these cells showed large gaps in the membrane staining (double arrowheads), suggesting that these cells lack an intact cytoplasmic membrane. By 120 min, more cells showed increased permeability to Sytox Green, DAPI, and discontinuous membranes, and we observed many spherical and tubular membrane projections (arrowheads). By 120 min, ~33% of all morphologically intact 3610 cells stained with Sytox Green, indicating they were permeablized, and 5% of the cells had protruding tubules (*SI Appendix*, Tables S2 and S3). By 300 min, very few intact cells remained in the Δ*spo0A* culture, whereas the PY79 culture still contained dividing cells, confirming the increased sensitivity of the Δ*spo0A* mutant to SDP. Time-lapse microscopy revealed that the membrane tubules were formed and released in a matter of seconds (Fig. 3*D* and Movie S1).

The domesticated strain PY79 and its Δ*spo0A* derivative (KP648) responded more slowly to SDP, with only ~4% of cells showing increased Sytox Green permeability at 60 min after treatment, and with major changes in cell morphology first observed 90 min after treatment. At 120 min, 13.7% of all morphologically intact PY79 cells stained with Sytox and increased to 19.8% in the PY79, Δ*spo0A* strain (*SI Appendix*, Table S2). These results confirm our initial hypothesis that the 4350 *m/z* ion, due to the overlap with the decreased growth phenotype of Δ*spo0A* in the coculture of Δ*spo0A* with PY79, is the major cannibalistic factor. Furthermore, the data indicate that SDP does not rapidly lyse all of the Spo0A-OFF cells and that a subpopulation of Δ*spo0A* cells remains viable even after several hours of treatment, suggesting an additional degree of multicellular behavior in a population of genetically identical *B. subtilis* cells.

Dual Nature of SKF- and SDP-Mediated Killing of Sister Cells. Having failed to detect any biological affect of purified SKF using the above liquid culture assays, we wanted to evaluate the ability of SKF and SDP to work independently on solid media. To assess this, we set out to determine whether purified SDP or SKF inhibited the growth of Δ*spo0A* on solid media. Spotting 2 μg SDP resulted in a large zone of decreased growth, and 2 μg SKF resulted in a smaller zone in which the lawn appeared somewhat thinner, whereas the control 10% DMSO did not have an effect on the growth (Fig. 4*A*). This indicates that both SDP and SKF reduce the growth of *B. subtilis* on solid media, although purified SDP has a much stronger effect than SKF.

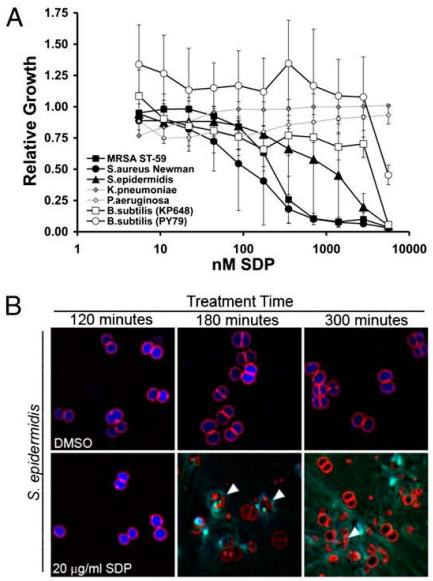

Fig. 5. Biological activity of SDP on clinically relevant human pathogens. (*A*) SDP inhibition curves for pathogenic microbes. Relative growth of *P. aeruginosa*, *K. pneumoniae*, *B. subtilis* strains KP648 (Δ*spo0A*), and PY79, *S. aureus* Newman strain, a clinical isolate of methicillin-resistant *S. aureus*, and *S. epidermidis* with the presence of increasing concentrations of SDP is shown in the curve. (*B*) Fluorescence micrograph showing growing cells of *S. epidermidis* treated with DMSO or 20 μg/mL SDP in DMSO for the time indicated and stained with FM 4-64 (red), DAPI (blue), and Sytox (green), as in Fig. 3.

We next sought to determine whether SDP and SKF produced independent killing effects of similar magnitude when overproduced on solid medium. To do so, we used a spot assay in which PY79, Δ*spo0A*, Δ*skf*, Δ*sdp*, and SKF- or SDP-overexpressing strains are spotted on *B. subtilis* lawns. When PY79 was spotted on the Δ*spo0A* lawn, a large zone of clearing was observed (Fig. 4*B*), as previously reported (6). This phenomenon is mostly dependent on SDP, as the inhibitory effect was still observed with a Δ*skf* strain but was abolished when *sdpABC* genes were deleted or not induced (Fig. 4*B*). We next overexpressed SKF in an *sdpABCIR* deletion background to eliminate the effect of SDP (P_{hyspac}*skf*, Δ*sdpABCIR*), and observed a killing effect toward lawns of PY79, Δ*skf* and Δ*spo0A* (Fig. 4*C*). These results indicate that although most of the killing effect of PY79 on a Δ*spo0A* lawn is mediated by SDP rather than SKF, overexpression of the *skf* operon still mediates a killing activity. Thus, either SKF or SDP can independently mediate cannibalism on solid culture medium, but SDP is much more potent than SKF.

SDP but Not SKF Has Antibacterial Activities Against Pathogens. The above results indicate that both SKF and SDP mediate cannibalistic effects. We therefore set out to determine whether these two molecules would also display activity against human pathogens by screening purified SKF and SDP for inhibitory activity against a panel of pathogenic microbes (including *B. subtilis* strains PY79 and its Δ*spo0A* derivative for comparison). We used a growth assay that measures differences in cell density compared with untreated controls. This screen revealed that SKF had no effect on growth, whereas SDP decreased cell density of members of the Gram-positive genus *Staphylococcus* to a greater extent than *B. subtilis*, but it did not affect the tested Gram-negative pathogens *Pseudomonas aeruginosa* or *Klebsiella pneumoniae* (Fig. 5*A*). SDP exhibited potent inhibitory activity against two *S. aureus* variants, the Newman strain used extensively in laboratory studies of *S. aureus* virulence, as well as a clinical isolate of methicillin-resistant *S. aureus* (MRSA) sequence type ST59. The IC_{50} against these *S. aureus* strains were 210 and 110 nM, respectively, slightly more active than the leading contemporary pharmacological agent for treatment of MRSA infection, vancomycin (IC_{50} 360, 270 nM, respectively). SDP also inhibited growth of *S. epidermidis*, an opportunistic pathogen associated with nosocomial infections of catheters and the urinary tract and invasive infections in human premature neonates (IC_{50} 990 nM). SDP has a relatively simple chemical structure, and might therefore provide an antibiotic candidate for future development of derivatives with smaller size and optimized activity against MRSA and closely related species.

In summary, this paper highlights the need for the development of new technologies to study and discover biologically active molecules, a cornerstone of chemical biology as well as therapeutic discovery (20). Thin-layer agar MALDI-IMS of cocultures of bacterial colonies enabled the discovery, isolation, and structural elucidation of two biologically active factors, SKF and SDP, one of which was cyclized and uniquely posttranslationally modified with a thioether linkage to the α-position of a methionine. MALDI-IMS can also be used to predict the function of metabolites. In this study, we observed an overlap of SDP extending from the cocultured strain PY79 with the region of Δ*spo0A* that was inhibited, enabling us to formulate a hypothesis that SDP, but not SKF, was the main cannibalistic factor. Indeed, when we tested the biological activities of the purified compounds, only SDP showed inhibitory activity in liquid cultures. On the other hand, both SDP and SKF mediated inhibition on solid cultures when overexpressed in whole cells grown on solid medium or when the purified compounds were spotted onto solid media. However, SKF, was much less potent than SDP, and our data indicate that SDP is the primary toxin that mediates cannibalism. Finally, screening both SKF and SDP for their antibacterial activities allowed us to demonstrate that SDP, but not SKF, inhibits growth of *Staphylococci* to a greater extent than it inhibits *B. subtilis* growth. This suggests that SDP also participates in defensive or predatory behavior directed at other species (14, 15), as well as cannibalism (6). The fact that SDP inhibited clinically relevant pathogens also demonstrates a unique application of studying metabolic exchange by IMS in the discovery of biologically active molecules, and therefore represents that IMS can be used as a tool in efforts to discover new classes of therapeutic agents.

Methods

Structural elucidation of SKF and SDP, as well as the annotation of SKF biosynthetic gene cluster, are described in *SI Appendix, SI Text*. Details regarding strains, culture conditions, bioassays are provided in *SI Appendix, SI Methods*. The procedures used in thin-layer agar MALDI IMS, purification of SKF and SDP, SKF derivatization, MS, NMR, and fluorescence microscopy are also detailed in *SI Appendix, SI Methods*.

ACKNOWLEDGMENTS. We thank the staff at the Losick laboratory (Harvard University, Cambridge, MA) for providing *skf* and *sdp* mutant strains, Michael Fischbach (University of California San Francisco, San Francisco, CA) for providing the *S. epidermidis* strain, and William H. Gerwick (University of California San Diego, La Jolla, CA) for critically reviewing the manuscript. Funding for the Dorrestein laboratory was provided by the Beckman Foundation and National Institute of General Medical Sciences Grant NIHGM086283 (to P.C.D. and P.A.P.). W.-T.L. was supported in part by study abroad Grant SAS-98116-2-US-108 from Taiwan. N.M.H and J.Y.Y. were supported by Ruth L. Kirschstein National Research Service Award (NRSA) from National Institutes of Health Grants 1 F31 GM90658-01 and 1 T32 EB009380-01, respectively. P.A.P. was supported by the National Center for Research Resources of National Institutes of Health via Grant P-41-RR024851. Funding for the Joe Pogliano lab was provided by National Institute of General Medical Sciences Grant NIHGM073898. Funding for the Kit Pogliano laboratory was provided by National Institute of General Medical Sciences Grant NIHGM57045.

1. Shank EA, Kolter R (2009) New developments in microbial interspecies signaling. *Curr Opin Microbiol* 12:205–214.
2. Tam NKM, et al. (2006) The intestinal life cycle of *Bacillus subtilis* and close relatives. *J Bacteriol* 188:2692–2700.
3. Aguilar C, Vlamakis H, Losick R, Kolter R (2007) Thinking about *Bacillus subtilis* as a multicellular organism. *Curr Opin Microbiol* 10:638–643.
4. Earl AM, Losick R, Kolter R (2008) Ecology and genomics of *Bacillus subtilis*. *Trends Microbiol* 16:269–275.
5. Kunst F, et al. (1997) The complete genome sequence of the gram-positive bacterium *Bacillus subtilis*. *Nature* 390:249–256.
6. González-Pastor JE, Hobbs EC, Losick R (2003) Cannibalism by sporulating bacteria. *Science* 301:510–513.
7. Ellermeier CD, Hobbs EC, Gonzalez-Pastor JE, Losick R (2006) A three-protein signaling pathway governing immunity to a bacterial cannibalism toxin. *Cell* 124:549–559.
8. Engelberg-Kulka H, Amitai S, Kolodkin-Gal I, Hazan R (2006) Bacterial programmed cell death and multicellular behavior in bacteria. *PLoS Genet* 2:e135.
9. Claverys JP, Håvarstein LS (2007) Cannibalism and fratricide: Mechanisms and raisons d'être. *Nat Rev Microbiol* 5:219–229.
10. López D, Vlamakis H, Losick R, Kolter R (2009) Cannibalism enhances biofilm development in *Bacillus subtilis*. *Mol Microbiol* 74:609–618.
11. Burbulys D, Trach KA, Hoch JA (1991) Initiation of sporulation in *B. subtilis* is controlled by a multicomponent phosphorelay. *Cell* 64:545–552.
12. Fawcett P, Eichenberger P, Losick R, Youngman P (2000) The transcriptional profile of early to middle sporulation in *Bacillus subtilis*. *Proc Natl Acad Sci USA* 97:8063–8068.
13. Molle V, et al. (2003) The Spo0A regulon of *Bacillus subtilis*. *Mol Microbiol* 50:1683–1701.
14. Lin D, Qu LJ, Gu H, Chen ZA (2001) A 3.1-kb genomic fragment of Bacillus subtilis encodes the protein inhibiting growth of Xanthomonas oryzae pv. oryzae. *J Appl Microbiol* 91:1044–1050.
15. Nandy SK, Bapat PM, Venkatesh KV (2007) Sporulating bacteria prefers predation to cannibalism in mixed cultures. *FEBS Lett* 581:151–156.
16. Cornett DS, Reyzer ML, Chaurand P, Caprioli RM (2007) MALDI imaging mass spectrometry: Molecular snapshots of biochemical systems. *Nat Methods* 4:828–833.
17. Seeley EH, Caprioli RM (2008) Molecular imaging of proteins in tissues by mass spectrometry. *Proc Natl Acad Sci USA* 105:18126–18131.
18. Yang YL, Xu Y, Straight P, Dorrestein PC (2009) Translating metabolic exchange with imaging mass spectrometry. *Nat Chem Biol* 5:885–887.
19. Zeigler DR, et al. (2008) The origins of 168, W23, and other *Bacillus subtilis* legacy strains. *J Bacteriol* 190:6983–6995.
20. Li JW, Vederas JC (2009) Drug discovery and natural products: End of an era or an endless frontier? *Science* 325:161–165.

Supplementary Materials

Imaging mass spectrometry of intraspecies metabolic exchange revealed the cannibalistic factors of *Bacillus subtilis*

Wei-Ting Liu,[a,1] Yu-Liang Yang,[b,1] Yuquan Xu,[b,1] Anne Lamsa,[c] Nina M Haste,[b,d] Jane Y. Yang,[a] Julio Ng,[e] David Gonzalez,[a] Craig D. Ellermeier,[f] Paul D. Straight,[g] Pavel A. Pevzner,[e,h] Joe Pogliano,[c] Victor Nizet,[b,d,i], Kit Pogliano,[c] Pieter C. Dorrestein,[a,b,d,2]

[a]*Departments of Pharmacology, Department of Chemistry and Biochemistry, University of California, San Diego, La Jolla, CA 92093.*
[b]*Skaggs School of Pharmacy and Pharmaceutical Sciences, University of California, San Diego, La Jolla, CA 92093.*
[c]*Division of Biological Sciences, University of California, San Diego, La Jolla, CA 92093.*
[d]*Center for Marine Biotechnology and Biomedicine, University of California, San Diego, La Jolla, CA 92093.*
[e]*Department of Computer Science, University of California San Diego, La Jolla, CA 92093.*
[f]*Department of Microbiology, University of Iowa, Iowa, 52242.*
[g]*Department of Biochemistry and Biophysics, Texas A&M University, College Station, TX 77843.*
[h]*University of California San Diego NCRR Center for Computational Mass Spectrometry, La Jolla, CA 92093.*
[i]*Department of Pediatrics, University of California San Diego, La Jolla, CA 92093.*

[1]The authors contributed equally to this work.
[2]Corresponding author
To whom correspondence should be directed, E-mail: pdorrest@ucsd.edu. Mailing address: Skaggs School of Pharmacy and Pharmaceutical Sciences, Biomedical Science Building (BSB), Room 4090 9500 Gilman Drive, La Jolla, CA 92093-0636. Phone: +1(858)534-6607. Fax: +1(858)822-0041.

A. Supporting text

Structural elucidation of SDP and SKF

The purified SDP was subjected to high resolution Fourier transform ion cyclotron resonance mass spectrometry (FT-ICR MS) to obtain a monoisotopic mass *m/z* 4311.209 $[M+H]^+$ (Fig. S3), and this mass matched Cys^{141}-Ser^{182} of SdpC-2.016 Da, indicating the likely presence of a disulfide crosslink. The fragmentation by collision-induced dissociation (CID) and FT-ICR MS analysis confirmed the sequence with a disulfide crosslink localized to residues Cys^{141} and Cys^{147} (Fig. 2, Fig. S5, Table S4). The N-terminal boundary of SDP is in agreement with the N-terminal Edman amino acid sequencing previously performed on SDP (1).

Purified SKF was also analyzed by high-resolution mass spectrometry and found to have a mass of 2781.302 Da (Fig. S3). This mass could not be readily matched to the C- or N-terminal portions of the 55 amino acid protein precursor SkfA (1). When purified SKF was subjected to high-resolution tandem mass spectrometry, the sequence tag WASKSI was obtained (Fig. S8*A*, Fig. S9). To define the number of amino acids that were involved in the mature SKF metabolite, a ^{15}N feeding experiment was performed. The feeding experiment with 98% pure [^{15}N]ammonium chloride resulted in a 36 Da increase in mass, indicating that SKF contained 36 nitrogen atoms which matched to the number of nitrogens in the last 26 amino acids of the SkfA sequence, CMGCWASKSIAMTRVCALPHPAMRAI (Fig. S8*B*). The calculated mass of this peptide is 2803.340, and therefore, the mature form of SkfA is 22.038 Da less than that expected from the intact peptide sequence. The absence of observable *y* ions provided an indication that SKF may be cyclic (2). We postulated that SKF was cyclic accounting for 18.011 of the 22.038 Da mass differences. The remaining 4.027 Da difference between the parent SkfA peptide and the cyclized precursor could be explained by two crosslinks, possibly a disulfide and a thioether.

To confirm that SKF was indeed cyclic, all thiols were replaced with a proton using a reductive dethiolation reaction composed of $NiCl_2$ and $NaBH_4$ (Fig. S10) (3). Subjecting SKF to this reaction resulted in an ion with a mass of 2551.444 Da. Tandem mass spectrometry by collision induced dissociation (CID) confirmed the sequence to the 26 amino acids on the C-terminal end of SkfA as well as a cyclic head-to-tail linkage between isoleucine and cysteine. The calculated mass of this molecule is 2551.450. To define the connection of the thioether linkage, the reductive dethiolation was repeated but with deuterated solvents and $NiCl_2/NaBD_4$ and resulted in a species with mass of 2558.491, 7.041 Da larger compared to the product resulted from $NiCl_2/NaBH_4$ reaction, suggesting 7 thiol connections. Six deuteriums were introduced from the replacement of three methionine and three cysteine side chains with deuterons while the remaining deuterium was introduced at the site of the thioether linkage (Fig. S11*A*). Therefore, it became possible to map out the position of the thioether linkage by locating this extra deuterium that gave rise to the 1 Da mass shift. To map the thioether linkage, multiple stages of tandem mass spectrometry were obtained on the deuterated dethiolated

SKF. To find the position of the additional deuterium, a mass list with manually deconvoluted fragment ions was analyzed by an algorithm NRP-comparative dereplication (4) against the theoretical structure of SKF with a deuterium labeled on each desulfurized position (Fig. S11*A*). NRP-dereplication matched the MS fragments with the structure and Met^{12} had the lowest score indicated the strongest correlation of the 1 Da increase between the observed ions in the tandem mass spectrometry experiment when compared to the theoretically predicted ions of the deuterated dethiolated SKF template (Fig. S8*C* and Fig. S11*B*). Guided by the NPR-dereplication result, manual annotation was performed, again verifying the extra deuterium on Met^{12} (Fig. S11*C* and Table S5, S6).

The position of the disulfide bond was determined by reduction, iodoacetamide alkylation and tandem mass spectrometry. Reduction and alkylation of SKF resulted in a mass increase of 116.061 Da, in agreement with two free thiols (Fig. S10). Via tandem mass spectrometry, the alkylated residues were found to be Cys^1 and Cys^{16}, positioning the disulfide between these two cysteines. Even though the tandem mass spectrometry of the desulfurized SKF indicated that the thioether linkage is connected to the methionine, it did not provide regiochemical information to which carbon of Met^{12} that Cys^4 was connected. To determine the regiospecificity of the tetrahedral linkage, we resorted to nuclear magnetic resonance (NMR) spectroscopy (Figs. S12 and Table S7). To determine the relevant proton signals, the NMR signal that corresponded to the methionine involved in the thioether cross-link needed to be identified. To find the modified methionine with an absent proton, a ^1H-^1H total correlation spectroscopy (TOCSY) was obtained first. From the TOCSY, one set of methionine correlations lacking an α-proton was observed, and suggested that the linkage of Cys^4 to Met^{12} is via the α-carbon of the latter residue (Fig. S12*B* and C). An α-connection would result in a ^{13}C-chemical shift at this α-carbon of about 70 ppm while a β-connection would result in ^{13}C-chemical shift of 40-50 ppm (3). The ^{13}C-chemical shift information was obtained indirectly by heteronuclear multiple bond correlation (HMBC) (Fig. S8*D* and *E*, Fig. S12*D*), because of the small quantities of pure SKF available. The same methionine that was missing the proton in the TOCSY was scrutinized in the HMBC spectrum. In the HMBC, in agreement with the findings by TOCSY, there was no evidence of an α-proton in Met^{12}; however, the β-proton possessed long range correlations between the β-protons and two quaternary carbons, located at δ 67.9 and 180.7 (Fig. S8*D* and *E*), and thus consistent with a thioether bridge connecting to the α-carbon of Met^{12}. A post-translational modification of a cysteine to the α-carbon of methionine has not been previously reported (5).

The functional annotation of the *skf* biosynthetic operon.

Based on the structure of SKF, it is now possible to propose the role of each gene on the *skf* operon involved in SKF biosynthesis. The *skf* operon was previously predicted to contain a stop codon due to sequencing errors in the original genome that resulted in an incorrect open reading frame assignment for *skfC*

and *skfD* (1). Thus, *skfC* and *skfD* are in fact a single open reading frame, and therefore we have omitted the designation *skfD*. Therefore the *skf* operon has seven genes, *skfABCEFGH* (Fig. S13). SkfA is a prepropeptide that is post-translationally modified to the mature SKF (1). SkfB belongs to the radical SAM superfamily that includes genes such as *albA*, *lipA*, *bioB*, which are involved in the biosynthesis of C-S linkages in subtilosin, lipoic acid, and biotin, respectively (Fig. S14*A*) (3, 6-8). We propose that SkfB is responsible for the C-S linkage of Cys^4 to the α-carbon of Met^{12} similar to the proposed reaction catalyzed by AlbA on the subtilosin pathway (3, 9). SkfC belongs to the CaaX family of proteases (Fig. S14*B*) which, in eukaryotes, are responsible for the proteolysis of C-terminal prenylated cysteines (10). Since this is the only protease candidate on the *skf* gene cluster, we propose it is involved in the cyclization reaction, which would represent a new function for a CaaX family member of proteins. SkfE is homologous to the cytoplasmic ATPase domain of ABC transporters, while SkfF is a polytopic membrane protein; both are predicted to be involved in the export and immunity of SKF (1). SkfG showed homology to several HEAT-repeat containing proteins, although the role of SkfG remains unclear. SkfH is a thioredoxin-oxidoreductase like protein and may be involved in the generation of the disulfide bond analogous to the proposed function of the oxidoreductase on the sublancin 168 biosynthetic pathway (Fig. S14*C*) (11).

B. Supplementary Methods

Strains used in this study

Bacillus	Genotype	Background	Source – Ref.
3610	Prototroph		S. Branda – 12
PY79	Prototrophic derivative of *B. subtilis* 168		K. Pogliano – 13
KP648	Δ*spo0A::erm*	PY79	K. Pogliano – 14,1
ALB1035	Δ*spo0A::erm*	3610	This study
EG208	$P_{spac\text{-}hy}$-*skfABCDEFGH(kan)*	PY79	R. Losick – 1
EG165	Δ*skfA::spc*	PY79	R. Losick – 1
EH273	*sdpABC*::*kan*	PY79	R. Losick – 16
ALB1046	Δ*skf::cat*	PY79	This study
ALB1085	$P_{spac\text{-}hy}$-*skfABCDEFGH(kan), ΔsdpABIC::tet*	PY79	This study
CDE1160	*amyE::*$P_{spac\text{-}hy}$-*sdpC(spec), sdpC::tet,* $P_{spac\text{-}hy}$-*sdpAB(cat)*	PY79	This study

Thin-layer agar MALDI-IMS

Sample preparation for thin-layer agar MALDI-IMS experiments was performed using a modified method adjusted from reference 17. 0.2-1 µL of bacterial overnight cultures grown in LB media were spotted on 100 O.D. x 25 mm Petri dishes (Fisherbrand) containing ISP2 solid agar. For testing individual cultures in isolation, strains were spotted at the center of Petri dishes; for the PY79 and Δ*spo0A* co-culturing experiment, both strains were spotted on the same plate with a distance between spots of 0.75 cm. The Petri dishes were sealed with parafilm and incubated for 2-4 days as indicated. After culturing, a rectangular section containing the colonies

was transferred to a MALDI target plate. It is critical to avoid any air bubbles because it will cause the agar to peel off during the IMS process. After taking a photograph, a 1:1 mixture of α-cyano-4-hydroxycinnamic acid and 2,5-dihydroxybenzoic acid was sprinkled on top of the culture using a 20 μm sieve method (17, 18), and was dried in a 37 °C oven for three hours. The detailed instrument parameters for collecting image data were described in reference 17. Briefly, the sample was subjected to Bruker microflex MALDI-TOF MS for imaging MS acquisition and the data was analyzed using the FlexImaging 2.0 software.

Purification of SKF and SDP

PY79 was cultured on approximately 1000 IPS2 agar plates and cultured at 28 °C for 2 days. The bacteria were scraped from agar plates and then re-suspended in milli-Q water. Equal amount of *n*-BuOH was used to extract SKF and SDP from aqueous layer. The crude *n*-BuOH extract was lyophilized, re-dissolved and then eluted via Sephadex LH-20 column using isopropanol/MeOH = 1:9. Each fraction was analyzed by MALDI MS and the fractions containing signals *m/z* 2782 or *m/z* 4312 were collected into two separate tubes. The two tubes that contained crude SKF or SDP, respectively, were purified subsequently by HPLC (C-18, 250 x 4.6 mm) running a gradient from 25% solvent A to 70% solvent A in 60 minutes with flow rate 1mL/min. Solvent A is isopropanol/MeCN = 7:3 containing 0.1% TFA; solvent B is 0.1% TFA (aq). SKF and SDP were eluted at 14, and 34.5 min, respectively (Fig. S3). Purified SKF and SDP were lyophilized and stored at -80°C before using for bioassay and structural elucidation. The yield for SKF and SDP was ~ 0.5 μg each per plate.

SKF derivatization

Dethiolated SKF was prepared by dissolving 1 μg of SKF with 1.5 μg $NaBH_4$/$NaBD_4$ and 1.5 μg $NiCl_2$ in 6.25 μL of 60% MeOH/MeOD. This reaction was incubated at 50 °C, and an additional 1.5 μg of $NaBH_4$/$NaBD_4$ and $NiCl_2$ were added into the reaction 5 and 10 minutes after initiation of the reaction to ensure complete conversion of SKF into dethiolated SKF. The mixture was then centrifuged for 1 min at 14500 rpm to remove the insoluble particles and then purified by HPLC using an Agilent Eclipse XDB-C18 column running MeCN gradients or by C18 ZipTip (Millipore) following the manufacturer's protocol prior to MS analysis.

For disulfide bond reduction, 1 μg SKF was dissolved in 40 mM ammonium bicarbonate buffer, pH 8.0, containing 10% MeCN. TCEP was added to reach a final concentration of 20 mM and incubated at 85 °C for 1hr. To prevent the free thiols from reforming disulfide bond, iodoacetamide was used to cap the cysteine thio group. To accomplish this, 50 mM Tris buffer, pH 7.4 was added to TCEP treated SKF solution to a final concentration of 1 mM to bring up the pH to neutral (checked by pH paper). 5 μg of iodoacetamide powder was directly added into the reaction mixture and allowed to react at RT for 5 min followed by quenching with an

equal volume of 10% formic acid.

General MS procedure for the characterization of SKF

For the MS data acquisition, each compound was dissolved in spray solvent 50:50 MeOH/H_2O containing 1% formic acid, and underwent nanoelectrospray ionization on a biversa nanomate (Advion Biosystems, Ithaca, NY) using a back pressure of 0.3-0.5 p.s.i. and the spray voltage of 1.4 -1.5 kV. MS spectra were acquired on a 6.42 T Finnigan LTQ-FTICR MS or a Finnigan LTQ-MS (Thermo-Electron Corporation, San Jose, CA) running Tune Plus software version 1.0 and Xcalibur software version 1.4 SR1. The instrument was first autotuned on the *m/z* value of the ion to be fragmented. Then, the ions were isolated by the linear ion trap and fragmented by collision induced dissociation (CID) (isolation window: 3-10 *m/z*; collision energy: 30).

NMR measurement of SKF

400 µg SKF was dissolved in 40 µL of CD_3OD for NMR data acquisition. NMR spectra were recorded on Bruker Avance III 600 MHz NMR with 1.7 mm Micro-CryoProbe at 300 K, with standard pulse sequences provided by Bruker. 2D TOCSY spectra were recorded with mixing times of 90 ms. 2D ^{1}H-^{13}C HMBC spectra were recorded with ^{2}J or $^{3}J_{H\text{-}C}$ coupling constants at 7 Hz, 2D ^{1}H-^{13}C HSQC spectra were recorded with $^{1}J_{H\text{-}C}$ coupling constants at 145 Hz.

Effect of SKF and SDP on *B subtilis* cell growth curve

The effect of SKF and SDP on *B. subtilis* cell growth was performed using 96 well microtiter plates. A 2 mL overnight culture in LB media was centrifuged at 6000g for 10 minutes and supernatants discarded. The cell pellets were resuspended using 2 mL of ISP2 media. OD_{595} of the resuspended cells were measured (ELx808 Ultra Microplate Reader, Bio-TEK Instruments), and the final OD_{595} was adjusted to 0.03 with ISP2 media. 100 µL diluted culture with indicated working concentrations of SKF or SDP were aliquoted into each well. The plate was shaken at 37°C, 120 rpm. OD_{595} were measured and recorded at each time point. To evaluate the effect of SDP on an exponentially growing culture, SDP was added at 3 or 6 hours to a final concentration of 20 µg/mL, and the OD_{595} was measured at each time point.

Fluorescence microscopy

The effects of SDP on individual *B. subtilis* cells were investigated in 15 µL cultures prepared in the following manner. Cultures were grown in LB media to an OD_{600} of 0.3, centrifuged, resuspended in 1/10 the volume and 14.25 µL of concentrated cells were added to 1.7 mL microcentrifuge tubes. At t = 0, 0.75 µL of 10% DMSO or 400 µg/mL SDP (in 10% DMSO) was added to different aliquots of cells. The tubes were capped and incubated

at 37°C in a roller. Samples were collected for imaging every 30 minutes. 2 µL of cells were added to 0.5 µL of a stain mix containing 30 µg/mL FM 4-64, 2.5 µM Sytox Green and 1 µg/mL DAPI prepared in 1X T-base. Cells were immobilized with Poly-L-Lysine and imaged on an Applied Precision Spectris Microscope (19). Images were deconvoluted and the medial focal planes shown. Time-lapse imaging showing the formation of membrane tubules and projections was performed on these slides, collecting images of cell membranes every 3 seconds for 1 minute.

Quantification of the amount of cellular lysis was performed by determining the percent cells showing clearly discontinuous membranes and increased permeability to Sytox Green relative to the number of intact cells. This data showed that the 3610 strain, both with and without the Δ*spo0A* mutation (ALB1035) showed the most rapid onset of cell lysis (first evident at t = 60 minutes) and the highest frequency of lysis. The strains in PY79 background were affected more slowly and in a lower percent of cells. We did not score later time points in this manner, because the extensive cell lysis made it impossible to determine the percent cell lysis, since it was unclear how many cells produced the debris.

Spot assay

Lawns were created by mixing 50 µl exponentially growing cells (OD_{600} = 0.4-0.6) with 3.5 ml 0.35% LB agar and pouring the mixture onto LB plates. When indicated, IPTG was added to a final concentration of 1 mM. After the top agar solidified, 5 µl of exponentially growing cells or purified compounds were spotted on top of the lawn and allowed to dry. The plates were then incubated overnight at 30°C.

Screen of antibacterial activities against pathogens

The activities of SDP and SKF were tested in a microtiter based screen for growth inhibitory activity against a variety of Gram-positive and Gram–negative bacterial species. Then, the IC_{50} of these compounds was assessed against a smaller set of representative organisms. For this assessment, SDP was tested against three organisms whose growth it inhibited, methicillin-resistant *Staphylococcus aureus* (MRSA) sequence type 59 (ST59), *S. aureus* Newman, *Staphylococcus epidermidis* (ATCC35984), and two that were unaffected, *Klebsiella pneumoniae* (ATCC700603) and *Pseudomonas aeruginosa* (ATCC 10145). SKF had no effect in the microtiter assay for any species and the MIC assay was performed with *S. aureus* MRSA ST59, *K. pneumoniae* (ATCC700603 and ATCC 35657), *Burkholderia cepacia* (ATCC 17765) and *Escherichia coli* (ATCC 25922).

IC_{50} assays were performed by a microbroth dilution assay. The overnight culture of the tested strain was diluted 1:200 in cation-adjusted Mueller-Hinton broth (MHB, Hardy Diagnostics, Santa Maria, CA) and grown with shaking at 37°C to mid-logarithmic phase after which they were centrifuged and pellets were resuspended

in phosphate-buffered saline to an OD_{600} of 0.4 – 0.5. Prior to the addition of this pre-culture, 96-well polystyrene test plates (Costar® #3288, Corning, NY) containing duplicate samples of serially diluted test compounds, SDP or SKF, and appropriate antibiotic controls were prepared in CAMHB. Bacteria were added to the test plate to a final concentration of $5x10^5$ CFU/ml in a volume of 80 µl/well. The control antibiotics included vancomycin (Hospira, Lake Forest, IL, USA) for *Staphylococcal* strains, ciprofloxacin (Fluka, Sigma-Adlrich) for *Pseudomonas aeruginosa* and sulfamethoxazole, trimethoprim (SMX-TMP Sicor ™ Irvine, CA) for *K. pneumoniae* and *E. coli* strains. Following the addition of bacteria, test plates were incubated at 37°C in a shaking incubator for 20 - 22h. Finally the plates were assessed for bacterial growth by the presence of turbidity at OD_{600}. The absorbance at each tested concentration were normalized to the negative control (absence of test compound) to determine relative growth at a given concentration of SDP or SKF. The IC_{50} values of SDP were determined from this data.

C. Supplementary Figures

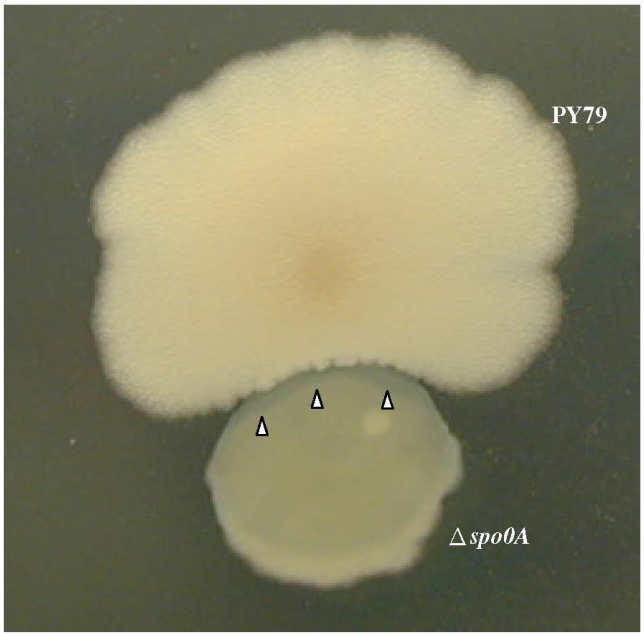

Supplementary Fig. 1. PY79 inhibits Δ*spo0A* (KP648) strain. The arrows (Δ) indicate the glassy region in the Δ*spo0A* colony.

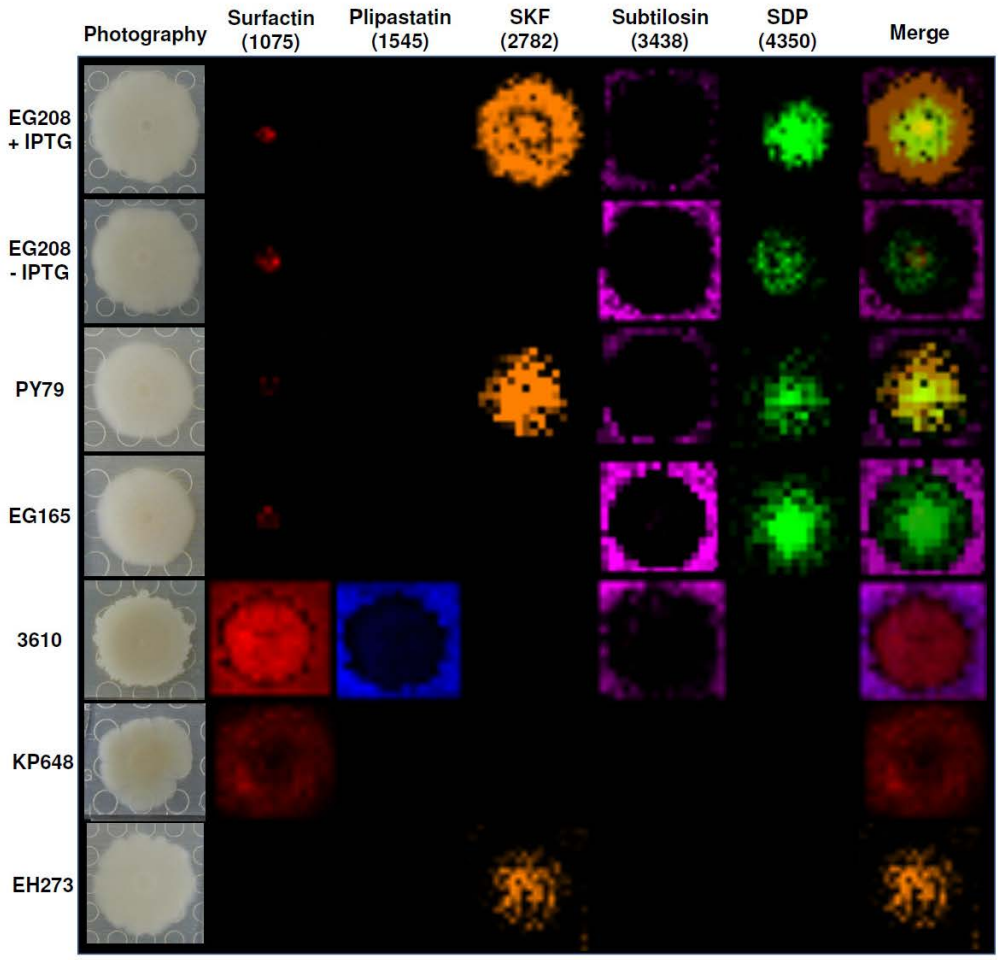

Supplementary Fig. 2. Metabolic profile of the strains used in this study. Strains were inoculated on an ISP2 agar plate and allowed to grow for 96 hours at room temperature and subjected to thin-layer agar IMS. The number labeled below each metabolite is the representative ion observed (*m/z*). *m/z* 1045, 1545, 3438 and 4350 are potassium adduct form $[M+K]^+$. For brief genotype description, 3610 is a wild type strain; PY79 is a laboratory domesticated wild type; EG208 contains the *skf* gene cluster under control of an IPTG inducible promoter; EG165, KP648, EH273 are *skfA, spo0A, sdpABC* deletion strains, respectively. All four mutants are constructed under PY79 background. The ion intensity was reflected by the intensity of colors. Each column of ions was displayed using same intensity scale optimized per each metabolite. The scale range in normalized relative ion intensity for each ion was specified in FlexImaging 2.0 (Bruker) as follows: surfactin 10%-100%; plipastatin 10-80%; SKF 30-60%; subtilosin 20-60%; SDP 1-30%.

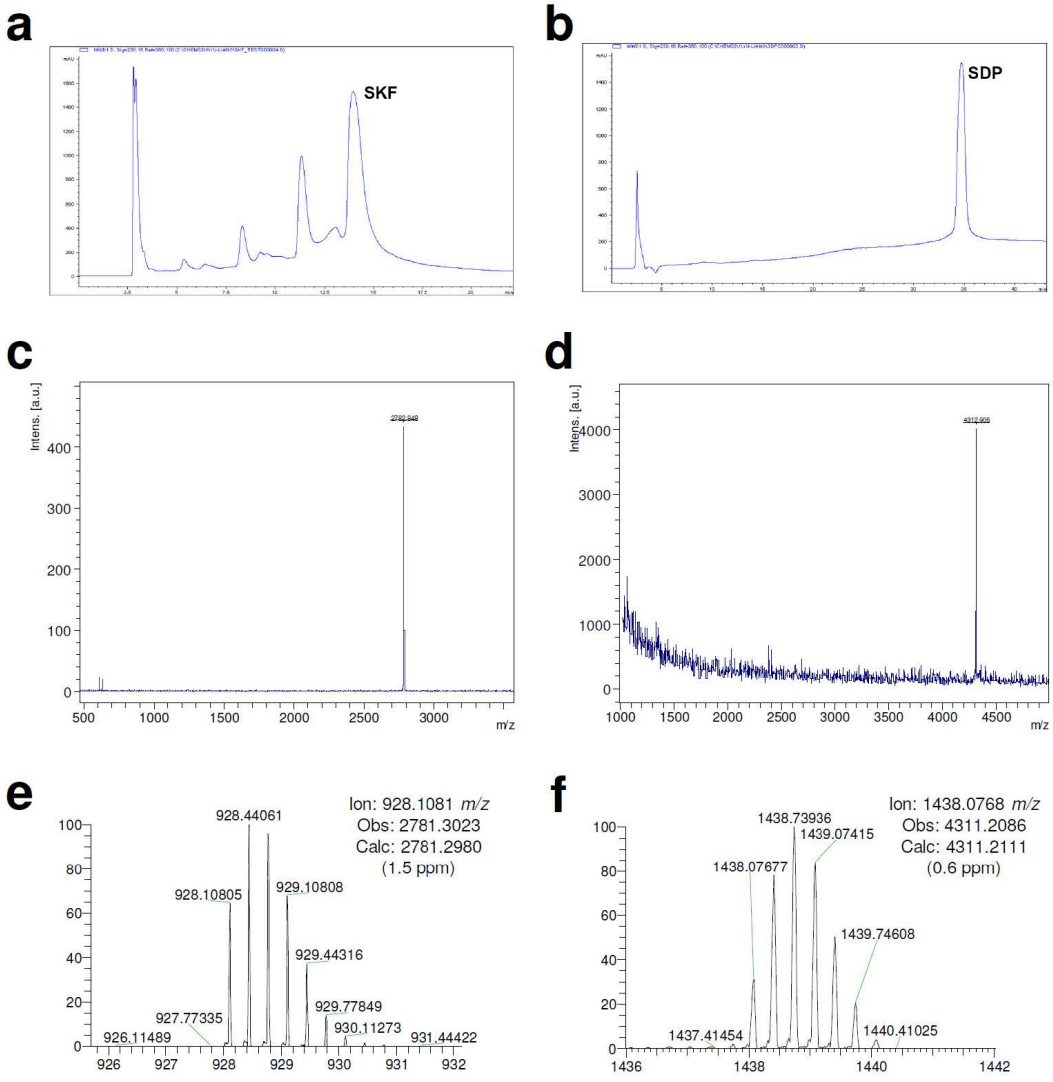

Supplementary Fig. 3. SKF and SDP purification. a, b) Crude SKF and SDP fractions obtained from an initial separations using Sephadex LH-20 column were further purified by HPLC (solvent system and gradients were specified in **Supplementary methods**). UV 230 nm was used to detect SKF and SDP. SKF and SDP were eluted at 14, and 34.5 min, respectively. **c**) MALDI-TOF MS spectrum of purified SKF. **d**) MALDI-TOF MS spectrum of purified SDP. **e**) FT-ICR MS spectrum of purified SKF. **f**) FT-ICR MS spectrum of purified SDP.

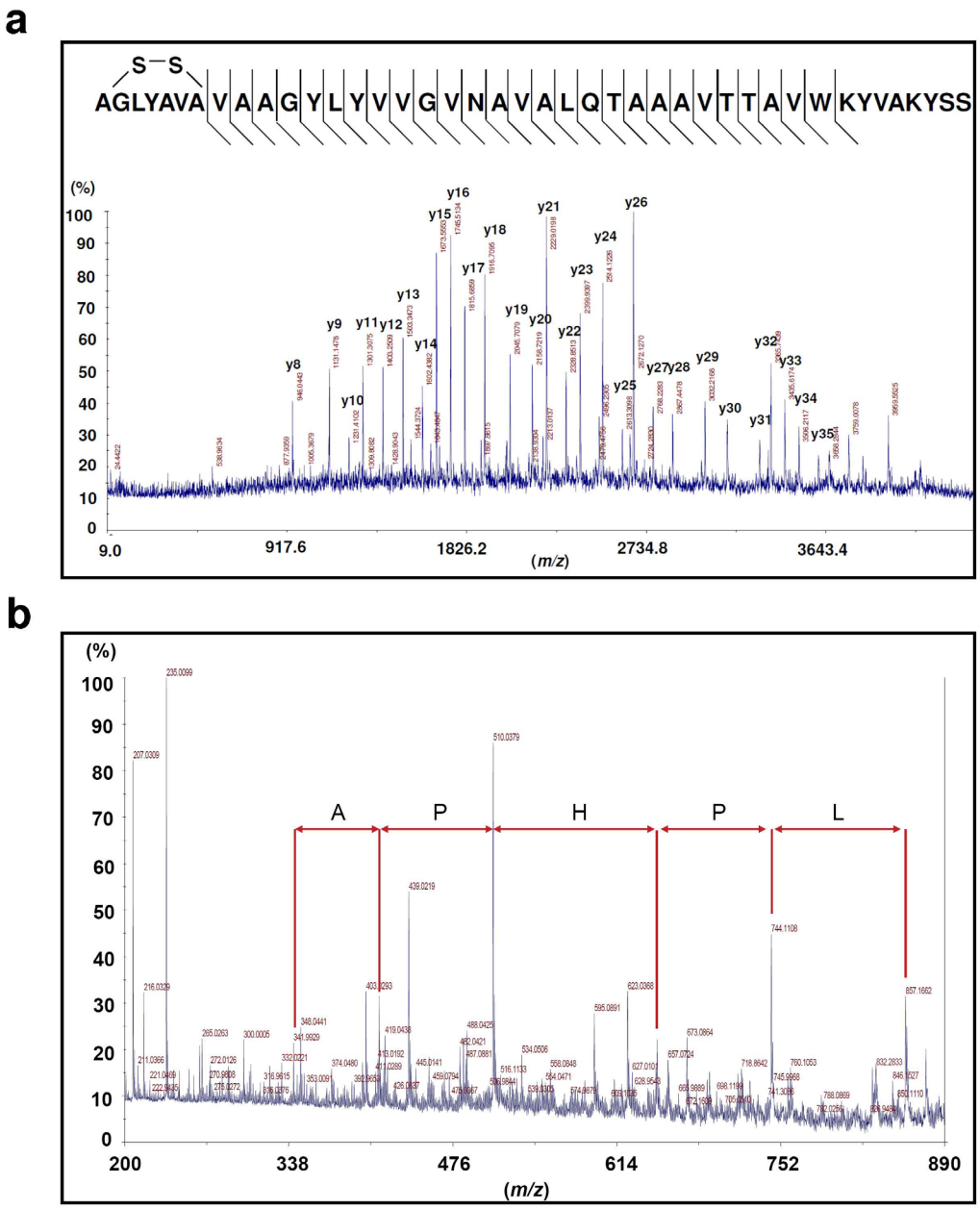

Supplementary Fig. 4. Intact cell MALDI TOF/TOF spectrum. a) Intact cell MALDI TOF/TOF spectrum of ion at *m/z* 4312. The corresponding ion table is showed in **Supplementary Table 1. b)** Intact cell MALDI TOF/TOF spectrum of ion at *m/z* 2782. The observed sequence tag that matched to SkfA is shown.

a)

```
atgaaaagtaaattacttaggctattgattgtttccatggtaacgatattggtttttttca
ttagtaggactctctaaggagtcaagtacatctgctaaagaaaaccatacattttctgga
gaagattactttagaggacttttatttggacaaggggaagttggtaaattaatttcaaac
gatttggaccctaaactcgtaaaagaggcaaatagtacagaaggtaaaaagttagtaaat
gatgtagtcaaatttataaaaaaagatcaaccacaatatatggatgaattgaaacaatcg
attgacagcaaagaccctaaaaaactcattgaaaatatgaccaaagcagaccaacttatc
caaaaatatgctaagaaaaatgaaaacgtaaaatactcttctaataaagttactccatct
tgtgggctttatgccgtctgtgtagcagctggatatttatatgttgtgggcgttaacgca
gttgcattacaaacggctgccgcagtaacaactgcagtgtggaaatacgttgccaaatat
tcctcttcagcttctaataattctgatttagaagcggctgctgcaaaaaccctaaaattg
attcatcaataa
```

b)

```
        10         20         30         40         50         60
MKSKLLRLLI VSMVTILVFS LVGLSKESST SAKENHTFSG EDYFRGLLFG QGEVGKLISN
        70         80         90        100        110        120
DLDPKLVKEA NSTEGKKLVN DVVKFIKKDQ PQYMDELKQS IDSKDPKKLI ENMTKADQLI
       130        140        150        160        170        180
QKYAKKNENV KYSSNKVTPS CGLYAVCVAA GYLYVVGVNA VALQTAAAVT TAVWKYVAKY
       190        200
SSSASNNSDL EAAAAKTLKL IHQ
```

Supplementary Fig. 5. a) *sdpC* gene sequence. b) SdpC protein sequence. Mature SDP is highlighted in yellow. A disulfide bridge exists between C^{141} and C^{147}.

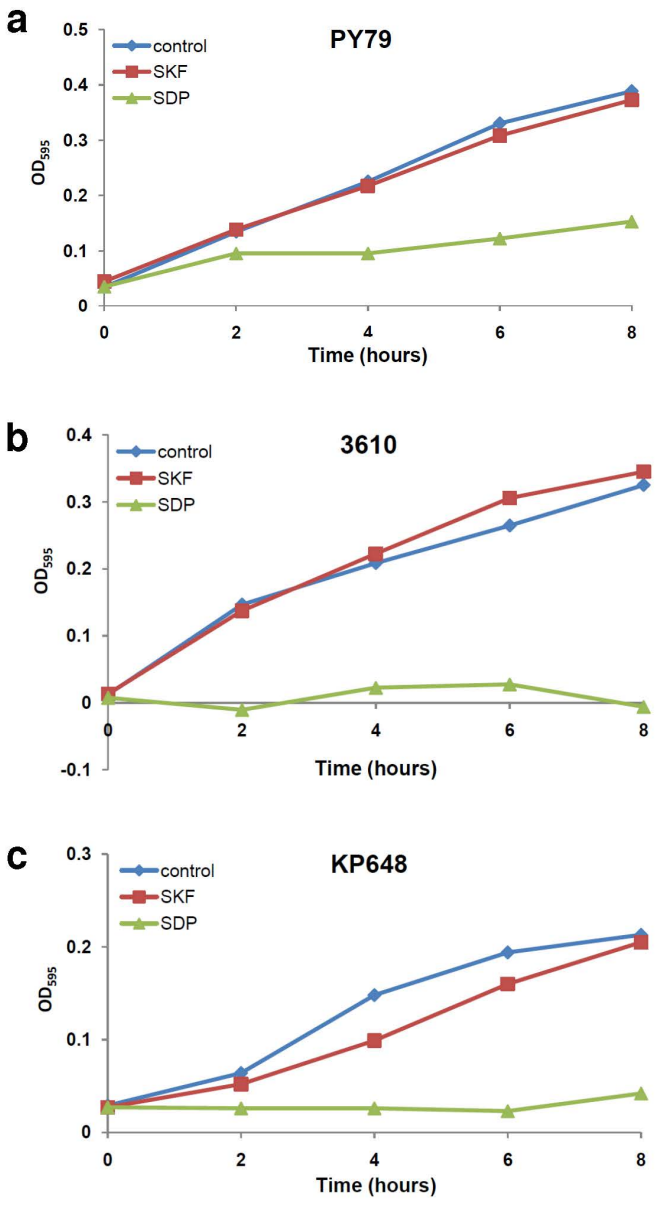

Supplementary Fig. 6. The effects of SDP and SKF on growth of *B. subtilis* strains in ISP2 media. The overnight culture was diluted into ISP2 media to OD_{595} 0.03, and SKF or SDP were added into 100 µL of diluted cultures to a final concentration of 20 µg/mL. The plate was shaken at 37 °C, 120 rpm. The OD_{595} was measured at each time point.

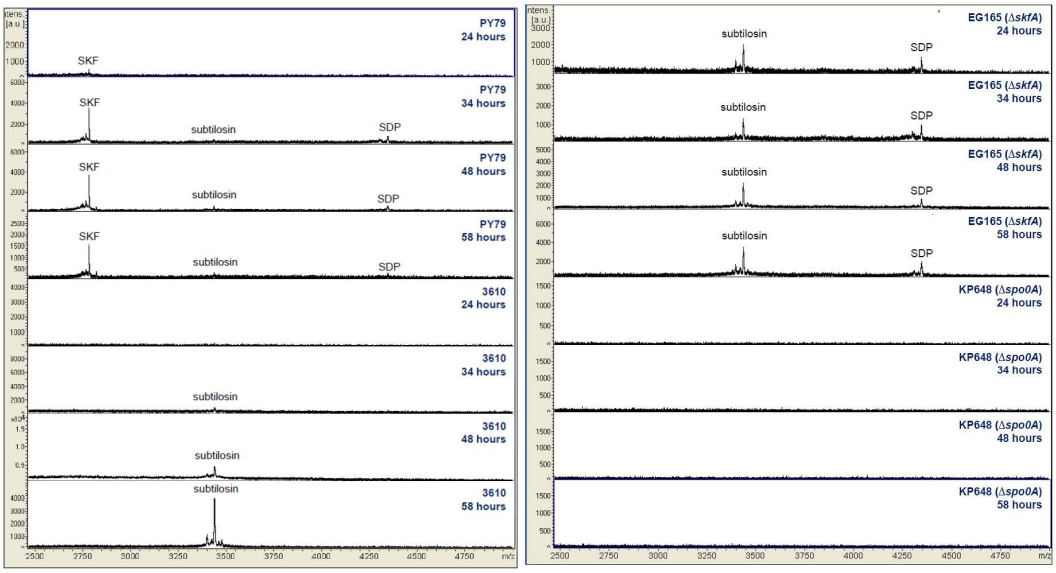

Supplementary Fig. 7. Time course of *B. subtilis* wildtype and mutant strains collected by intact cell MALDI-TOF MS (20, 21). Each strain was allowed to grow on ISP2 solid agar for 24, 34, 48 and 58 hours at 28 ºC. Each spectrum shown is an average of 200 single spectra. EG165 and KP648 are *skfA* or s*po0A* gene deletion strains, respectively. The metabolic outputs for 96 hours cultures are shown in **Supplementary Fig. 2**.

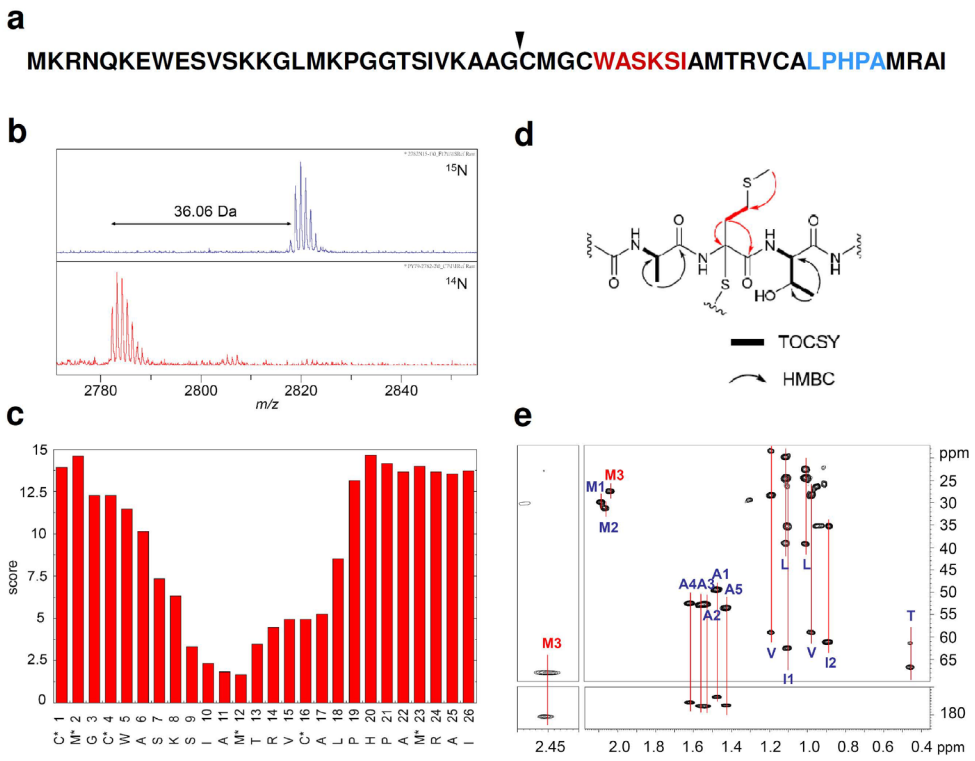

Supplementary Fig. 8. The structural characterization of SKF. (**a**) The SkfA sequence. ▼ indicates a protease cleavage site. The sequence tags observed by tandem mass spectrometry generated by FT-ICR MS/MS (red) and MALDI TOF/TOF (blue) are highlighted. (**b**) The MALDI-TOF analysis of SKF from cells grown in ^{15}N-media. (**c**) Comparative dereplication of deuterated-dethiolated SKF. (**d**) A schematic representation of the ^{1}H-^{13}C long range correlations and ^{1}H-^{1}H TOCSY correlations of the modified methionine and neighbor residues in SKF. (**e**) The ^{1}H-^{13}C HMBC spectrum of SKF showing the important ^{13}C-chemical shift supporting the α-connection to the methionine. The full TOCSY and HMBC spectra and tables of the observed chemical shifts are provided in the supporting information.

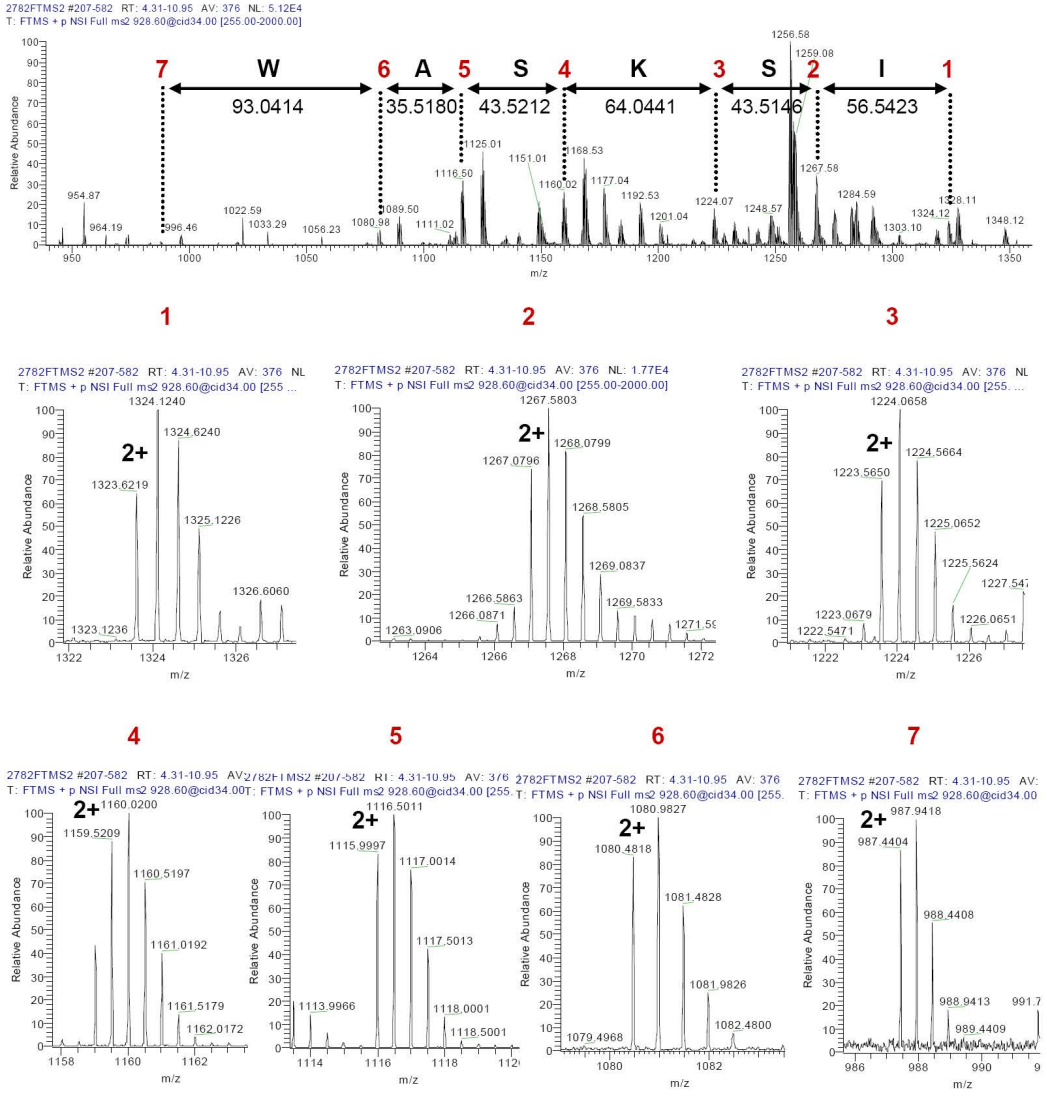

Supplementary Fig. 9. FT MS/MS spectrum of ion *m/z* 928.60 (2+ charge state). The observed mass difference and isotope profiles of each ion (2+ charge state) are shown.

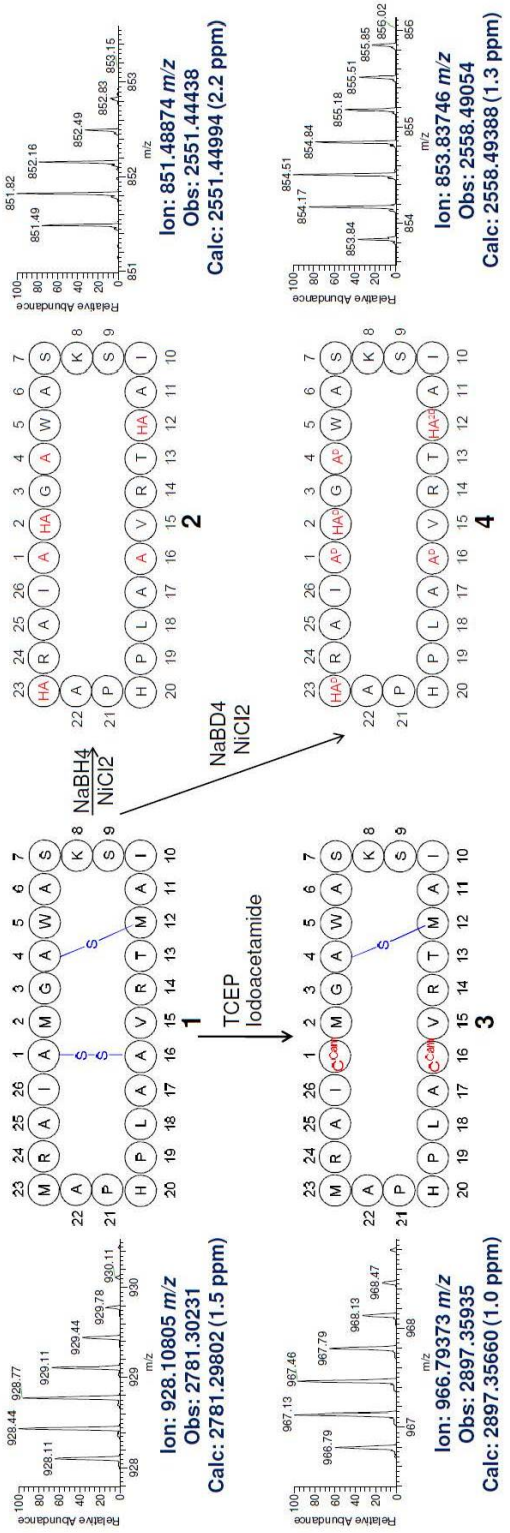

Supplementary Fig. 10. Chemical derivatization of SKF. TCEP reduction followed by iodoacetamide alkylation yielded a species with 116 Da addition (compound 2), corresponding to two carboxyamidomethylated cysteines (C^{Cam}) with the retaining of the thioether linkage. $NaBH_4$ and $NaBD_4$ reduction yielded dethiolated SKF derivatives with cysteine reduced to alanine, and methionine to homoalanine (HA) (compound 3,4). Deuteriums were labeled on the reductive cleavage positions under deuterated condition (compound 4). Zoom in MS1 spectrum of 3+ charge state species analyzed by FT-ICR MS as well as observed (Obs) and calculated (Calc) masses were showed beside each derivative.

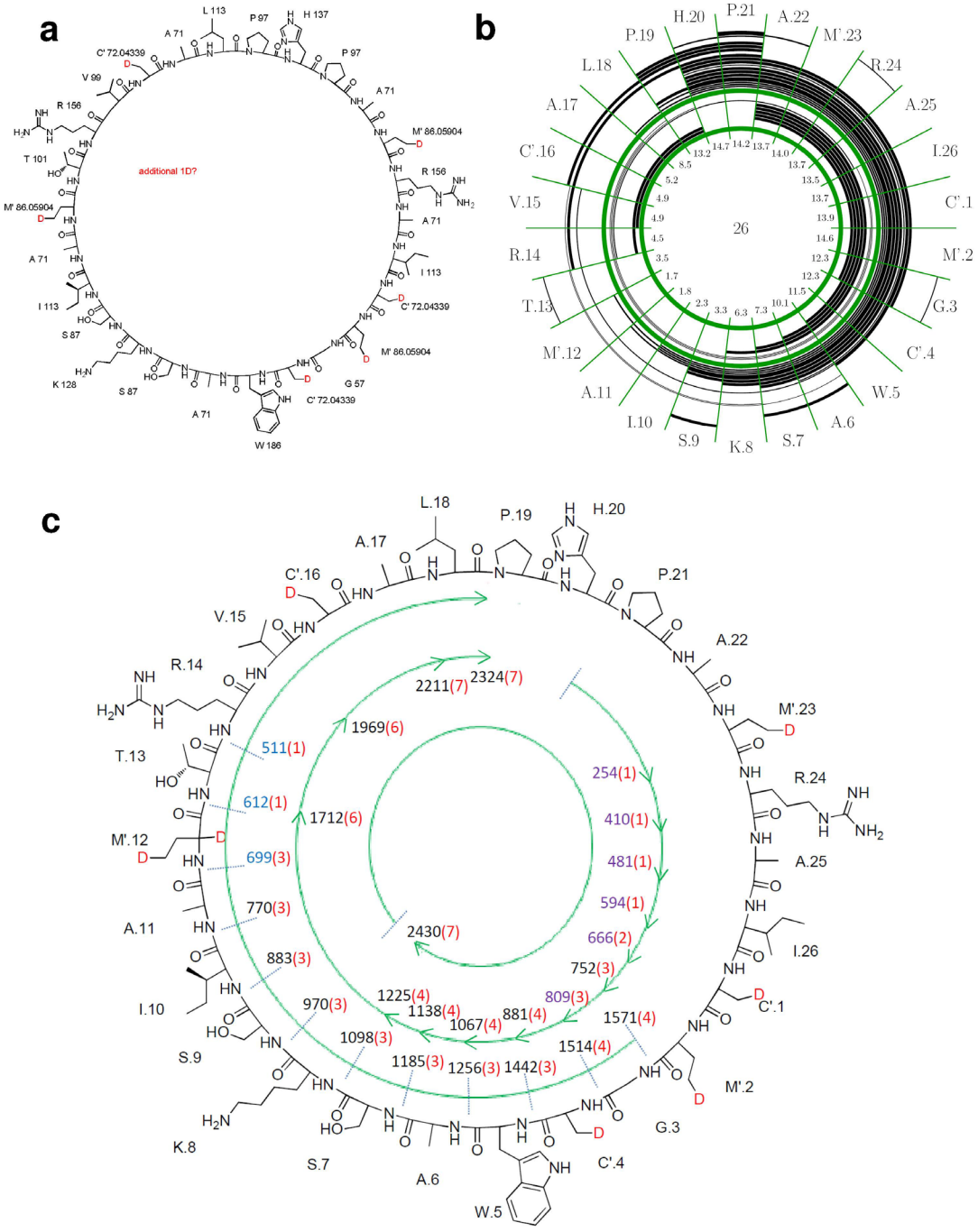
a
b
c
additional 1D?
26

Supplementary Fig. 11. Comparative dereplication of SKF. a) SKF template used for comparative dereplication. Under $NaBD_4/NiCl_2$ dethiolation reaction, seven deuteriums were obtained. Six deuteriums can be predicted to be introduced from the replacement of three methionine and three cysteine side chains (red color labeled), whereas the remaining deuterium is introduced at the site of the thioether linkage. This template and the dethiolated SKF MS/MS spectrum were subjected to NPR-dereplication algorithm to compute for correlation. The least correlated residue indicates the location of the extra deuterium which allows to infer the location of thioether linkage. **b)** Comparative dereplication suggested thioether linkage on Met^{12}. Each semicircle represents an annotated peak in the MS spectrum. Peaks with multiple annotations split their count equally among the repeats. Inner numbers are the count/score of the supporting peaks for the conservation of the given amino acid. Amino acid codes have an extra index number to disambiguate repeated amino acids by their position. $Methionine^{12}$ has the lowest score indicating it bears the extra deuterium. **c)** Summary of fragments observed by CID fragmentation of deuterated dethiolated SKF. Incorporated deuteriums were labeled on structure with D (in red). Each number labeled inner the chemical structure is the mass of observed fragment with semi-circle representing the sequence. Associated number in parenthesis represents the number of deuterium within certain fragment. Each residue was labeled with one letter amino acid code as well as corresponding masses showed outside the chemical structure. Ions observed in MS^2 were showed in black color. Further supporting ions observed from MS^3 spectrum of ion *m/z* 883 were shown in blue and ions observed from MS^3 spectrum of ion *m/z* 881 were shown in purple. The corresponding ion tables are showed in **Supplementary Tables 5** and **6.**

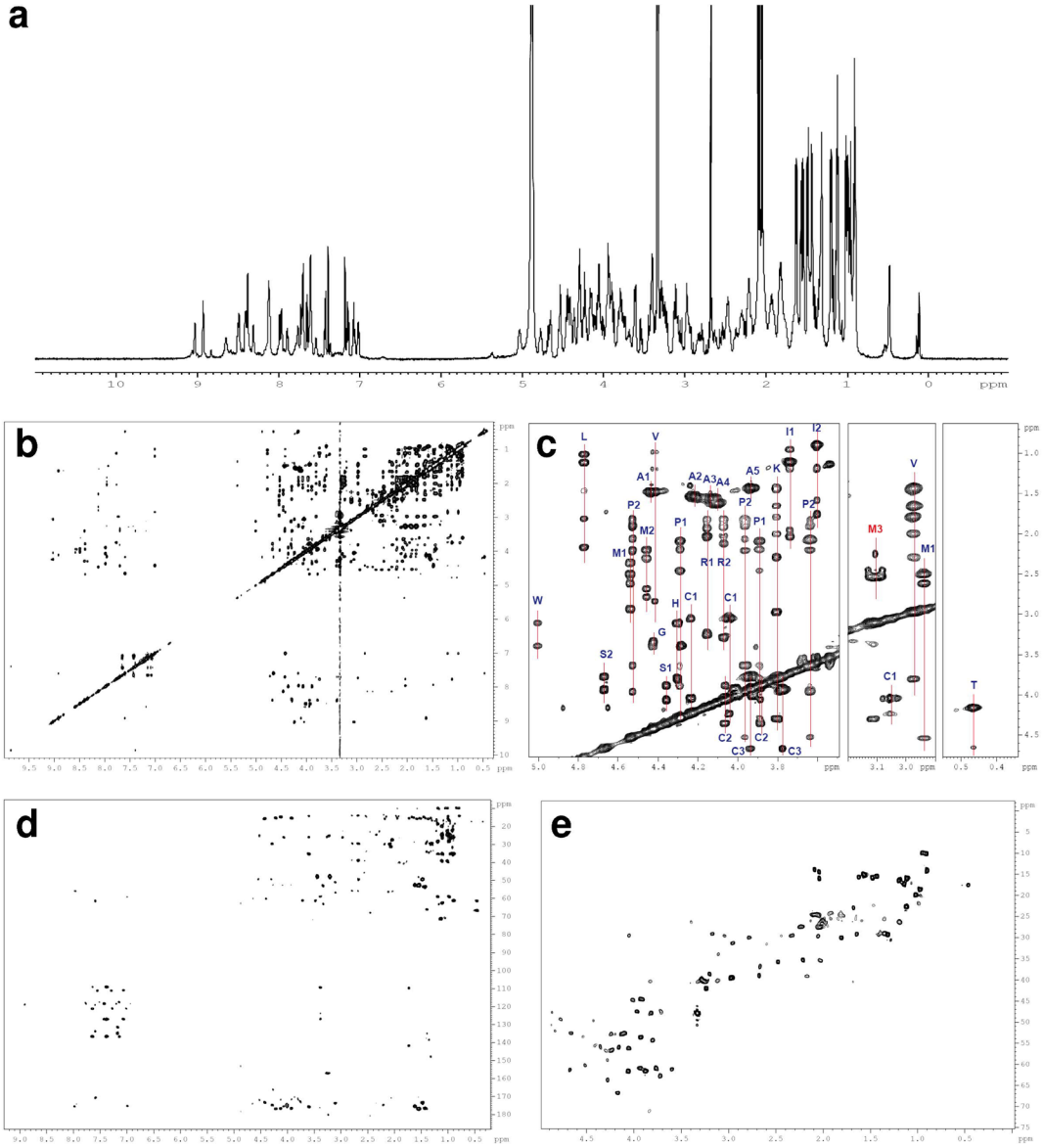

Supplementary Fig. 12. NMR spectra of SKF. a) ^{1}H NMR spectrum of SKF. The spectrum was observed in CD_3OD, 600 MHz. The detailed annotations were listed in **Supplementary Table 6**. **b, c**) ^{1}H-^{1}H TOCSY spectra and annotations of SKF. The spectrum was observed in CD_3OD, 600 MHz, with mixing time = 90 ms. subfigure b is a full spectrum whereas subfigure c is a zoom in spectrum as well as annotations. **d**) ^{1}H-^{13}C

HMBC spectrum of SKF. The spectrum was observed in CD_3OD, 600 MHz, with $^{2,3}J_{1H/13C}$ = 7 Hz. Full ^{1}H-^{13}C HMBC spectrum is shown. The annotations for critical signals supporting modified methionine are displayed in Fig 2e. **e**) ^{1}H-^{13}C HSQC spectrum of SKF. The spectrum was observed in CD_3OD, 600 MHz, with $^{1}J_{1H/13C}$ = 145 Hz. ^{1}H-^{13}C HSQC spectrum was collected to assist in HMBC spectrum annotation.

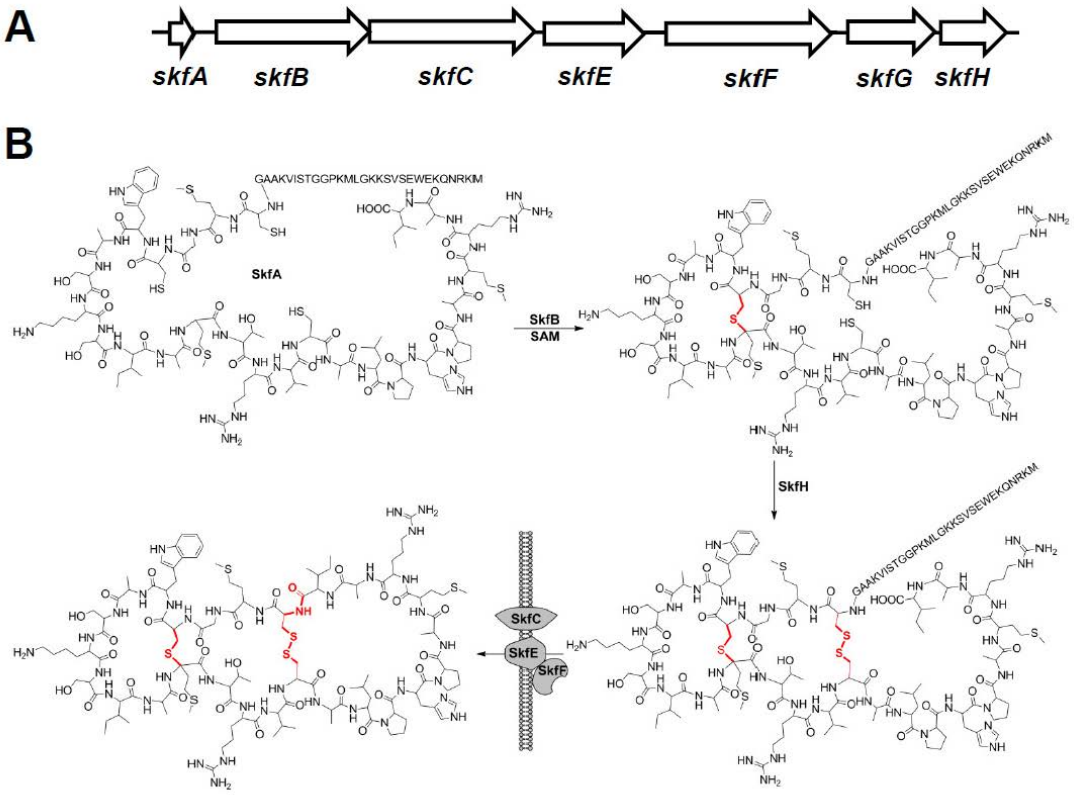

Supplementary Fig. 13. The functional annotation of the *skf* operon. (**a**) The *skf* operon. (**b**) The proposed biosynthetic pathway of SKF.

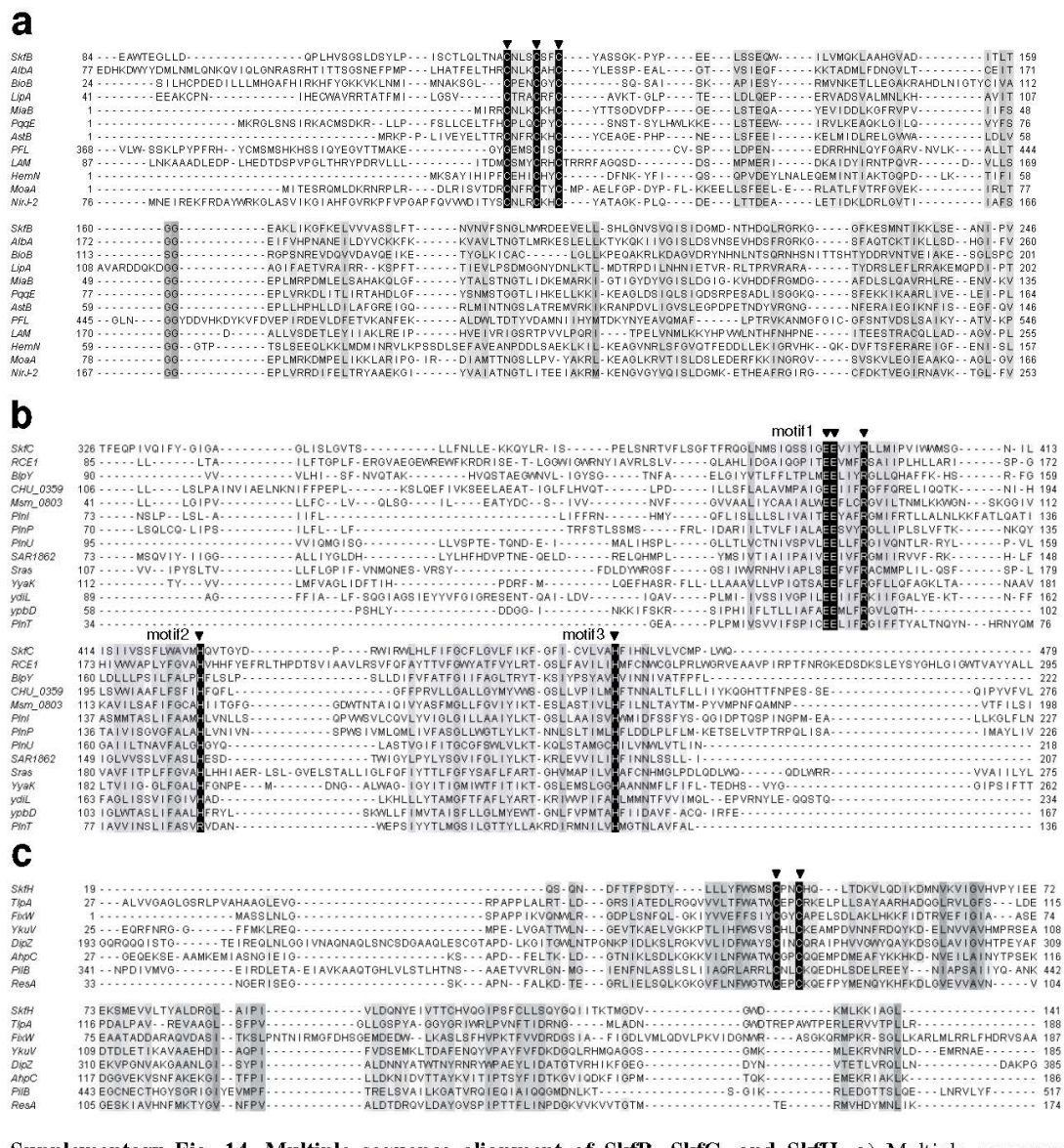

Supplementary Fig. 14. Multiple sequence alignment of SkfB, SkfC, and SkfH. a) Multiple sequence alignment of SkfB. SkfB belongs to radical SAM superfamily, along with some well-known proteins such as LAM, PFL, BioB, LipA. All members of this family show a conserved motif of CXXXCXXC (marked by ▼) which act to coordinate the iron in [4Fe-4S] cluster. **b**) Multiple sequence alignment of SkfC. Three conserved motifs are showed. The first motif contains two adjacent glutamic acid usually follows by a highly conserved

arginine spaced by three resides. The first Glu in motif1 as well as the two histidines are thought to involve in zinc binding whereas the second Glu is responsible for catalytic activity. **c**) Multiple sequence alignment of SkfH. SkfH homologs to thioredoxin showed a characteristic CXXC motif. Only the highly conserved regions are displayed due to the length variation of each protein. Alignment was done by kalign (22) using default settings. Only the highly conserved regions are displayed due to the length variation of each protein.

D. Supplementary Tables

Supplementary Table 1. Annotation of ion *m/z* 4312.6 intact cell MALDI TOF/TOF MS spectra.

Seq.	Ion	Calc. mass	Obs. Ion	Obs. Mass	Error (Da)	Seq.	Ion	Calc. mass	Obs. Ion	Obs. Mass	Error (Da)
C*	y42	4311.2111				**A**	y21	2228.1841	2229.0198	2228.0125	0.17
G	y41	4210.2176				**L**	y20	2157.1470	2158.7219	2157.7146	0.57
L	y40	4153.1961				**Q**	y19	2044.0629	2045.7079	2044.7006	0.64
Y	y39	4040.1121				**T**	y18	1916.0043	1916.7095	1915.7022	0.30
A	y38	3877.0487				**A**	y17	1814.9567	1815.6859	1814.6786	0.28
V	y37	3806.0116				**A**	y16	1743.9195	1745.5134	1744.5061	0.59
C*	y36	3706.9432				**A**	y15	1672.8824	1673.5553	1672.5480	0.33
V	y35	3603.9340	3605.5808	3604.5735	0.64	**V**	y14	1601.8453	1602.4382	1601.4309	0.41
A	y34	3504.8656	3506.2117	3505.2044	0.34	**T**	y13	1502.7769	1503.3473	1502.3400	0.44
A	y33	3433.8285	3435.6174	3434.6101	0.78	**T**	y12	1401.7292	1403.2509	1402.2436	0.51
G	y32	3362.7914	3365.7439	3364.7366	1.95	**A**	y11	1300.6816	1302.3075	1301.3002	0.62
Y	y31	3305.7699	3307.0168	3306.0095	0.24	**V**	y10	1229.6444	1231.4102	1230.4029	0.76
L	y30	3142.7066	3143.8500	3142.8427	0.14	**W**	y9	1130.5760	1131.1478	1130.1405	-0.44
Y	y29	3029.6226	3032.2168	3031.2095	1.59	**K**	y8	944.4967	946.0443	945.0370	0.54
V	y28	2866.5592	2867.4478	2866.4405	0.12	**V**	y7	816.4018			
V	y27	2767.4908	2768.2283	2767.2210	0.27	**Y**	y6	653.3384			
G	y26	2668.4224	2669.2111	2668.2038	0.22	**A**	y5	554.2700			
V	y25	2611.4009	2613.3098	2612.3025	0.90	**K**	y4	483.2329			
N	y24	2512.3325	2514.1226	2513.1153	0.78	**Y**	y3	355.1380			
A	y23	2398.2896	2399.9397	2398.9324	0.64	**S**	y2	192.0746			
V	y22	2327.2525	2328.8513	2327.8440	0.59	**S**	y1	105.0426			

Supplementary Table 2. Sytox Green cell permeability over time of SDP treatment.

Average Percent Permeabilized Cells[1] ±SD[2] (# of cells scored in each experiment)				
Timepoint	**3610[3]**	**ALB1035[3]**	**PY79**	**KP648**
30 min DMSO	1.9% (313)	0% (111)	0.6% (353)	0.3% (292)
60 min DMSO	1.1% (379)	0.7% (153)	0.8%±0.3% (186,313,318,260)	1.1%±0.1% (284,437)
90 min DMSO	2.7% (331)	0.3% (337)	0.5%±0.5% (247,320,326,435)	0.6%±0.4% (326,350)
120 min DMSO	0.3% (290)	0% (265)	0.5%±0.5 (166,329,365,321)	1.2%±1.6% (225,300)
30 min SDP	10.3% (339)	1.3% (156)	0.6% (174)	2.4% (252)
60 min SDP	4.7% (342)	7.5% (308)	4.2%±2.9% (224,250,313,215)	3.5%±1.5% (309,367)
90 min SDP	28.0% (336)	16.3% (1295)	7.5%±2.2% (271,375,290,304)	13.6%±15.1% (274,305)
120 min SDP	32.8% (344)	34.3% (507)	13.7%±1.5% (134,248,203,307)	19.8%±5.8% (301,255)

[1]The percentage of permeabilized cells for individual experiments were calculated and then averaged to generate the average percent permeabilized cells. Cell debris was not scored unless it clearly was derived from a single cell. Membrane spheres and tubules were not counted as cells.

[2]The standard deviation was calculated based on the percent permeabilized cells in repeated experiments

[3]Experiments on these strains were performed once, so no standard deviation is available

Supplementary Table 3. Membrane staining irregularities in strain 3610 after 120 minutes of SDP treatment.

Cell type	% cells (# scored)
Intact cells[1]	64% (314)
Irregular membrane	29% (140)
Clear gaps in membrane	7% (36)
Tubules	5% (27)[2]
Spheres	5% (26)[2]

[1]Includes permeabilized cells that had no obvious membrane deformation.

[2]Membrane tubules and spheres are subcellular particles, so the scoring indicates the frequency with which such structures were observed relative to the total number of cells scored.

Supplementary Table 4. Annotations of SDP FT MS/MS spectrum. Errors are in ppm.

Seq.	Ion	Calc. mass	Obs. ion	Obs. mass	Error	Ion	Calc. mass	Obs. ion	Obs. mass	Error
C*	b1	103.0092				y42	4311.2111			
G	b2	160.0307				y41	4210.2176			
L	b3	273.1147				y40	4153.1961			
Y	b4	436.1780				y39	4040.1121			
A	b5	507.2152				y38	3877.0487			
V	b6	606.2836				y37	3806.0116			
C*	b7	707.2771	708.2770	707.2697	10.42	y36	3706.9432			
V	b8	806.3455	807.3433	806.3360	11.76	y35	3603.9340	1802.9338	3603.8530	22.47
A	b9	877.3826	878.3798	877.3725	11.50	y34	3504.8656	1753.4027	3504.7908	21.34
A	b10	948.4197	949.4153	948.4080	12.34	y33	3433.8285	1717.8869	3433.7592	20.17
G	b11	1005.4412	1006.4351	1005.4278	13.29	y32	3362.7914	1682.3684	3362.7222	20.57
Y	b12	1168.5045	1169.4938	1168.4865	15.40	y31	3305.7699	1653.8592	3305.7038	20.00
L	b13	1281.5886	1282.5748	1281.5675	16.42	y30	3142.7066	1572.3325	3142.6504	17.87
Y	b14	1444.6519	1445.6347	1444.6274	16.95	y29	3029.6226	1515.7906	3029.5666	18.45
V	b15	1543.7203	1544.7019	1543.6946	16.64	y28	2866.5592			
V	b16	1642.7887	1643.7614	1642.7541	21.06	y27	2767.4908	1384.7287	2767.4428	17.33
G	b17	1699.8102	1700.7851	1699.7778	19.04	y26	2668.4224	1335.1968	2668.3790	16.25
V	b18	1798.8786	1799.8453	1798.8380	22.55	y25	2611.4009	1306.6889	2611.3632	14.44
N	b19	1912.9215	1913.8818	1912.8745	24.57	y24	2512.3325	1257.1545	2512.2944	15.16
A	b20	1983.9586				y23	2398.2896	1200.1330	2398.2514	15.91
V	b21	2083.0270				y22	2327.2525	1164.6165	2327.2184	14.63
A	b22	2154.0642				y21	2228.1841	1115.0821	2228.1496	15.46
L	b23	2267.1482				y20	2157.1470	1079.5659	2157.1172	13.78
Q	b24	2395.2068				y19	2044.0629	1023.0255	2044.0364	12.95
T	b25	2496.2545				y18	1916.0043	958.9989	1915.9832	11.01
A	b26	2567.2916				y17	1814.9567	1815.9249	1814.9176	21.50
A	b27	2638.3287				y16	1743.9195	1744.8932	1743.8859	19.28
A	b28	2709.3658				y15	1672.8824	1673.8595	1672.8522	18.06
V	b29	2808.4342				y14	1601.8453	1602.8207	1601.8134	19.91
T	b30	2909.4819				y13	1502.7769	1503.7552	1502.7479	19.29
T	b31	3010.5296				y12	1401.7292	1402.7101	1401.7028	18.84
A	b32	3081.5667				y11	1300.6816	1301.6685	1300.6612	15.63
V	b33	3180.6351				y10	1229.6444	1230.6321	1229.6248	15.96
W	b34	3366.7144				y9	1130.5760	1131.5661	1130.5588	15.22
K	b35	3494.8094				y8	944.4967	945.4916	944.4843	13.13
V	b36	3657.8727				y7	816.4018	817.3993	816.3920	11.93
Y	b37	3756.9411				y6	653.3384			
A	b38	3827.9782				y5	554.2700			
K	b39	3956.0732				y4	483.2329			
Y	b40	4119.1365				y3	355.1380			
S	b41	4206.1685				y2	192.0746			
S	b42	4293.2006				y1	105.0426			

Supplementary Table 5. Annotations of critical ions observed in deuterated dethiolated SKF MS/MS spectrum analyzed by FT-ICR MS.

Calc. Mass 1[a]	D number[b]	Calc. Mass 2[c]	Obs Mass	Error (ppm)	Annotation[d]
749.4547	3	752.4736	752.4733	-0.3	PAM'RAIC'M'
767.4654	3	770.4842	770.4802	-5.2	AM'TRVC'AL
877.5133	4	881.5384	881.5395	1.2	PAM'RAIC'M'GC'
880.5495	3	883.5683	883.5648	-3.9	IAM'TRVC'AL
967.5815	3	970.6003	970.6006	0.3	SIAM'TRVC'AL
1063.5926	4	1067.6177	1067.6171	-0.6	PAM'RAIC'M'GC'W
1095.6765	3	1098.6953	1098.6955	0.2	KSIAM'TRVC'AL
1134.6298	4	1138.6548	1138.6530	-1.6	PAM'RAIC'M'GC'WA
1182.7085	3	1185.7273	1185.7267	-0.5	SKSIAM'TRVC'AL
1221.6618	4	1225.6869	1225.6763	-8.6	PAM'RAIC'M'GC'WAS
1253.7456	3	1256.7644	1256.7656	1.0	ASKSIAM'TRVC'AL
1439.8249	3	1442.8438	1442.8402	-2.4	WASKSIAM'TRVC'AL
1510.8621	4	1514.8871	1514.8793	-5.2	C'WASKSIAM'TRVC'AL
1567.8835	4	1571.9086	1571.8966	-7.7	GC'WASKSIAM'TRVC'AL
1705.9627	6	1712.0004	1711.9916	-5.1	PAM'RAIC'M'GC'WASKSIAM'
1963.1115	6	1969.1492	1969.1343	-7.5	PAM'RAIC'M'GC'WASKSIAM'TR
2204.2542	7	2211.2981	2211.3032	2.3	PAM'RAIC'M'GC'WASKSIAM'TRVC'A
2317.3384	7	2324.3822	2324.3689	-5.7	PAM'RAIC'M'GC'WASKSIAM'TRVC'AL
2423.3550	7	2430.3989	2430.3984	-0.2	SIAM'TRVC'ALPHPAMRAIC'M'GC'WAS

a. Theoretical mass of fragment ions resulted from $NaBH_4$ reduction (dethiolated SKF).

b. D number represents for the number of deuterium labeled within certain fragments.

c. Theoretical mass of fragment ions resulted from $NaBD_4$ reduction (deuterated dethiolated SKF).

d. Residue C and M are marked due to the reason that these two residues are derivatized after reaction.

Supplementary Table 6. Annotations of critical ions observed in additional fragmentation (MS3) of deuterated dethiolated SKF analyzed by IT-MS.

Calc. Mass 1[a]	D number[b]	Calc. Mass 2[c]	Obs Mass	Error (Da)	Annotation[d]
510.33	1	511.33	511.26	-0.07	RVC'AL
611.38	1	612.38	612.35	-0.03	TRVC'AL
696.43	3	699.45	699.44	0.00	M'TRVC'AL
806.48	3	809.50	809.44	-0.05	PAM'RAIC'M'G
664.40	2	666.41	666.44	0.03	PAM'RAIC'
593.36	1	594.37	594.44	0.07	PAM'RAI
480.28	1	481.29	481.35	0.07	PAM'RA
409.24	1	410.25	410.35	0.10	PAM'R
253.14	1	254.15	253.99	-0.16	PAM'

a. Theoretical mass of fragment ions resulted from $NaBH_4$ reduction (dethiolated SKF).

b. D number represents for the number of deuterium labeled within certain fragments.

c. Theoretical mass of fragment ions resulted from $NaBD_4$ reduction (deuterated dethiolated SKF).

d. Residue C and M are marked due to the reason that these two residues are derivatized after reaction.

Supplementary Table 7. ^{1}H NMR data of SKF.

	NH	α	β	γ	others
A1	7.93	4.43	1.48		
A2	7.98	4.22	1.54		
A3	8.11	4.13	1.56		
A4	8.91	4.1	1.62		
A5	8.40	3.93	1.43		
C1	9.02	4.23	3.05, 4.04		
C2	7.98	4.35	3.88, 4.06		
C3	8.38	4.67	3.78, 3.93		
G	8.39	3.39, 4.28			
H	8.03	5.00	3.10, 3.40		8.58 (NH), 7.18
I1	7.60	3.74	2.04	1.11 (CH_3), 1.19, 1.96	1.01 (δ)
I2	8.47	3.6	1.76	0.89 (CH_3), 1.19, 1.59	0.91 (δ)
K	7.73	4.28	2.29	1.79, 1.99	1.43 (δ), 1.65 (δ), 2.97 (ε)
L	7.60	4.77	1.46, 2.17	1.81	1.01 (δ), 1.12 (δ)
M1	7.52	4.54	2.36, 2.51	2.62, 2.94	2.09 (SCH_3)
M2	8.13	4.46	2.20, 2.31	2.69, 2.79	2.07 (SCH_3)
M3	ND	-	2.25, 2.46	2.54, 3.10	2.04 (SCH_3)
P1	-	4.29	2.09, 2.46	2.09, 2.19	3.65 (δ), 3.90 (δ)
P2	-	4.53	1.91, 2.21	1.81, 2.07	3.64 (δ), 3.97 (δ)
R1	7.96	4.15	2.03	1.83, 1.94	7.44 (NH), 3.25 (δ)
R2	7.98	4.07	2.10	1.82, 1.92	7.53 (NH), 3.28 (δ)
S1	7.99	4.36	3.88, 4.07		
S2	8.38	4.67	3.77, 3.93		
T	7.59	4.65	4.16	0.47	
V	7.77	4.42	2.84	0.98, 1.20	
W	8.34	4.30	3.11, 3.80		9.85 (NH), 7.39 (s), 7.66 (d), 7.07 (t), 7.15 (t), 7.43 (d)

D. References

S1. Gonzalez-Pastor JE, Hobbs EC, Losick R (2003) Cannibalism by sporulating bacteria. *Science* 301:510–513.

S2. Ngoka LCM, Gross ML (1999) Multistep tandem mass spectrometry for sequencing cyclic peptides in an ion-trap mass spectrometer. *J Am Soc Mass Spectrom* 10:732–746.

S3. Kawulka KE, et al. (2004) Structure of subtilosin A, a cyclic antimicrobial peptide from *Bacillus subtilis* with unusual sulfur to alpha-carbon crosslinks: Formation and reduction of alpha-thio-alpha-amino acid derivatives. *Biochemistry* 43:3385–3395.

S4. Ng J, et al. (2009) Dereplication and *de novo* sequencing of nonribosomal peptides. *Nat Methods* 6:596–599.

S5. Oman TJ, van der Donk WA (2010) Follow the leader: the use of leader peptides to guide natural product biosynthesis. *Nat Chem Biol* 6:9–18.

S6. Miller JR, et al. (2000) *Escherichia coli* LipA is a lipoyl synthase: *In Vitro* biosynthesis of lipoylated pyruvate dehydrogenase complex from octanoyl-acyl carrier protein. *Biochemistry* 39:15166–15178.

S7. Sofia HJ, Chen G, Hetzler BG, Reyes-Spindola JF, Miller NE (2001) Radical SAM, a novel protein superfamily linking unresolved steps in familiar biosynthetic pathways with radical mechanisms: functional characterization using new analysis and information visualization methods. *Nucl Acids Res* 29:1097–1106.

S8. Berkovitch F, Nicolet Y, Wan JT, Jarrett JT, Drennan CL (2004) Crystal structure of biotin synthase, an S-adenosylmethionine-dependent radical enzyme. *Science* 303:76–79.

S9. McIntosh JA, Donia MS, Schmidt EW (2009) Ribosomal peptide natural products: bridging the ribosomal and nonribosomal worlds. *Nat Prod Rep* 26:537–559.

S10. Pei J, Grishin NV (2001) Type II CAAX prenyl endopeptidases belong to a novel superfamily of putative membrane-bound metalloproteases. *Trends Biochem Sci* 26:275–277.

S11. Dorenbos R, et al. (2002) Thiol-disulfide oxidoreductases are essential for the production of the lantibiotic sublancin 168. *J Biol Chem* 277:16682–16688.

S12. Branda SS, Gonzalez-Pastor JE, Ben-Yehuda S, Losick R, Kolter R (2001) Fruiting body formation by *Bacillus subtilis*. *Proc Natl Acad Sci* USA 98:11621–11626.

S13. Youngman P, Perkins JB, Losick R (1984) Construction of a cloning site near one end of Tn917 into which foreign DNA may be inserted without affecting transposition in Bacillus subtilis or expression of the transposon-borne erm gene. *Plasmid* 12:1–9.

S14. Pogliano J, Sharp M, Pogliano K (2002) Chromosome partitioning during establishment of cellular asymmetry in *Bacillus subtilis*. *J Bact* 184:1743–1749.

S15. Ireton K, Rudner DZ, Siranosian KJ, Grossman AD (1993) Integration of multiple developmental signals in Bacillus subtilis through the Spo0A transcription factor. *Genes Dev* 7:283–294.

S16. Ellermeier CD, Hobbs EC, Gonzalez-Pastor JE, Losick RA (2006) Three-Protein Signaling Pathway Governing Immunity to a Bacterial Cannibalism Toxin. *Cell* 124:549–559.

S17. Yang YL, Xu Y, Straight P, Dorrestein PC (2009) Translating metabolic exchange with imaging mass spectrometry. *Nat Chem Biol* 5:885–887.

S18. Puolitaival SM, Burnum KE, Cornett DS, Caprioli RM (2008) Solvent-free matrix dry-coating for MALDI imaging of phospholipids. *J Am Soc Mass Spectrom* 19:882–886.

S19. Becker EC, Pogliano K (2007) Cell-specific SpoIIIE assembly and DNA translocation polarity are dictated by chromosome orientation. *Mol Microbiol* 66:1066–1079.

S20. Leenders F, Stein TH, Kablitz B, Franke P, Vater J (1999) Rapid Typing of Bacillus subtilis Strains by their Secondary Metabolites Using Matrix-Assisted Laser Desorption/Ionization Mass Spectrometry of Intact Cells *Rapid Commun Mass Spectrom* 13:943–949.

S21. Erhard M, von Döhren H, Jungblut P (1997) Rapid typing and elucidation of new secondary metabolites of intact cyanobacteria using MALDI-TOF mass spectrometry. *Nat Biotechnol* 15:906–909.

S22. Lassmann T, Sonnhammer ELL (2006) Kalign, Kalignvu and Mumsa: web servers for multiple sequence alignment. *Nucl Acids Res* 34:596–599.

Chapter 2, in full, is a reprint of the material as it appears in *Proceedings of the National Academy of Sciences* 2010 (Vol.107(37) pp. 16286-16290). I was a secondary author and developed the microculture techniques required for the fluorescence microscopy and performed the experiments for the cell biology work displayed in Figures 3, 4, and 5B.

Chapter 3

The *Bacillus subtilis* cannibalism toxin SDP collapses the proton motive force and induces autolysis

Molecular Microbiology (2012) 84(3), 486–500 ■

doi:10.1111/j.1365-2958.2012.08038.x
First published online 2 April 2012

The *Bacillus subtilis* cannibalism toxin SDP collapses the proton motive force and induces autolysis

Anne Lamsa,[1] Wei-Ting Liu,[2] Pieter C. Dorrestein[2,3,4] and Kit Pogliano[1]*

[1]*Division of Biological Sciences,* [2]*Department of Chemistry and Biochemistry,* [3]*Skaggs School of Pharmacy and Pharmaceutical Sciences and* [4]*Center for Marine Biotechnology and Biomedicine, University of California, San Diego, La Jolla, CA 92093, USA.*

Summary

Bacillus subtilis **SDP is a peptide toxin that kills cells outside the biofilm to support continued growth. We show that purified SDP acts like endogenously produced SDP; it delays sporulation, and the SdpI immunity protein confers SDP resistance. SDP kills a variety of Gram-positive bacteria in the phylum Firmicutes, as well as *Escherichia coli* with a compromised outer membrane, suggesting it participates in defence of the *B. subtilis* biofilm against Gram-positive bacteria as well as cannibalism. Fluorescence microscopy reveals that the effect of SDP on cells differs from that of nisin, nigericin, valinomycin and vancomycin-KCl, but resembles that of CCCP, DNP and azide. Indeed, SDP rapidly collapses the PMF as measured by fluorometry and flow cytometry, which triggers the slower process of autolysis. This secondary consequence of SDP treatment is not required for cell death since the autolysin-defective *lytC, lytD*, *lytE*, *lytF* strain fails to be lysed but is nevertheless killed by SDP. Collapsing the PMF is an ideal mechanism for a toxin involved in cannibalism and biofilm defence, since this would incapacitate neighbouring cells by inhibiting motility and secretion of proteins and toxins. It would also induce autolysis in many Gram-positive species, thereby releasing nutrients that promote biofilm growth.**

Introduction

Bacterial species must compete with a multitude of other species in the environment for both space and nutrients. Due to the diversity and density of microbes present in the environment, competition is constant as each species attempts to find and maintain a niche. In the environment, many bacteria exist primarily in biofilms, communities of cells held together by exopolysaccharides, proteins and other substances (Hibbing *et al.*, 2010; Abee *et al.*, 2011). Biofilms enable bacteria to claim territories by excluding competitors, by adhering to surfaces and they confer increased resistance to a variety of environmental stresses, including antibacterial compounds. Differentiation of cells within the biofilm can allow a great variety of niches to be simultaneously occupied, by one species or by a mixed population (Haussler, 2010; Hibbing *et al.*, 2010; Lopez *et al.*, 2010). Thus, biofilms provide a ubiquitous means for bacteria to compete and cooperate with other species, and to form spatially organized and functionally differentiated communities to maximally exploit the environment.

A commonly implemented competition mechanism is the production of secreted metabolites that have diverse effects on intra- and inter-species interactions. This includes modulating development, promoting biofilm dispersal, killing competitors or inhibiting toxin production in a competitor (Straight and Kolter, 2009; Yang *et al.*, 2009; Hibbing *et al.*, 2010; Gonzalez *et al.*, 2011). These secreted metabolites can also stimulate growth by facilitating acquisition of iron and other metals or by facilitating extracellular electron transfer to insoluble electron acceptors for respiratory growth (D'Onofrio *et al.*, 2010; Skaar, 2010; Bird *et al.*, 2011). *Bacillus subtilis* secretes many secondary metabolites, including subtilosin, surfactin, plipistatin and bacillaene (Babasaki *et al.*, 1985; Stein, 2005; Shelburne *et al.*, 2007; Asaduzzaman and Sonomoto, 2009), some of which play dual functions as antimicrobial compounds and signalling molecules. For example, the lipopeptides surfactin and plipistatin have antimicrobial properties (Vanittanakom *et al.*, 1986; Carrillo *et al.*, 2003; Gonzalez *et al.*, 2011) and together repress the production of toxin molecules by *Staphylococcus aureus* (Gonzalez *et al.*, 2011). Surfactin also mediates various behaviours, such as *B. subtilis* swarming motility (Kearns and Losick, 2003) and biofilm formation (Lopez *et al.*, 2009a), and the inhibition of aerial hyphae formation in *Streptomyces coelicolor* (Straight *et al.*, 2006; Yang *et al.*, 2009). Similarly, the polyketide bacillaene both inhibits bacterial translation (Patel *et al.*, 1995) and inhibits production of prodiginine

Accepted 9 March, 2012. *For correspondence. E-mail kpogliano@ucsd.edu; Tel. (+1) 858 822 1314; Fax (+1) 858 822 5740.

and several other molecules in *S. coelicolor* (Yang *et al.*, 2009). Thus, secreted metabolites are critical for mediating the outcome of inter-species interactions due to both their antibacterial effects and their signalling roles.

The *B. subtilis* biofilm also secretes antimicrobial products that mediate cannibalism by killing non-biofilm forming siblings (Gonzalez-Pastor *et al.*, 2003). These cannibal cells lyse genetically identical siblings and susceptible neighbours of other species (Nandy *et al.*, 2007; Liu *et al.*, 2010) to release nutrients that allow continued growth (Gonzalez-Pastor *et al.*, 2003; Lopez *et al.*, 2009b). This delays the initiation of sporulation, a starvation-induced developmental process that produces dormant spores. Sporulation is a lengthy committed pathway (Parker *et al.*, 1996; Dworkin and Losick, 2005), so if nutrients become available, sporulating cells are at a competitive disadvantage as they cannot resume growth until sporulation is complete. Therefore, using cannibalistic toxins to lyse susceptible neighbours would provide an advantageous mechanism to delay sporulation until absolutely necessary (Gonzalez-Pastor *et al.*, 2003). Cannibalism might also serve to eliminate cheater cells not directly contributing to biofilm development (Smukalla *et al.*, 2008; Mitri *et al.*, 2011) and to eliminate differentiated cell types that are no longer beneficial to the population, thereby allowing the biofilm to use the nutrients from these cells to produce new beneficial cell types. Thus, secreted metabolites may be used to sculpt a differentiated bacterial biofilm by removing and replacing unnecessary cell types, thereby allowing the biofilm to adapt even during starvation.

Critical to understanding the role of secreted metabolites in microbial populations is elucidating the mechanism by which these molecules affect bacterial cells. Secreted metabolites that inhibit bacterial growth do so by inhibiting a variety of essential cellular pathways, from transcription to cell wall biosynthesis. Furthermore, at the sublethal concentrations that one might expect to predominate early in an interaction, different compounds have distinct effects on gene expression and behaviour (Nalca *et al.*, 2006; Rogers *et al.*, 2007; Romero *et al.*, 2011). Teasing apart the role of these molecules in microbial population dynamics will therefore require understanding the effects they have on cells at both lethal and sublethal concentrations.

We here describe studies on the mechanism of action of the SDP cannibalistic toxin, which we previously demonstrated to cause lysis of *B. subtilis*, *S. aureus* and *S. epidermidis* (Liu *et al.*, 2010). The mature SDP toxin is a 42-amino-acid peptide with a single disulphide bond (Liu *et al.*, 2010) that is produced by processing and secretion of the product of the *sdpC* gene. We here demonstrate that purified SDP acts in a manner consistent with that of endogenously produced SDP, as it delays sporulation (Gonzalez-Pastor *et al.*, 2003) and resistance to purified SDP is mediated by SdpI (Ellermeier *et al.*, 2006). We further demonstrate that SDP rapidly collapses the proton motive force (PMF) of *B. subtilis*, as well as the *lptD4213 Escherichia coli* mutant that has a compromised outer membrane. This subsequently induces the dramatic autolysin mediated lysis that is a secondary consequence of SDP treatment in autolysis susceptible Gram-positive species, such as *B. subtilis*, *S. aureus* and *S. epidermidis* (Tipper, 1969; Jolliffe *et al.*, 1981; Sieradzki *et al.*, 1998). Collapsing the PMF is an ideal mechanism of action for a cannibalistic and defensive toxin, as it would rapidly eliminate the ability of neighbouring species and non-biofilm producing *B. subtilis* cells (which do not produce SdpI) to respond by moving away, while autolysis would release nutrients that can be readily used to promote biofilm growth.

Results

Purified and endogenously produced SDP have the same biological effects

Prior to investigating the mechanism by which purified SDP kills cells, we first verified that purified SDP affected *Bacillus subtilis* cells by a mechanism relevant to *in vivo* studies that used endogenously produced or inducible SDP (Gonzalez-Pastor *et al.*, 2003; Butcher and Helmann, 2006; Ellermeier *et al.*, 2006). SDP was originally identified as delaying the onset of sporulation (Gonzalez-Pastor *et al.*, 2003), so we first tested if treatment with purified SDP delayed sporulation. To do so, we used the undomesticated strain 3610 because PY79 did not sporulate in the small scale culture conditions used to document the cell biological effects of purified SDP (Liu *et al.*, 2010). Briefly, in this method, cells are grown in LB to mid-log phase, then concentrated 10-fold in the same medium and 15 μl aliquots transferred to microfuge tubes for further incubation with or without SDP. Under these conditions, 3610 showed significant levels of sporulation by 5 h (Fig. 1A and B), when asymmetrically positioned sporulation septa at various stages of engulfment were visible in 36% of DMSO-treated cells. SDP treatment reduced the frequency of sporulation to 1%. Thus, SDP treatment dramatically reduces the frequency of sporulation, in keeping with previous publications (Gonzalez-Pastor *et al.*, 2003; Lopez *et al.*, 2009b).

Next, we tested if previously identified SDP-resistance mechanisms also provided resistance against purified SDP. The primary SDP resistance mechanism is SdpI, a membrane protein that is induced in response to SDP and conveys resistance to high levels of SDP (Ellermeier *et al.*, 2006). A secondary resistance mechanism, which functions in the absence of SdpI, is mediated through the extracytoplasmic function (ECF) sigma factor σ^W (Butcher & Helmann, 2006 and Fig. S1), and this requires two

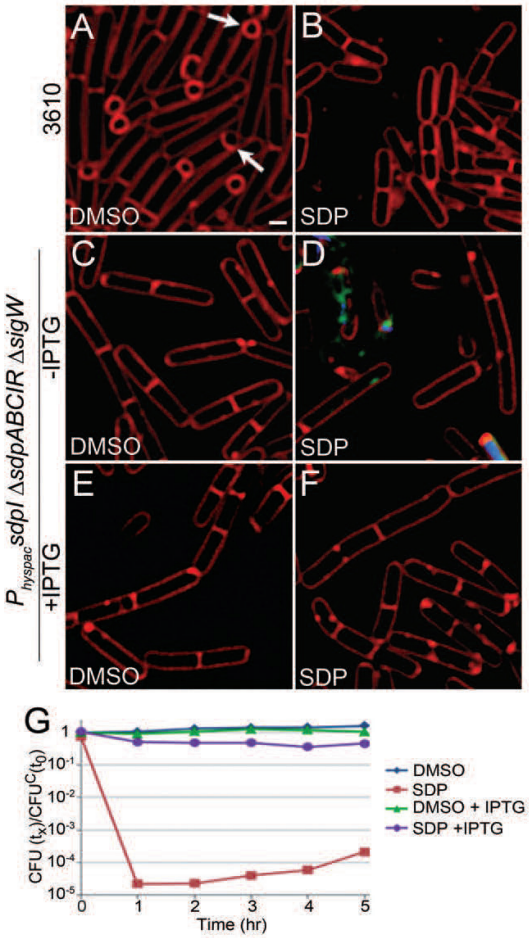

Fig. 1. Purified SDP acts in a manner similar to endogenously produced SDP.
A and B. Purified SDP delays sporulation. Strain 3610 was grown for 5 h after treatment with DMSO (A) or 20 μg ml^{-1} SDP (B), which is 2–5× above the MIC (Supporting Information). Membranes were stained with FM 4–64 (red) before fluorescence microscopy. Arrows indicate cells with sporulation septa at various stages of engulfment. Scale bar represents 1 μm.
C–F. SdpI is sufficient for protection against purified SDP. *P*$_{hyspac}$*sdpIΔsdpABCIRΔsigW* (TPM758) cells were treated for 3 h with 0.5% DMSO (C and E) or 20 μg ml^{-1} SDP (D and F) either without (C and D) or with (E and F) induction of *sdpI* with 1 mM IPTG. Cells were stained with FM 4–64 (red), and two DNA stains, DAPI (blue) and SYTOX Green (green). SYTOX Green is membrane impermeable and only stains permeabilized cells.
G. Effect of SdpI production on viability of *P*$_{hyspac}$*sdpI ΔsdpABCIR ΔsigW* (TPM758) cells treated with SDP ($n = 2$). Viability is shown as the ratio of colony-forming units (cfu) at the indicated time and treatment to the cfu at t_0 for the DMSO control (cfu^C).

potential SDP resistance systems, *yknW-Z*, an ABC transporter, and *yhfL*, an SdpI paralogue (Butcher and Helmann, 2006). Thus, if purified SDP kills cells by the same mechanism as endogenously produced SDP, overexpression of SdpI should be sufficient for high level SDP resistance even in the absence of the backup systems induced by σ^W. We used fluorescence microscopy to test this prediction. To do so, we employed a *ΔsdpABCIR ΔsigW* strain lacking the normal resistance mechanisms that also had *sdpI* under the control of the IPTG inducible promoter *P*$_{hyspac}$ (TPM758). In the absence of IPTG, and hence SdpI, SDP treatment caused significant lysis by 3 h (Fig. 1D), and viable cell counts showed that viability dropped nearly 5 logs in 1 h (Fig. 1G, red). However, when *sdpI* was induced with IPTG, we failed to observe lysis (Fig. 1F) or any loss of viability (Fig. 1G, purple). These results demonstrate that SdpI is sufficient for protection against purified SDP, as expected based on previous results with endogenously produced SDP (Butcher and Helmann, 2006; Ellermeier *et al.*, 2006).

SDP affects both Gram-positive and Gram-negative bacteria

We next explored the ability of SDP to kill additional Gram-positive bacteria, to extend previous studies showing that it kills *Listeria monocytogenes* (Palmer *et al.*, 2009) *S. aureus* and *S. epidermidis* (Liu *et al.*, 2010). We chose five species from the phylum Firmicutes and one from the phylum Actinobacteria. Of the species tested, only the Actinobacterium *Micrococcus luteus* was resistant to SDP (Fig. 2A, red) at the concentration tested. All of the Firmicutes species tested were sensitive to SDP, with *B. megaterium* showing the most sensitivity, as it was no longer viable at the initial time point (Fig. 2A, purple). *S. epidermidis* was the least sensitive to SDP, but still showed a 2.5 log drop in viability by 5 h (Fig. 2A, green). This experiment demonstrates that SDP is active against a wide variety of Gram-positive bacteria within the phylum Firmicutes.

Our previous studies failed to show any effect of SDP on the Gram-negative species tested (Liu *et al.*, 2010), suggesting that either the outer membrane of Gram-negative bacteria provides a barrier to entry of SDP or that SDP has a Gram-positive specific target. To test these hypotheses, we took advantage of an *E. coli* strain that has a defect in the *lptD* gene that encodes a protein required for outer membrane biogenesis. This mutation permeabilizes the outer membrane and renders *E. coli* sensitive to drugs such as vancomycin and nisin that normally target only Gram-positive bacteria (Sampson *et al.*, 1989; Braun and Silhavy, 2002; Wu *et al.*, 2006). Fluorescence microscopy and viable cell counts demonstrated that wild-type *E. coli* (MC4100) is unaffected by SDP treatment, and that by 3 h of treatment the cells had the small cell morphology characteristic of stationary phase cells (Fig. 2B). However, upon SDP treatment, the *lptD* (NR698) cells stopped dividing, became slightly wider and longer than untreated cells and were hyper-permeabilized to DAPI (Fig. 2C). Cell

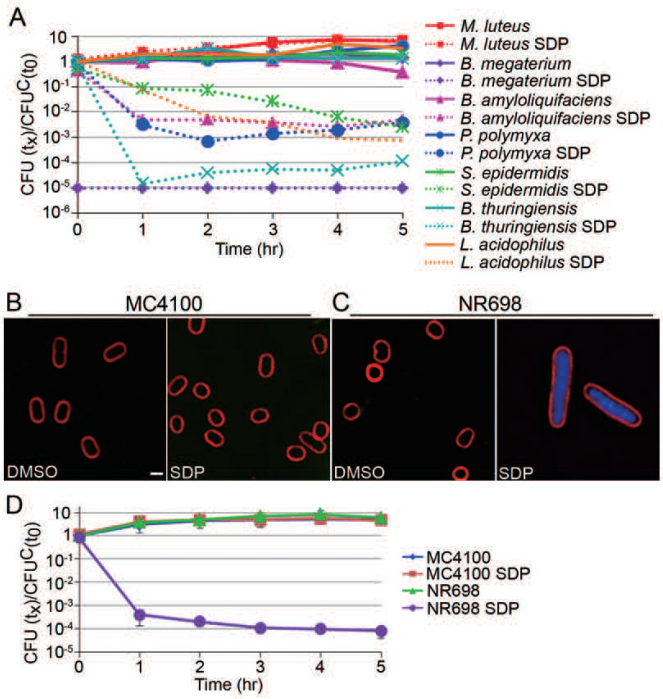

Fig. 2. Effects of SDP on Gram-positive species and *E. coli*.
A. Effect of 20 μg ml^{-1} SDP on viability of a variety of Gram-positive species ($n = 2$), calculated as in Fig. 1G. We were unable determine if *M. luteus* was sensitive to higher concentrations of SDP due to our limited supply.
B. Fluorescence micrograph of *E. coli* wt (MC4100) treated with 0.5% DMSO or 20 μg ml^{-1} SDP for 5 h and stained with FM 4–64 (red) and DAPI (blue). Scale bar represents 1 μm.
C. Fluorescence micrograph of *lptD4213* (NR698) cells treated with 0.5% DMSO or 20 μg ml^{-1} SDP for 5 h. SDP treatment produces cells that are hyper-permeabilized to DAPI and that fail to enter stationary phase and therefore remain elongated.
D. Effect of SDP on *E. coli* wt (MC4100) and *lptD4213* (NR698, *lptD4213*) viability, calculated as in Fig. 1G. Error bars show the standard error of ≥ 3 experiments.

viability also dropped almost 4 orders of magnitude (Fig. 2D, purple). Therefore, SDP recognizes a target that is broadly distributed in bacteria, but is unable to penetrate the outer membrane of Gram-negative species.

Comparison of the cytological effects of SDP and other membrane active compounds

SDP induces dramatic lysis of *B. subtilis* cells that is characterized by the extrusion of membrane vesicles and tubules after 1–2 h of treatment (Liu *et al.*, 2010). We used fluorescence microscopy to investigate this characteristic lysis phenotype by comparing the cell biological effects of SDP to antibiotics with known mechanisms of action. We focused on antibacterial compounds that target the cell wall, the cytoplasmic membrane and cellular energy production (vancomycin, nisin, CCCP, DNP, azide; Fig. 3A–H). Three compounds, the energy poisons CCCP, DNP and sodium azide, showed SDP-like phenotypes and a similar rate and extent of viability loss. These compounds killed cells within 1–2 h (Fig. 3K), although SDP-treated cells showed increasing numbers of viable cells over time. This is likely because at the onset of treatment, a few cells in the culture express SdpI, and this SDP-resistant population survives and resumes growth. Fluorescence microscopy revealed that after 2 h of treatment with SDP, CCCP, DNP and sodium azide, some cells showed large gaps in the cytoplasmic membrane, extracellular membrane vesicles of variable size, permeability to SYTOX Green, increased permeability to DAPI and diffuse chromosomal DNA (Fig. 3B–E).

The channel forming toxin nisin also caused cell lysis, as evidenced by cells with gaps in the cytoplasmic membrane and increased permeability. However, unlike the other compounds nisin uniformly hyper-permeabilized the cells to DAPI and SYTOX Green (Fig. 3H), likely because of the large, non-specific channels it forms in the cytoplasmic membrane (Lubelski *et al.*, 2008; these changes in permeability are discussed and quantified below). The membranes of nisin-treated cells showed highly uneven staining and no external vesicles were observed (Fig. 3H). The cell wall-active drug vancomycin caused the cells to accumulate extra membrane material in a few locations along the lateral cell wall (Fig. 3G), perhaps because vancomycin titrates peptidoglycan precursors and slows peptidoglycan synthesis without slowing membrane biogenesis (Molenkamp and Veerkamp, 1976). Thus, compounds with different mechanisms of action have different effects on bacterial cell architecture. SDP produces a cytological profile similar to CCCP, DNP and azide suggesting that it depletes cellular energy stores (the PMF and/or ATP).

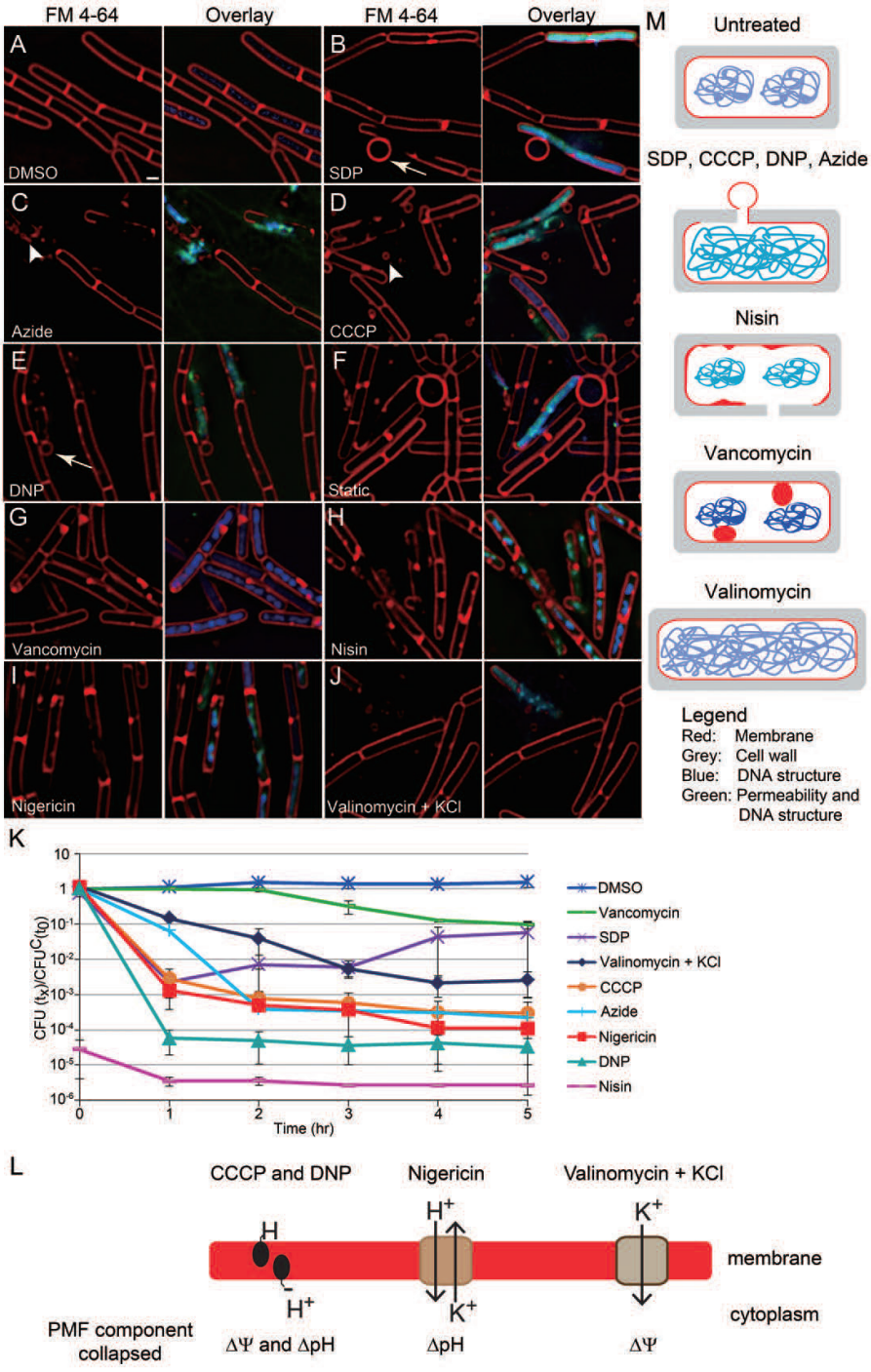

Fig. 3. Effects of antibacterial compounds on *B. subtilis* cell architecture.
A–J. Fluorescence micrographs of growing cells of PY79 treated with (A) 0.5% DMSO, (B) 20 μg ml^{-1} SDP, (C) 10 mM sodium azide, (D) 100 μM CCCP, (E) 2 mM DNP, (G) 250 μg ml^{-1} vancomycin, (H) 10 μg ml^{-1} nisin, (I) 62.5 μM nigericin, (J) 125 μM valinomycin with 200 mM KCl (F) incubated statically, for 2 h (A–F, I–J), 1 h (H) or 3 h (G). Cells are stained with FM 4–64 (red), DAPI (blue) and SYTOX Green (green), as in Fig. 1. Arrowheads indicate small membrane vesicles and debris. Arrows indicate large vesicles. Scale bar represents 1 μm.
K. Effects of treatments on PY79 viability, calculated as in Fig. 2. Error bars show the standard error of ≥ 3 experiments.
L. Cartoon demonstrating the mechanism of PMF component collapse for CCCP, DNP, nigericin and valinomycin + KCl.
M. Cartoon showing representations of the cytological profiles (A–E, G–H, J).

SDP rapidly collapses the PMF

Many antimicrobial peptides collapse the PMF by forming channels in the cytoplasmic membrane (Peters *et al.*, 2010; Wilmes *et al.*, 2011; Nan *et al.*, 2011b). We therefore hypothesized that this was more likely to be the primary mechanism of action for SDP. Prior to determining if SDP collapses the PMF, we tested how rapidly it affected cell viability and growth. Short-term viable cell counts showed that SDP-treated cells showed a several log drop in viability by 10 min (Fig. 4D), although lysis was not observed until > 60 min. Time-lapse fluorescence microscopy demonstrated that cells treated with SDP for 20 min failed to divide, with lysis starting ~ 60 min after treatment (Fig. S2). Thus, SDP is fast acting and its effects are irreversible within 10 min (Fig. 4D).

We used two complimentary assays to determine if SDP collapses the PMF, fluorometry and flow cytometry. First, to measure the effect of SDP on *B. subtilis*, we used a fluorometry assay that allows the effects of compounds on the PMF to be followed over time, starting as soon as it is possible to load the sample after treatment, about 30 s with the small sample volume used here (which precluded adding SDP during the experiment). This assay measures the average effects on all the cells in the population. This assay uses $DiSC_3(5)$, a dye that enters polarized cells, is quenched, and is released when the cells depolarize, leading to increased fluorescence (Sims *et al.*, 1974; Strahl and Hamoen, 2010). SDP caused depolarization in *B. subtilis* strain PY79 at concentrations as low as 1 μg ml^{-1} with a timescale similar to that of nisin (Fig. 4E, green and blue). In contrast, 10 μg ml^{-1} vancomycin had no

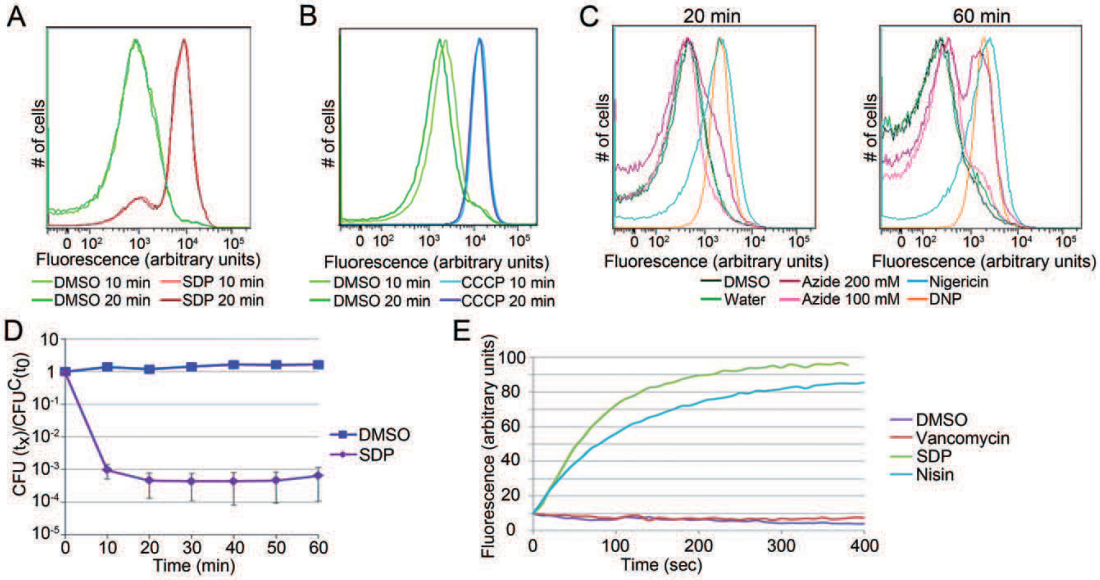

Fig. 4. SDP rapidly depletes the PMF and slowly induces autolysis.
A–C. Flow cytometry assay of $DiBAC_4(5)$ stained *E. coli lptD4213* (NR698) cells. (A and B) Cells were treated for 10 min (light) or 20 min (dark) with DMSO (green), 4 μg ml^{-1} SDP (red) or 500 μM CCCP (blue) and subjected to flow cytometry. (C) Cells were treated for 20 min or 60 min, as indicated, with DMSO (dark green), Water (green), 200 mM Azide (crimson), 100 mM Azide (pink), 125 μM Nigericin (aqua), or 20 mM DNP (orange) and subjected to flow cytometry.
D. Treatment of PY79 with 20 μg ml^{-1} SDP reduces *B. subtilis* PY79 viability (calculated as in Fig. 2) within 10 min; the limited quantities of SDP available precluded doing additional shorter time points. Error bars represent the standard error of ≥ 3 experiments.
E. Fluorometry assay of $DiSC_3(5)$ stained *B. subtilis* PY79 cells treated with DMSO (purple), 10 μg ml^{-1} vancomycin (red), 1 μg ml^{-1} SDP (green) or 11 μg ml^{-1} nisin (blue).

impact on the PMF. Thus, SDP rapidly collapses the PMF in *B. subtilis*.

Second, we used flow cytometry to quantify the fraction of cells affected by various treatments. This assay cannot be performed with *B. subtilis* because it grows in chains that preclude analysis by flow cytometry without either gating the cell size to analyse only individual cells, which comprise < 5% of the population, or by fixing and physically separating the cells (Aguilar *et al.*, 2010), which makes it impossible to measure the PMF. We therefore used the *E. coli lptD* strain (NR698; Ruiz *et al.*, 2005), which grows as single cells. Cells were treated with SDP and a variety of control compounds and then resuspended in 1× PBS with 5 μg ml^{-1} DiBAC$_4$(5), a potential sensitive dye that only enters depolarized cells and then binds to membranes and proteins, resulting in increased fluorescence (Jepras *et al.*, 1995; 1997). Cells treated with SDP at concentrations as low as 4 μg ml^{-1} show increased fluorescence within 10 min of treatment. (Fig. 4A, red; see SDP titration experiment in Fig. S3A). This shift is comparable to that seen with CCCP (Fig. 4B, blue), DNP (Fig. 4C, orange), nigericin (Fig. 4C, blue) and nisin treatment (Fig. S3B). In contrast, azide only depolarized the membranes in a fraction of the cells at the highest concentration after an hour (Fig. 4C, crimson). Thus, SDP rapidly collapses the PMF of both *B. subtilis* and *E. coli*, suggesting that this is its primary mechanism of action.

SDP treatment most closely resembles treatments that collapse both ΔΨ (membrane potential) and ΔpH

The data above indicate that SDP collapses the PMF, but they do not discriminate between decreases in the individual components of the PMF, ΔΨ (membrane potential) and ΔpH. We therefore expanded our list of reference compounds to include those that specifically collapse the ΔΨ or the ΔpH (unlike CCCP, DNP and azide, which collapse both components). To discriminate between these two activities, we tested the effects of nigericin and valinomycin on *B. subtilis* cells. Nigericin inserts into the membrane and facilitates the equal exchange of extracellular H^+ for intracellular K^+ ions, dissipating ΔpH while maintaining ΔΨ since this is a charge neutral exchange. Valinomycin moves K^+ ions from high to low concentrations, so in the presence of high extracellular concentrations of K^+ it collapses ΔΨ with no effect on ΔpH, as there is no change in the proton gradient. Somewhat surprisingly, the cell biological effects of these two compounds were easily distinguishable from each other and from SDP, CCCP, DNP and azide. Nigericin induces cell lysis and accumulation of membrane at septa, like those that collapse both components of the PMF; however, the DNA in lysed cells is more compacted, extracellular vesicles are rarely seen, and there are subtle accumulations of membrane pools along the side of the cell (Fig. 3I, with entire fields shown in Fig. S4). Valinomycin-KCl treatment produces elongated cells with smooth membranes, decondensed chromosomes, and cell lysis produces many extracellular vesicles but small membrane gaps are not observed. Thus, somewhat surprisingly, compounds that specifically deplete the ΔΨ or ΔpH appear different from one another, and different from compounds that collapse both components of the PMF. Our data suggest that SDP might collapse both the ΔΨ and the ΔpH, similar to CCCP and DNP.

Quantitative discrimination between mechanisms of action using cell biology

Our cell biological studies demonstrated that compounds with different mechanisms of action had different effects on membrane and DNA architecture and on cell permeability, even after short times of treatment (20 min). Specifically, all of the compounds that target components of the PMF produce cells with decondensed chromosomes and reduced DAPI staining (Fig. 5B, E, F, H and L) compared with untreated cells (Fig. 5A, D, G and K). Quantification demonstrated that these cells have lower DAPI fluorescence intensity per cell than controls (Fig. 5N), suggesting that DAPI might require the PMF for uptake (similar to kanamycin; Taber *et al.*, 1987). In contrast, nisin-treated cells showed increased chromosome condensation and increased DAPI fluorescence intensity per cell compared with the control (Fig. 5A and C). This suggests that intact cells take up less DAPI than nisin-treated cells. Nisin-treated cells were also rapidly permeabilized to SYTOX Green (Fig. 5C) and showed a 130× increase in SYTOX fluorescence intensity (Fig. 5M). This increased cell permeability is likely due to the ability of nisin to form non-specific channels in the cytoplasmic membrane (Lubelski *et al.*, 2008). Vancomycin (at > 10× the MIC) has little effect on DAPI or SYTOX Green fluorescence, but FM 4–64 staining was uneven, suggesting that the cells contained membrane invaginations. Thus, at short times of treatment, SYTOX Green permeability and chromosome condensation can discriminate between compounds that affect the PMF, which decondense the chromosomes, and those which produce large membrane channels, which rapidly permeabilized the cells and cause chromosome condensation.

Autolysis is a secondary consequence of SDP treatment

During our cytological profiling experiments, we noted that cells treated with SDP lyse in a manner identical to that observed when untreated *B. subtilis* cells are moved from aerated to static culture (Fig. 3F). This suggested that autolysis, which is also induced by CCCP and azide (Jolliffe *et al.*, 1981), might be responsible for the dramatic

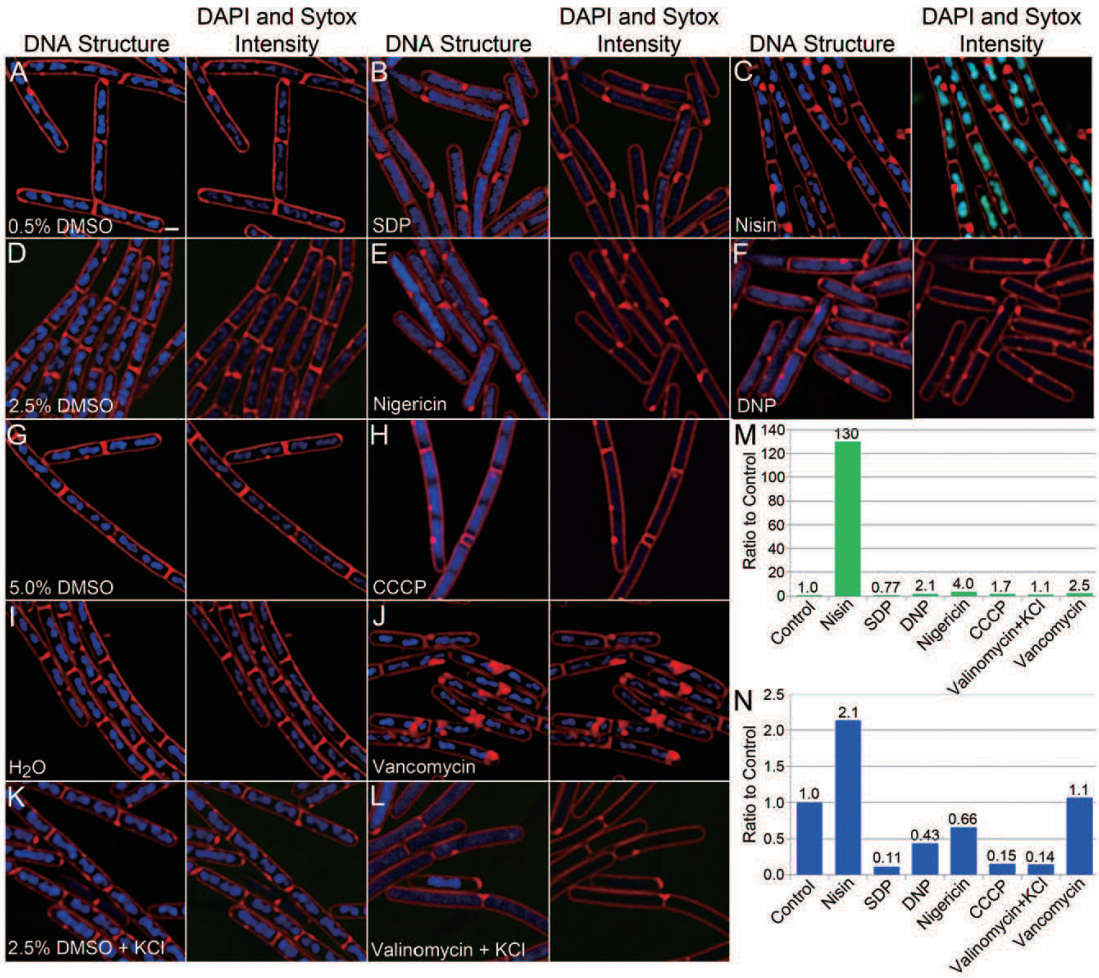

Fig. 5. The short-term consequences of various compounds on cell structure. PY79 cultures were treated with the indicated compounds for 20 min at the concentrations specified in Fig. 3 (except CCCP is 500 μM and DNP is 10 mM), stained with FM 4–64 (red), DAPI (blue) and SYTOX Green (green) and imaged.
A–L. Overlays are shown following adjustment of DAPI images to visualize DNA structure (left) and of the DAPI and SYTOX Green images to reveal changes in fluorescence intensity (right) as described in the methods. Scale bar represents 1 μm.
M. Graph showing the ratio of average SYTOX Green fluorescence intensity/pixel for cells treated with various compounds for 20 min to the appropriate controls. Only nisin significantly permeabilizes the cells.
N. Graph of the ratio of average DAPI fluorescence intensity/pixel for cells treated with various compounds for 20 min to the appropriate controls. SDP, CCCP, DNP, nigericin and valinomycin-treated cells show significantly decreased fluorescence intensity, whereas nisin shows increased fluorescence intensity and vancomycin shows no change.

lysis that is a late consequence of SDP treatment. Autolysis is caused by cellular enzymes called autolysins that digest peptidoglycan during processes such as cell separation and elongation, and can cause cell lysis when deregulated (Jolliffe *et al.*, 1981; Smith *et al.*, 2000). To test the hypothesis that SDP induces autolysis, we used a strain missing the four major *B. subtilis* autolysins LytC, LytD, LytE, LytF (ALB1111) that is resistant to autolysis induced by a lack of aeration and by certain membrane active compounds, including CCCP and azide (Margot *et al.*, 1999). When treated with SDP, the autolysin-deficient strain failed to lyse, showing neither increased SYTOX permeability nor external membrane vesicles, even after 5 h (Fig. 6B), although it accumulated internal membrane vesicles. However, viable cell counts showed that the mutant cells lost viability as rapidly as the wild-

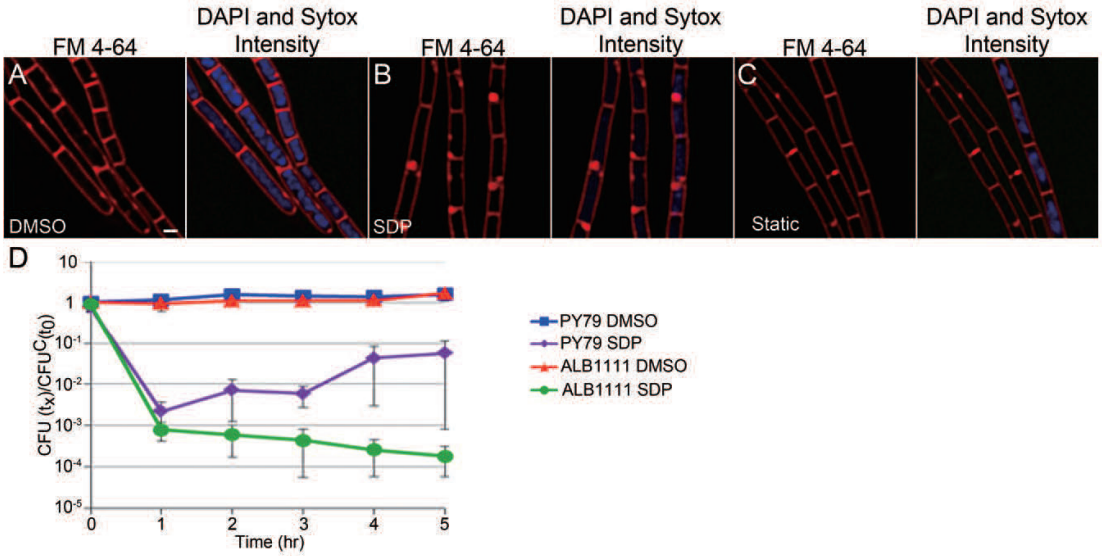

Fig. 6. Effect of autolysins on cell lysis and death.
A–C. Fluorescence micrographs of autolysin deficient cells *ΔlytABC ΔlytD ΔlytE ΔlytF* (ALB1111) treated for 5 h with (A) DMSO, (B) 20 μg ml^{-1} SDP, or (C) statically incubated. Cells are stained with FM 4–64 (red), DAPI (blue), and SYTOX Green (green). Scale bar represents 1 μm. No change in SYTOX Green permeability is observed.
D. Cell viability in SDP-treated PY79 and *ΔlytABC ΔlytD ΔlytE ΔlytF* (ALB1111) cells. (The PY79 curves are the same as those shown in Fig. 3). Both strains lose viability upon SDP treatment. Error bars represent the standard error of ≥ 3 experiments.

type strain after SDP treatment (Fig. 6D, green). This indicates that autolysis is a secondary consequence of SDP treatment and not the primary cause of cell death.

Discussion

Our studies of the mechanism of action of SDP were greatly facilitated by cell biological studies of the effects of membrane active antibacterial compounds on the structure of bacterial cells. These studies indicated that SDP likely collapses the PMF (as confirmed by more specific assays) and that this subsequently induces autolysis. Cytological profiling is capable of discriminating between two compounds that bind the lipid II precursor for peptidoglycan biogenesis (vancomycin and nisin), as only one (nisin) makes large channels in the membrane that permeabilize the cells to SYTOX Green (Fig. 5C and Fig. S4). This assay also discriminates between compounds that collapse both components of the PMF (CCCP, DNP), those that collapse or dissipate a single component of the PMF (ΔpH or ΔΨ; nigericin, valinomycin) and those that make non-specific channels in the cytoplasmic membrane (nisin). Our studies suggest that SDP rapidly collapses both components of the PMF and that this is responsible for its immediate toxicity to bacterial cells. Thus, cytological profiling can rapidly provide insight into the possible mechanisms of action of newly identified antibacterial compounds that affect the cell membrane, and thereby limit the number of more specific assays required to fully document the mechanism of action.

We favour the hypothesis that SDP collapses both components of the PMF by translocating protons across the membrane, perhaps forming a channel that allows protons but not larger molecules to diffuse freely across the membrane (Fig. 7). Interestingly, many cationic antimicrobial peptides produced by the human immune system and bacteria kill cells by inserting into the membrane and assembling channels that collapse the PMF (Peters *et al.*, 2010; Nan *et al.*, 2011b). Thus, SDP, which is also a cationic peptide, shares a mechanism of action with many other peptides that play an evolutionarily ancient role in protecting eukaryotes and bacteria against invading bacteria.

A secondary consequence of PMF collapse in many Gram-positive bacteria, including *B. subtilis* and *S. aureus*, is autolysis, which we have demonstrated produces the dramatic lysis associated with SDP treatment. Autolysis involves enzymes that cleave peptidoglycan during cell elongation and cell separation, which are deregulated or hyperactivated by PMF collapse, leading to cell lysis. The mechanism by which loss of the PMF induces autolysis is not completely clear, but our observation that different cytological profiles are produced by collapse of either ΔpH or ΔΨ or both suggests that collapse

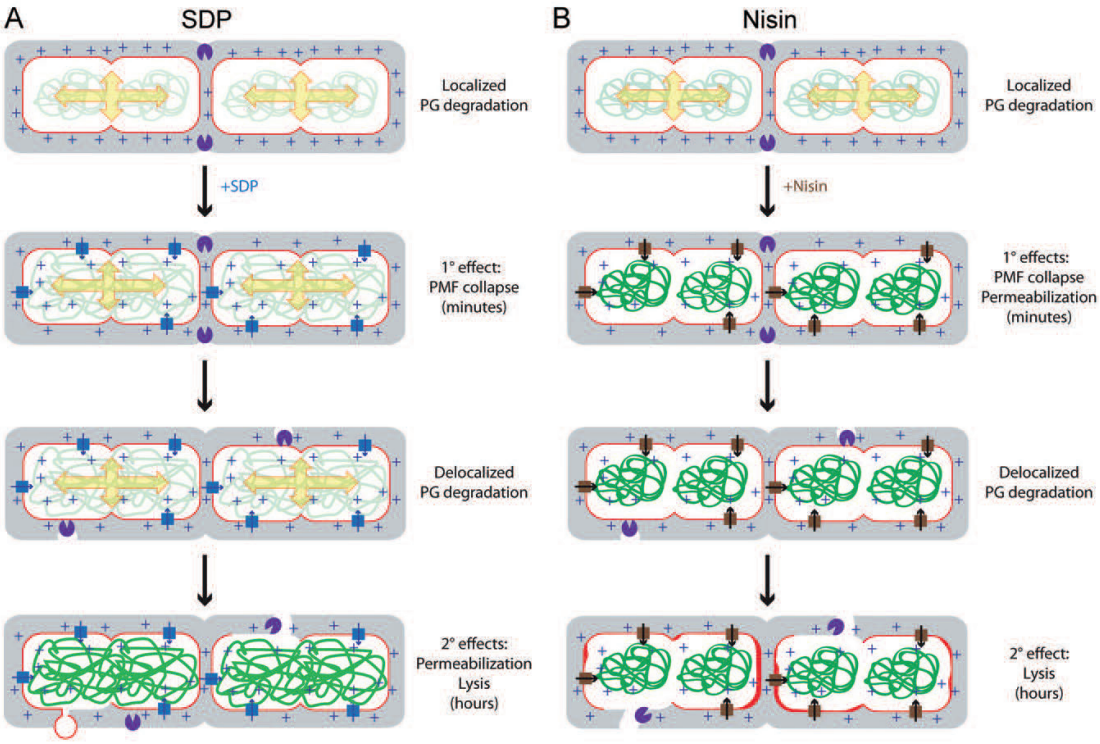

Fig. 7. Comparison of the cytological profiles and mechanisms of action and for SDP and nisin. Key: grey – cell wall; red – cytoplasmic membrane; light green – DNA structure; dark green – cell permeability; + – protons; purple – autolysins; blue – SDP; brown – nisin.
A. SDP (blue) depolarizes the membrane, and we propose that it inserts into the membrane and forms a proton channel, causing PMF collapse and chromosome decondensation. Autolysin activity is deregulated and delocalized peptidoglycan degradation causes holes in the cell wall. After hours, this induces autolysis, with extrusion of membrane tubules and vesicles caused by high internal osmotic pressure (red), and increased SYTOX Green permeability.
B. Nisin (brown) inserts into the membrane and forms a large non-specific channel that rapidly permeabilizes the cells, collapsing the PMF, osmotically equilibrating the cells, and condensing the chromosomes. Autolysin activity is deregulated and delocalized peptidoglycan degradation causes holes in the cell wall. After hours, autolysis occurs, but in the absence of a high internal osmotic pressure, the cell implodes to form internal membranes rather than exploding to form external membrane vesicles and tubules.

of each component of the PMF might activate enzymes with distinct substrate specificities or localization. Previous results suggest that ΔpH is coupled to autolysin activity via the acidic wall polymer teichoic acid, which maintains a pH gradient across the cell wall. During respiration, teichoic acid is proposed to retain protons close to the cytoplasmic membrane, which are replaced by $K+$ or $Na+$ from the medium at the outer surface of the wall. This inhibits autolysin activity near the membrane of respiring cells, thereby restricting autolysin activity to the outer surface of the cells (Neuhaus and Baddiley, 2003; Rice and Bayles, 2008). Such autolysins would therefore be deregulated upon collapse of the ΔpH but not by collapse of $\Delta\Psi$. There are two attractive models for sensing $\Delta\Psi$. First, some bacteriophages regulate host cell lysis by PMF collapse, which triggers the release and activation of membrane-anchored endolytic enzymes (the SAR-endolysins; Park *et al.*, 2007; Rice and Bayles, 2008). The PMF governs the insertion of charged transmembrane proteins into the membrane (Celebi *et al.*, 2008), likely via the $\Delta\Psi$. Second, $\Delta\Psi$ is required for localization of a variety of cell division proteins (Strahl and Hamoen, 2010), suggesting that depolarization might release the autolytic enzymes from their usual site of activity at the septum or the outer layers of the wall. Further studies are required to identify the autolytic enzymes that are induced by collapse of the ΔpH or $\Delta\Psi$, and to understand the mechanism by which collapse of each component of the PMF leads to autolysis.

Regardless of the mechanism by which the ΔpH and $\Delta\Psi$ govern autolysin activity, delocalized peptidoglycan degradation ultimately produces holes in the cell wall (Rice and Bayles, 2008; Vollmer *et al.*, 2008). In otherwise intact cells, the osmotic pressure would then force the membrane through these holes, leading to the extrusion of membrane

vesicles and to permeabilization of the cell to larger molecules such as SYTOX Green. We hypothesize that the number and distribution of the holes in the cell wall is dictated by the specific autolysins activated by each treatment, and that this in turn determines if cells lyse with the extrusion of relatively few large vesicles or with the production of many smaller vesicles. In contrast, cells that have been permeabilized with molecules that assemble large non-specific pores, such as nisin, would lack an internal osmotic pressure as the pores would allow the osmotic equilibration of the cell with the medium. Thus, by the time the autolysins produce holes in the cell wall, cell lysis would simply entail an internal collapse of the cell membrane rather than the extrusion of membrane vesicles.

Potential role of SDP in mediating inter- and intra-species interactions

SDP acts as a cannibalistic toxin that kills a subset of *B. subtilis* cells within the biofilm to allow continued growth thereby delaying the onset of sporulation (Ellermeier *et al.*, 2006; Liu *et al.*, 2010). We here demonstrate that SDP is active against a variety of bacterial species in the Firmicutes phylum, including species closely related to *B. subtilis* such as *B. amyloliquifaciens* and also more distantly related species such as *Lactobacillus acidophilus*. This expands the list of Gram-positive species sensitive to SDP beyond those previously published (Palmer *et al.*, 2009; Liu *et al.*, 2010) and suggests that SDP might play a more general role in defending the *B. subtilis* colony against invading species. We speculate that in this broader context, depleting cellular energy stores might be the ideal mechanism of action for a defensive extracellular metabolite. First, sublethal concentrations of compounds that collapse the PMF rapidly inhibit flagellar motility in a variety of species (Ridgway, 1977; Goulbourne and Greenberg, 1980; Nan *et al.*, 2011a). This could prevent motility-driven invasion of *B. subtilis* colonies as well as swarming away from the *B. subtilis* colony. Second, collapsing the PMF disrupts biofilm formation in *Pseudomonas aeruginosa* and *Shewanella oneidensis* (Ikonomidis *et al.*, 2008; Saville *et al.*, 2011), suggesting that SDP could inhibit biofilm formation by neighbouring species, and thus reduce competition for a niche. Third, the PMF is necessary for protein secretion and the export of many toxic secreted metabolites (Geller, 1991; Driessen, 1992), so SDP might reduce the ability of neighbouring species to produce or respond to toxic molecules. Finally, and perhaps most importantly, a variety of Gram-positive species undergo autolysis when the PMF is compromised (Jolliffe *et al.*, 1981; Reith and Mayer, 2011), but not when pathways such as transcription or translation are inhibited by antibiotics (Jolliffe *et al.*, 1981; Falk *et al.*, 2010). Thus, inducing autolysis would be advantageous for a cannibalistic or defensive toxin as it would lead to the release of nutrients from target cells without the need to secrete enzymes to lyse neighbouring bacteria. The SDP toxin is therefore ideally suited for its roles in eliminating unnecessary cell types from the colony and in defending it from invasion by competing species.

Experimental procedures

Strains and culture conditions

The strains used in this study are listed in Table 1. All cultures were grown in LB medium at 37°C, except cultures for fluorometry. All cells treated with compounds were treated in concentrated microcultures (described below), except cultures for fluorometry, which were grown in LB supplemented with 50 mM HEPES pH 7.5, 300 mM KCl and 0.1% glucose.

Solutions of SDP and other toxins were prepared using the following concentrations and solvents: 400 μg ml^{-1} SDP (10% DMSO, purified as described in (Liu *et al.*, 2010), 100 mM sodium azide (H_2O, Sigma), 2 mM CCCP (20% DMSO, Sigma) or 10 mM CCCP (100% DMSO, Sigma), 5 mg ml^{-1} valinomycin (100% DMSO, Sigma), 2.5 mg ml^{-1} nigericin (100% DMSO, Calbiochem), 400 mM dinitrophenol (100% DMSO, Sigma) 5 mg ml^{-1} vancomycin (H_2O, Sigma), and 100 μg ml^{-1} nisin (10% DMSO, Sigma). One mM IPTG was used to induce SdpI in TPM758 cells.

Concentrations of antibiotics in solid culture were as follows: MLS (1 μg ml^{-1} erythromycin, 25 μg ml^{-1} lincomycin), 10 μg ml^{-1} tetracycline, 100 μg ml^{-1} spectinomycin. Except when otherwise noted, SDP was used at 20 μg ml^{-1}, which we estimate is between 2 × and 5 × the MIC (Table S1).

Fluorescence microscopy

Cells were cultured for fluorescence microscopy as described in Liu *et al.* (2010). The effects of compounds on individual *B. subtilis* cells were investigated in concentrated 15 μl microcultures prepared in the following manner. Cultures were grown in LB media to an OD_{600} of 0.3, centrifuged, resuspended in 1/10 the volume and 14.25 or 13.5 μl (depending on the volume of compound to be added) of concentrated cells were added to 1.7 ml microcentrifuge tubes. At $t = 0$, 0.75 μl or 1.5 μl of the indicated compound was added to aliquots of cells. Compounds were used at the following final concentrations: 0.5% DMSO, 2.5% DMSO, 5.0% DMSO, 20 μg ml^{-1} SDP, 10 mM azide, 100 μM CCCP (Fig. 3), 500 μM CCCP (Fig. 5), 2 mM DNP (Fig. 3), 10 mM DNP (Fig. 5), 62.5 μM nigericin, 125 μM valinomycin, 250 μg ml^{-1} vancomycin, 10 μg ml^{-1} nisin. Cultures to be treated with valinomycin were grown in LB supplemented with 200 mM KCl (Fig. 3), or 300 mM KCl (Fig. 5). Tubes were capped and incubated at 37°C in a roller. Samples were collected for imaging every hour. Three microlitres of cells were added to 0.75 μl of a stain mix containing 30 μg ml^{-1} FM 4–64, 2.5 μM SYTOX Green and 1.2 μg ml^{-1} DAPI prepared in 1× T-base. *E. coli* cultures were treated identically to *B. subtilis* cultures, but the treatment was extended to 5 h. The pH of control cultures was monitored after incubation, and found to be unchanged from the starting medium (pH 6.5–7.0).

Table 1. Strains used in this study.

Strains	Genotype	Background	Reference
B. subtilis			
3610	Prototroph, undomesticated parent of 168		Branda *et al.* (2001)
PY79	Prototrophic derivative of *B. subtilis* 168		Youngman *et al.* (1984)
EH273	*sdpABC::kan*	PY79	Ellermeier *et al.* (2006)
TPM758	*ΔsdpABCIR::tet, ΔsigW::kan amyE::*P_{hyspac}*sdpI*$^{+}$*Ωspec*	PY79	Ellermeier lab
KP3034	*lacA::spec*	PY79	BGSC1A785→PY79
SCB751	*amyE::mifM-yidC2*^{6}*-lacZΩcat*	PY79	Chiba *et al.* (2009)
ALB1039	*ΔsigW::mls*	PY79	This study
ALB1088	*ΔsdpABCIR::tet*	PY79	This study
ALB1142	*ΔsdpABCIR::tet, ΔsigW::mls*	PY79	This study
ALB1111	*lytABC::neo, lytD:: tet, lytF::spec, lytE::cm lytD::tet*	PY79	This study
HB0020	*ΔsigW::mls trpC2 ΔSPβ*	168	Cao *et al.* (2001)
L16601	Prototrophic derivative of *B. subtilis* 168		Margot and Karamata (1996)
L16648	*lytABC::neo, lytF::spec, lytE::cm, lytD::tet*	L16601	Margot *et al.* (1999)
CDE433	*ΔsdpABCIR::tet, ΔsigW::kan*	PY79	Ellermeier and Losick (2006)
E. coli			
MC4100	*F–, [araD139]*$_{B/r}$*, Δ(argF-lac)169, lambda–, e14–, flhD5301, Δ(fruK-yeiR)725(fruA25), relA1, rpsL150(strR), rbsR22, Δ(fimB-fimE)632(::IS1), deoC1*		Casadaban (1976)
NR698	*lptD4213*	MC4100	Ruiz *et al.* (2005)
Other species			
ATCC9341	*Micrococcus luteus*		Lab collection
ATCC12872	*Bacillus megaterium*		Lab collection
FZB42	*Bacillus amyloliquifaciens*		Lab collection
ATCC35646	*Bacillus thuringiensis*		Lab collection
ATCC4356	*Lactobacillus acidophilus*		Lab collection
ATCC842	*Paenibacillus polymyxa*		Lab collection
ATCC35984	*Staphylococcus epidermidis*		Lab collection

Cells were immobilized on an agarose pad (1/10 LB, 0.375 μg ml^{-1} FM 4–64, 0.025 μg ml^{-1} DAPI) and imaged on an Applied Precision Spectris Microscope described in (Liu *et al.*, 2006). Images were deconvolved using softWoRx v3.3.6 (Applied Precision) and the medial focal planes shown. The DAPI and SYTOX Green images in Figs 1–3, 6, S1 and S4 were normalized within each figure based on intensity and exposure length to reflect intensities relative to the treatment with the highest fluorescence intensity in each figure.

Sporulation conditions

To quantify the impact of SDP on sporulation, concentrated microcultures in LB were prepared as described above, and incubated with rolling at 37°C. Samples were harvested after 5 h, and stained with FM 4–64 and prepared for microscopy as described above. The number of cells with asymmetric septa in a 3610 culture was counted after treatment with 0.5% DMSO or 20 μg ml^{-1} SDP for 5 h. At least 100 cells were counted per treatment per experiment. Numbers reflect the average of three experiments.

Viable cell counts

Viable cell counts were obtained through dilution and plating of cells from the same cultures as those subjected to microscopy. Ten-fold serial dilutions were made at the indicated time in 1× T-base and spotted onto LB plates. The first dilution reduces the concentration of SDP and other antimicrobial compounds below their minimal inhibitory concentrations. We therefore infer that cell death is due to compounds that bound the cell before dilution. Colonies were counted after growth and colony-forming units (cfu) per ml calculated. Shown is the ratio of cfu at time x [cfu(t_x)] to cfu of the control at t_0 [cfu^{C}(t_0)].

Flow cytometry

Measurement of the PMF by flow cytometry used NR698 (*E. coli lptD4213*) grown as for microscopy. After SDP treatment at 37°C for 10 or 20 min (as indicated in the figure), 3–15 μl of culture was resuspended in 1× PBS with 5 μg ml^{-1} $DiBAC_4(5)$ and 100 000 events counted using a BD LSR II flow cytometer. Fluorescence data were collected using the 561 nm laser. Area under the curve (dsRed-A) was used as the fluorescence intensity measurement.

Fluorometry

Measurement of the PMF by fluorometry was conducted similarly to Strahl and Hamoen (2010). *B. subtilis* strain PY79 cells were grown in LB supplemented with 50 mM HEPES pH 7.5, 300 mM KCl and 0.1% glucose to an OD_{600} of 0.3–0.35, spun down, then resuspended in 0.5 volume 50 mM HEPES pH 7.5, 300 mM KCl and 0.1% glucose. $DiSC_3(5)$ (1 μM final), cells, and DMSO (0.5% final), vancomycin (10 μg ml^{-1} final), nisin (11 μg ml^{-1} final), or SDP (1 μg ml^{-1} final) were mixed together in a final volume of 50 μl and transferred into a capillary cuvette. The fluorescence was monitored with a Fluoromax-4 spectrofluorometer at excitation 544-10 nm and emission 660-10 nm. The representative

curves shown were normalized so that each started at the same level of fluorescence.

Quantification of DAPI and SYTOX Green staining intensity

Cells used for DAPI and SYTOX Green quantification were treated with the indicated compound for 20 min at 37°C prior to immobilization on an agarose pad for fluorescence microscopy. The DAPI and SYTOX staining intensities are sensitive to both cell permeabilization and to chromosome architecture. Thus, more permeabilized cells show brighter staining, as do more condensed chromosomes, which is why we show two images. First, to show chromosome architecture in the panels titled 'DNA structure', the DAPI images were adjusted to allow the optimal visualization of the chromosomes. Second, to show staining intensity relative to untreated controls in the panels titles 'DAPI and Sytox intensity', the DAPI and SYTOX Green images were adjusted to normalize the brightness relative to that of the brightest sample (nisin), based on exposure length and intensity. This more accurately displayed relative fluorescence intensities. Thus, the manner in which we quantified the data in Fig. 5 primarily reflects uptake, since we quantified total DAPI staining intensity per cell rather than per area occupied by the chromosome.

Average DAPI and SYTOX Green fluorescence intensity/pixel for each cell was calculated from non-deconvolved images and the background values subtracted. A total of $\geq$ 100 cells were measured per treatment. Briefly, a polygon was drawn in Image J using the membrane as a guide. To calculate background fluorescence, polygons were drawn in areas without cells. Values for DAPI and SYTOX Green fluorescence intensity/pixel were adjusted to reflect a 0.3 s exposure time. Finally, the average fluorescence intensity for each sample was divided by the average fluorescence intensity of the appropriate solvent control.

Time-lapse microscopy

Time-lapse fluorescence microscopy (Becker and Pogliano, 2007) was conducted on concentrated microcultures treated with 0.5% DMSO or 20 μg ml^{-1} SDP at 37°C for 20 min. After treatment, 3.0 μl of cells was added to 9.0 μl of a stain mix in 1$\times$ T-base, containing 0.67 μg ml^{-1} FM 4–64 and 0.67 μM SYTOX Green, applied to agarose pads (1/5 LB, 0.3 μg ml^{-1} FM 4–64, 0.5 μM SYTOX Green) and grown at 30°C for ~ 20 min prior to microscopy. Pictures were taken every 10 min for 2 h.

Statistical analysis

Viable cell counts after drug treatment (Figs 2C, 3K, 4D and E): $n \geq 3$ separate experiments, the average value is plotted, and error bars represent standard error. Spot assay viable cell quantification (Fig. S1): bars represent the average of $n \geq 3$ separate experiments. Error bars represent the standard deviation.

Acknowledgements

We thank Poochit Nonejuie and Joe Pogliano (UCSD) for assistance in the development of cytological profiling. We also thank Richard Losick (Harvard University) and Craig Ellermeier (University of Iowa) for providing strains, the Elena Zuniga laboratory (UCSD) for use of the LSR II flow cytometer, the Patricia Jennings laboratory (UCSD) for instruction and use of the Fluorometer, and Craig Ellermeier and Carol Gross (UCSF) for helpful discussions. Funding for this project in the Pogliano and Dorrestein laboratories was provided by the National Institute of Health (AI095125). Anne Lamsa was supported, in part, by an NIH training grant (GM7240). Wei-Ting Liu was supported, in part, by a study abroad grant from Taiwan (SAS-98116-2-US-108).

References

Abee, T., Kovacs, A.T., Kuipers, O.P., and van der Veen, S. (2011) Biofilm formation and dispersal in Gram-positive bacteria. *Curr Opin Biotechnol* **22:** 172–179.

Aguilar, C., Vlamakis, H., Guzman, A., Losick, R., and Kolter, R. (2010) KinD is a checkpoint protein linking spore formation to extracellular-matrix production in *Bacillus subtilis* biofilms. *MBio* **1:** e00035-10.

Asaduzzaman, S.M., and Sonomoto, K. (2009) Lantibiotics: diverse activities and unique modes of action. *J Biosci Bioeng* **107:** 475–487.

Babasaki, K., Takao, T., Shimonishi, Y., and Kurahashi, K. (1985) Subtilosin A, a new antibiotic peptide produced by *Bacillus subtilis* 168: isolation, structural analysis, and biogenesis. *J Biochem* **98:** 585–603.

Becker, E.C., and Pogliano, K. (2007) Cell-specific SpoIIIE assembly and DNA translocation polarity are dictated by chromosome orientation. *Mol Microbiol* **66:** 1066–1079.

Bird, L.J., Bonnefoy, V., and Newman, D.K. (2011) Bioenergetic challenges of microbial iron metabolisms. *Trends Microbiol* **19:** 330–340.

Branda, S.S., Gonzalez-Pastor, J.E., Ben-Yehuda, S., Losick, R., and Kolter, R. (2001) Fruiting body formation by *Bacillus subtilis*. *Proc Natl Acad Sci USA* **98:** 11621–11626.

Braun, M., and Silhavy, T.J. (2002) Imp/OstA is required for cell envelope biogenesis in *Escherichia coli*. *Mol Microbiol* **45:** 1289–1302.

Butcher, B.G., and Helmann, J.D. (2006) Identification of *Bacillus subtilis* sigma-dependent genes that provide intrinsic resistance to antimicrobial compounds produced by Bacilli. *Mol Microbiol* **60:** 765–782.

Cao, M., Bernat, B.A., Wang, Z., Armstrong, R.N., and Helmann, J.D. (2001) FosB, a cysteine-dependent fosfomycin resistance protein under the control of sigma(W), an extracytoplasmic-function sigma factor in *Bacillus subtilis*. *J Bacteriol* **183:** 2380–2383.

Carrillo, C., Teruel, J.A., Aranda, F.J., and Ortiz, A. (2003) Molecular mechanism of membrane permeabilization by the peptide antibiotic surfactin. *Biochim Biophys Acta* **1611:** 91–97.

Casadaban, M.J. (1976) Transposition and fusion of the *lac* genes to selected promoters in *Escherichia coli* using bacteriophage lambda and Mu. *J Mol Biol* **104:** 541–555.

Celebi, N., Dalbey, R.E., and Yuan, J. (2008) Mechanism and hydrophobic forces driving membrane protein insertion of subunit II of cytochrome bo 3 oxidase. *J Mol Biol* **375:** 1282–1292.

Chiba, S., Lamsa, A., and Pogliano, K. (2009) A ribosome-nascent chain sensor of membrane protein biogenesis in *Bacillus subtilis*. *EMBO J* **28:** 3461–3475.

D'Onofrio, A., Crawford, J.M., Stewart, E.J., Witt, K., Gavrish, E., Epstein, S., *et al.* (2010) Siderophores from neighboring organisms promote the growth of uncultured bacteria. *Chem Biol* **17:** 254–264.

Driessen, A.J. (1992) Precursor protein translocation by the *Escherichia coli* translocase is directed by the protonmotive force. *EMBO J* **11:** 847–853.

Dworkin, J., and Losick, R. (2005) Developmental commitment in a bacterium. *Cell* **121:** 401–409.

Ellermeier, C.D., and Losick, R. (2006) Evidence for a novel protease governing regulated intramembrane proteolysis and resistance to antimicrobial peptides in *Bacillus subtilis*. *Genes Dev* **20:** 1911–1922.

Ellermeier, C.D., Hobbs, E.C., Gonzalez-Pastor, J.E., and Losick, R. (2006) A three-protein signaling pathway governing immunity to a bacterial cannibalism toxin. *Cell* **124:** 549–559.

Falk, S.P., Noah, J.W., and Weisblum, B. (2010) Screen for inducers of autolysis in *Bacillus subtilis*. *Antimicrob Agents Chemother* **54:** 3723–3729.

Geller, B.L. (1991) Energy requirements for protein translocation across the *Escherichia coli* inner membrane. *Mol Microbiol* **5:** 2093–2098.

Gonzalez, D.J., Haste, N.M., Hollands, A., Fleming, T.C., Hamby, M., Pogliano, K., *et al.* (2011) Microbial competition between *Bacillus subtilis* and *Staphylococcus aureus* monitored by imaging mass spectrometry. *Microbiology* **157:** 2485–2492.

Gonzalez-Pastor, J.E., Hobbs, E.C., and Losick, R. (2003) Cannibalism by sporulating bacteria. *Science* **301:** 510–513.

Goulbourne, E.A., Jr, and Greenberg, E.P. (1980) Relationship between proton motive force and motility in *Spirochaeta aurantia*. *J Bacteriol* **143:** 1450–1457.

Haussler, S. (2010) Multicellular signalling and growth of *Pseudomonas aeruginosa*. *Int J Med Microbiol* **300:** 544–548.

Hibbing, M.E., Fuqua, C., Parsek, M.R., and Peterson, S.B. (2010) Bacterial competition: surviving and thriving in the microbial jungle. *Nat Rev Microbiol* **8:** 15–25.

Ikonomidis, A., Tsakris, A., Kanellopoulou, M., Maniatis, A.N., and Pournaras, S. (2008) Effect of the proton motive force inhibitor carbonyl cyanide-m-chlorophenylhydrazone (CCCP) on *Pseudomonas aeruginosa* biofilm development. *Lett Appl Microbiol* **47:** 298–302.

Jepras, R.I., Carter, J., Pearson, S.C., Paul, F.E., and Wilkinson, M.J. (1995) Development of a robust flow cytometric assay for determining numbers of viable bacteria. *Appl Environ Microbiol* **61:** 2696–2701.

Jepras, R.I., Paul, F.E., Pearson, S.C., and Wilkinson, M.J. (1997) Rapid assessment of antibiotic effects on *Escherichia coli* by bis-(1,3-dibutylbarbituric acid) trimethine oxonol and flow cytometry. *Antimicrob Agents Chemother* **41:** 2001–2005.

Jolliffe, L.K., Doyle, R.J., and Streips, U.N. (1981) The energized membrane and cellular autolysis in *Bacillus subtilis*. *Cell* **25:** 753–763.

Kearns, D.B., and Losick, R. (2003) Swarming motility in undomesticated Bacillus subtilis. *Mol Microbiol* **49:** 581–590.

Liu, N.J., Dutton, R.J., and Pogliano, K. (2006) Evidence that the SpoIIIE DNA translocase participates in membrane fusion during cytokinesis and engulfment. *Mol Microbiol* **59:** 1097–1113.

Liu, W.T., Yang, Y.L., Xu, Y., Lamsa, A., Haste, N.M., Yang, J.Y., *et al.* (2010) Imaging mass spectrometry of intraspecies metabolic exchange revealed the cannibalistic factors of *Bacillus subtilis*. *Proc Natl Acad Sci USA* **107:** 16286–16290.

Lopez, D., Fischbach, M.A., Chu, F., Losick, R., and Kolter, R. (2009a) Structurally diverse natural products that cause potassium leakage trigger multicellularity in *Bacillus subtilis*. *Proc Natl Acad Sci USA* **106:** 280–285.

Lopez, D., Vlamakis, H., Losick, R., and Kolter, R. (2009b) Cannibalism enhances biofilm development in *Bacillus subtilis*. *Mol Microbiol* **74:** 609–618.

Lopez, D., Vlamakis, H., and Kolter, R. (2010) Biofilms. *Cold Spring Harb Perspect Biol* **2:** a000398.

Lubelski, J., Rink, R., Khusainov, R., Moll, G.N., and Kuipers, O.P. (2008) Biosynthesis, immunity, regulation, mode of action and engineering of the model lantibiotic nisin. *Cell Mol Life Sci* **65:** 455–476.

Margot, P., and Karamata, D. (1996) The wprA gene of *Bacillus subtilis* 168, expressed during exponential growth, encodes a cell-wall-associated protease. *Microbiology* **142** (Pt 12)**:** 3437–3444.

Margot, P., Pagni, M., and Karamata, D. (1999) *Bacillus subtilis* 168 gene lytF encodes a gamma-D-glutamate-meso-diaminopimelate muropeptidase expressed by the alternative vegetative sigma factor, sigmaD. *Microbiology* **145** (Pt 1)**:** 57–65.

Mitri, S., Xavier, J.B., and Foster, K.R. (2011) Social evolution in multispecies biofilms. *Proc Natl Acad Sci USA* **108** (Suppl. 2)**:** 10839–10846.

Molenkamp, G.C., and Veerkamp, J.H. (1976) Effects of antibiotics on metabolism of peptidoglycan, protein, and lipids in *Bifidobacterium bifidum* subsp. *pennsylvanicus*. *Antimicrob Agents Chemother* **10:** 786–794.

Nalca, Y., Jansch, L., Bredenbruch, F., Geffers, R., Buer, J., and Haussler, S. (2006) Quorum-sensing antagonistic activities of azithromycin in *Pseudomonas aeruginosa* PAO1: a global approach. *Antimicrob Agents Chemother* **50:** 1680–1688.

Nan, B., Chen, J., Neu, J.C., Berry, R.M., Oster, G., and Zusman, D.R. (2011a) Myxobacteria gliding motility requires cytoskeleton rotation powered by proton motive force. *Proc Natl Acad Sci USA* **108:** 2498–2503.

Nan, Y.H., Park, I.S., Hahm, K.S., and Shin, S.Y. (2011b) Antimicrobial activity, bactericidal mechanism and LPS-neutralizing activity of the cell-penetrating peptide pVEC and its analogs. *J Pept Sci* **17:** 812–817.

Nandy, S.K., Bapat, P.M., and Venkatesh, K.V. (2007) Sporulating bacteria prefers predation to cannibalism in mixed cultures. *FEBS Lett* **581:** 151–156.

Neuhaus, F.C., and Baddiley, J. (2003) A continuum of anionic charge: structures and functions of d-alanyl-teichoic acids in gram-positive bacteria. *Microbiol Mol Biol Rev* **67:** 686–723.

Palmer, M.E., Wiedmann, M., and Boor, K.J. (2009) sigma(B)

and sigma(L) contribute to *Listeria monocytogenes* 10403S response to the antimicrobial peptides SdpC and nisin. *Foodborne Pathog Dis* **6:** 1057–1065.
Park, T., Struck, D.K., Dankenbring, C.A., and Young, R. (2007) The pinholin of lambdoid phage 21: control of lysis by membrane depolarization. *J Bacteriol* **189:** 9135–9139.
Parker, G.F., Daniel, R.A., and Errington, J. (1996) Timing and genetic regulation of commitment to sporulation in *Bacillus subtilis*. *Microbiology* **142** (Pt 12)**:** 3445–3452.
Patel, P.S., Huang, S., Fisher, S., Pirnik, D., Aklonis, C., Dean, L., *et al.* (1995) Bacillaene, a novel inhibitor of procaryotic protein synthesis produced by *Bacillus subtilis*: production, taxonomy, isolation, physico-chemical characterization and biological activity. *J Antibiot (Tokyo)* **48:** 997–1003.
Peters, B.M., Shirtliff, M.E., and Jabra-Rizk, M.A. (2010) Antimicrobial peptides: primeval molecules or future drugs? *PLoS Pathog* **6:** e1001067.
Reith, J., and Mayer, C. (2011) Peptidoglycan turnover and recycling in Gram-positive bacteria. *Appl Microbiol Biotechnol* **92:** 1–11.
Rice, K.C., and Bayles, K.W. (2008) Molecular control of bacterial death and lysis. *Microbiol Mol Biol Rev* **72:** 85–109.
Ridgway, H.F. (1977) Source of energy for gliding motility in *Flexibacter polymorphus*: effects of metabolic and respiratory inhibitors on gliding movement. *J Bacteriol* **131:** 544–556.
Rogers, P.D., Liu, T.T., Barker, K.S., Hilliard, G.M., English, B.K., Thornton, J., *et al.* (2007) Gene expression profiling of the response of *Streptococcus pneumoniae* to penicillin. *J Antimicrob Chemother* **59:** 616–626.
Romero, D., Traxler, M.F., Lopez, D., and Kolter, R. (2011) Antibiotics as signal molecules. *Chem Rev* **111:** 5492–5505.
Ruiz, N., Falcone, B., Kahne, D., and Silhavy, T.J. (2005) Chemical conditionality: a genetic strategy to probe organelle assembly. *Cell* **121:** 307–317.
Sampson, B.A., Misra, R., and Benson, S.A. (1989) Identification and characterization of a new gene of *Escherichia coli* K-12 involved in outer membrane permeability. *Genetics* **122:** 491–501.
Saville, R.M., Rakshe, S., Haagensen, J.A., Shukla, S., and Spormann, A.M. (2011) Energy-dependent stability of *Shewanella oneidensis* MR-1 biofilms. *J Bacteriol* **193:** 3257–3264.
Shelburne, C.E., An, F.Y., Dholpe, V., Ramamoorthy, A., Lopatin, D.E., and Lantz, M.S. (2007) The spectrum of antimicrobial activity of the bacteriocin subtilosin A. *J Antimicrob Chemother* **59:** 297–300.
Sieradzki, K., Villari, P., and Tomasz, A. (1998) Decreased susceptibilities to teicoplanin and vancomycin among coagulase-negative methicillin-resistant clinical isolates of staphylococci. *Antimicrob Agents Chemother* **42:** 100–107.
Sims, P.J., Waggoner, A.S., Wang, C.H., and Hoffman, J.F. (1974) Studies on the mechanism by which cyanine dyes measure membrane potential in red blood cells and phosphatidylcholine vesicles. *Biochemistry* **13:** 3315–3330.
Skaar, E.P. (2010) The battle for iron between bacterial pathogens and their vertebrate hosts. *PLoS Pathog* **6:** e1000949.
Smith, T.J., Blackman, S.A., and Foster, S.J. (2000) Autolysins of *Bacillus subtilis*: multiple enzymes with multiple functions. *Microbiology* **146** (Pt 2)**:** 249–262.
Smukalla, S., Caldara, M., Pochet, N., Beauvais, A., Guadagnini, S., Yan, C., *et al.* (2008) FLO1 is a variable green beard gene that drives biofilm-like cooperation in budding yeast. *Cell* **135:** 726–737.
Stein, T. (2005) *Bacillus subtilis* antibiotics: structures, syntheses and specific functions. *Mol Microbiol* **56:** 845–857.
Strahl, H., and Hamoen, L.W. (2010) Membrane potential is important for bacterial cell division. *Proc Natl Acad Sci USA* **107:** 12281–12286.
Straight, P.D., and Kolter, R. (2009) Interspecies chemical communication in bacterial development. *Annu Rev Microbiol* **63:** 99–118.
Straight, P.D., Willey, J.M., and Kolter, R. (2006) Interactions between *Streptomyces coelicolor* and *Bacillus subtilis*: role of surfactants in raising aerial structures. *J Bacteriol* **188:** 4918–4925.
Taber, H.W., Mueller, J.P., Miller, P.F., and Arrow, A.S. (1987) Bacterial uptake of aminoglycoside antibiotics. *Microbiol Rev* **51:** 439–457.
Tipper, D.J. (1969) Mechanism of autolysis of isolated cell walls of *Staphylococcus aureus*. *J Bacteriol* **97:** 837–847.
Vanittanakom, N., Loeffler, W., Koch, U., and Jung, G. (1986) Fengycin – a novel antifungal lipopeptide antibiotic produced by *Bacillus subtilis* F-29-3. *J Antibiot (Tokyo)* **39:** 888–901.
Vollmer, W., Joris, B., Charlier, P., and Foster, S. (2008) Bacterial peptidoglycan (murein) hydrolases. *FEMS Microbiol Rev* **32:** 259–286.
Wilmes, M., Cammue, B.P., Sahl, H.G., and Thevissen, K. (2011) Antibiotic activities of host defense peptides: more to it than lipid bilayer perturbation. *Nat Prod Rep* **28:** 1350–1358.
Wu, T., McCandlish, A.C., Gronenberg, L.S., Chng, S.S., Silhavy, T.J., and Kahne, D. (2006) Identification of a protein complex that assembles lipopolysaccharide in the outer membrane of *Escherichia coli*. *Proc Natl Acad Sci USA* **103:** 11754–11759.
Yang, Y.L., Xu, Y., Straight, P., and Dorrestein, P.C. (2009) Translating metabolic exchange with imaging mass spectrometry. *Nat Chem Biol* **5:** 885–887.
Youngman, P., Perkins, J.B., and Losick, R. (1984) Construction of a cloning site near one end of Tn917 into which foreign DNA may be inserted without affecting transposition in *Bacillus subtilis* or expression of the transposon-borne erm gene. *Plasmid* **12:** 1–9.

Supporting information

Additional supporting information may be found in the online version of this article.

Please note: Wiley-Blackwell are not responsible for the content or functionality of any supporting materials supplied by the authors. Any queries (other than missing material) should be directed to the corresponding author for the article.

Supplemental data

Quantification of the relative contribution of SdpI and σ^W to SDP resistance *in vivo*

We investigated the relative contributions of σ^W and SdpI to protection against endogenously produced SDP by spotting wild type (PY79) or *sdpABC* (EH273) mutant strains on lawns of wild type, *sigW* (ALB1039), *sdpABCIR* (ALB1088), and *sigW sdpABCIR* (ALB1142) double mutant strains. This produces halos of variable diameter and variable clearness surrounding the spot (Fig. S1A). We noted that halos could be obscured by swarming or swimming, and were therefore concerned that killing of bacteria in the lawn might be obscured by movement of bacteria from the spot into the halo. We therefore specifically quantified colony forming units of the lawn bacteria by plating on media containing an antibiotic the lawn bacteria are resistant to (MLS (Δ*sigW*), tetracycline (Δ*sdpABCIR*, Δ*sdpABCIR*Δ*sigW*), or spectinomycin (*wt*)) (Fig.S1B) and we quantified total bacteria on media without antibiotics. This unambiguous assay demonstrated that the *sigW* (ALB1039) single mutation did not reduce survival of the lawn bacteria, whereas the *sdpABCIR* (ALB1088) mutation reduced survival by ~15 fold. However, the absence of both σ^W and SdpI completely abolished survival of the lawn. Thus, SdpI is sufficient for protection against both purified and endogenously produced SDP and σ^W contributes to SDP resistance in the absence of SdpI.

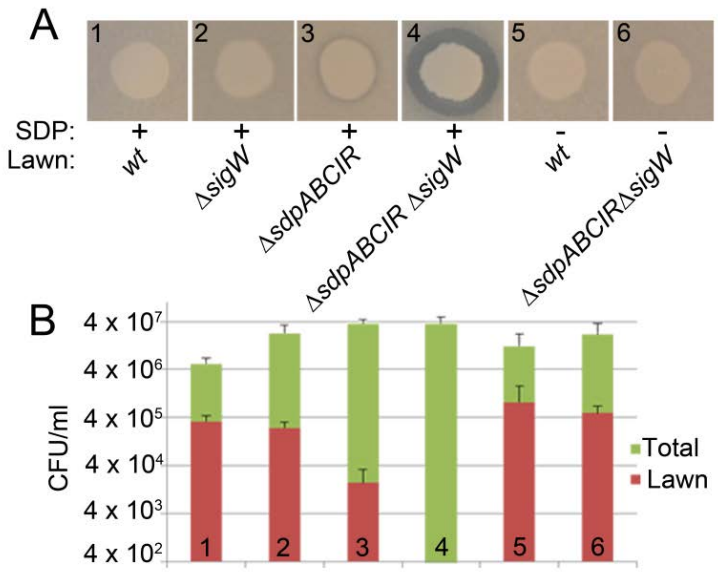

Figure S1: (A) The lawn assay for killing a bacterial lawn of the indicated genotype by spots of wild type (+) or *sdpABC* (EH273) cultures (-). Halos indicative of killing are observed in samples 3 and 4. Lawns were made by mixing 50 µl of exponentially growing cells in LB (OD_{600} = 0.3-0.6) with 3.5 ml 0.35% LB agar and pouring the mixture onto LB plates. After the top agar solidified, 5 µl of exponentially growing cells were spotted on top of the lawn and allowed to dry. The plates were then incubated overnight at 30°C. (B) Survival of the lawn in (A) was quantified by excising an agar plug from the center of each spot with a Pasteur pipet and resuspending the plug in 200 µl 1X T-base. 10-fold serial dilutions were made and spotted on plain LB (to quantify total bacteria) and LB containing the following drugs to quantify survival of the bacteria in the lawn: methicillin-lincomycin (MLS) *(ΔsigW)*, Tetracycline (Δ*sdpABCIR*, Δ*sdpABCIR*Δ*sigW*), or Spectinomycin (*wt*). The total CFU ml^{-1} (green) and lawn CFU ml^{-1} (red) were calculated after incubation. Error bars show the standard deviation of >3 experiments. Numbers on the bars correspond to the spot assays in (A).

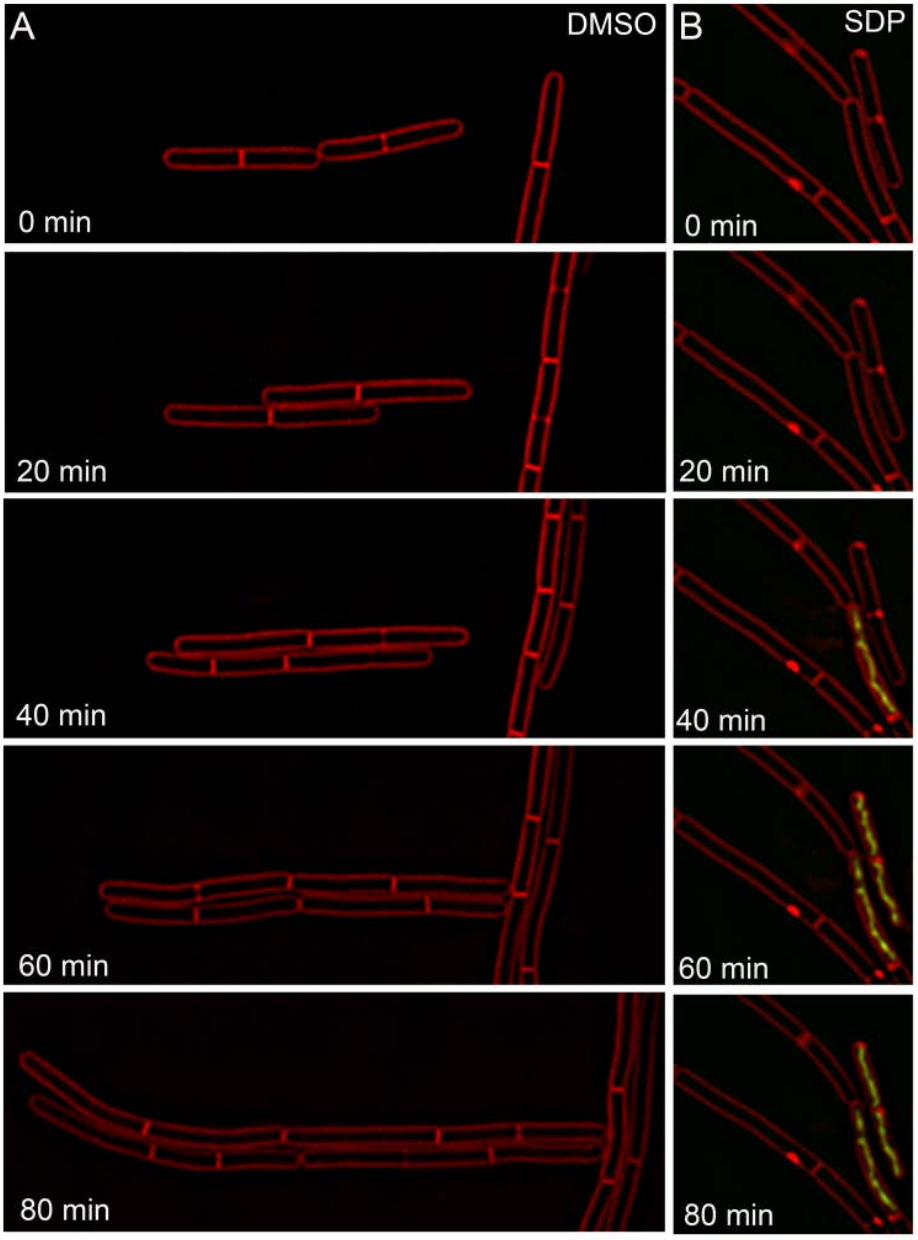

Figure S2: SDP treated cells fail to divide. Timelapse microscopy of PY79 cells treated with DMSO (A) or 20 µg ml^{-1} SDP (B) for 20 min prior to growth on an agarose pad without SDP at 30°C. Cells are stained with FM 4-64 (red) and SYTOX Green (green).

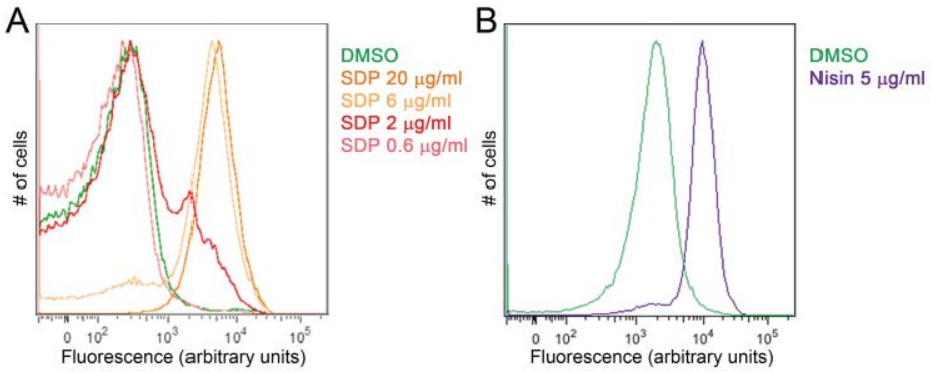

Figure S3: Measurement of PMF collapse using flow cytometry. Flow cytometry assay of $DiBAC_4(5)$ stained *E. coli lptD4213* (NR698) cells. Cells were treated for (A) 60 min with DMSO (green), 20 μg ml^{-1} SDP (dark orange), 6 μg ml^{-1} SDP (light orange), 2 μg ml^{-1} SDP (red), or 0.6 μg ml^{-1} SDP (pink), or for (B) 10 min with DMSO (green), or 5 μg ml^{-1} Nisin (purple) and subjected to flow cytometry. This experiment suggests that the minimum concentration of SDP required to collapse the PMF in most cells (at least temporarily) is 6 μg ml^{-1}.

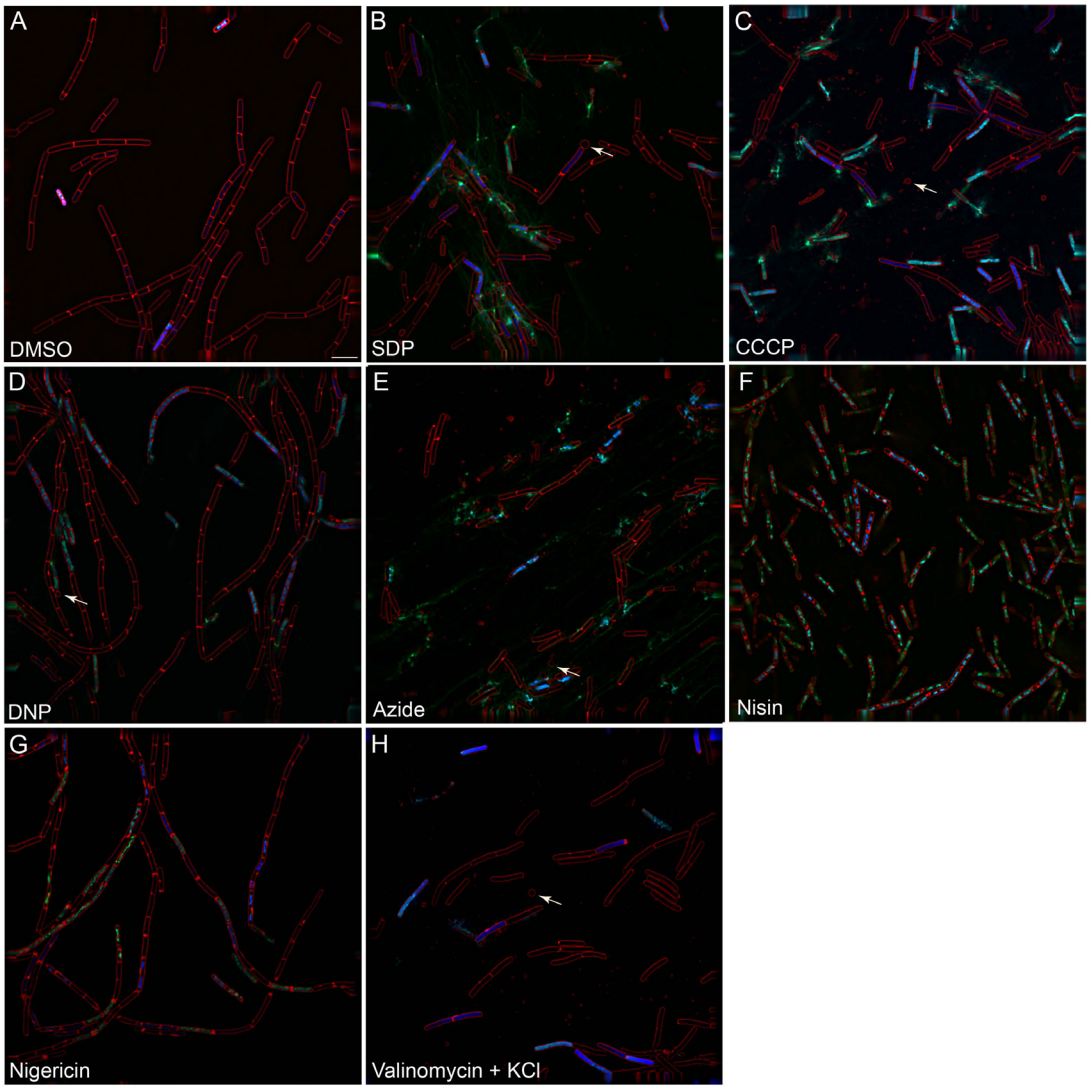

Figure S4: Effects of antibacterial compounds on *B. subtilis* cell architecture. Fluorescence micrographs of cells treated identically to those in Fig. 3. (A) 0.5% DMSO (B) 20 μg ml^{-1} SDP (C) 100 μM CCCP10 (D) 2 mM DNP (E) 10 mM sodium azide (F) 10 μg ml^{-1} nisin (G) 62.5 μM nigericin (H) 125 μM valinomycin with 200 mM KCl for 2 hr (A-E, G-H), or 1 hr (F). Cells are stained with FM 4-64 (red), DAPI (blue), and SYTOX Green (green), as in Fig. 1. Arrows indicate membrane vesicles. Scale bar represents 5 μm.

Table S1: Effect of different concentrations of SDP on viability[1] of *B. subtilis* strain PY79[2]				
	CFU (t_x)/CFU^C(t_0)			
Treatment	0 hr	1 hr	0 hr	1 hr
DMSO	1.0	1.0	1.0	1.13
SDP 20 µg ml^{-1}	0.29	1.52 x 10^{-4}	0.43	1.33 x 10^{-5}
SDP 10 µg ml^{-1}	0.91	7.14 x 10^{-4}	0.83	0.80
SDP 5 µg ml^{-1}	1.14	0.62	0.90	0.90

[1]Viability was determined as described in the materials and methods section of the main paper.
[2]Two separate experiments were shown. In the first (left), the MIC was 10 µg ml^{-1}, whereas in the second (right), the MIC was 20 µg ml^{-1}.

Chapter 3, in full, is a reprint of the material as it appears in *Molecular Microbiology* 2012 (Vol. 84(3) pp. 486-500) and in the online supplement. I was the primary author of this work, conducted all the experiments and made all of the figures.

Chapter 4

Application of cytological profiling to molecules with unknown mechanisms of action

A. Abstract

Recent advances in natural product discovery have led to the isolation of a plethora of new potentially bioactive natural products, many from interspecies interactions. However, current technology for mechanism of action (MOA) determination is not high-throughput enough to keep up with the rate at which natural products are being isolated. This creates a bottleneck at the step of MOA determination, which is crucial for understanding the role of these molecules in interspecies interactions, or their potential as an antibiotic. Cytological profiling using fluorescence microscopy was previously applied to determine the MOA of the cannibalistic toxin SDP in *B. subtilis*. I here utilize cytological profiling on several newly isolated natural products with unknown MOAs: a bromoalterochromide, spirohexenolide A, chlorothricin, and stenothricin. I found that cytological profiling can easily distinguish between the effects of each natural product, but only one of the four possessed an easily distinguishable MOA. This molecule, a bromoalterochromide, exhibited a cytological profile indistinguishable from nisin, and thus I conclude that it acts through a MOA of pore formation. Testing of a crude extract from the *Pseudoalteromonas sp.* that produces the bromoalterochromide revealed a cytological profile the same as the bromoalterochromide. Although the MOA of most of the natural products could not be identified, this study shows that with a large enough range of control compounds, cytological profiling will be a viable method of MOA determination, with applications as early in the process of natural product discovery as the screening of crude extracts for antimicrobial activity.

B. Introduction

Microbes have long been a source of natural products with useful bioactive properties, such as those used as antibiotics. In recent years, innovations in sequencing technologies have allowed rapid sequencing of whole genomes, and mining of these genomes has resulted in the realization that the genetic potential for natural product production in microbes is almost limitless (1-3). The number of molecules that a single microbe can produce is staggering. A good representative of this fact is *Streptomyces coelicolor* A3(2). Analysis of the genome sequence of *S. coelicolor* revealed 30 gene clusters predicted to produce natural products, only a fraction of which had been characterized (1). The collection of small molecules produced by a species has been termed the parvome (from the Latin *parvus* for small) (4, 5). The molecules that comprise the parvome function in all aspects of microbial life, including biofilm formation, cell differentiation, and interspecies signaling or competition (4-8).

New ways to identify these small molecules in the context of a colonies or interspecies interactions have been made possible through recent advancements in mass spectrometry (MS) techniques such as MALDI-TOF IMS (matrix assisted laser desorption ionization-time of flight imaging mass spectrometry) and nanoDESI (nano-spray desorption electrospray ionization) (9, 10). MS data can be accompanied with bioinformatics techniques to determine the identity of each ion observed during MS data collection and has led to the isolation and structural characterization of a plethora of new potentially bioactive compounds (11, 12). These new molecules have been

isolated because they either are known to have interesting bioactive properties or because their distribution in an interspecies interaction implies bioactive properties. However, the role of many of these molecules in interspecies interactions remains unclear. Indeed, even for those compounds that inhibit the growth of competing species, a bottleneck remains in identifying their specific cellular target or their mechanism of action (MOA). Determination of a MOA can provide a variety of clues as to the function of the molecule in the environment, as well as its potential for development as an antibiotic. With so many new molecules being isolated, there is a need for a simple and high-throughput method for quickly determining the MOA of these molecules in a way that utilizes a minimal amount of compound. This would allow molecules of particular interest to be identified as quickly as possible so they can be pursued further.

A microscopy-based method of MOA determination has been effectively demonstrated in eukaryotic cells utilizing microscopy of cells with various stains as an output (13, 14). These stains allow for the measurement of the effects of drugs on variables including, but not limited to, DNA content, organelle shape and size, microtubule architecture and protein synthesis. This data can then be quantified and compared to that of cells treated with compounds with known MOAs. If the data from a compound matches to the data of a control compound, then a MOA can be assigned and more targeted studies performed (13, 14). This method, termed cytological profiling, is high-throughput and is attractive as a method to be adapted for use with prokaryotes. In Chapter 3, I used cytological profiling in *Bacillus subtilis* to determine the MOA of the cannibalistic toxin sporulation delaying protein (SDP) produced by *B.*

subtilis. Through the use of high magnification and resolution fluorescence microscopy to compare the effects of SDP on cell architecture to the effects of other antibiotics, in conjunction with traditional PMF assays, I showed that SDP acts by collapsing the PMF of susceptible Gram-positive species. These studies demonstrated that cytological profiling works on *B. subtilis* cells as well as eukaryotic cells, given a microscopy system of sufficient resolution and a robust method to keep cells alive during imaging, which is non-trivial in bacteria.

I here apply this powerful technique to the study of several interesting molecules. The first is a bromoalterochromide produced by a *Pseudoalteromonas sp.* isolated from a soft coral (Fig. 4.1). Bromoalterochromides were first isolated from *Pseudoalteromonas maricaloris* and are commonly produced by *Pseudoalteromonas sp,* but so far as we know, they have not been tested for activity against bacteria (15, 16). The second molecule is spirohexenolide A, a spirotetronate antibiotic produced by *Streptomyces platensis* that has shown both anti-tumor and anti-bacterial activities (Fig. 4.1) (17). The third is chlorothricin, another member of the spirotetronate family that early results suggested inhibits bacterial pyruvate carboxylase and potentially interacts with phospholipid tails in the membrane (Fig. 4.1) (18, 19). Lastly, I look at stenothricin, a lipopeptide first isolated and characterized from *Streptomyces griseus* (20), and produced by some *Bacillus* isolates (21). The stenothricin we test (Fig. 4.1), is one of three species of stenothricins that differ in lipid chain length isolated from *Streptomyces roseosporus*, which also produces the antibacterial compound arylomycin and the clinically relevant antibiotic daptomycin (11). The cytological profiling of these molecules demonstrates the technique's ability to easily distinguish

the effect of the molecules, although there is not yet enough data to identify the MOA of all the molecules.

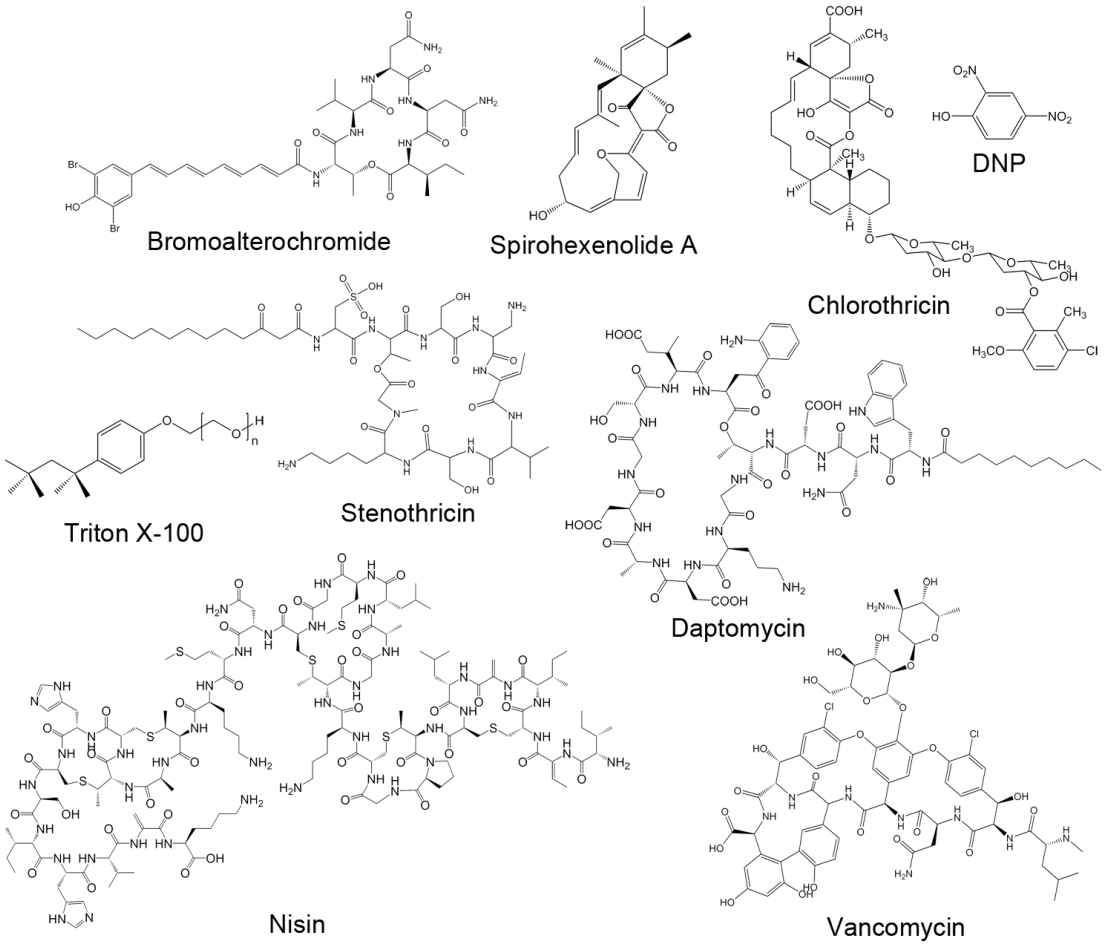

Figure 4.1 Structures of compounds used in this study.

C. Materials and Methods

Strains and culture conditions

The strains used in this chapter are PY79, a prototrophic *B. subtilis* laboratory strain (22) and *Escherichia coli* NR698 (23), a MC4100 *lptD* mutant also referred to as *imp4213* in the literature. All *B. subtilis* cultures were grown in LB medium at 37˚C, except for cultures to be treated with daptomycin, which were supplemented

with 50 μg/ml $CaCl_2$. *E. coli lptD* cultures were grown in LB at 30˚C. Stock solutions of compounds were prepared using the following concentrations and solvents: 9 mg/ml bromoalterochromide (100% DMSO), 22 mg/ml OT59 extract (100% DMSO), 500 μg/ml nisin (10% DMSO, Sigma), 400 mM DNP (100% DMSO, Sigma), 10 mM spirohexenolide A (100% DMSO, purified as described in(17)), 5 mg/ml chlorothricin (100% DMSO, Santa Cruz Biotechnology), 5 mg/ml vancomycin (water, Sigma), 5 mg/ml daptomycin (water, Cubist), 100% Triton X-100 (Sigma), 400 μg/ml stenothricin (10% DMSO). Stenothricin and the bromoalterochromide were provided by the lab of Dr. Pieter Dorrestein; Spirohexenolide A was provided by the lab of Dr. Michael Burkart.

Fluorescence microscopy

For the bromoalterochromide studies, cells were cultured for fluorescence microscopy as described in (24). Compounds were used at the following final concentrations: 0.83% DMSO, 75 μg/ml, 25 μg/ml, or 8.3 μg/ml bromoalterochromide (as indicated), 1.1 mg/ml OT59 crude extract, 10 mM DNP, 10 μg/ml, 3 μg/ml, or 1 μg/ml nisin (as indicated). 15 μl concentrated cultures were incubated in 1.7 ml tubes in a roller at 37˚C. Samples were collected for imaging at 20 minutes. 3 μl of cells were added to 0.75 μl of a stain mix containing 30 μg/ml FM 4-64, 2.5 μM SYTOX green and 1.2 μg/ml DAPI prepared in 1X T-base. Cells were immobilized on an agarose pad (10% LB, 1% agarose, 0.375 μg/ml FM 4-64, 0.025 μg/ml DAPI) prior to microscopy. DAPI images were collected, but are not shown.

For the spirotetronate studies *E. coli lptD* cells were cultured overnight in LB, and the culture was diluted 1:100 to inoculate 20 ml LB in a flask at 30˚C. 100-500 μl

of culture were then transferred to a 13 mm glass test tube and the appropriate amount of compound added. Compounds were used at the following final concentrations (5X the MIC, except for DMSO): 2.5% DMSO, 250 μM spirohexenolide A, 10 μg/ml chlorothricin, 2.5 μg/ml nisin. Tubes were incubated at 30˚C in a roller. Samples were stained with 1 μg/ml FM 4-64, 2 μg/ml DAPI and 0.5uM SYTOX green, then spun down and concentrated ~10X prior to collecting for imaging at 30 and 120 minutes. Cells were immobilized on an agarose pad (20% LB, 1.2% agarose) prior to microscopy.

B. subtilis cells were cultured for fluorescence microscopy as follows. Cells were cultured in LB at 37˚C in a flask until 0.2 OD_{600}. 100-500 μl of culture were then transferred to a 13 mm glass test tube and the appropriate amount of compound added. Compounds were used at the following final concentrations (5x the MIC, except for DMSO): 0.6% DMSO, 60 μM spirohexenolide A, 62.5 μg/ml chlorothricin, 7.5 mM DNP, 10 μg/ml nisin. Tubes were incubated at 37˚C in a roller. Samples were collected for imaging at 20 minutes and 60 minutes, concentrated approximately 10 times, and 3 μl of concentrated cells were added to 0.75 μl of the stain mix listed above. Cells were immobilized on an agarose pad (10% LB, 1% agarose, 0.375 μg/ml FM 4-64, 0.025 μg/ml DAPI) prior to microscopy.

For the stenothricin studies, cells were cultured for fluorescence microscopy as follows. A pre-culture was grown to ~0.2-0.4 OD_{600} for *B. subtilis* or to saturation for *E.coli lptD*, then diluted 1:100 into 20 ml LB. For cultures to later be treated with daptomycin, 90 μl of 100 mM $CaCl_2$ was added at this stage (final concentration 50 μg/ml). Flasks were incubated at 37˚C until 0.2 OD_{600}. Cultures were then mixed with

the appropriate amount of compound. Compounds were used at the following final concentrations: 0.5% DMSO, 20 μg/ml, 10 μg/ml, 5 μg/ml, or 2 μg/ml stenothricin (as indicated), 1.5 μg/ml vancomycin, 0.1% or 0.5% Triton X-100 (as indicated), 6 μg/ml nisin, 10 μg/ml daptomycin. 15 μl of treated cells were transferred into a 1.7 ml tube and incubated at 37˚C in a roller. Samples were collected for imaging at 20 minutes. 6 μl of cells were added to 1.5 μl of dye mix (described above) and immobilized on an agarose pad (20% LB, 1.2% agarose, 0.375 μg/ml FM 4-64, 0.025 μg/ml DAPI) prior to microscopy.

All microscopy was performed on an Applied Precision Spectris microscope as described in (25). Images were deconvolved using softWoRx V 5.5.1 and the medial focal plane shown. In figure 4.5, SYTOX intensity in the SYTOX intensity panels was normalized within the figure, and in figure 4.6, the DAPI and SYTOX green images were normalized within the figure based on intensity and exposure length relative to the treatment with the highest fluorescence intensity.

Viable cell counts

Viable cell counts were obtained through dilution and plating of cells from the same culture as those subjected to microscopy. Ten-fold serial dilutions were made at the indicated time in 1X T-base and spotted onto LB plates. Colonies were counted after growth and colony forming units (CFU) per ml calculated. Shown is the ratio of CFU at time x [$CFU(t_x)$] to CFU of the control at t_0 [$CFU^c(t_0)$]. Graphs with error bars indicate the standard error of at least three separate experiments.

D. Results

Cytological profiling of a bromoalterochromide

The bromoalterochromides are a structurally unique family of compounds that has not been tested for activity against bacteria, and thus no MOA data is available (15, 16). To determine the MOA of the bromoalterochromide purified from a *Pseudoalteromonas sp.* by Pieter Dorrestein's lab, we employed cytological profiling in conjunction with viable cell counts to determine the minimal concentration necessary to affect growth and viability. Concentrated *B. subtilis* cultures were treated with different amounts of the molecule, fluorescence microscopy was performed to examine the physiological effects it had on cell morphology, and viable cell counts were used to determine if cell death was induced at the different concentrations. Treatment with 75 μg/ml of the bromoalterochromide resulted in a greater than 3-log drop in viability at the initial timepoint (0 hr) (Fig. 4.2A squares). Treatment with 25 μg/ml resulted in an initial drop of viability of only 1-log, but a drop of over 3-logs by one hour (Fig 4.2A circles). The 3-log drop in viability might have occurred on a shorter timescale than an hour, but due to the small quantities of the bromoalterochromide, and its extreme sensitivity to light and oxidation, only a limited number of experiments could be performed and I was unable to test viability at a timepoint between zero and one hour. Treatment at 8.3 μg/ml resulted in an initial viability drop similar to than seen with a concentration of 25 μg/ml, but with rapid recovery (Fig 4.2A asterisks). Thus, under the conditions tested, the minimal bactericidal concentration (MBC) of the bromoalterochromide was 25 μg/ml.

Cells treated with the bromoalterochromide at 3X the MBC (75 μg/ml) were uniformly permeabilized to SYTOX green within 20 minutes and possessed aberrant

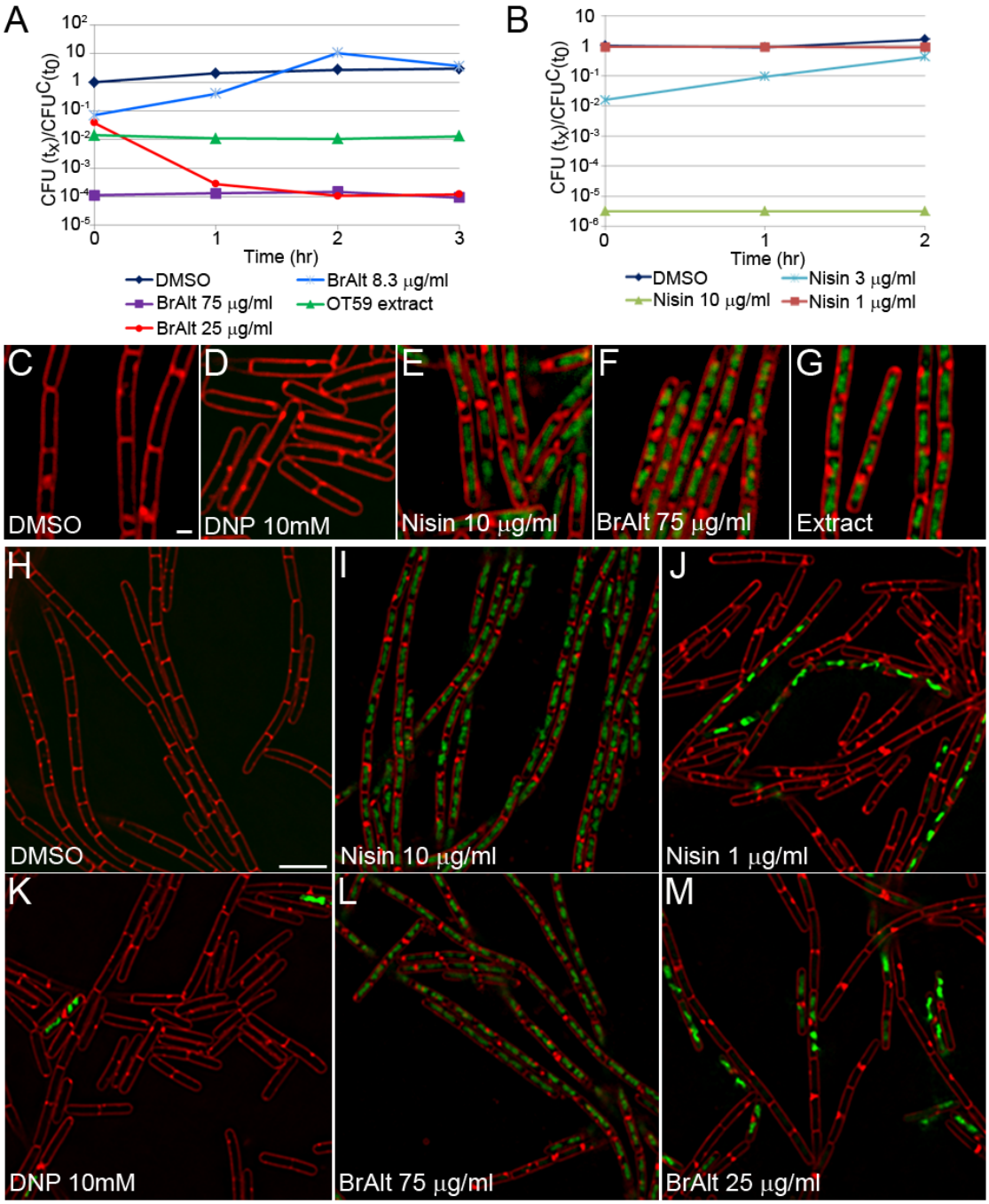

Figure 4.2 Effects of the bromoalterochromide and other antimicrobials on *B. subtilis* viability and cell architecture. (A) Effects of different amounts of bromoalterochromide and 1.1 mg/ml OT59 crude extract on PY79 cell viability. (B) Effects of different amounts of nisin on PY79 cell viability. Cell viability is shown as the ratio of colony-forming units (CFU) at the indicated time and treatment to the CFU at t_0 for the control (CFU^C). C-M Fluorescence micrographs of growing PY79 cells treated with (C,H) 0.83% DMSO (D,K) 10 mM DNP (E,I) 10 μg/ml nisin (F,L) 75 μg/ml bromoalterochromide (G) 1.1 mg/ml OT59 crude extract (J) 1 μg/ml nisin (M) 25 μg/ml bromoalterochromide for 20 min. Cells are stained with FM 4-64 (red), and SYTOX green (green). SYTOX green is membrane impermeable and only stains cells with compromised membranes. Scale bar represents 1 μm (A) or 5 μm (H).

septa and membrane blobs identical to those seen in cells treated with nisin (Fig 4.2F,L). The only other compound tested so far, other than nisin, that induced uniform SYTOX green permeability is the detergent Triton X-100 (Fig 4.6K,L), but this produces large internal membrane accumulations seen in neither nisin nor bromoalterochromide treated cells. The viability curves were also similar to nisin, since cells treated with both compounds at 3X above the MBC were rendered inviable within the first few minutes (Fig 4.2A squares, B triangles). Treatment with a lower concentration of the bromoalterochromide (25 μg/ml) resulted in only a fraction of the cells becoming permeabilized to SYTOX green within 20 minutes (Fig 4.2M), similar to the pattern seen with a low concentration of nisin (Fig 4.2J). These similarities suggest that the bromoalterochromide acts in a manner similar to nisin, rapidly forming pores in the membrane large enough for SYTOX green (MW = ~600) to pass through.

Mechanism of action determination from a crude extract

Purification of a compound is a lengthy and expensive process. We therefore tested whether the MOA of a compound of interest could be determined directly from a crude extract, allowing the processes of MOA determination and activity guided purification to occur simultaneously. Concentrated cultures were treated with a crude extract from the *Pseudoalteromonas sp.* that produces the bromoalterochromide. Mass spectrometry in Pieter Dorrestein's lab showed that this extract contained the bromoalterochromide, as well as a variety of other bromoalterochromides and several other molecules (Fig 4.3). Cells treated with this crude extract looked identical to those treated with the bromoalterochromide alone (Fig 4.2G) and exhibited the full

extent of the viability drop at the initial timepoint (Fig 4.2A triangles), thus giving validity to the idea of using crude extracts in cytological profiling to screen for molecules of interest.

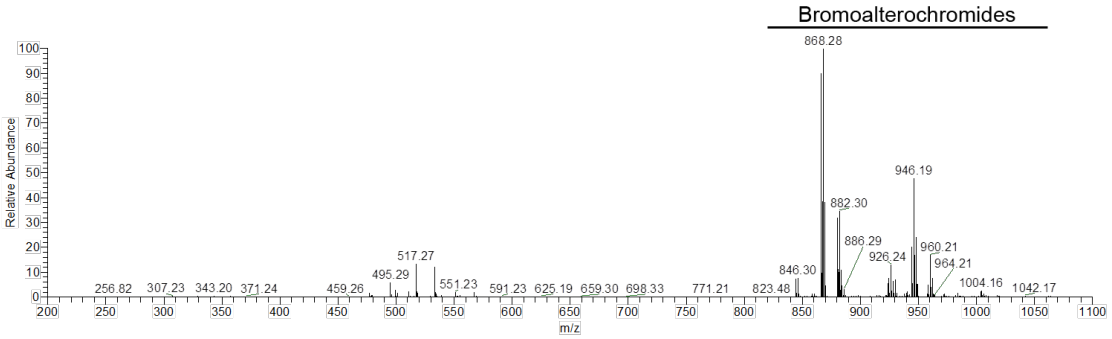

Figure 4.3. Mass spectra of OT59 crude extract

Cytological profiling of spirotetronate compounds

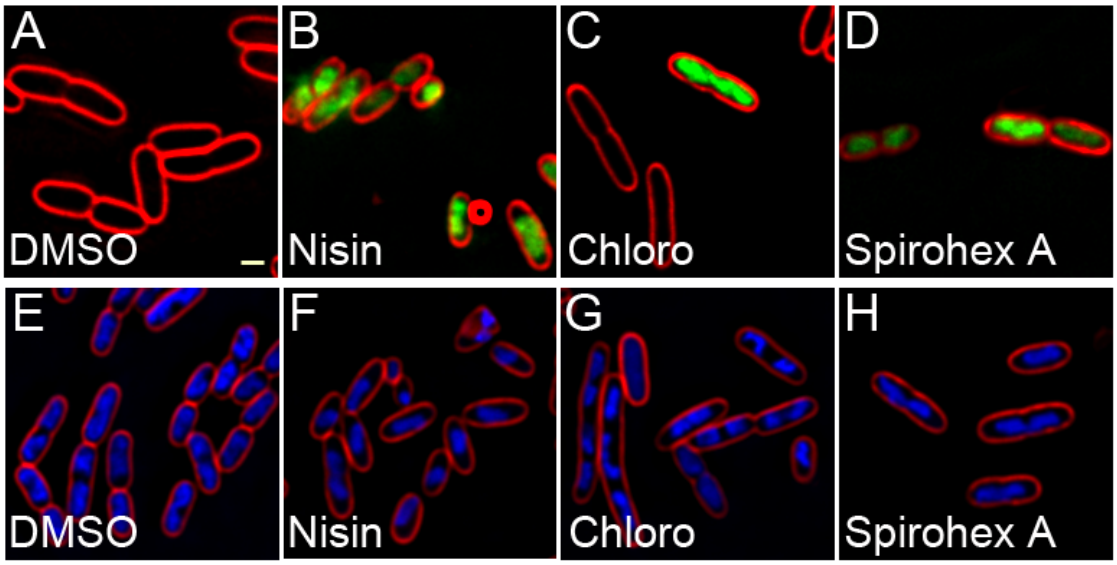

Figure 4.4 Effects of antimicrobials on *E. coli* cell architecture. A-H Fluorescence micrographs of growing *E. coli lptD* cells treated with (A,E) 2.5% DMSO (B,F) 2.5 µg/ml nisin (C,G) 10 µg/ml chlorothricin (D,H) 250 µg/ml spirohexenolide A for 30 min (A-D) or 2h (E-H). Cells are stained with FM 4-64 (red) and SYTOX green (green, A-D) or DAPI (blue, E-H). Scale bar represents 1 µM.

The spirotetronate antibiotics are a class of antibiotics effective against Gram-positive bacteria. Chlorothricin is the only member with proposed MOAs, inhibition

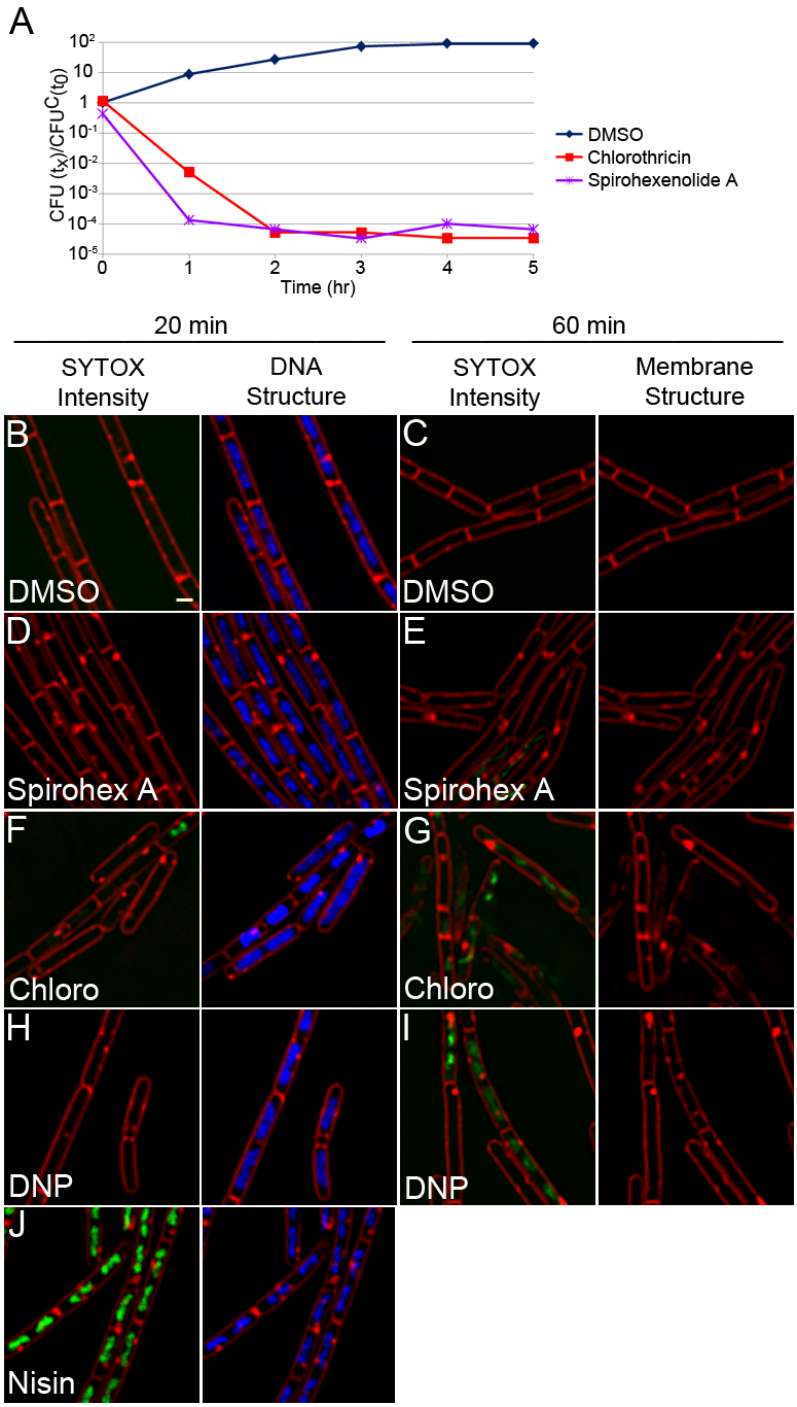

Figure 4.5 Effects of antimicrobials on *B. subtilis* viability and cell architecture. (A) Effects of chlorothricin and spirohexenolide A on PY79 viability. Cell viability is shown as the ratio of colony-forming units (CFU) at the indicated time and treatment to the CFU at t_0 for the control (CFU^C). B-J. Fluorescence micrographs of growing PY79 cells treated with (B,C) 0.6% DMSO (D,E) 60 µM spirohexenolide (F,G) 62.5 µg/ml chlorothricin (H,I) 7.5 mM DNP (J) 10 µg/ml nisin for 20 min (B,D,F,H,J) or 60 min (C,E,G,I). Cells are stained with FM 4-64 (red) and DAPI (blue, DNA structure panels) or SYTOX green (green, SYTOX Intensity panels). SYTOX green is membrane impermeable and only stains cells with compromised membranes. Scale bar represents 1 µm.

of pyruvate carboxylase (26, 27) and interaction with the hydrophobic tails of phospholipids in the membrane (19). However, pyruvate carboxylase inhibition is unlikely to be the mechanism by which chlorothricin kills bacteria in LB, since the enzyme is not necessary for growth in rich medium (28). Poochit Nonejuie in Joe Pogliano's lab performed cytological profiling of spirohexenolide A and chlorothricin using the *E. coli lptD* mutant (also referred to as *imp4213*). The results at an early timepoint (30 minutes) indicated that both seemed to act in a manner similar to nisin, rapidly permeabilizing many of the cells to SYTOX Green (Fig 4.4B-D).

To further investigate and validate the MOA of spirohexenolide A and chlorothricin, I conducted cytological profiling in *B. subtilis* using exponentially growing cells in conjunction with viable cell counts of the cultures. After spirohexenolide A and chlorothricin treatment at 5X the MIC, viability dropped less than a log initially, with additional drops of 4-logs by one hour (Fig 4.5A asterisks and squares). This is in contrast to nisin treated cells, which are rendered inviable by the initial timepoint (Fig 4.6B Xs). Thus, both compounds take longer to kill *B. subtilis* cells than nisin.

Cytological profiling demonstrated that cells treated with spirohexenolide A at 5X the MIC showed no SYTOX green permeability at 20 minutes, and very little by one hour (Fig 4.5D,E), in contrast to cells treated with nisin, which are uniformly permeabilized within 20 minutes (Fig 4.5J). Additionally, no lysis was observed in the spirohexenolide A treated cells (Fig 4.5E), in contrast to cells treated with either nisin or with any compound that collapses the PMF (Fig 4.5I). The spirohexenolide A-treated cells appeared somewhat elongated at both timepoints, and they contained

membrane vesicles somewhat smaller than those observed in vancomycin-treated cells (Fig 4.5D,E). Treatment with higher concentrations of spirohexenolide A did not produce a more rapid loss of viability or an increase in the number of cells permeabilized to SYTOX green (not shown). Furthermore, although spirohexenolide A collapsed the PMF of *E. coli lptD* within 10 minutes of treatment (not shown), I was unable to demonstrate a PMF collapse in *B. subtilis* cells under our assay conditions (data not shown). These data suggest that spirohexenolide A kills *B. subtilis* cells by a different mechanism than that demonstrated for *E. coli* (production of membrane channels). Further experiments are required to identify the MOA in *B. subtilis*.

Treatment of exponentially growing *B. subtilis* with 5X the MIC of chlorothricin resulted in 34% of the cells being permeabilized to SYTOX green (Fig 4.5G); treatment with chlorothricin at 10X the MIC did not increase permeabilization (not shown). Chlorothricin treated cells also produced membrane blobs, mostly at newly initialized septa and near the cell poles after 20 minutes of treatment (Fig 4.5F). Many of the permeabilized cells had begun lysing by one hour in a manner similar to cells treated with compounds that collapse the PMF (Fig 4.5G), although the lysis occurred at an earlier timepoint than we see with PMF collapsing compounds such as DNP. Thus, chlorothricin causes rapid permeabilization of a fraction of the cells, and the remaining cells are elongated with membrane vesicles, ultimately undergoing autolysis. This combination of cytological effects is unlike other compounds I have tested so far.

A previous study demonstrated that in model membranes chlorothricin interacts with the hydrocarbon chains of the phospholipids and thus one of the

mechanisms of chlorothricin might be targeted at the membrane (19), which could account for the lysis. The cells showed a mixture of permeabilized cells with compacted DNA and non-permeabilized cells with fairly diffuse DNA at 20 minutes and an hour (Fig 4.5F,G), indicating the possibility of a dual MOA. Interestingly, heterogeneity of cell size is seen with *E. coli lptD* after two hours of treatment (Fig. 4.4G), suggesting that the compound might have a dual MOA in both species.

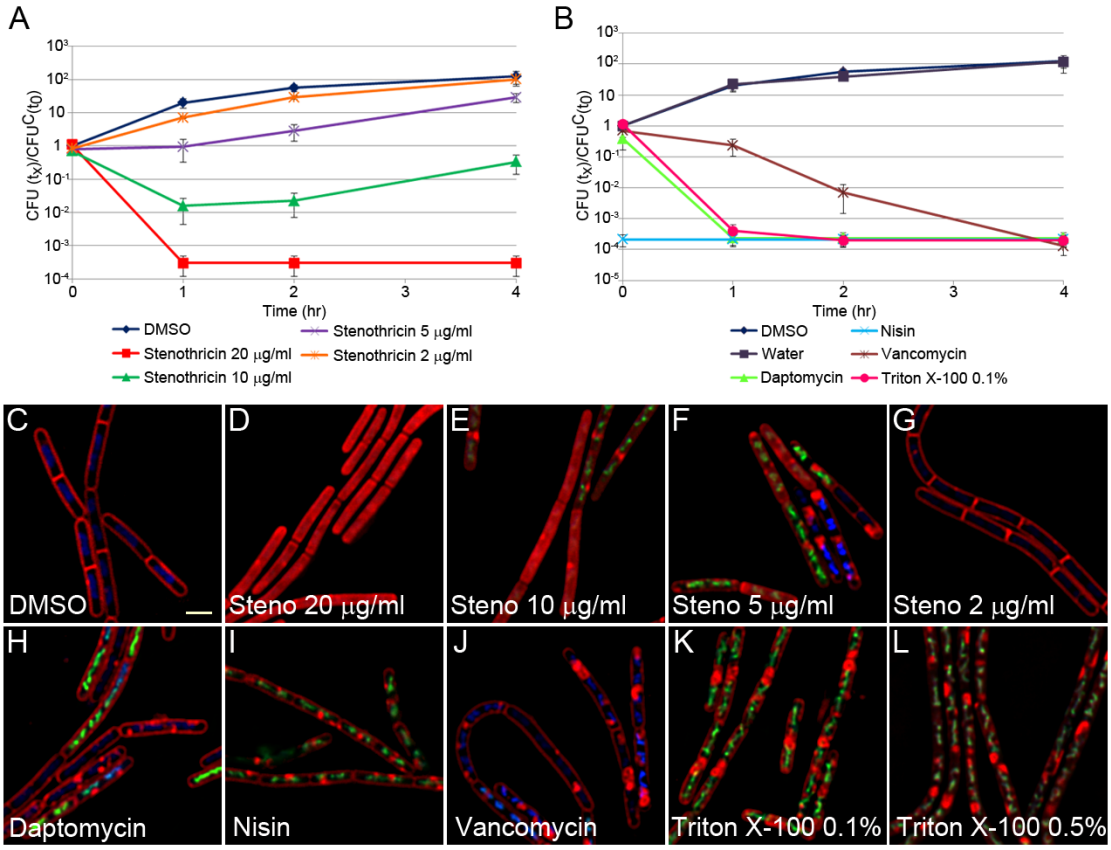

Figure 4.6 Effects of stenothricin and other antimicrobials on *B. subtilis* viability and cell architecture. (A) Effects of different amounts of stenothricin on PY79 cell viability. (B) Effects of control treatments on PY79 viability. Cell viability is shown as the ratio of colony-forming units (CFU) at the indicated time and treatment to the CFU at t_0 for the control (CFU^C). Error bars show the standard error of ≥3 experiments. C-L Fluorescence micrographs of growing PY79 cells treated with (C) 0.5% DMSO (D) 20 μg/ml stenothricin (E) 10 μg/ml stenothricin (F) 5 μg/ml stenothricin (G) 2 μg/ml stenothricin 1132 (H) 10 μg/ml daptomycin (I) 6 μg/ml nisin (J) 1.25 μg/ml vancomycin (K) 0.1% Triton X-100 (L) 0.5% Triton X-100 for 20 minutes. Cells are stained with FM 4-64 (red), DAPI (blue), and SYTOX green. SYTOX green is membrane impermeable and only stains cells with compromised membranes. Scale bar represents 2 μm.

Cytological profiling of stenothricin

The only previous publication on stenothricin (20) failed to detect activity against their *B. subtilis* strain in a filter disk assay (20), but we were able to see activity under our conditions. Specifically, we found that treatment of cells with 20 μg/ml stenothricin caused viability to irreversibly drop 3 logs by one hour, while treatment with 10 μg/ml caused a transient drop in viability, and 5 μg/ml caused a slight lag in growth (Fig 4.6A). Clearly, stenothricin is bactericidal to *B. subtilis* cells, in contrast to the early publication. It remains unclear if this is due to a difference in the chemical structures of the stenothricin, the *B. subtilis* strains, or a lack of sensitivity in the previously used disk assay.

We next performed cytological profiling of stenothricin on exponentially growing microcultures of *B. subtilis*. Treatment with 20 μg/ml stenothricin for 20 minutes resulted in cells with membrane staining throughout the cell and compact chromosomes that weakly stained with DAPI and SYTOX green (Fig 4.6D). Weak DNA staining is generally observed when the cells are especially damaged and there is much debris from lysis. The weak staining could be due to low concentrations of DNA due to diffusion of degradation, or the properties of DNA binding of the dyes when the cell has equilibrated with the outside environment. The membrane staining throughout the cell appears to be due to detachment of the cell membrane from the peptidoglycan and possible solubilization of the membrane, since the cells appear smaller and the septa are unstained. As the concentration of stenothricin is lowered, viability drops less, producing a transient growth arrest at 5 μg/ml (Fig 4.6A Xs). At this concentration, the majority of cells have lost the cytoplasmic membrane staining

phenotype. Instead, they are permeabilized to SYTOX and show large membrane blobs and internal vesicles (Fig 4.6F), similar to those seen with vancomycin and detergent treatment (Fig 4.6J-L). These cells are growth arrested but have not undergone the greater than a log drop in viability seen at the higher concentrations, so it is not clear if these cytological effects represent the lethal effect of stenothricin. We also compared stenothricin treated cells to those treated with another antibiotic produced by the same species, daptomycin, at 3X the MIC and found that daptomycin produced elongated cells containing small membrane vesicles, with some of the cells permeabilized to SYTOX (Fig 4.6H).

None of the compounds I have tested so far, nor any tested by Poochit Nonejuie in his systematic tests in *E. coli*, produce cells with membrane staining throughout the cell as seen in the 20 μg/ml stenothricin treated cells (Fig 4.6D). Indeed, levels of detergent (Triton X-100) higher than the bactericidal concentration produce in patchy membrane throughout the cell (Fig 4.6L), rather than the consistent levels seen in cells treated with 20 ug/ml stenothricin. However, we need to profile a cationic detergent, since stenothricin is a cationic lipopeptide, while triton is nonionic. Thus, my studies to date suggest that stenothricin has a unique MOA.

E. Discussion

This study demonstrates the potential of cytological profiling for MOA determination in bacteria, however the technique it is still in its infancy. We were able to demonstrate that the MOA of a bromoalterochromide is pore-formation, and we could detect this activity in a crude extract. Identifying activities in crude extracts

could be of great use in the screening of extracts for interesting MOAs, and for guidance during purification. In some cases, an activity might be detectable by cytological profiling at a sub-MIC level of compound that would not be detected in standard activity assays that only take into account growth inhibition. For example, if high enough levels of stenothricin for growth inhibition were not obtained in a crude extract, no activity would be detected, but in our cytological profiling experiments, we were able to see an effect at levels below the bactericidal concentration (Fig. 4.6F). A common screening method is to design screens to detect activity against a specific cellular target, therefore limiting discovery to a narrow range of molecules. However, cytological profiling provides a way to screen for all MOAs in the same assay and to identify some activities prior to purification. Thus, the technique provides a more general screen that will allow the discovery of molecules with new activities against intact bacterial cells.

Although cytological profiling is a powerful technique, it clearly requires additional development. I was only able to unambiguously identify the MOA of one out of the four molecules I tested, however, this is likely due to the youth of the technique and will likely be overcome merely by profiling a larger variety of compounds with known MOAs (an effort underway in both *E. coli* and *B. subtilis*). I am confident that once a large library of control compounds has been screened, the MOA of a much larger fraction of the natural products we are given will be easily identified. This has been successfully done in eukaryotes (13, 14), and though bacteria are less architecturally complex than eukaryotes, we have shown that the effects of different compounds on cell architecture are still easily distinguishable. The resulting

data will provide a reference set against which new compounds can be compared in the future. We can also use our data to eliminate MOAs we have already profiled, still giving us valuable information.

As seen through the examples of spirohexenolide A and chlorothricin, not all compounds have the same effect in different organisms. We've previously found that compounds that collapse the PMF induce autolysis in *B. subtilis*, but *E.coli* does not lyse even though the MOA of the compounds is the same in both species (24). In the case of spirohexenolide A and chlorothricin though, the MOA prediction based on the two species does not agree. At this point in time, we do not know if spirohexenolide A and chlorothricin are exhibiting different MOAs in *E.coli* than in *B. subtilis*, or if it is an artifact of using a strain of *E. coli* with a defective outer membrane. This requires us to be careful in our conclusions, but can also provide a greater level of information to help us tease apart the difference in MOA between compounds. Most of the standard antibiotics we use do have consistent phenotypes between *B. subtilis* and *E. coli lptD*, and thus profiling in both organisms provides a wealth of information. It is obvious from our experience with these new molecules that there is enormous untapped potential out there for molecules that have unique MOAs, many of which could be developed as antibiotics and provide much needed new scaffolds for antibiotic development.

F. References

1. Nett, M., H. Ikeda, and B.S. Moore, Genomic basis for natural product biosynthetic diversity in the actinomycetes. Nat Prod Rep, 2009. **26**(11): p. 1362-84.

2. Zotchev, S.B., O.N. Sekurova, and L. Katz, Genome-based bioprospecting of microbes for new therapeutics. Curr Opin Biotechnol, 2012.

3. Medema, M.H., K. Blin, P. Cimermancic, V. de Jager, P. Zakrzewski, M.A. Fischbach, T. Weber, E. Takano, and R. Breitling, antiSMASH: rapid identification, annotation and analysis of secondary metabolite biosynthesis gene clusters in bacterial and fungal genome sequences. Nucleic Acids Res, 2011. **39**(Web Server issue): p. W339-46.

4. Davies, J. and K.S. Ryan, Introducing the parvome: bioactive compounds in the microbial world. ACS Chem Biol, 2012. **7**(2): p. 252-9.

5. Davies, J., Darwin and microbiomes. EMBO Rep, 2009. **10**(8): p. 805.

6. Shank, E.A. and R. Kolter, New developments in microbial interspecies signaling. Curr Opin Microbiol, 2009. **12**(2): p. 205-14.

7. Straight, P.D. and R. Kolter, Interspecies chemical communication in bacterial development. Annu Rev Microbiol, 2009. **63**: p. 99-118.

8. Lopez, D., H. Vlamakis, and R. Kolter, Biofilms. Cold Spring Harb Perspect Biol, 2010. **2**(7): p. a000398.

9. Yang, J.Y., V.V. Phelan, R. Simkovsky, J.D. Watrous, R.M. Trial, T.C. Fleming, R. Wenter, B.S. Moore, S.S. Golden, K. Pogliano, and P.C. Dorrestein, Primer on agar-based microbial imaging mass spectrometry. J Bacteriol, 2012. **194**(22): p. 6023-8.

10. Watrous, J., P. Roach, T. Alexandrov, B.S. Heath, J.Y. Yang, R.D. Kersten, M. van der Voort, K. Pogliano, H. Gross, J.M. Raaijmakers, B.S. Moore, J. Laskin, N. Bandeira, and P.C. Dorrestein, Mass spectral molecular networking of living microbial colonies. Proc Natl Acad Sci U S A, 2012. **109**(26): p. E1743-52.

11. Liu, W.T., R.D. Kersten, Y.L. Yang, B.S. Moore, and P.C. Dorrestein, Imaging mass spectrometry and genome mining via short sequence tagging identified the anti-infective agent arylomycin in *Streptomyces roseosporus*. J Am Chem Soc, 2011. **133**(45): p. 18010-3.

12. Kersten, R.D., Y.L. Yang, Y. Xu, P. Cimermancic, S.J. Nam, W. Fenical, M.A. Fischbach, B.S. Moore, and P.C. Dorrestein, A mass spectrometry-guided genome mining approach for natural product peptidogenomics. Nat Chem Biol, 2011. **7**(11): p. 794-802.

13. Tanaka, M., R. Bateman, D. Rauh, E. Vaisberg, S. Ramachandani, C. Zhang, K.C. Hansen, A.L. Burlingame, J.K. Trautman, K.M. Shokat, and C.L. Adams, An unbiased cell morphology-based screen for new, biologically active small molecules. PLoS Biol, 2005. **3**(5): p. e128.

14. Perlman, Z.E., M.D. Slack, Y. Feng, T.J. Mitchison, L.F. Wu, and S.J. Altschuler, Multidimensional drug profiling by automated microscopy. Science, 2004. **306**(5699): p. 1194-8.

15. Speitling, M., O.F. Smetanina, T.A. Kuznetsova, and H. Laatsch, Bromoalterochromides A and A', unprecedented chromopeptides from a marine *Pseudoalteromonas maricaloris* strain KMM 636T. J Antibiot (Tokyo), 2007. **60**(1): p. 36-42.

16. Vynne, N.G., M. Mansson, K.F. Nielsen, and L. Gram, Bioactivity, chemical profiling, and 16S rRNA-based phylogeny of *Pseudoalteromonas* strains collected on a global research cruise. Mar Biotechnol (NY), 2011. **13**(6): p. 1062-73.

17. Kang, M., B.D. Jones, A.L. Mandel, J.C. Hammons, A.G. DiPasquale, A.L. Rheingold, J.J. La Clair, and M.D. Burkart, Isolation, structure elucidation, and antitumor activity of spirohexenolides A and B. J Org Chem, 2009. **74**(23): p. 9054-61.

18. Schindler, P.W. and H. Zahner, [Metabolic products of microorganisms. 96. Mechanism of action of the macrolide-type antibiotic, chlorothricin. I. Inhibitor of the pyruvate carboxylase from *Bacillus subtilis*]. Arch Mikrobiol, 1972. **82**(1): p. 66-75.

19. Pache, W. and D. Chapman, Interaction of antibiotics with membranes: chlorothricin. Biochim Biophys Acta, 1972. **255**(1): p. 348-57.

20. Hasenbohler, A., H. Kneifel, W.A. Konig, H. Zahner, and H.J. Zeiler, [Metabolic products of microorganisms. 134. Stenothricin, a new inhibitor of the bacterial cell wall synthesis (author's transl)]. Arch Microbiol, 1974. **99**(4): p. 307-21.

21. Wulff, E.G., C.M. Mguni, K. Mansfeld-Giese, J. Fels, M. Lübeck, and J. Hockenhull, Biochemical and molecular characterization of *Bacillus amyloliquefaciens*, *B. subtilis* and *B. pumilus* isolates with distinct antagonistic potential against *Xanthomonas campestris pv. campestris*. Plant Pathology, 2002. **51**(5): p. 574-584.

22. Youngman, P., J.B. Perkins, and R. Losick, Construction of a cloning site near one end of Tn917 into which foreign DNA may be inserted without affecting

transposition in *Bacillus subtilis* or expression of the transposon-borne erm gene. Plasmid, 1984. **12**(1): p. 1-9.

23. Ruiz, N., B. Falcone, D. Kahne, and T.J. Silhavy, Chemical conditionality: a genetic strategy to probe organelle assembly. Cell, 2005. **121**(2): p. 307-17.

24. Lamsa, A., W.T. Liu, P.C. Dorrestein, and K. Pogliano, The *Bacillus subtilis* cannibalism toxin SDP collapses the proton motive force and induces autolysis. Mol Microbiol, 2012.

25. Liu, N.J., R.J. Dutton, and K. Pogliano, Evidence that the SpoIIIE DNA translocase participates in membrane fusion during cytokinesis and engulfment. Mol Microbiol, 2006. **59**(4): p. 1097-113.

26. Schindler, P.W. and M.C. Scrutton, Mode of action of the macrolide-type antibiotic, chlorothricin. Effect of the antibiotic on the catalytic activity and some structural parameters of pyruvate carboxylases purified from rat and chicken liver. Eur J Biochem, 1975. **55**(3): p. 543-53.

27. Schindler, P.W. and H. Zahner, Mode of action of the macrolide-type antibiotic, chlorothricin. Kinetic study of the inhibition of pyruvate carboxylase from *Bacillus stearothermophilus*. Eur J Biochem, 1973. **39**(2): p. 591-600.

28. Diesterhaft, M.D. and E. Freese, Role of pyruvate carboxylase, phosphoenolpyruvate carboxykinase, and malic enzyme during growth and sporulation of *Bacillus subtilis*. J Biol Chem, 1973. **248**(17): p. 6062-70.

The bromoalterochromide used in chapter 4 was purified in Pieter Dorrestein's lab by Don Nguyen, Xiling Zhao, and Wilna Moree. Stenothricin was purified in Pieter Dorrestein's lab by Wei-Ting Liu. Spirohexenolide A was provided by Mike Burkhart's lab. Poochit Nonejuie provided the *E. coli* cytological profiling data.

Chapter 5

A ribosome-nascent chain sensor of membrane protein biogenesis in *Bacillus subtilis*

The EMBO Journal (2009) 28, 3461–3475 | © 2009 European Molecular Biology Organization | All Rights Reserved 0261-4189/09
www.embojournal.org

THE EMBO JOURNAL

A ribosome–nascent chain sensor of membrane protein biogenesis in *Bacillus subtilis*

Shinobu Chiba[1], Anne Lamsa and Kit Pogliano*

Division of Biological Sciences, University of California, San Diego, CA, USA

Proteins in the YidC/Oxa1/Alb3 family have essential functions in membrane protein insertion and folding. *Bacillus subtilis* encodes two YidC homologs, one that is constitutively expressed (*spoIIIJ/yidC1*) and a second (*yqjG/yidC2*) that is induced in *spoIIIJ* mutants. Regulated induction of *yidC2* allows *B. subtilis* to maintain capacity of the membrane protein insertion pathway. We here show that a gene located upstream of *yidC2 (mifM/yqzJ)* serves as a sensor of SpoIIIJ activity that regulates *yidC2* translation. Decreased SpoIIIJ levels or deletion of the MifM transmembrane domain arrests *mifM* translation and unfolds an mRNA hairpin that otherwise blocks initiation of *yidC2* translation. This regulated translational arrest and *yidC2* induction require a specific interaction between the MifM C-terminus and the ribosomal polypeptide exit tunnel. MifM therefore acts as a ribosome–nascent chain complex rather than as a fully synthesized protein. *B. subtilis* MifM and the previously described secretion monitor SecM in *Escherichia coli* thereby provide examples of the parallel evolution of two regulatory nascent chains that monitor different protein export pathways by a shared molecular mechanism.

The EMBO Journal (2009) **28,** 3461–3475. doi:10.1038/emboj.2009.280; Published online 24 September 2009
Subject Categories: membranes & transport; proteins
Keywords: membrane protein insertion; Oxa1p/Alb3/YidC; ribosome; SecM; translational regulation

Introduction

Approximately 30% of cellular proteins are translocated across or inserted into the membrane using a conserved and essential membrane translocation apparatus. In the Eubacteria, movement of proteins across the membrane depends on three integral membrane proteins that assemble a protein-conducting channel, SecY and SecE, which are present in all cells, and SecG, which is replaced by Sec61β in eukaryotes and archaea (reviewed by Pohlschroder *et al*, 2005; Papanikou *et al*, 2007; Rapoport, 2007; Driessen and Nouwen, 2008). Bacterial protein secretion depends on the SecA ATPase, which functions as a motor to translocate secreted proteins through the SecYEG channel. The insertion of integral membrane proteins into the membrane is also essential and the machinery for this process partially overlaps with the secretory apparatus: most substrates seem to require the SecYEG protein-conducting channel, but only substrates with large extracellular domains require the SecA ATPase for membrane insertion (Kol *et al*, 2008; Xie and Dalbey, 2008). The membrane insertion of many proteins also requires YidC, a conserved membrane protein in the YidC/Oxa1/Alb3 family that is required for membrane protein insertion and assembly of membrane protein complexes in bacteria, mitochondria and chloroplasts (Yi and Dalbey, 2005; van der Laan *et al*, 2005; Kiefer and Kuhn, 2007). Biochemical experiments suggest that some membrane proteins first interact with the SecYEG channel and are later transferred to YidC for integration into the lipid bilayer or for folding into functional state (Urbanus *et al*, 2001; van der Laan *et al*, 2001). However, certain membrane proteins that lack large extracellular domains are inserted into the membrane in a manner that depends on YidC but not on SecYEG, suggesting flexibility in the pathway for membrane protein biogenesis (Kiefer and Kuhn, 2007; Xie and Dalbey, 2008). The cryoelectron microscopy images of YidC (Lotz *et al*, 2008; Kohler *et al*, 2009) and the ability of purified YidC to insert certain proteins into the membrane in the absence of the Sec proteins (Serek *et al*, 2004; van der Laan *et al*, 2004), suggest that YidC provides a second protein-conducting channel.

The essentiality of protein secretion and membrane protein biogenesis makes it likely that all cells can respond to decreased secretion capacity by either prioritizing certain substrates, as in eukaryotes (Kang *et al*, 2006; Oyadomari *et al*, 2006; Hegde and Kang, 2008), or by increasing the secretion capacity of the cell. Indeed, *Escherichia coli* and closely related bacteria have a feedback mechanism to maintain cellular protein secretion capacity by increasing SecA translation when the SecYEG pathway is compromised (Oliver and Beckwith, 1982; Schmidt and Oliver, 1989). This feedback mechanism depends on a gene located upstream of *secA, secM*, that acts as a ribosome–nascent chain complex to monitor protein secretion capacity (McNicholas *et al*, 1997; Schmidt *et al*, 1988; Nakatogawa and Ito, 2001, 2002). Prior data suggested that *Bacillus subtilis* cells might have the ability to monitor the YidC-dependent membrane protein insertion pathway (Rubio *et al*, 2005). Specifically, *B. subtilis*, like many other Gram-positive bacteria, encodes two YidC homologs (SpoIIIJ and YqjG) either of which can support viability (Murakami *et al*, 2002; Tjalsma *et al*, 2003). However, the role of these proteins in *B. subtilis* remains unclear (Murakami *et al*, 2002; Tjalsma *et al*, 2003), in contrast those encoded by *Streptococcus mutans*, which clearly has a role in membrane protein insertion

*Corresponding author. Division of Biological Sciences, University of California, San Diego, 9500 Gilman Drive La Jolla, San Diego, CA 92093-0377, USA. Tel.: +1 858 822 1314; Fax: +1 858 822 5740; E-mail: kpogliano@ucsd.edu
[1]Present address: Institute for Virus Research, Kyoto University, Sakyo-ku, Kyoto 606-8507, Japan

Received: 5 June 2009; accepted: 12 August 2009; published online: 24 September 2009

(Hasona *et al*, 2005; Dong *et al*, 2008; Funes *et al*, 2009). The *B. subtilis spoIIIJ* gene is likely the primary *yidC* homolog (YidC1), because it is constitutively expressed and located in a similar chromosomal context as *E. coli yidC* (Errington *et al*, 1992). The second *yidC* homolog (*yqjG*; here renamed *yidC2*) is likely the backup system for *spoIIIJ* (*yidC1*), because it is induced in *spoIIIJ* mutants (Rubio *et al*, 2005). This latter observation suggests that *B. subtilis* has a mechanism by which it can sense changing SpoIIIJ activity and increase YidC2 levels as needed to maintain appropriate cellular levels of YidC activity.

We here describe the mechanism by which *B. subtilis* monitors SpoIIIJ (YidC1) activity. Specificially, we show that YidC2 induction involves the product of the upstream gene, *yqzJ*, which is in an operon with *yidC2*, and an mRNA hairpin that occludes the *yidC2* Shine–Dalgarno (SD) site. The *yqzJ* gene encodes a small membrane protein with an N-terminal transmembrane (TM) segment that is a likely substrate of SpoIIIJ (Xie and Dalbey, 2008). YqzJ also has a C-terminal translational arrest domain that interacts with the ribosomal polypeptide exit tunnel to induce a stable translational arrest when SpoIIIJ is absent or limiting. This translational arrest positions the stalled ribosome over the 5′ region of the mRNA hairpin, thereby exposing the *yidC2* SD site and allowing increased translational initiation. Membrane insertion relieves the translational arrest, so when membrane protein insertion is inhibited, the hairpin remains unfolded for longer periods of time, allowing additional YidC2 to be synthesized until cellular membrane protein insertion capacity is restored. Thus, YqzJ acts as a cellular monitor of SpoIIIJ-dependent membrane protein insertion while it is a ribosome–nascent chain complex, rather than as a fully synthesized protein.

The regulatory mechanism we describe bears striking similarities to the *E. coli* protein secretion monitor SecM. We therefore propose renaming *yqzJ* as *mifM*, for membrane protein insertion and folding monitor. However, genomic and sequence comparisons between MifM and SecM reveal that the translational arrest motifs of these two regulatory proteins share no detectable sequence similarity and that they are found in different bacterial kingdoms. This suggests that SecM and MifM are independently evolved ribosome–nascent chain sensors that use a common molecular mechanism to monitor different protein export pathways.

Results

Disruption of spoIIIJ upregulates yidC2 expression at the translational level

To understand the mechanism of *yidC2* (*yqjG*) induction in *spoIIIJ* mutants, we first investigated whether regulation occurs at the level of transcription, translation or protein stability. The *yidC2* gene is in an operon with the ORF *yqzJ* (here renamed *mifM*, as described below), which encodes a 95 amino acid protein (Figure 1A). As shown earlier (Rubio *et al*, 2005), an in-frame fusion of *lacZ* to the stop codon of *yidC2* (*yidC2*^{275}–*lacZ*; Figure 1Aa) exhibits elevated β-galactosidase activity in *spoIIIJ* strains (Figure 1Ba). This was also the case for an in-frame fusion of *lacZ* after the 6th codon of *yidC2* (*yidC2*^{6}–*lacZ*; Figure 1Ab and Bb), so it is unlikely that YidC2 induction is due to increased proteolytic stability of YidC2 in the absence of SpoIIIJ. If *yidC2* induction occurs by modulating *mifM–yidC2* transcription or *mifM* translational initiation, then an in-frame fusion of *lacZ* after the 5th codon of *mifM* (*mifM*^{5}–*lacZ*: Figure 1Ac) should also show elevated β-galactosidase activity in *spoIIIJ* strains. However, identical levels of β-galactosidase activity were observed in the wild-type and *spoIIIJ* strains with the *mifM*^{5}–*lacZ* fusion (Figure 1Bc). Thus, the absence of SpoIIIJ is likely to induce *yidC2* translation in a manner independent of *mifM* transcription and translational initiation.

mifM translation disrupts a stem loop that blocks yidC2 translation

To further understand the mechanism by which *yidC2* is regulated, we performed a genetic screen to isolate mutants that induce *yidC2*. A strain containing the *yidC2*^{6}–*lacZ* fusion was mutagenized with NTG (*N*-methyl-*N*′-nitro-*N*-nitrosoguanidine) and plated on DSM plates containing the β-galactosidase indicator XG. Blue, Lac+ colonies were picked and purified. Of the 150 Lac+ mutants, 37 contained mutations in *spoIIIJ* and 17 were 100% linked to the *yidC2*^{6}–*lacZ* reported gene. DNA sequence analysis revealed that eight of the *spoIIIJ* mutations altered the SD sequence (Supplementary data), suggesting that reducing the level SpoIIIJ protein is sufficient to induce *yidC2*. All of the mutations linked to *yidC*^{6}–*lacZ* were within the upstream ORF, *mifM*. Ten *mifM* mutants had the same point mutation, a G-A transition at nucleotide 16, causing a glutamate to lysine substitution at the 6th amino acid of MifM; hereafter referred to as the class I mutation. The remaining seven mutations were at three sites near the 3′ end of *mifM*, C275T (Ser92Thr), C277T (Leu93Phe) or C280T (Leu94Phe); hereafter referred to as the class II mutations. These results suggested that *mifM* has an important function in regulation of *yidC2* expression.

Examination of the 5′ end of *yidC2* revealed a potential stem loop that could mask the *yidC2* SD site (Figure 1C). The 5′ half of the stem loop is located within the 3′ end of *mifM*, where the class II mutations are located (Figure 1C). We therefore hypothesized that the stem loop repressed the initiation of *yidC2* translation. In keeping with this idea, all class II mutations disrupt G-C pairing of the stem loop, suggesting that the mutations destabilize the structure, thereby leading to high-level constitutive expression of *yidC2*. To test this model, we introduced silent mutations that disrupt the structure without changing the MifM amino acid sequence (*yidC2*^{6}–*lacZ*(Δ*stem*); Figure 1Df). Disrupting the stem loop indeed caused high-level constitutive expression of *yidC2* in wild-type and *spoIIIJ* strains (Figure 1E), suggesting that the stem loop inhibits *yidC2* translation. To test whether *mifM* translation is necessary for *yidC2* translation, we first terminated translation before the ribosome reached the stem loop by introducing a TAA stop codon at codon 86 (Figure 1Dg). This abolished *yidC2* induction in a *spoIIIJ* strain and slightly reduced *yidC2* expression in wild type (Figure 1Fg). We next duplicated six *mifM* codons (91–96) including the stop codon, so that wild-type MifM was synthesized but translation stopped before the ribosome moved into the stem loop (Figure 1Dh). This also resulted in low and constitutive expression of *yidC2* (Figure 1Fh) that was increased when the stem loop was disrupted (not shown). We conclude that translation of *mifM* into the 5′ half of the stem loop is necessary for high-level *yidC2* expression.

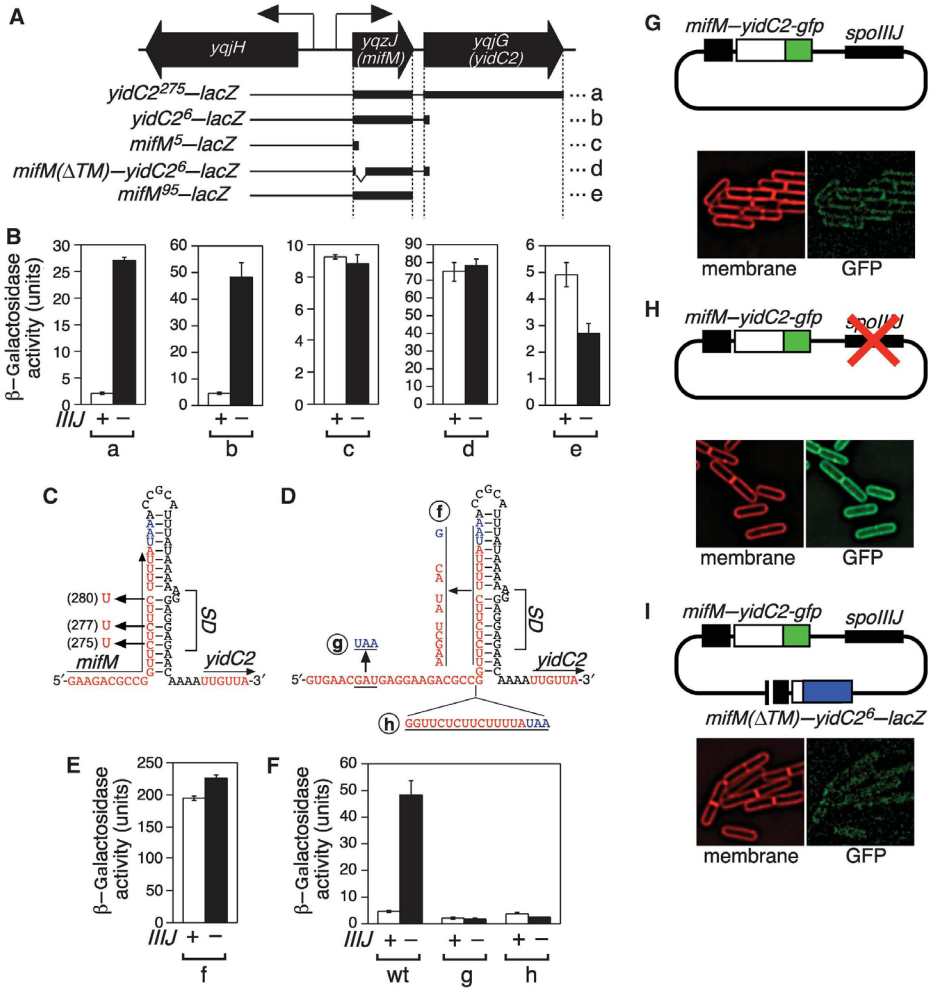

Figure 1 *mifM* regulates *yidC2* expression. (**A**) Genetic context of *yqjG* (*yidC2*) and in frame translational *lacZ* fusions to the 3′-end of *yidC2* (a) or *mifM* (e), producing YidC2^{275}–LacZ and MifM^{95}–LacZ, respectively, and after *yidC2* codon 6 (b, d) and *mifM* codon 5 (c). Construct (d) also contains an in-frame deletion of the *mifM* region encoding the transmembrane (TM) segment. (**B**) β-galactosidase (β-gal) activity in wild type (white) or the *spoIIIJ* mutant (black). The fusions (a–e) correspond to those shown in (A). (**C**) Predicted secondary structure of *mifM–yidC2* mRNA. SD, Shine–Dalgarno site recognized by the ribosome to initiate translation. The class II mutations of *mifM* are indicated by arrows with residue's numbers. (**D**) Diagram of *mifM* mutants in the *yidC2*^{6}*–lacZ* fusion. (f) Silent mutations to disrupt the hairpin without changing MifM amino acids (*yidC2*^{6}*–lacZ(Δstem)*). (g) Stop codon at codon 86. (h) Duplication of codons 91–96 (including the stop codon) to allow translation of full-length *mifM* without unfolding the hairpin. (**E**) β-gal activity with the stem-loop mutation shown in (D) (f). (**F**) Translation through the hairpin is required for *yidC2* expression. β-gal activity of strain with mutations (g) and (h) from (D). wt, wild type. (**G–H**) *mifM* functions *in cis*. Expression of *yidC2-GFP* monitored by fluorescence microscopy with identical GFP (green) exposures and image adjustments for each strain; membranes were stained with FM 4-64 (red). (**G**) Expression of *yidC2-GFP* downstream of wild-type *mifM* in wild type (**H**) Expression of *yidC2-GFP* downstream of wild-type *mifM* in *spoIIIJ* (**I**) MifMΔTM expressed in a wild-type strain with *yidC2-gfp* downstream of wild-type *mifM*.

MifM senses membrane protein insertion

SpoIIIJ and YidC2 are likely involved in membrane protein biogenesis or protein secretion (Tjalsma *et al*, 2003; Camp and Losick, 2008). Interestingly, MifM is predicted to be a small membrane protein with a single N-terminal TM segment (amino acids 12–34) and a C-terminal cytoplasmic domain (amino acids 35–95). This topology is similar to that of *E. coli* proteins that are inserted into the membrane in a manner dependent on the SpoIIIJ homologue YidC (Xie and Dalbey, 2008), suggesting that MifM is inserted into the membrane by SpoIIIJ. Interestingly, the class I MifM mutation changes the charge of the N-terminal domain from negative to positive, which might produce a membrane insertion defect that induces *yidC2*, thereby mimicking SpoIIIJ limitation. To test this model, we deleted the region encoding the MifM TM segment and found that it caused elevated *yidC2* expression in wild-type cells (Figure 1Ad and Bd). These results suggest that MifM serves as a sensor of

SpoIIIJ activity that upregulates *yidC2* when SpoIIIJ activity is limiting and membrane insertion is blocked.

MifM is a cis-acting regulator of yidC2 translation

If *mifM* translation unfolds the stem loop in a manner regulated by SpoIIIJ-dependent membrane insertion of MifM, then it should regulate YidC2 expression only *in cis*. To test this prediction, we expressed MifM(ΔTM) *in trans* to *yidC2-gfp* with wild-type *mifM* upstream. The strain carrying only *yidC2-gfp* showed weak GFP fluorescence in wild-type cells (Figure 1G), and stronger membrane-associated GFP fluorescence in the *spoIIIJ* background (Figure 1H) as expected (Rubio *et al*, 2005). Expression of MifM(ΔTM) did not elevate the YidC2-GFP signal (Figure 1I) unless it was encoded upstream of YidC2-GFP, indicating that *mifM* functions only *in cis*. Together these results suggest that MifM is a *cis*-acting regulator of *yidC2* translation that senses SpoIIIJ activity, likely when it is inserted into the membrane as a ribosome-associated nascent chain. We therefore renamed its gene (formerly *yqzJ*) *mifM* for membrane insertion and folding monitor.

MifM is incompletely translated in the absence of SpoIIIJ

The above results suggest that in the absence of SpoIIIJ, the *mifM–yidC2* stem loop is more efficiently unfolded than in the presence of SpoIIIJ. Unfolding could be accomplished either by allowing more ribosomes to translate *mifM–yidC2* mRNA or by having ribosomes move more slowly across the stem loop so it remains unfolded for longer times. The former model is unlikely because the initiation of *mifM* translation occurs at similar levels in the presence or absence of SpoIIIJ (Figure 1Ac and Bc). We therefore hypothesized that the absence of SpoIIIJ might stall the ribosome in a location that occluded the 5′ side of the stem loop thereby exposing the *yidC2* SD. To test this idea, we fused *lacZ* at the 3′-end of the *mifM* coding sequence (producing $mifM^{95}$*–lacZ*; Figure 1Ae). This fusion showed lower β-galactosidase activity when *spoIIIJ* was disrupted, as expected if *mifM* translation was attenuated under these conditions (Figure 1Be). This suggests that *mifM* translation is arrested when membrane insertion of MifM is blocked by the *spoIIIJ* mutation or deletion of the MifM TM domain.

Detection of a MifM translational intermediate

If *mifM* translation is arrested in the absence of membrane insertion, it might be possible to observe a translational intermediate in *mifM(ΔTM)* strains. We therefore constructed strains expressing an N-terminal fusion of GFP to MifM lacking its N-terminal TM domain with or without a C-terminal FLAG-tag for detection of the full-length protein (Figure 2A; GFP–$MifM^{35–95}$–FLAG and GFP–$MifM^{35–95}$, respectively). Immunoblotting using GFP-specific antibodies detected two major products in the strain expressing GFP–$MifM^{35–95}$ (Figure 2B, lane 2) and an additional larger minor product in the strain expressing GFP–$MifM^{35–95}$–FLAG (Figure 2B, lane 3). This minor product (band a) was detected with both GFP- and FLAG-specific antibodies (Figure 2B, lanes 3 and 6), so it must be full-length GFP–$MifM^{35–95}$–FLAG. However, the shorter products (bands b and c) were not detected by FLAG-specific antibodies, so they must be N-terminal fragments (Figure 2A). To test whether these

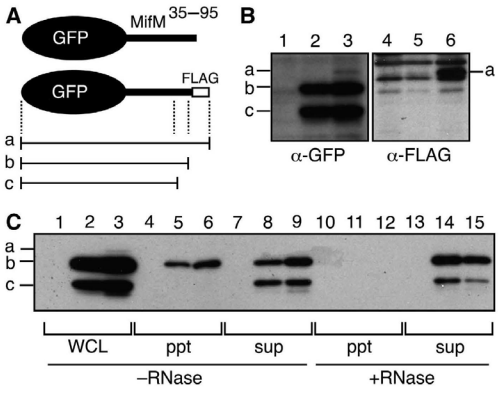

Figure 2 Visualization of MifM translational arrest. (**A**) The C-terminus of GFP was fused to amino acids 35–95 of MifM with or without the C-terminal FLAG-tag. (a–c) Products visualized in immunoblots. (**B**) Immunoblotting of GFP–$MifM^{35–95}$ derivatives. Proteins from strains expressing GFP–$MifM^{35–95}$ (lanes 2, 5), GFP–$MifM^{35–95}$–FLAG (3, 6) or no GFP fusion (1, 4) analysed by immunoblotting with anti-GFP (left panel) or anti-FLAG (right panel). (**C**) CTABr fractionation of GFP–$MifM^{35–95}$. Proteins from strains expressing GFP–$MifM^{35–95}$ (lanes 2, 5, 8, 11, 14), GFP–$MifM^{35–95}$–FLAG (3, 6, 9, 12, 15) or no GFP fusion (1, 4, 7, 10, 13) analysed by immunoblotting with anti-GFP after CTABr precipitation. Samples 10–15 were treated with RNaseA before CTABr. WCL, whole cell lysate; ppt, precipitated fraction; sup, supernatant.

shorter products were translational intermediates or degradation products, we used CTABr precipitation (Gilmore *et al*, 1991; Nakatogawa and Ito, 2001), which precipitates RNA and RNA–protein complexes such as translational intermediates that retain a covalently attached tRNA at the C-terminus. Fragment b but not fragment c was precipitated by CTABr (Figure 2C) and this CTABr precipitation was abolished by RNase treatment. Thus, fragment b is an MifM translational intermediate whereas fragment c is likely a degradation product. These results show that *mifM(ΔTM)* undergoes a strong translational arrest such that the arrest species appears more abundant than full-length protein. The apparent size of fragment b suggests that the elongation arrest occurs within the 3′-region of *mifM*, a position at which the arrested ribosome could prevent formation of the mRNA hairpin that blocks *yidC2* translation.

A specific amino acid sequence is required for MifM translational arrest

To further elucidate the mechanism by which *mifM* regulates *yidC2*, we tested the relative importance of the *mifM* mRNA and amino acid sequences in the region of the hairpin. To do so, we designed a frame-shift mutation within *mifM* that would produce an mRNA sequence almost identical to native *mifM* but encode a completely different amino acid sequence. We first introduced an extra stop codon and a silent mutation (Figure 3Aa) to prevent out of frame translation from producing a product much longer than native MifM, and to prevent premature translational termination, respectively. The $yidC2^{6}$*–lacZ* fusion with these two mutations showed low-level expression in the wild-type strain and induction in the *spoIIIJ* strain to levels similar to the wild-type fusion

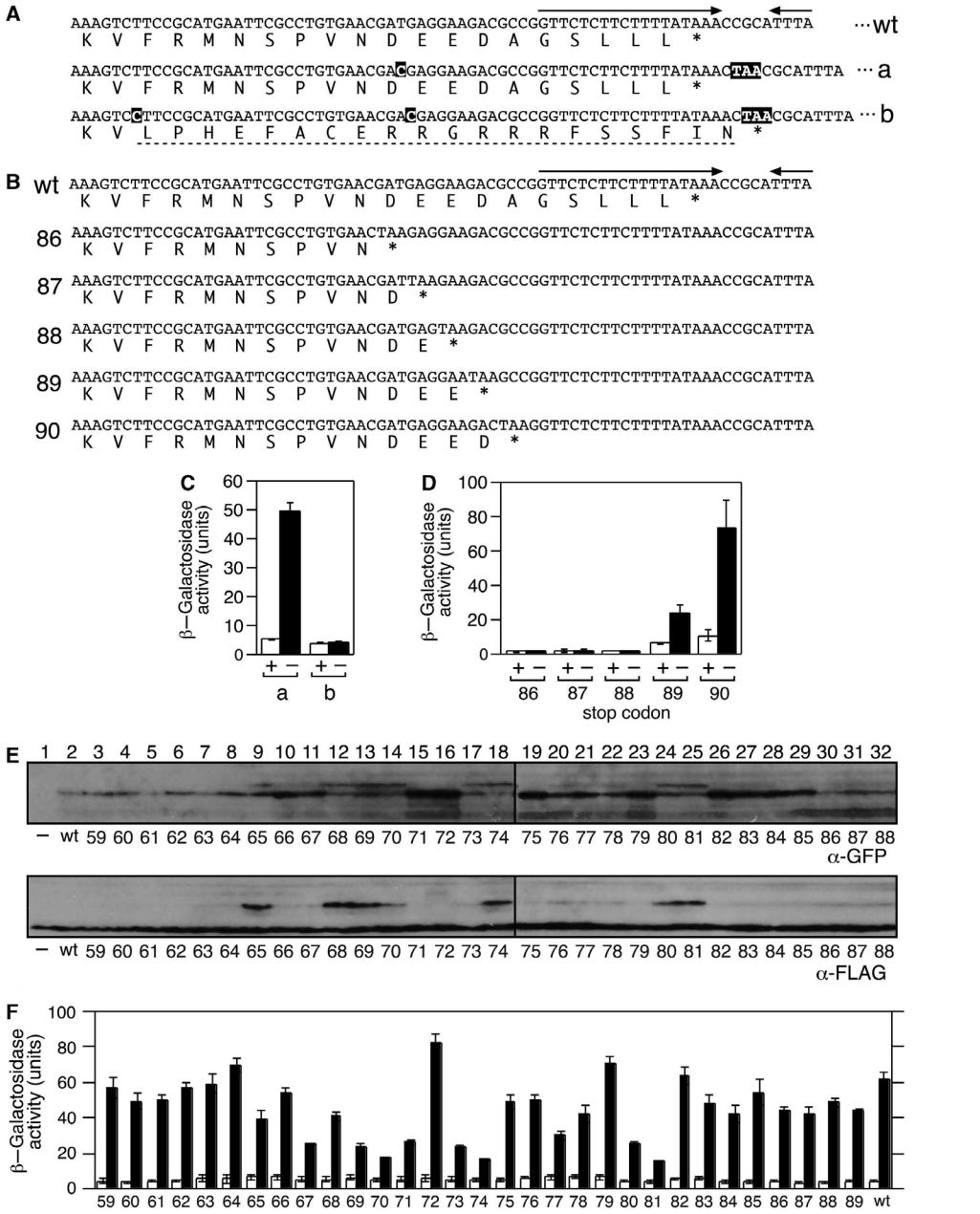

Figure 3 Identification of MifM amino acids required for translational arrest. (**A**) The *mifM* frame-shift mutant; white characters in black box indicate the mutations. Arrows show site of stem loop. (**B**) Introduction of stop codons in *mifM* (*). The number at left represents the codon substituted by a TAA stop codon. (**C**) β-gal activity of mutants in A in wild type (white) or *spoIIIJ* (black). (**D**) β-gal activity of mutants in B in wild type (white) or *spoIIIJ* (black). (**E**) Ala-replacement of GFP–MifM$^{35-95}$–FLAG at the *mifM* codons indicated by numbers. Immunoblotting with anti-GFP and anti-FLAG. Arrest-defective substitutions accumulate full-length protein. (**F**) β-gal activity of *yidC2*^{6}*–lacZ* containing the indicated MifM Ala-replacements, in wild type (white) or *spoIIIJ* (black).

(Figure 3Ca). When then introduced a frame-shift mutation at codon 78 (Figure 3Ab), which resulted in low and constitutive *yidC2*^{6}*–lacZ* expression (Figure 3Cb), showing that the translational arrest was abolished. We conclude that a specific amino acid sequence at the MifM C-terminus is required for translational arrest.

Identification of the site of translational arrest

Stop codons before the translational arrest site should prematurely release the ribosome from the mRNA, allowing the stem loop to refold and inhibiting YidC2 expression, whereas those after the arrest site should have no effect. We therefore introduced stop codons immediately to the 5′ of the stem loop to determine whether the mutation prevented *yidC2* induction in the *spoIIIJ* strain (Figure 3B). Stop codons before codon 88 blocked *yidC2* induction (Figure 3D), whereas a stop codon at codon 90 showed wild-type induction (Figure 3D). These results indicate that *mifM* translation must continue to codon 88 to allow *yidC2* expression and that codon 90 is dispensable for translational arrest. Codon 89 was not fully essential for the induction of *yidC2*, though it might participate in stabilizing the translational arrest, because substitution of codon 89 by a stop codon showed intermediate *yidC2* expression. These data indicate that the translational arrest occurs near the MifM C-terminus, most likely after codon 88 is translated, consistent with the estimated molecular weight of the translational arrest product of GFP–MifM$^{35\ 95}$ (~35 kDa, Figure 2B, band b). Translating ribosomes cover approximately 6–9 nucleotides of mRNA to the 3′ of the A site (Culver, 2001; Yusupova *et al*, 2001, 2006; Takyar *et al*, 2005), which would allow a ribosome arrested at codon 88 to partially cover the 5′ side of the stem loop (see Figure 1C), thereby exposing the *yidC2* SD for the duration of the arrest.

Arrest requires amino acids within the ribosomal polypeptide exit tunnel

To identify amino acids required to arrest MifM translation, we mutagenized the C-terminal region of MifM. Codons 59–89 were targeted because the above results suggested that arrest occurred near codon 89, which would place this codon near the peptidyl transfer site of the ribosome, and because the C-terminal 30–40 amino acids of nascent polypeptides lie within the polypeptide exit tunnel of the ribosome and are therefore well positioned to mediate a translational arrest (Krieg *et al*, 1989; Mothes *et al*, 1994; Frank *et al*, 1995; Matlack and Walter, 1995; Ban *et al*, 2000; Daniel *et al*, 2008). We constructed a series of alanine replacements in GFP–MifM$^{35\ 95}$–FLAG and monitored accumulation of the arrest species by immunoblotting with GFP- and FLAG-specific antibodies. Changing I65, H68, R69, I70, W73, I74, M80, N81 to alanine clearly increased accumulation of full-length MifM (Figure 3E), suggesting they might be required for the arrest, whereas other substitutions had more subtle effects. These substitutions could affect protein or mRNA stability as well as translation, so we introduced identical substitutions in wild-type *mifM* in the context of *yidC2–lacZ* to assess the ability of these proteins to induce YidC2 in the *spoIIIJ* strain. Substitutions at amino acids Y67, R69, I70, T71, W73, I74, M80 or N81 reduced YidC2 induction in the *spoIIIJ* strain as expected for mutations that reduce the translational arrest (Figure 3F). Amino acids that both increased production of full-length MifMΔTM and reduced *yidC2* induction in the *spoIIIJ* strain allowed us to identify a minimal set of amino acids that are clearly critical for the arrest (R69, I70, W73, I74, M80, N81); these are upstream of the translational arrest that occurs at E88 or D89. Interestingly, substitutions at the site of the arrest (E88A, D89A) had only minor effects in either assay, indicating that the specific amino acid or peptidyl–tRNA at the site at which translation arrests is not critical (although it is critical that translation continues beyond these amino acids, Figure 3D). The amino acids necessary for translational arrest lie within the polypeptide exit tunnel of the ribosome and distal to the peptidyl transferace centre (PTC) at which elongation occurs.

A mutation that alters the polypeptide exit tunnel of the ribosome compromises elongation arrest

The above results suggest that an interaction between the MifM nascent polypeptide and the ribosomal polypeptide exit tunnel arrests translation. If so, then mutations that alter the polypeptide exit tunnel could impair the interaction and prevent the translational elongation arrest. To isolate arrest-defective ribosomes, we took advantage of the similarity in the mode of action of MifM and erythromycin, which binds within the exit tunnel to inhibit polypeptide elongation (Schlunzen *et al*, 2003; Tu *et al*, 2005; Vazquez-Laslop *et al*, 2008). This effect can be prevented by mutations that change the amino acids and rRNA that line the exit tunnel, which convey erythromycin resistance (Erm^R; (Gaynor and Mankin, 2003; Zaman *et al*, 2007; Diner and Hayes, 2009). Certain Erm^R mutants in *E. coli* are defective in translational arrests mediated by regulatory nascent chains, such as the SecAYEG monitor SecM (Nakatogawa and Ito, 2002; Lawrence *et al*, 2008), the tryptophan sensor TnaC (Cruz-Vera *et al*, 2005), the erythromycin sensor ErmCL (Vazquez-Laslop *et al*, 2008) and the chloramphenicol sensor Crb^{cmlA} (Lawrence *et al*, 2008). We therefore isolated spontaneous Erm^R mutants from independent *B. subtilis* cultures. These mutants all had an identical duplication of seven amino acids in the L22 protein (^{94}SQINKRT^{100}; Figure 4A). On the basis of crystal structure of the ribosome (Ban *et al*, 2000), it is likely that this duplication causes a seven amino acid insertion within the interior of the ribosome exit tunnel (Figure 4A and E), in a region that can be mutated to Erm^R in other bacteria (Franceschi *et al*, 2004; Zaman *et al*, 2007).

We tested whether the Erm^R mutation affected YidC2 induction by introducing it into strains in which MifMΔTM is encoded upstream of *yidC2–lacZ* (*mifM(ΔTM)–yidC2^6–lacZ*), which would normally express high levels of YidC2 because of the prolonged translational arrest caused by the absence of membrane insertion (Figure 1Ad). Expression of *yidC2–lacZ* was drastically decreased in the Erm^R strain compared with wild type (Figure 4B). However, when the stem-loop mutation was introduced to relieve the dependence of *yidC2* expression on translational arrest (*mifM–yidC2^6–lacZ(Δstem)*: Figure 1Df), the Erm^R strain showed wild-type expression. Thus, the Erm^R mutation does not affect translation or folding of β-galactosidase. We next used GFP–MifM$^{35\ 95}$–FLAG to directly compare levels of the arrest and full-length species by immunoblotting. In the Erm^R mutant full-length MifM was the major species with only a small amount of the arrest product accumulated (Figure 4C, lanes 3 and 6), the opposite of the wild-type strain in which little full-length MifM accumulated (lanes 2 and 5). Thus, a mutation in the polypeptide exit tunnel of the ribosome compromises both MifM translational arrest and *yidC2* induction. We conclude that the elongation arrest of MifM is mediated by interaction between the C-terminal region of MifM and the polypeptide exit tunnel of the ribosome (Figure 4E).

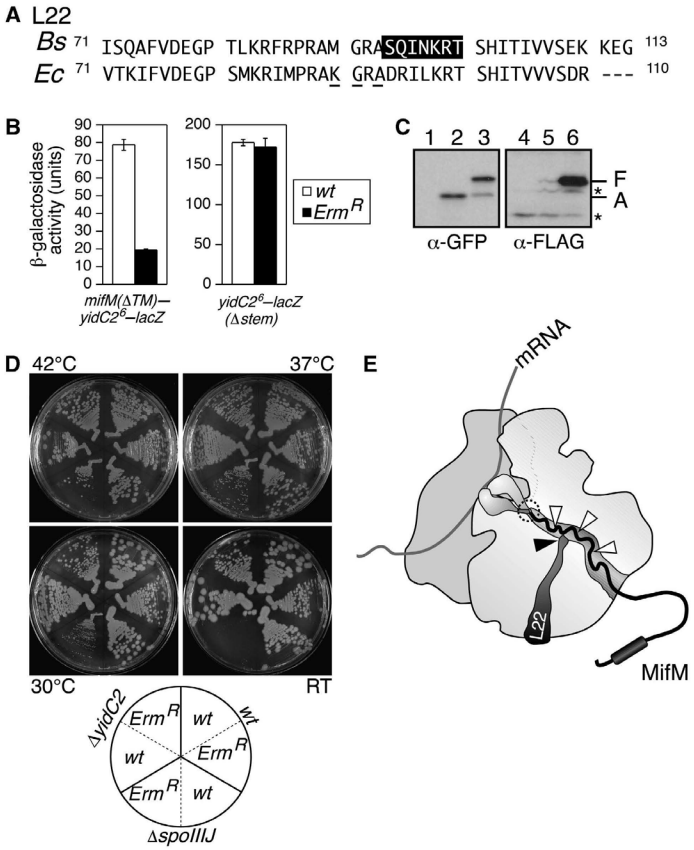

Figure 4 A mutation affecting the ribosomal protein L22 compromises elongation arrest (**A**) The spontaneous Erm^R mutant has a seven amino acid duplication in L22 (white letters on black). Alignment of this region of *B. subtilis (Bs)* and *E. coli* (*Ec*) L22; underlined amino acids affect elongation arrest of *E. coli tnaC* (K90; Cruz-Vera *et al*, 2005) or *secM* (G91 and A93; Nakatogawa and Ito, 2002). (**B**) β-gal activity of *mifM(ΔTM)-yidC2*^{6}*–lacZ* (left) or the stem-loop mutant (right) in Erm^R (black) and wild-type (white) strains. (**C**) Immunoblotting of GFP–$MifM^{35-95}$–FLAG in the Erm^R mutant with GFP and FLAG-specific antibodies. Strains with (2, 3, 5, 6) or without GFP fusion (1, 4) in wild type (lanes 1, 2, 4 and 5) or Erm^R (3, 6). *, non-specific bands (**D**) Synthetic cold sensitive growth is observed in the *erm spoIIIJ* double mutant. Strains were streaked on LB plates and incubated at the indicated temperature (RT, room temperature ~24°C). (**E**) View of the ribosome polypeptide exit tunnel, showing approximate positions of L22 (black arrowheads) and MifM (white arrowheads) amino acids required for arrest. Dotted circle shows PTC.

During the course of these studies we noted that the arrest-defective Erm^R strain showed a cold sensitive growth defect in the *spoIIIJ* background, whereas the single *erm* or *yidC2 erm* double mutant showed only a minor growth phenotype (Figure 4D). We surmise that the Erm^R mutant expresses sufficient YidC2 to support growth in the absence of SpoIIIJ at high temperatures, likely because of the residual translational arrest observed in western blots (Figure 4C). However, the reduced arrest activity prevents YidC2 from being fully induced, thereby limiting YidC2 activity and resulting in cold sensitive growth, as is also observed for *E. coli* mutants in the *sec* genes (Pogliano and Beckwith, 1993) and *yidC* (Yuan *et al*, 2007). These results suggest that erythromycin resistance might decrease the ability of a bacterium to survive events that compromise membrane protein insertion.

Phylogenetic distribution of yidC2 and mifM

Our results indicate that MifM allows *B. subtilis* cells to produce additional YidC2 protein when the activity or level of the primary YidC protein (SpoIIIJ) is reduced. We performed a phylogenetic analysis to determine how many bacteria have two copies of *yidC* and which of these were in an operon with a *mifM*-like gene. Our analysis indicated that the genomes of most Gram-negative bacteria had just one copy of *yidC*, whereas the genomes of many Gram-positive bacteria had more than one (Figure 5A; Supplementary Table S1). However, not all Gram-positive bacteria encode two YidC proteins. Within the phylum Firmicutes, most Lactobacillales have two *yidC* genes (for an average of 1.98 *yidC* genes/genome), whereas most Clostridiales have one (for an average of 1.14 *yidC* genes/genome). Most species within the order Bacillales have two *yidC* genes (for an average of 1.8 *yidC* genes/genome). *Staphylococcus aureus* is a notable exception in *Staphylococci* sp. as it encodes just one *yidC* gene. We were unable to detect MifM in the Actinobacteria, the Lactobacillales or the Clostridiales. Within the Bacillales, *mifM*-like genes were identified upstream of *yidC2* in

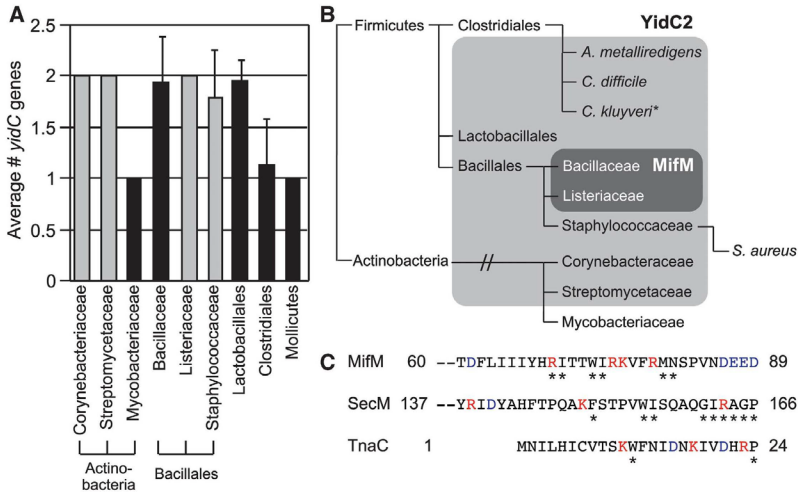

Figure 5 Phylogenetic distribution of *yidC2* and *mifM* in selected bacterial groups. (**A**) Average number of *yidC* genes in selected bacterial genera. Those shown in grey have five or fewer sequenced species. (**B**) Plot showing the distribution of *yidC2* in different bacterial genomes. *Clostridium kluyveri* has three *yidC* genes. (**C**) Alignment of the MifM with SecM and TnaC aligning the proteins from the C-terminal amino acid in the arrest product. Blue (acidic amino acids), Red (basic amino acids), stars, sites at which mutations reduce the arrest activity.

Bacillus sp., *Listeria* sp. and *Geobacillus* sp. (Figure 5B; Supplementary Table S2) but absent from the genomes of *Staphylococci* sp. that encoded both *yidC1* and *yidC2*. The restriction of the *mifM–yidC2* system to a subset of the Bacillales is similar to the distribution of the *secM-secA* system, which is restricted to a subset of the γ-proteobacteria (van der Sluis and Driessen, 2006).

Discussion

Our results support the following model for the mechanism by which *B. subtilis* upregulates its secondary membrane protein insertase (YidC2) when activity of the primary membrane protein insertase (SpoIIIJ/YidC1) is limited. When membrane protein secretion capacity is high, *yidC2* translation is repressed by a stem loop that masks the *yidC2* SD, thereby inhibiting *yidC2* translation (Figure 6A and I). However, when membrane insertion of MifM is prevented by a *spoIIIJ* mutation or by deletion of the MifM TM segment, *mifM* translation is arrested. The arrested ribosome is positioned over the 5′ half of the stem loop, thereby exposing the *yidC2* SD and allowing *yidC2* translation (Figure 6A and V). This regulatory mechanism requires two distinct communication events between the MifM nascent polypeptide, the ribosome and the membrane insertion apparatus. First, our genetic data indicate that translational arrest requires an interaction between the arrest motif near the MifM C-terminus and the polypeptide exit tunnel of the ribosome. This interaction within the ribosome must be communicated back to the peptidyl transferase site at which elongation occurs. Second, the translational arrest is relieved by an event that is likely to be the insertion of MifM into the membrane, as it requires the N-terminal TM domain of MifM and SpoIIIJ (YidC1). This event must also be communicated back to the peptidyl transferase site to allow continued elongation. The MifM–YidC2 system provides the first example of a mechanism in which a bacterial cell senses the activity of the YidC pathway and the second example of a regulatory nascent chain that senses interactions outside the ribosome.

Many regulatory nascent chains are short polypeptides encoded in the 5′ end of an operon. These short nascent chains mediate translational arrest in response to a cofactor (amino acid or antibiotic) that directly or indirectly modifies the interaction between the nascent chain and the ribosome to mediate stalling (reviewed by Yanofsky, 1981; Yanofsky *et al*, 1996; Tenson and Ehrenberg, 2002). This translational arrest can govern either transcription or translation of downstream genes. For example, the *E. coli tna* operon, which controls tryptophan catabolism, is regulated by a translational arrest within the 5′ *tnaC* gene, which encodes a polypeptide of 24 amino acids. Translation of *tnaC* is arrested when tryptophan concentration increases and free tryptophan binds to the ribosome, stalling translation (Tenson and Ehrenberg, 2002; Cruz-Vera *et al*, 2005; Yanofsky, 2007). The stalled ribosome prevents Rho-dependent transcriptional termination, thereby inducing the downstream genes. Operons conferring resistance to antibiotics that target the ribosome often are regulated in a manner that directly parallels the mechanism by which *yidC2* is regulated. For example, the *ermC* gene (which confers erythromycin resistance) is regulated by a short upstream ORF in which translation is arrested in the presence of erythromycin (Narayanan and Dubnau, 1987). This arrest unfolds a stem loop thereby revealing the *ermC* SD sequence and allowing translation of *ermC*, which confers erythromycin resistance. Common features of the short regulatory nascent chains described to date are that they respond to binding of antibiotics or cofactors within the ribosome and that they are short polypeptides that are mostly accommodated within the ribosome.

MifM provides the second example of a long regulatory nascent chain that monitors an event sensed outside the ribosome. The first to be described is *E. coli* SecM, which monitors protein secretion through the SecYEG pathway and upregulates the SecA protein translocation ATPase when

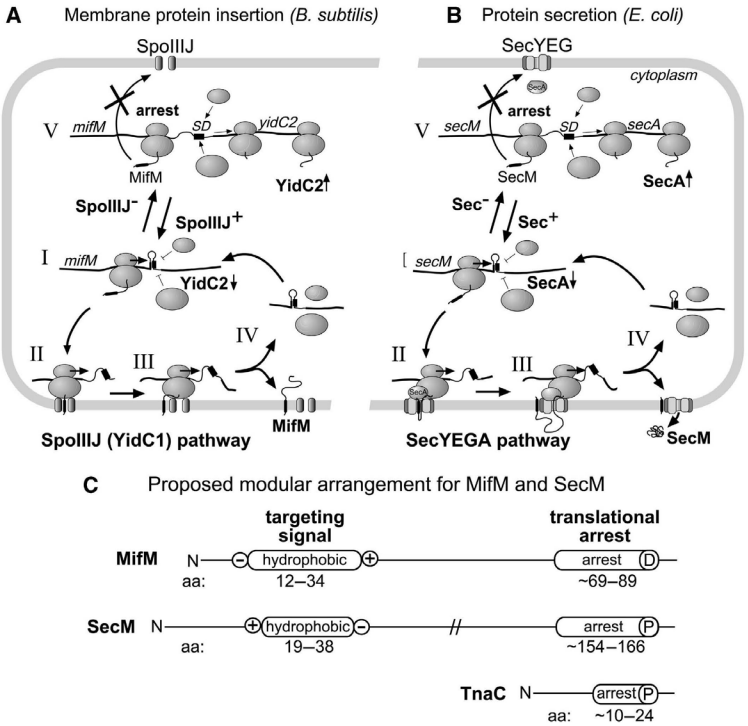

Figure 6 Model for the *B. subtilis* membrane protein insertion monitor MifM and comparison to the *E. coli* protein secretion monitor SecM. (**A**) Model for YidC2 regulation. The mRNA hairpin masks the *yidC2* SD site to block *yidC2* translation (I). When MifM inserts into the membrane, the translational arrest is transient or does not occur, thereby allowing only transient unfolding of the mRNA secondary structure by the ribosome (II–IV). When membrane insertion of MifM is impaired, *mifM* translation is arrested and the ribosome unfolds the mRNA, allowing ribosomes to recognize the *yidC2* SD and initiate translation (V). (**B**) Comparison to the protein secretion monitor *secM*. Formation of the mRNA hairpin masks the *secA* SD and blocks *secA* translation. When SecM is secreted, the translational arrest is released, transiently exposing the *secA* SD and basal levels of SecA are synthesized (I–IV). When secretion is impaired, SecM is not secreted and a prolonged translational arrest occurs (V), unfolding the mRNA and allowing elevated SecA synthesis. (**C**) Proposed modular arrangement of MifM and SecM. The N-terminus of each protein contains a targeting signal comprised of either the putative transmembrane domain of MifM, which likely directs the protein to the SpoIIIJ (YidC1) membrane protein biogenesis pathway, or the signal sequence of SecM, which directs the protein to the SecYEG protein secretion pathway. Positive and negative charges flanking the hydrophobic core of these signals are indicated. The C-terminus of each protein contains a translational arrest motif comprising ~12–20 amino acids preceding the final amino acid required for translational arrest (indicated by a D or P). This motif is located within the polypeptide exit tunnel of the ribosome, whereas the final amino acid translated is a peptidyl–tRNA at the PTC. TnaC is shown for comparison.

protein secretion capacity is limiting (Oliver and Beckwith, 1982; Schmidt and Oliver, 1989). The mechanism by which SecM monitors protein export is strikingly similar to the mechanism by which MifM monitors membrane protein insertion. Specifically, under conditions of limiting protein secretion capacity or when SecM secretion is blocked by deletion of the signal peptide, *secM* translation is arrested (McNicholas *et al*, 1997; Nakatogawa and Ito, 2001, 2002). This arrest positions the ribosome over the 5′ side of a stem loop that occludes the SecA SD sequence, allowing increased *secA* translation (Figure 6B). Similar to *mifM*, *secM* encodes a protein with a C-terminal motif that interacts with the exit tunnel of the ribosome to induce a translational arrest (Figure 6C). Both proteins also include an N-terminal targeting motif that dictates the cellular pathway that the regulatory nascent chain monitors: SecM has an N-terminal signal peptide that directs the protein to the SecYEGA translocase for movement across the cytoplasmic membrane, whereas MifM has a single predicted TM segment and an intracellular domain. These two proteins are likely moved across the membrane by separate cellular pathways, as SecM is secreted by the SecYEGA preprotein translocase, whereas the predicted topology of MifM is similar to that of *E. coli* proteins that are inserted into the bilayer in a YidC-dependent but SecYEGA-independent manner (Xie and Dalbey, 2008). These results suggest that long regulatory nascent chains have a modular arrangement, with the N-terminal domain specifying which event outside the ribosome is monitored and a C-terminal arrest motif (Figure 6C). This modular structure raises the possibility that additional regulatory nascent chains that sense events outside the ribosome exist, such as chaperone-mediated protein folding or the assembly of protein complexes.

Our data indicate that the *mifM* translational arrest is mediated by specific interactions between the C-terminus of the MifM nascent chain and the polypeptide exit tunnel of the ribosome (Figure 4E), as is the case for other nascent chain-mediated translational arrest mechanisms. Similar to *tnaC*

and *secM*, *mifM* translational arrest depends on regions of the nascent chain that are located away from the PTC at which translation is arrested, within in the polypeptide exit tunnel (Gong and Yanofsky, 2002; Nakatogawa and Ito, 2002; Cruz-Vera *et al*, 2005, 2007). Furthermore, mutations that affect the L22 ribosomal protein, which forms a constriction in the middle of the exit tunnel, compromise *mifM* translational arrest as is the case for *secM, ermC* and *tnaC* (Nakatogawa and Ito, 2002; Cruz-Vera *et al*, 2005; Vazquez-Laslop *et al*, 2008). These data suggest that this region of the polypeptide exit tunnel senses arrest motifs and triggers a signal transduction event that inhibits polypeptide elongation at the PTC.

We were surprised to find no primary sequence similarity in the arrest motifs of MifM, SecM and TnaC (Figure 5C) and to find that genetic analysis revealed several differences between the architecture of the MifM arrest motif and these two well-studied examples. First, single amino acid substitutions near the site of the MifM translational arrest had little effect, whereas changing the C-terminal proline codons of *tnaC* and *secM* strongly inhibits translational arrest (Nakatogawa and Ito, 2002; Cruz-Vera and Yanofsky, 2008). Alignment of MifM homologs revealed a conserved cluster of negatively charged amino acids near the site of the translational arrest (Supplementary Table S2), so it is possible that arrest can occur at any of these sites. Second, no single amino acid substitution in MifM completely blocked the arrest, whereas a single substitution within SecM (at Arg^{163}, two amino acids away from the translational arrest) abolished translational arrest (Yap and Bernstein, 2009). Together these results suggest that MifM translational arrest might be mediated by multiple interactions that independently contribute to the arrest rather than by a limited number of critical amino acids. These differences in arrest motif architecture and the lack of sequence similarity suggest that there could be more than one mechanism to induce translational arrest and that many polypeptides might be capable of serving as regulatory nascent chains.

The release of the MifM and SecM translational arrests requires the interaction of the stalled ribosome with SpoIIIJ (YidC1) or with the SecYEG protein translocation channel, respectively. This suggests that at least one substrate of the *B. subtilis* YidC homologues is targeted co-translationally, although it remains unclear if this is also the case for other substrates in *B. subtlis* or in *E. coli*. It is interesting that two different protein translocation machineries can mediate the release of similar translational arrests. It has been proposed that the translational arrest of SecM is released by a pulling force generated by the SecA ATPase motor during the translocation of the C-terminal domain of SecM across the membrane (Nakatogawa and Ito, 2002; Butkus *et al*, 2003; Nakatogawa *et al*, 2004). In this context, it is somewhat surprising that the MifM translational arrest is released by YidC-dependent membrane insertion, because the MifM C-terminus is likely to remain in the cytoplasm, so membrane insertion is not necessarily expected to generate a large pulling force. Furthermore, YidC-dependent membrane insertion can occur in the absence of an ATPase such as SecA (Samuelson *et al*, 2000; Serek *et al*, 2004), and only in some examples does YidC-mediated membrane protein insertion depend on the proton motif force or the signal recognition particle, which has GTPase activity (Facey *et al*, 2007; Celebi *et al*, 2008). Thus, although insertion of the TM segment into the hydrophobic membrane might generate a local pulling force, it is unclear whether this force would be of similar magnitude as that generated by the ATP-driven export of a protein across the membrane. It is also possible that the release might be mediated by the direct interaction between the ribosome–nascent chain complex and membrane protein insertion apparatus, which could trigger signal transduction that rearranges the environment of the exit tunnel or the PTC so that the translational arrest of *mifM* is canceled. In keeping with this model, it has recently been shown that the ribosome–nascent chain makes nearly identical contacts with the YidC and SecYEG channels and that this interaction causes similar structural changes in the large subunit of the ribosome (Kohler *et al*, 2009). Additional studies are necessary to elucidate the precise mechanism for release of the MifM translational arrest.

Mitochondria, chloroplasts and certain Gram-positive bacteria express more than one YidC/Oxa1/Alb3 protein. In some cases, the YidC proteins are functionally differentiated. For example, mitochondrial Oxa1 has a C-terminal extension that interacts with the mitochondrial ribosome and thereby mediates cotranslational membrane insertion, whereas the homolog Cox18 lacks the C-terminal extension and functions at later steps of membrane protein insertion (reviewed by Bonnefoy *et al*, 2009). A similar functional differentiation has been proposed in the Gram-positive bacterium *S. mutans*, in which YidC2 possesses a C-terminal ribosome-docking site and is involved in co-translational membrane protein insertion, whereas YidC1 lacks this domain (Funes *et al*, 2009). Interestingly, neither *B. subtilis* SpoIIIJ nor YidC2 has this C-terminal extension, although our data suggest that at least one SpoIIIJ substrate, MifM, is targeted to SpoIIIJ co-translationally. SpoIIIJ and YidC2 clearly share an essential function, as it is possible to genetically inactivate one but not both genes. YidC2 therefore provides a backup for this essential function, allowing cells to survive an otherwise lethal event. The *mifM* sensing system we here describe allows this backup function to be inducible, perhaps reducing the fitness cost associated with expressing YidC2 when it is not needed. SpoIIIJ and YidC2 also seem to have at least one non-overlapping function. Specifically, YidC2 is unable to substitute for SpoIIIJ during sporulation (Errington *et al*, 1992; Murakami *et al*, 2002; Tjalsma *et al*, 2003), suggesting that certain membrane proteins might specifically require SpoIIIJ for their biogenesis (such as SpoIIIAE; Camp and Losick, 2008). It is interesting to speculate that YidC2 might also be specifically required in a particular environment, or during a specific developmental pathway or stress response that is shared by those Gram-positive species that encode more than one YidC protein. We suspect that accessory YidC proteins might have different functions in different bacterial species, because not all *yidC2* genes are preceded by *mifM* (Figure 5B; Supplementary Table S2). This might also be the case for SecA and SecY, which are frequently duplicated in Gram-positive bacteria (Cao and Saier, 2003; Rigel and Braunstein, 2008; Siboo *et al*, 2008; Mistou *et al*, 2009).

Our phylogentic analysis indicates that the membrane protein insertion monitor MifM evolved in a different group of bacteria than the protein secretion monitor SecM (van der Sluis and Driessen, 2006). This, together with the absence of sequence similarity in the arrest motif of the two proteins, suggests that MifM and SecM represent the parallel evolution

Table I Strains used in these studies

Strains	Genotype	Reference or source
PY79	wild type	Youngman *et al* (1984)
KP3034	*lacA::spec*	This study
KP11086	*amyE::yidC2^{275}–lacZΩcat*	Rubio *et al* (2005)
KP11131	*amyE::yidC2^{275}–lacZΩcat, ΔspoIIIJ-jag::cat::spc*	Rubio *et al* (2005)
KP11268	*yidC2-gfpΩspc*	This study
SCB406	*amyE::mifM^{95}–lacZΩcat*	This study
SCB416	*amyE::mifM^{95}–lacZΩcat, ΔspoIIIJ-jag::cat::spc*	This study
SCB421	*amyE::mifM^{S}–lacZΩcat*	This study
SCB426	*amyE::mifM^{S}–lacZΩcat, ΔspoIIIJ-jag::cat::spc*	This study
SCB429	*yidC2-gfpΩspc, amyE::mifM(ΔTM)–yidC2^{6}–lacZΩcat*	This study
SCB430	*yidC2-gfpΩspc, ΔspoIIIJ-jag::cat::tet*	This study
SCB454	*amyE::mifM(ΔTM)–yidC2^{6}–lacZΩcat*	This study
SCB461	*amyE::mifM(ΔTM)–yidC2^{6}–lacZΩcat, ΔspoIIIJ-jag::cat::spc*	This study
SCB467	*amyE::mifM(91-96rp)yidC2^{6}–lacZΩcat*	This study
SCB474	*amyE::mifM(91-96rp)yidC2^{6}–lacZΩcat, ΔspoIIIJ-jag::cat::spc*	This study
SCB495	*amyE::mifMyidC2^{6}–lacZ(Δstem)Ωcat*	This study
SCB501	*amyE::mifMyidC2^{6}–lacZ(Δstem)Ωcat, ΔspoIIIJ-jag::cat::spc*	This study
SCB560	*amyE::mifM(D86stop)–yidC2^{6}–lacZΩcat*	This study
SCB561	*amyE::mifM(A90stop)–yidC2^{6}–lacZΩcat*	This study
SCB562	*amyE::mifM(frameshift)–yidC2^{6}–lacZΩcat*	This study
SCB566	*amyE::mifM(D86stop)–yidC2^{6}–lacZΩcat, ΔspoIIIJ-jag::cat::spc*	This study
SCB567	*amyE::mifM(A90stop)–yidC2^{6}–lacZΩcat, ΔspoIIIJ-jag::cat::spc*	This study
SCB568	*amyE::mifM(frameshift)–yidC2^{6}–lacZΩcat, ΔspoIIIJ-jag::cat::spc*	This study
SCB610	*ybaCΩloxP-kan-loxP*	This study
SCB625	*ybaCΩloxP-kan-loxP, erm^{R}*	This study
SCB663	*amyE::mifM(E87stop)–yidC2^{6}–lacZΩcat*	This study
SCB664	*amyE::mifM(E88stop)–yidC2^{6}–lacZΩcat*	This study
SCB665	*amyE::mifM(D89stop)–yidC2^{6}–lacZΩcat*	This study
SCB669	*amyE::mifM(E87stop)–yidC2^{6}–lacZΩcat, ΔspoIIIJ-jag::cat::spc*	This study
SCB670	*amyE::mifM(E88stop)–yidC2^{6}–lacZΩcat, ΔspoIIIJ-jag::cat::spc*	This study
SCB671	*amyE::mifM(D89stop)–yidC2^{6}–lacZΩcat, ΔspoIIIJ-jag::cat::spc*	This study
SCB675	*amyE::mifM(I66A)–yidC2^{6}–lacZΩcat*	This study
SCB676	*amyE::mifM(Y67A)–yidC2^{6}–lacZΩcat*	This study
SCB677	*amyE::mifM(H68A)–yidC2^{6}–lacZΩcat*	This study
SCB678	*amyE::mifM(R69A)–yidC2^{6}–lacZΩcat*	This study
SCB680	*amyE::mifM(T71A)–yidC2^{6}–lacZΩcat*	This study
SCB681	*amyE::mifM(T72A)–yidC2^{6}–lacZΩcat*	This study
SCB682	*amyE::mifM(W73A)–yidC2^{6}–lacZΩcat*	This study
SCB683	*amyE::mifM(I74A)–yidC2^{6}–lacZΩcat*	This study
SCB685	*amyE::mifM(K76A)–yidC2^{6}–lacZΩcat*	This study
SCB686	*amyE::mifM(V77A)–yidC2^{6}–lacZΩcat*	This study
SCB687	*amyE::mifM(F78A)–yidC2^{6}–lacZΩcat*	This study
SCB688	*amyE::mifM(R79A)–yidC2^{6}–lacZΩcat*	This study
SCB689	*amyE::mifM(I70A)–yidC2^{6}–lacZΩcat*	This study
SCB689	*amyE::mifM(M80A)–yidC2^{6}–lacZΩcat*	This study
SCB691	*amyE::mifM(S82A)–yidC2^{6}–lacZΩcat*	This study
SCB692	*amyE::mifM(P83A)–yidC2^{6}–lacZΩcat*	This study
SCB693	*amyE::mifM(V84A)–yidC2^{6}–lacZΩcat*	This study
SCB694	*amyE::mifM(N85A)–yidC2^{6}–lacZΩcat*	This study
SCB695	*amyE::mifM(D86A)–yidC2^{6}–lacZΩcat*	This study
SCB696	*amyE::mifM(E87A)–yidC2^{6}–lacZΩcat*	This study
SCB697	*amyE::mifM(E88A)–yidC2^{6}–lacZΩcat*	This study
SCB705	*amyE::mifM(D86silent)-TAA-yidC2^{6}–lacZΩcat*	This study
SCB706	*amyE::mifM(I66A)–yidC2^{6}–lacZΩcat, ΔspoIIIJ-jag::cat::spc*	This study
SCB707	*amyE::mifM(Y67A)–yidC2^{6}–lacZΩcat, ΔspoIIIJ-jag::cat::spc*	This study
SCB708	*amyE::mifM(H68A)–yidC2^{6}–lacZΩcat, ΔspoIIIJ-jag::cat::spc*	This study
SCB709	*amyE::mifM(R69A)–yidC2^{6}–lacZΩcat, ΔspoIIIJ-jag::cat::spc*	This study
SCB710	*amyE::mifM(I70A)–yidC2^{6}–lacZΩcat, ΔspoIIIJ-jag::cat::spc*	This study
SCB711	*amyE::mifM(T71A)–yidC2^{6}–lacZΩcat, ΔspoIIIJ-jag::cat::spc*	This study
SCB712	*amyE::mifM(T72A)–yidC2^{6}–lacZΩcat, ΔspoIIIJ-jag::cat::spc*	This study
SCB713	*amyE::mifM(W73A)–yidC2^{6}–lacZΩcat, ΔspoIIIJ-jag::cat::spc*	This study
SCB714	*amyE::mifM(I74A)–yidC2^{6}–lacZΩcat, ΔspoIIIJ-jag::cat::spc*	This study
SCB716	*amyE::mifM(K76A)–yidC2^{6}–lacZΩcat, ΔspoIIIJ-jag::cat::spc*	This study
SCB717	*amyE::mifM(V77A)–yidC2^{6}–lacZΩcat, ΔspoIIIJ-jag::cat::spc*	This study
SCB718	*amyE::mifM(F78A)–yidC2^{6}–lacZΩcat, ΔspoIIIJ-jag::cat::spc*	This study
SCB719	*amyE::mifM(R79A)–yidC2^{6}–lacZΩcat, ΔspoIIIJ-jag::cat::spc*	This study
SCB720	*amyE::mifM(M80A)–yidC2^{6}–lacZΩcat, ΔspoIIIJ-jag::cat::spc*	This study
SCB722	*amyE::mifM(S82A)–yidC2^{6}–lacZΩcat, ΔspoIIIJ-jag::cat::spc*	This study
SCB723	*amyE::mifM(P83A)–yidC2^{6}–lacZΩcat, ΔspoIIIJ-jag::cat::spc*	This study
SCB724	*amyE::mifM(V84A)–yidC2^{6}–lacZΩcat, ΔspoIIIJ-jag::cat::spc*	This study
SCB725	*amyE::mifM(N85A)–yidC2^{6}–lacZΩcat, ΔspoIIIJ-jag::cat::spc*	This study
SCB726	*amyE::mifM(D86A)–yidC2^{6}–lacZΩcat, ΔspoIIIJ-jag::cat::spc*	This study
SCB727	*amyE::mifM(E87A)–yidC2^{6}–lacZΩcat, ΔspoIIIJ-jag::cat::spc*	This study
SCB728	*amyE::mifM(E88A)–yidC2^{6}–lacZΩcat, ΔspoIIIJ-jag::cat::spc*	This study

Table I Continued

Strains	Genotype	Reference or source
SCB736	*amyE::mifMD86(silent)-TAA-yidC2^{6}–lacZΩcat, ΔspoIIIJ-jag::cat::spc*	This study
SCB751	*amyE::yidC2^{6}–lacZΩcat*	This study
SCB757	*amyE::yidC2^{6}–lacZΩcat, ΔspoIIIJ-jag::cat::spc*	This study
SCB762	*amyE::mifM(N81A)–yidC2^{6}–lacZΩcat*	This study
SCB767	*amyE::mifM(N81A)–yidC2^{6}–lacZΩcat, ΔspoIIIJ-jag::cat::spc*	This study
SCB803	*amyE::mifM(T60A)–yidC2^{6}–lacZΩcat*	This study
SCB804	*amyE::mifM(D61A)–yidC2^{6}–lacZΩcat*	This study
SCB805	*amyE::mifM(F62A)–yidC2^{6}–lacZΩcat*	This study
SCB806	*amyE::mifM(L63A)–yidC2^{6}–lacZΩcat*	This study
SCB807	*amyE::mifM(I65A)–yidC2^{6}–lacZΩcat*	This study
SCB814	*amyE::mifM(T60A)–yidC2^{6}–lacZΩcat, ΔspoIIIJ-jag::cat::spc*	This study
SCB815	*amyE::mifM(D61A)–yidC2^{6}–lacZΩcat, ΔspoIIIJ-jag::cat::spc*	This study
SCB816	*amyE::mifM(F62A)–yidC2^{6}–lacZΩcat, ΔspoIIIJ-jag::cat::spc*	This study
SCB817	*amyE::mifM(L63A)–yidC2^{6}–lacZΩcat, ΔspoIIIJ-jag::cat::spc*	This study
SCB818	*amyE::mifM(I65A)–yidC2^{6}–lacZΩcat, ΔspoIIIJ-jag::cat::spc*	This study
SCB828	*amyE::rbsm1-gfp–mifM$^{35-95}$–yidC2^{6}–lacZΩcat*	This study
SCB832	*amyE::mifM(R75A)–yidC2^{6}–lacZΩcat*	This study
SCB839	*amyE::mifM(R75A)–yidC2^{6}–lacZΩcat, ΔspoIIIJ-jag::cat::spc*	This study
SCB844	*amyE::yidC2^{6}–lacZΩcat, lacA::spc*	This study
SCB846	*amyE::mifM(R59A)–yidC2^{6}–lacZΩcat*	This study
SCB847	*amyE::mifM(D89A)–yidC2^{6}–lacZΩcat*	This study
SCB851	*amyE::rbsm1-gfp–mifM$^{35-95}$–flag-yidC2^{6}–lacZΩcat*	This study
SCB858	*amyE::mifM(R59A)–yidC2^{6}–lacZΩcat, ΔspoIIIJ-jag::cat::spc*	This study
SCB859	*amyE::mifM(D89A)–yidC2^{6}–lacZΩcat, ΔspoIIIJ-jag::cat::spc*	This study
SCB966	*ybaCΩloxP-kan-loxP, ΔspoIIIJ-jag::cat::spc*	This study
SCB967	*ybaCΩloxP-kan-loxP, erm^{R}, ΔspoIIIJ-jag::cat::spc*	This study
SCB968	*ybaCΩloxP-kan-loxP, ΔyidC2::spc*	This study
SCB969	*ybaCΩloxP-kan-loxP, erm^{R}, ΔyidC2::spc*	This study
SCB972	*amyE::mifM(ΔTM)–yidC2^{6}–lacZΩcat, ybaCΩloxP-kan-loxP*	This study
SCB973	*amyE::mifM(ΔTM)–yidC2^{6}–lacZΩcat, ybaCΩloxP-kan-loxP, erm^{R}*	This study
SCB976	*amyE::P$_{mifM}$-rbsm1-gfp–mifM$^{35-95}$–flag–yidC2^{6}–lacZΩcat, ybaCΩloxP-kan-loxP*	This study
SCB993	*amyE::P$_{mifM}$-rbsm1-gfp–mifM$^{35-95}$–flag–yidC2^{6}–lacZΩcat, ybaCΩloxP-kan-loxP, erm^{R}*	This study
SCB994	*amyE::mifM(Δstem)yidC2^{6}–lacZΩcat, ybaCΩloxP-kan-loxP*	This study
SCB995	*amyE::mifM(Δstem)yidC2^{6}–lacZΩcat, ybaCΩloxP-kan-loxP, erm^{R}*	This study
SCB996	*amyE::mifM(I64A)–yidC2^{6}–lacZΩcat*	This study
SCB1002	*amyE::mifM(I64A)–yidC2^{6}–lacZΩcat, ΔspoIIIJ-jag::cat::spc*	This study
SCB1044	*amyE::P$_{mifM}$-gfp–mifM$^{35-95}$–flagΩcat*	This study
SCB1045	*amyE::P$_{mifM}$-gfp–mifM$^{35-95}$(R75A)–flagΩcat*	This study
SCB1049	*amyE::P$_{mifM}$-gfp–mifM$^{35-95}$(I74A)–flagΩcat*	This study
SCB1051	*amyE::P$_{mifM}$-gfp–mifM$^{35-95}$(R59A)–flagΩcat*	This study
SCB1052	*amyE::P$_{mifM}$-gfp–mifM$^{35-95}$(T60A)–flagΩcat*	This study
SCB1053	*amyE::P$_{mifM}$-gfp–mifM$^{35-95}$(D61A)–flagΩcat*	This study
SCB1054	*amyE::P$_{mifM}$-gfp–mifM$^{35-95}$(F62A)–flagΩcat*	This study
SCB1055	*amyE::P$_{mifM}$-gfp–mifM$^{35-95}$(L63A)–flagΩcat*	This study
SCB1056	*amyE::P$_{mifM}$-gfp–mifM$^{35-95}$(I64A)–flagΩcat*	This study
SCB1057	*amyE::P$_{mifM}$-gfp–mifM$^{35-95}$(I65A)–flagΩcat*	This study
SCB1058	*amyE::P$_{mifM}$-gfp–mifM$^{35-95}$(I66A)–flagΩcat*	This study
SCB1059	*amyE::P$_{mifM}$-gfp–mifM$^{35-95}$(Y67A)–flagΩcat*	This study
SCB1060	*amyE::P$_{mifM}$-gfp–mifM$^{35-95}$(H68A)–flagΩcat*	This study
SCB1061	*amyE::P$_{mifM}$-gfp–mifM$^{35-95}$(R69A)–flagΩcat*	This study
SCB1062	*amyE::P$_{mifM}$-gfp–mifM$^{35-95}$(I70A)–flagΩcat*	This study
SCB1064	*amyE::P$_{mifM}$-gfp–mifM$^{35-95}$(T72A)–flagΩcat*	This study
SCB1065	*amyE::P$_{mifM}$-gfp–mifM$^{35-95}$(W73A)–flagΩcat*	This study
SCB1066	*amyE::P$_{mifM}$-gfp–mifM$^{35-95}$(K76A)–flagΩcat*	This study
SCB1067	*amyE::P$_{mifM}$-gfp–mifM$^{35-95}$(V77A)–flagΩcat*	This study
SCB1068	*amyE::P$_{mifM}$-gfp–mifM$^{35-95}$(F78A)–flagΩcat*	This study
SCB1069	*amyE::P$_{mifM}$-gfp–mifM$^{35-95}$(R79A)–flagΩcat*	This study
SCB1070	*amyE::P$_{mifM}$-gfp–mifM$^{35-95}$(M80A)–flagΩcat*	This study
SCB1071	*amyE::P$_{mifM}$-gfp–mifM$^{35-95}$(N81A)–flagΩcat*	This study
SCB1072	*amyE::P$_{mifM}$-gfp–mifM$^{35-95}$(S82A)–flagΩcat*	This study
SCB1073	*amyE::P$_{mifM}$-gfp–mifM$^{35-95}$(P83A)–flagΩcat*	This study
SCB1074	*amyE::P$_{mifM}$-gfp–mifM$^{35-95}$(V84A)–flagΩcat*	This study
SCB1075	*amyE::P$_{mifM}$-gfp–mifM$^{35-95}$(N85A)–flagΩcat*	This study
SCB1076	*amyE::P$_{mifM}$-gfp–mifM$^{35-95}$(D86A)–flagΩcat*	This study
SCB1077	*amyE::P$_{mifM}$-gfp–mifM$^{35-95}$(E87A)–flagΩcat*	This study
SCB1078	*amyE::P$_{mifM}$-gfp–mifM$^{35-95}$(E88A)–flagΩcat*	This study
SCB1260	*amyE::P$_{mifM}$-gfp–mifM$^{35-95}$(T71A)–flagΩcat*	This study
SCB1261	*amyE::P$_{mifM}$-gfp–mifM$^{35-95}$(D89A)–flagΩcat*	This study
ALB185	*spoIIIJ-flagΩloxP-kan-loxP, lacA::spec*	This study
ALB198	*spoIIIJ (Shine–Dalgarno AGGAGG to AGGAAG), amyE::yidC2^{6}–lacZΩcat, lacA::spec*	This study
ALB228	*spoIIIJ (Shine–Dalgarno AGGAGG to AAGAGG), amyE::yidC2^{6}–lacZΩcat, lacA::spec*	This study
ALB396	*spoIIIJ (Shine–Dalgarno AGGAGG to AGAAGG), amyE::yidC2^{6}–lacZΩcat, lacA::spec*	This study

of protein sensors of two different pathways that act by similar molecular mechanisms. The increasing numbers of regulatory nascent chains that lack primary sequence identity suggests that the ribosome does not blindly translate the genetic code. Translation instead seems to represent an ongoing negotiation between the ribosome, the nascent polypeptide and other cellular components such as the machineries for membrane protein biogenesis and protein secretion. Although this might limit the usage of the genetic code, it allows cells to use nascent chains as regulatory switches that respond to different co-translational or translational events. Clearly nascent chains are not simply nonfunctional intermediates in proteins synthesis and instead are capable of interacting with a discriminating ribosome to provide regulatory mechanisms that enable cells to respond to changing intracellular environments.

Materials and methods

Strain and plasmid construction

B. subtilis strains (Table I) were constructed by transformation (Hoch, 1991). The Δ*spoIIIJ-jag* deletion strain used in these studies is a complete deletion in which the coding region was replaced by a *cat* gene that was subsequently replaced with the *tet* gene (Rubio *et al*, 2005) using pCm::Tc (Steinmetz and Richter, 1994). The *lacA::spec* mutation (Hartl *et al*, 2001) was transformed into PY79 for these studies. Plasmids (Supplementary Table S3) were constructed by standard cloning methods, PCR and site-directed mutagenesis (Sawano and Miyawaki, 2000) using the strategies described in Supplementary data and the oligonucleotides in Supplementary Table S4. Plasmids were verified by sequencing the coding region. Following introduction into the *B. subtilis* chromosome, recombinants were checked for their antibiotic resistance, the inactivation of *amyE* and the loss of any additional drug resistance markers on the plasmid backbone.

Growth conditions and general procedures

B. subtilis cells were cultured at 37°C in LB and CH media (Sterlini and Mandelstam, 1969) for western blotting and β-galactosidase activities assay, respectively. Cultures with $OD_{600} = 0.5–1.0$ were collected for each experiment. β-galactosidase assays (Miller, 1972; Rubio *et al*, 2005) and immunoblots (Blaylock *et al*, 2004) were performed as described earlier. Blots were probed with monoclonal anti-GFP (Roche), and either polyclonal (Figure 3F) or monoclonal (Figures 2 and 5) anti-FLAG (Sigma).

Isolation of mutants that overexpress yidC2

A 10 ml aliquot of SCB844 (*amyE::yidC2*^{6}*–lacZΩcat, lacA::spc*) culture with $OD_{600} = 0.5$ in LB media was collected, washed with the citrate buffer (100 mM citric acid, pH5.5) twice, suspended in 10 ml of the citrate buffer and divided into 10 tubes. The cells were treated with 0.1 mg/ml NTG for 30 min at 30°C, then washed with 1 ml of phosphate buffer (pH 7.0) and suspended in 1 ml of LB followed by addition of the same volume of 50% glycerol. The mutant pools were stored at −80°C until subjected to screening. The mutant pool was diluted and aliquots spread on DSM plates containing 60 μg/ml X-gal. Blue colonies were isolated at 37 and 42°C. Chromosomal DNA of Lac+ mutants was isolated and transformed into PY79 selecting for Cm^R encoded by *amyE::yidC2*^{6}*–lacZΩcat* to identify mutations linked to the fusion. Unlinked mutations were moved into an unmutagenized background by transformation into KP3034 (*lacA::spec*) competent cells using a high concentration of chromosomal DNA, selecting for Cm^R and isolating the rare blue colonies in which both the unknown mutation and the *lacZ* fusion had been co-transformed into the recipient. These backcrossed strains were checked for linkage to *spoIIIJ* by transformation with chromosomal DNA from strain ALB185 (Table I). The *spoIIIJ*-linked mutations were sequenced to identify the point mutations. Three different mutations affecting the SD sequence were identified (Supplementary data).

CTABr precipitation

CTABr precipitation was performed essentially as described (Gilmore *et al*, 1991; Nakatogawa and Ito, 2001), with the following modifications. To prepare lysates of *B. subtilis* cells, 1 ml of LB culture was washed with 1 ml of HSM (20 mM HEPES (pH 7.6), 20% sucrose, 20 mM $MgCl_2$) buffer and treated with 1 mg/ml lysozyme in the same buffer for 10 min at 37°C. Cells were then collected by centrifugation and resuspended in 200 μl of ice-cold 20 mM HEPES (pH 7.6), 150 mM NaCl and solubilized with 0.5% NP-40 on ice for 7 min. Insoluble particles were removed by centrifuge (4°C, 13 000 r.p.m. for 5 min) and 90 μl of each cell lysate was mixed with 500 μl of 2% CTABr and 500 μl of 0.5 M NaOAc (pH 4.7) for CTABr precipitation. The mixture was incubated on ice for 10 min, then at 30°C for 10 min, centrifuged at 14 000 r.p.m. for 15 min and the pellet washed by acetone/HCl (19:1) twice and solubilized in SDS sample buffer. The supernatants were collected and proteins precipitated with 10% TCA and washed by acetone/HCl (19:1) before solubilization in SDS sample buffer. RNase treatment was done by adding 0.5 μl of 4 mg/ml RNaseA into 90 μl of cell lysate and incubated for 10 min at 37°C before addition of CTABr.

Isolation and characterization of erythromycin resistant (Erm^R) mutations

Strain SCB610 (*ybaCΩloxP-kan-loxP*), which has a kanamycin resistance marker near the ribosomal protein operon was plated on LB plates with 2 μg/ml of erythromycin to select spontaneous Erm^R mutants. Genetic linkage between the *erm* mutation and the ribosomal operon was tested by transforming chromosomal DNA of each mutant into PY79 (wild type) on LB erythromycin plates and screening for kanamycin resistance; all were linked. The *rplV* gene of wild type (SCB610) and *erm* mutants was PCR amplified and sequenced.

Microscopy and image analysis

For GFP visualization, live cells were stained with 5 μg/ml FM 4–64 (Molecular Probes; (Sharp and Pogliano, 1999). Images were collected using an Applied Precision optical sectioning microscope (Liu *et al*, 2006) and deconvolved using softWoRx v3.3.6 (Applied Precision).

Supplementary data

Supplementary data are available at *The EMBO Journal* Online (http://www.embojournal.org).

Acknowledgements

This work was supported by the National Institute of Health (GM 57045). SC and AL performed the experiments; SC, AL and KP analysed the data. SC and KP prepared the paper.

Conflict of interest

The authors declare that they have no conflict of interest.

References

Ban N, Nissen P, Hansen J, Moore PB, Steitz TA (2000) The complete atomic structure of the large ribosomal subunit at 2.4 A resolution. *Science* **289:** 905–920

Blaylock B, Jiang X, Rubio A, Moran Jr CP., Pogliano K (2004) Zipper-like interaction between proteins in adjacent daughter cells mediates protein localization. *Genes Dev* **18:** 2916–2928

Bonnefoy N, Fiumera HL, Dujardin G, Fox TD (2009) Roles of Oxa1-related inner-membrane translocases in assembly of respiratory chain complexes. *Biochim Biophys Acta* **1793:** 60–70

Butkus ME, Prundeanu LB, Oliver DB (2003) Translocon 'pulling' of nascent SecM controls the duration of its translational pause and secretion-responsive secA regulation. *J Bacteriol* **185:** 6719–6722

Camp AH, Losick R (2008) A novel pathway of intercellular signalling in *Bacillus subtilis* involves a protein with similarity to a component of type III secretion channels. *Mol Microbiol* **69:** 402–417

Cao TB, Saier Jr MH (2003) The general protein secretory pathway: phylogenetic analyses leading to evolutionary conclusions. *Biochim Biophys Acta* **1609:** 115–125

Celebi N, Dalbey RE, Yuan J (2008) Mechanism and hydrophobic forces driving membrane protein insertion of subunit II of cytochrome bo 3 oxidase. *J Mol Biol* **375:** 1282–1292

Cruz-Vera LR, New A, Squires C, Yanofsky C (2007) Ribosomal features essential for tna operon induction: tryptophan binding at the peptidyl transferase center. *J Bacteriol* **189:** 3140–3146

Cruz-Vera LR, Rajagopal S, Squires C, Yanofsky C (2005) Features of ribosome-peptidyl-tRNA interactions essential for tryptophan induction of tna operon expression. *Mol Cell* **19:** 333–343

Cruz-Vera LR, Yanofsky C (2008) Conserved residues Asp16 and Pro24 of TnaC-tRNAPro participate in tryptophan induction of Tna operon expression. *J Bacteriol* **190:** 4791–4797

Culver GM (2001) Meanderings of the mRNA through the ribosome. *Structure* **9:** 751–758

Daniel CJ, Conti B, Johnson AE, Skach WR (2008) Control of translocation through the Sec61 translocon by nascent polypeptide structure within the ribosome. *J Biol Chem* **283:** 20864–20873

Diner EJ, Hayes CS (2009) Recombineering reveals a diverse collection of ribosomal proteins L4 and L22 that confer resistance to macrolide antibiotics. *J Mol Biol* **386:** 300–315

Dong Y, Palmer SR, Hasona A, Nagamori S, Kaback HR, Dalbey RE, Brady LJ (2008) Functional overlap but lack of complete cross-complementation of Streptococcus mutans and *Escherichia coli* YidC orthologs. *J Bacteriol* **190:** 2458–2469

Driessen AJ, Nouwen N (2008) Protein translocation across the bacterial cytoplasmic membrane. *Annu Rev Biochem* **77:** 643–667

Errington J, Appleby L, Daniel RA, Goodfellow H, Partridge SR, Yudkin MD (1992) Structure and function of the *spoIIIJ* gene of *Bacillus subtilis*: a vegetatively expressed gene that is essential for σ^G activity at an intermediate stage of sporulation. *J Gen Microbiol* **138** (Pt 12): 2609–2618

Facey SJ, Neugebauer SA, Krauss S, Kuhn A (2007) The mechanosensitive channel protein MscL is targeted by the SRP to the novel YidC membrane insertion pathway of *Escherichia coli*. *J Mol Biol* **365:** 995–1004

Franceschi F, Kanyo Z, Sherer EC, Sutcliffe J (2004) Macrolide resistance from the ribosome perspective. *Curr Drug Targets Infect Disord* **4:** 177–191

Frank J, Zhu J, Penczek P, Li Y, Srivastava S, Verschoor A, Radermacher M, Grassucci R, Lata RK, Agrawal RK (1995) A model of protein synthesis based on cryo-electron microscopy of the *E. coli* ribosome. *Nature* **376:** 441–444

Funes S, Hasona A, Bauerschmitt H, Grubbauer C, Kauff F, Collins R, Crowley PJ, Palmer SR, Brady LJ, Herrmann JM (2009) Independent gene duplications of the YidC/Oxa/Alb3 family enabled a specialized cotranslational function. *Proc Natl Acad Sci USA* **106:** 6656–6661

Gaynor M, Mankin AS (2003) Macrolide antibiotics: binding site, mechanism of action, resistance. *Curr Top Med Chem* **3:** 949–961

Gilmore R, Collins P, Johnson J, Kellaris K, Rapiejko P (1991) Transcription of full-length and truncated mRNA transcripts to study protein translocation across the endoplasmic reticulum. *Methods Cell Biol* **34:** 223–239

Gong F, Yanofsky C (2002) Instruction of translating ribosome by nascent peptide. *Science* **297:** 1864–1867

Hartl B, Wehrl W, Wiegert T, Homuth G, Schumann W (2001) Development of a new integration site within the *Bacillus subtilis* chromosome and construction of compatible expression cassettes. *J Bacteriol* **183:** 2696–2699

Hasona A, Crowley PJ, Levesque CM, Mair RW, Cvitkovitch DG, Bleiweis AS, Brady LJ (2005) Streptococcal viability and diminished stress tolerance in mutants lacking the signal recognition particle pathway or YidC2. *Proc Natl Acad Sci USA* **102:** 17466–17471

Hegde RS, Kang SW (2008) The concept of translocational regulation. *J Cell Biol* **182:** 225–232

Hoch JA (1991) Genetic analysis in *Bacillus subtilis*. *Methods Enzymol* **204:** 305–320

Kang SW, Rane NS, Kim SJ, Garrison JL, Taunton J, Hegde RS (2006) Substrate-specific translocational attenuation during ER stress defines a pre-emptive quality control pathway. *Cell* **127:** 999–1013

Kiefer D, Kuhn A (2007) YidC as an essential and multifunctional component in membrane protein assembly. *Int Rev Cytol* **259:** 113–138

Kohler R, Boehringer D, Greber B, Bingel-Erlenmeyer R, Collinson I, Schaffitzel C, Ban N (2009) YidC and Oxa1 form dimeric insertion pores on the translating ribosome. *Mol Cell* **34:** 344–353

Kol S, Nouwen N, Driessen AJ (2008) Mechanisms of YidC-mediated insertion and assembly of multimeric membrane protein complexes. *J Biol Chem* **283:** 31269–31273

Krieg UC, Johnson AE, Walter P (1989) Protein translocation across the endoplasmic reticulum membrane: identification by photocross-linking of a 39-kD integral membrane glycoprotein as part of a putative translocation tunnel. *J Cell Biol* **109:** 2033–2043

Lawrence MG, Lindahl L, Zengel JM (2008) Effects on translation pausing of alterations in protein and RNA components of the ribosome exit tunnel. *J Bacteriol* **190:** 5862–5869

Liu NJ, Dutton RJ, Pogliano K (2006) Evidence that the SpoIIIE DNA translocase participates in membrane fusion during cytokinesis and engulfment. *Mol Microbiol* **59:** 1097–1113

Lotz M, Haase W, Kuhlbrandt W, Collinson I (2008) Projection structure of YidC: a conserved mediator of membrane protein assembly. *J Mol Biol* **375:** 901–907

Matlack KE, Walter P (1995) The 70 carboxyl-terminal amino acids of nascent secretory proteins are protected from proteolysis by the ribosome and the protein translocation apparatus of the endoplasmic reticulum membrane. *J Biol Chem* **270:** 6170–6180

McNicholas P, Salavati R, Oliver D (1997) Dual regulation of *Escherichia coli secA* translation by distinct upstream elements. *J Mol Biol* **265:** 128–141

Miller JH (1972) *Experiments in Molecular Genetics*. Cold Spring Harbor, NY: Cold Spring Harbor Laboratory Press

Mistou MY, Dramsi S, Brega S, Poyart C, Trieu-Cuot P (2009) Molecular dissection of the *secA2* locus of group B *Streptococcus* reveals that glycosylation of the Srr1 LPXTG protein is required for full virulence. *J Bacteriol* **191:** 4195–4206

Mothes W, Prehn S, Rapoport TA (1994) Systematic probing of the environment of a translocating secretory protein during translocation through the ER membrane. *EMBO J* **13:** 3973–3982

Murakami T, Haga K, Takeuchi M, Sato T (2002) Analysis of the *Bacillus subtilis spoIIIJ* gene and its paralogue gene, *yqjG*. *J Bacteriol* **184:** 1998–2004

Nakatogawa H, Ito K (2001) Secretion monitor, SecM, undergoes self-translation arrest in the cytosol. *Mol Cell* **7:** 185–192

Nakatogawa H, Ito K (2002) The ribosomal exit tunnel functions as a discriminating gate. *Cell* **108:** 629–636

Nakatogawa H, Murakami A, Ito K (2004) Control of SecA and SecM translation by protein secretion. *Curr Opin Microbiol* **7:** 145–150

Narayanan CS, Dubnau D (1987) Demonstration of erythromycin-dependent stalling of ribosomes on the *ermC* leader transcript. *J Biol Chem* **262:** 1766–1771

Oliver DB, Beckwith J (1982) Regulation of a membrane component required for protein secretion in *Escherichia coli*. *Cell* **30:** 311–319

Oyadomari S, Yun C, Fisher EA, Kreglinger N, Kreibich G, Oyadomari M, Harding HP, Goodman AG, Harant H, Garrison JL, Taunton J, Katze MG, Ron D (2006) Cotranslocational degradation protects the stressed endoplasmic reticulum from protein overload. *Cell* **126:** 727–739

Papanikou E, Karamanou S, Economou A (2007) Bacterial protein secretion through the translocase nanomachine. *Nat Rev Microbiol* **5:** 839–851

Pogliano KJ, Beckwith J (1993) The Cs sec mutants of *Escherichia coli* reflect the cold sensitivity of protein export itself. *Genetics* **133:** 763–773

Pohlschroder M, Hartmann E, Hand NJ, Dilks K, Haddad A (2005) Diversity and evolution of protein translocation. *Annu Rev Microbiol* **59:** 91–111

Rapoport TA (2007) Protein translocation across the eukaryotic endoplasmic reticulum and bacterial plasma membranes. *Nature* **450:** 663–669

Rigel NW, Braunstein M (2008) A new twist on an old pathway—accessory Sec [corrected] systems. *Mol Microbiol* **69:** 291–302

Rubio A, Jiang X, Pogliano K (2005) Localization of translocation complex components in *Bacillus subtilis:* enrichment of the signal recognition particle receptor at early sporulation septa. *J Bacteriol* **187:** 5000–5002

Samuelson JC, Chen M, Jiang F, Moller I, Wiedmann M, Kuhn A, Phillips GJ, Dalbey RE (2000) YidC mediates membrane protein insertion in bacteria. *Nature* **406:** 637–641

Sawano A, Miyawaki A (2000) Directed evolution of green fluorescent protein by a new versatile PCR strategy for site-directed and semi-random mutagenesis. *Nucleic Acids Res* **28:** 78

Schlunzen F, Harms JM, Franceschi F, Hansen HA, Bartels H, Zarivach R, Yonath A (2003) Structural basis for the antibiotic activity of ketolides and azalides. *Structure* **11:** 329–338

Schmidt MG, Oliver DB (1989) SecA protein autogenously represses its own translation during normal protein secretion in *Escherichia coli*. *J Bacteriol* **171:** 643–649

Schmidt MG, Rollo EE, Grodberg J, Oliver DB (1988) Nucleotide sequence of the *secA* gene and *secA*(Ts) mutations preventing protein export in *Escherichia coli*. *J Bacteriol* **170:** 3404–3414

Serek J, Bauer-Manz G, Struhalla G, van den Berg L, Kiefer D, Dalbey R, Kuhn A (2004) *Escherichia coli* YidC is a membrane insertase for Sec-independent proteins. *EMBO J* **23:** 294–301

Sharp MD, Pogliano K (1999) An *in vivo* membrane fusion assay implicates SpoIIIE in the final stages of engulfment during *Bacillus subtilis* sporulation. *Proc Natl Acad Sci USA* **96:** 14553–14558

Siboo IR, Chaffin DO, Rubens CE, Sullam PM (2008) Characterization of the accessory Sec system of *Staphylococcus aureus*. *J Bacteriol* **190:** 6188–6196

Steinmetz M, Richter R (1994) Plasmids designed to alter the antibiotic resistance expressed by insertion mutations in *Bacillus subtilis*, through *in vivo* recombination. *Gene* **142:** 79–83

Sterlini JM, Mandelstam J (1969) Commitment to sporulation in Bacillus subtilis and its relationship to development of actinomycin resistance. *Biochem J* **113:** 29–37

Takyar S, Hickerson RP, Noller HF (2005) mRNA helicase activity of the ribosome. *Cell* **120:** 49–58

Tenson T, Ehrenberg M (2002) Regulatory nascent peptides in the ribosomal tunnel. *Cell* **108:** 591–594

Tjalsma H, Bron S, van Dijl JM (2003) Complementary impact of paralogous Oxa1-like proteins of Bacillus subtilis on post-translocational stages in protein secretion. *J Biol Chem* **278:** 15622–15632

Tu D, Blaha G, Moore PB, Steitz TA (2005) Structures of MLSBK antibiotics bound to mutated large ribosomal subunits provide a structural explanation for resistance. *Cell* **121:** 257–270

Urbanus ML, Scotti PA, Froderberg L, Saaf A, de Gier JW, Brunner J, Samuelson JC, Dalbey RE, Oudega B, Luirink J (2001) Sec-dependent membrane protein insertion: sequential interaction of nascent FtsQ with SecY and YidC. *EMBO Rep* **2:** 524–529

van der Laan M, Bechtluft P, Kol S, Nouwen N, Driessen AJ (2004) F1F0 ATP synthase subunit c is a substrate of the novel YidC pathway for membrane protein biogenesis. *J Cell Biol* **165:** 213–222

van der Laan M, Houben EN, Nouwen N, Luirink J, Driessen AJ (2001) Reconstitution of Sec-dependent membrane protein insertion: nascent FtsQ interacts with YidC in a SecYEG-dependent manner. *EMBO Rep* **2:** 519–523

van der Laan M, Nouwen NP, Driessen AJ (2005) YidC—an evolutionary conserved device for the assembly of energy-transducing membrane protein complexes. *Curr Opin Microbiol* **8:** 182–187

van der Sluis EO, Driessen AJ (2006) Stepwise evolution of the Sec machinery in Proteobacteria. *Trends Microbiol* **14:** 105–108

Vazquez-Laslop N, Thum C, Mankin AS (2008) Molecular mechanism of drug-dependent ribosome stalling. *Mol Cell* **30:** 190–202

Xie K, Dalbey RE (2008) Inserting proteins into the bacterial cytoplasmic membrane using the Sec and YidC translocases. *Nat Rev Microbiol* **6:** 234–244

Yanofsky C (1981) Attenuation in the control of expression of bacterial operons. *Nature* **289:** 751–758

Yanofsky C (2007) RNA-based regulation of genes of tryptophan synthesis and degradation, in bacteria. *RNA* **13:** 1141–1154

Yanofsky C, Konan KV, Sarsero JP (1996) Some novel transcription attenuation mechanisms used by bacteria. *Biochimie* **78:** 1017–1024

Yap MN, Bernstein HD (2009) The plasticity of a translation arrest motif yields insights into nascent polypeptide recognition inside the ribosome tunnel. *Mol Cell* **34:** 201–211

Yi L, Dalbey RE (2005) Oxa1/Alb3/YidC system for insertion of membrane proteins in mitochondria, chloroplasts and bacteria. *Mol Membr Biol* **22:** 101–111

Youngman P, Perkins JB, Losick R (1984) A novel method for the rapid cloning in *Escherichia coli* of *Bacillus subtilis* chromosomal DNA adjacent to Tn917 insertions. *Mol Gen Genet* **195:** 424–433

Yuan J, Phillips GJ, Dalbey RE (2007) Isolation of cold-sensitive *yidC* mutants provides insights into the substrate profile of the YidC insertase and the importance of transmembrane 3 in YidC function. *J Bacteriol* **189:** 8961–8972

Yusupova G, Jenner L, Rees B, Moras D, Yusupov M (2006) Structural basis for messenger RNA movement on the ribosome. *Nature* **444:** 391–394

Yusupova GZ, Yusupov MM, Cate JH, Noller HF (2001) The path of messenger RNA through the ribosome. *Cell* **106:** 233–241

Zaman S, Fitzpatrick M, Lindahl L, Zengel J (2007) Novel mutations in ribosomal proteins L4 and L22 that confer erythromycin resistance in *Escherichia coli*. *Mol Microbiol* **66:** 1039–1050

Plasmid construction

Plasmids listed in Table S3 were constructed as follows and verified by DNA sequencing of the coding region. To construct pCH735, a BamHI site at the 5' upstream of *mifM* on pAR27 (*amyE*::*mifM-yidC2*^{275}*-lacZΩcat*; Rubio et al., 2005) was mutagenized (from GGATCC to GGGTCC) and a new BamHI site was introduced just before stop codon of *mifM* by site-directed mutagenesis (Sawano and Miyawaki, 2000) using mutagenesis primers SP1 and SP4 (Table S4). The resulting plasmid was then digested by BamHI (which also cuts at the beginning of the *lacZ* coding region) and re-ligated to excise the *yidC2* coding region to allow the last sense codon of *mifM* to be followed both by a BamHI site and *lacZ* in frame. pCH743 was made by essentially the same procedure as pCH735 except using SP2 instead of SP4 in order to introduce a BamHI site after the 5th codon of *mifM* to excise both codons 6 through 95 of *mifM* and the entire *yidC2* coding region. pCH746 was constructed by eliminating the BamHI site at the 5' upstream of *mifM* from pAR70 (*amyE::mifM-yidC2*^{6}*-lacZΩcat*; Rubio et al., 2005) by site-directed mutagenesis using the SP1 mutagenesis primer. Two individual BamHI sites were introduced after the 5th and 34th codons of *mifM* on pCH746 respectively by site-directed mutagenesis using primers SP2 and SP3, generating pCH756. The resulting plasmid was digested by BamHI and re-ligated to excise the region encoding the transmembrane segment of MifM. pCH774, pCH792, pCH795 were constructed by site-directed mutagenesis using individual primer or mixed primers SP7 (for pCH774), SP5 (for pCH792) or mixture of SP12 and SP13 (for pCH795) and pCH746 as the template. pCH804 was constructed by two sequential site-directed mutagenesis using the primer SP12 and the template plasmid pCH746 for the first step to make pCH774 and primers SP13 and SP14 and the template plasmid pCH774 for the second step. pCH806 was constructed by the TA-cloning of a 0.6 kb PCR fragment of '*ybaC* coding region including the stop codon amplified from PY79 cDNA using primers SP16 and SP17 into the T-added SmaI site of pEB71 (a pUC19-derivative with *loxP-kan*^{R}*-loxP*). A stop codon or a codon for alanine was introduced by site-

directed mutagenesis using a template plasmid pCH746 and individual primers described in Table S5 to make a series of plasmids for the stop codon scanning or alanine scanning for *mifM-yidC2*^{6}*-lacZ* derivatives.

Plasmids for *gfp-mifM*$^{35-95}$ were constructed as follows. The transmembrane region of *mifM* flanked by two BamHI sites on pCH756 (described above) was replaced by a BamHI-digested *gfp* PCR fragment amplified from pCH507 (*gfp-spoIIQ*; (Chiba et al., 2007)) using primers SP9 and SP10 to generate pCH835 (*amyE::PmifM-gfp-mifM*$^{35-95}$*-yidC2*^{6}*-lacZΩcat*). An EcoRI fragment of pCH835 was cloned into the same site of pCH818 (*amyE::mifM-flagΩcat*) to make pCH985 (*amyE::P*$_{mifM}$*-gfp-mifM*$^{35-95}$*-flagΩcat*). pCH818 was constructed by cloning a SphI-SpeI fragment of pCH735 into the same sites of pCH801 (*amyE::mifM-yidC2-gfp-SpeI-flagΩcat*). pCH801 was made by introducing a SpeI site followed by eight codons for flag-tag into the 3' end of *gfp* on p*yqjG21* (*amyE::mifM-gfpΩcat*; Rubio et al., 2005) by site directed mutagenesis using primer SP52. A series of plasmids for alanine scanning mutagenesis of GFP-MifM$^{35-95}$-FLAG were constructed by site-directed mutagenesis using individual primers as described in Table S5 and pCH985 as the template. Plasmid pCH913 was constructed by introducing mutations in the Shine-Dalgarno sequence for *gfp-mifM*$^{35-95}$ by site-directed mutagenesis using primer SP8 and the template plasmid pCH805, which is identical to pCH835 but constructed independently in the same procedure. pCH929 was constructed by cloning of a SphI-HindIII fragment of pCH913 into the same sites of pCH892 (*amyE::P*$_{mifM}$*-gfp-mifM*$^{35-95}$*-flag-yidC2*^{6}*-lacZΩcat*), which has been constructed by site-directed mutagenesis using primer SP11 and pCH835 as the template. Plasmids were verified by DNA sequencing of the coding region.

pCH706 encodes a *kanR* gene linked to *spoIIIJ*. It was constructed by TA-cloning of the 3' half of *spoIIIJ* that was PCR amplified with primers SP53 and SP54 from PY79 cDNA and cloning the fragment into the T-added SmaI site of pEB71 to generate a *'spoIIIJ271-flagΩloxP-kan-loxP* allele. This plasmid was integrated into the native *spoIIIJ* locus of PY79.

Isolation of mutations that reduce SpoIIIJ (YidC1) synthesis and induce *yidC2*

Mutations linked to *spoIIIJ* were sequenced. Nine contained mutations in three different sites within the Shine-Dalgarno sequence (with no additional mutations in the coding region) as indicated in Table S5. These mutations reduced the spore titer from 4-10 fold and induced *yidC2*^{6}*-lacZ*, demonstrating that reducing the level of otherwise wildtype SpoIIIJ induces *yidC2*.

Table S1: Phylogenetic distribution of YidC homologues in various bacterial phyla

	Number of species with:						
	one YidC	two YidC	three YidC	total species	total number YidC	Average copy number	Standard deviation
Firmicutes-Clostridiales	26	2	1	29	33	1.14	0.44
Firmicutes-Bacillales	5	20	1	26	48	1.85	0.46
Firmicutes-Lactobacillales	1	27	0	28	55	1.96	0.19
Mollicutes	19	0	0	19	19	1	0
Cyanobacteria	9	0	0	9	9	1	0
Actinobacteria-Corynebacteriaceae	0	5	0	5	10	2	0
Actinobacteria-Mycobacteriaceae	10	0	0	10	10	1	0
Actinobacteria-Streptomycetaceae	0	3	0	3	6	2	0
Actinobacteria-Micrococcaceae	2	2	0	4	6	1.5	0.58
Actinobacteria-Nocardioidaceae	3	1	0	4	5	1.25	0.5
Firmicutes-Bacillaceae	2	13	1	16	31	1.94	0.44
Firmicutes-Listeriaceae	0	3	0	3	6	2	0
Firmicutes-Staphylococcaceae	1	4	0	5	9	1.8	0.45
Firmicutes-Lactobacillaceae	0	14	0	14	28	2	0
Firmicutes-Leuconostocaceae	0	3	0	3	6	2	0
Firmicutes-Streptococcaceae	0	10	0	10	20	2	0
Firmicutes-Clostridiaceae	11	2	1	14	18	1.29	0.61
Firmicutes-Peptococcaceae	5	0	0	5	5	1	0

BLASTP was used to identify YidC homologues starting in May 2009, using *B. subtilis* SpoIIIJ as the query sequence and an e-value of 0.07 as the cutoff. Only a single strain was analyzed per species.

Table S2: Sequence alignments of MifM-like proteins

A

```
L. monocytogenes          ----MISILQILLEPEFISLTVTFLLMLTIFSYWSAITLLKPKMVLPADAICIKPVKISL 56
L. welshimeri             -MRGMISILQLLLEPEFISLTVTFLLMLTIFSYWSAITLLKPKMVLPADAICLKPVKITL 59
L. innocua                ----MISILQLLLEPEFISLTVTFLLMLTIFSYWSAITLLKPKMVLPADATCLKPVKTLL 56
G. kaustophilus           ----MEAPIDLLV---YMSLVGALWIIMK--GYMGAHRTAKS-LFYEPALASVREREAGG 50
G. thermodenitrificans    ----MEAPIELLW---YMSLVGVLFVIVK--GYMGIHRVTKS-LSYESAWTTVREYRAGA 50
B. amyloliquefaciens      --MILESMNDFLFLVDFFTIILPALTAIG-IAFLLRERRAGEHWRTKR-IDEHQAVVQLN 56
B. subtilis               MTMFVESINDVLFLVDFFTIILPALTAIG-IAFLLRECRAGEQWKSKR-TDEHQTVFHIN 58
B. licheniformis          --MILESFNDAFFLIEFFTIVLPALTAIG-IALILKDCSTGDSWKTKR-FEEYHAIQFVS 56
B. pumilus                --MIIDTFNEVFFLVEFFTIILPALTAIG-IAFLLKDCRMNEHLGGHR-LEELDAS-LLN 55
B. anthracis              ---MEFLLQDAILYISFVTTALCLLEVFF-LANVSRFVRQQASSGRQRAFALVDTCEDSA 56
B. cereus                 ---MEFLLQDAILYISFVTTALCLLEVFF-LANVSRFVRQQASSGRQRAFALVDTCEDSA 56
B. thuringiensis          ---MEFLLQDAILYISFVTTALCLLEVFF-LANVSRFVRQQASSGRQRAFALVDTCEDSA 56
B. halodurans             ---MLDVLSEMVALSLTIALAVMVITAFTPLYFRTVDRPFRLNWQRKQ----LDSTHMSS 53
B. clausii                ---MIDLIMELPMLWVSVAPVMVVVAMVA---YEN-FKLRRMHMRMKR---TVHDTDKTG 50
                                     :       .:        .

L. monocytogenes          RAHFYRTS--PNFVINWLAITRKCSAITDDEDSFSFSNV------ 93
L. welshimeri             RAHFYRSS--PNFIINWLAITMKCSAITDDEDSFSFSNI------ 96
L. innocua                RAHFVRTS--PNFIINWLAITKKCSAITDDEDSFSFSNR------ 93
G. kaustophilus           GAERAALPWRPLFLPQRRKIPVRERTSRTDEDGRPFPL------- 88
G. thermodenitrificans    ATGFVALPSRPLFLPQRRKIPIRERTNRTDEDGRPFS-------- 87
B. amyloliquefaciens      RTDFLIIIY--HRITTWIRKVIRMNSPANDDEDVSFLLL------ 93
B. subtilis               RTDFLIIIY--HRITTWIRKVFRMNSPVNDEEDAGSLLL------ 95
B. licheniformis          AVDFLIILY--HRITVWISKVIRMKASSNDDEDHRFLLLSI---- 95
B. pumilus                RTDFLFIIY--DRITTWISKVIRMKRSSNDDEDH-LLPLSN---- 93
B. anthracis              GNVPLFSIF--YKYG-MIRSVRRQESSEENDEVGPYTPMFR---- 94
B. cereus                 GNVPLFSIF--YKYG-MIRSVRRQESSEENDEVGPYTPMFR---- 94
B. thuringiensis          GNVPLFSIF--YKYG-MIRSVRRQESSEENDEVGPYTPMFR---- 94
B. halodurans             DVSAFIRP---LSVVHHPKVHSIKDKSSADEEAPSFILA------ 89
B. clausii                CVDMTPVRP--LALWARPKIPYFRDKGCQDDDGPYPCCMHQQIAA 93
                                                  ...
```

A. Protein sequence alignment for putative MifM-like proteins in the Bacillales. Protein sequences of gene ID: 16803420 (*Lm*), 116872812 (*Lw*), 16800485 (*Li*), 56420358 (*Gk*), 138895364 (*Gt*), 154686650 (*Bam*), 50812265 (*Bs*), 52348809 (*Bl*), 157692894 (*Bp*), 30265066 (*Ban*), 42784208 (*Bce*), 49480767 (*Bt*), 15613731 (*Bh*), 56965672 (*Bcl*) were aligned by ClustalW2. Hydrophobic, acidic and basic residues were labeled as pink, blue and red, respectively.

Table S3: Plasmids used in these studies

Plasmid	Gene	Primer
pCH706	*'spoIIIJ271-flagΩloxP-kan-loxP*	SP53, SP54
pCH735	*amyE::mifM95-lacZΩcat*	SP1, SP4
pCH743	*amyE::mifM^{5}-lacZΩcat*	SP1, SP2
pCH746	*amyE::yidC2^{6}-lacZΩcat*	SP1
pCH767	*amyE:mifM(ΔTM)-yidC2^{6}-lacZΩcat*	SP2, SP3
pCH774	*amyE::mifM(91-96rp)yidC2^{6}-lacZΩcat*	SP7
pCH792	*amyE::mifMyidC2^{6}-lacZ(Δstem)Ωcat*	SP5
pCH795	*amyE::mifMD86(silent)-TAA-yidC2^{6}-lacZΩcat*	SP12, SP13
pCH802	*amyE::mifMD86(stop)-yidC2^{6}-lacZΩcat*	SP6
pCH803	*amyE::mifMA90(stop)-yidC2^{6}-lacZΩcat*	SP15
pCH804	*amyE::mifM(frameshift)-yidC2^{6}-lacZΩcat*	SP12, SP13, SP14
pCH806	*'ybaCΩloxP-kan-loxP*	SP16, SP17
pCH823	*amyE::mifME87(stop)-yidC2^{6}-lacZΩcat*	SP18
pCH824	*amyE::mifME88(stop)-yidC2^{6}-lacZΩcat*	SP19
pCH825	*amyE::mifMD89(stop)-yidC2^{6}-lacZΩcat*	SP20
pCH838	*amyE::mifM(I66A)-yidC2^{6}-lacZΩcat*	SP21
pCH839	*amyE::mifM(Y67A)-yidC2^{6}-lacZΩcat*	SP22
pCH840	*amyE::mifM(H68A)-yidC2^{6}-lacZΩcat*	SP23
pCH841	*amyE::mifM(R69A)-yidC2^{6}-lacZΩcat*	SP24
pCH842	*amyE::mifM(I70A)-yidC2^{6}-lacZΩcat*	SP25
pCH843	*amyE::mifM(T71A)-yidC2^{6}-lacZΩcat*	SP26
pCH844	*amyE::mifM(T72A)-yidC2^{6}-lacZΩcat*	SP27
pCH845	*amyE::mifM(W73A)-yidC2^{6}-lacZΩcat*	SP28
pCH846	*amyE::mifM(I74A)-yidC2^{6}-lacZΩcat*	SP29
pCH848	*amyE::mifM(K76A)-yidC2^{6}-lacZΩcat*	SP30
pCH849	*amyE::mifM(V77A)-yidC2^{6}-lacZΩcat*	SP31
pCH850	*amyE::mifM(F78A)-yidC2^{6}-lacZΩcat*	SP32
pCH851	*amyE::mifM(R79A)-yidC2^{6}-lacZΩcat*	SP33
pCH852	*amyE::mifM(M80A)-yidC2^{6}-lacZΩcat*	SP34
pCH854	*amyE::mifM(S82A)-yidC2^{6}-lacZΩcat*	SP35
pCH855	*amyE::mifM(P83A)-yidC2^{6}-lacZΩcat*	SP36
pCH856	*amyE::mifM(V84A)-yidC2^{6}-lacZΩcat*	SP37
pCH857	*amyE::mifM(N85A)-yidC2^{6}-lacZΩcat*	SP38

pCH858	*amyE*::*mifM(D86A)-yidC2*^{6}*-lacZΩcat*	SP39	
pCH859	*amyE*::*mifM(E87A)-yidC2*^{6}*-lacZΩcat*	SP40	
pCH860	*amyE*::*mifM(E88A)-yidC2*^{6}*-lacZΩcat*	SP41	
pCH872	*amyE*::*mifM(N81A)-yidC2*^{6}*-lacZΩcat*	SP42	
pCH905	*amyE*::*mifM(T60A)-yidC2*^{6}*-lacZΩcat*	SP43	
pCH906	*amyE*::*mifM(D61A)-yidC2*^{6}*-lacZΩcat*	SP44	
pCH907	*amyE*::*mifM(F62A)-yidC2*^{6}*-lacZΩcat*	SP45	
pCH908	*amyE*::*mifM(L63A)-yidC2*^{6}*-lacZΩcat*	SP46	
pCH909	*amyE*::*mifM(I65A)-yidC2*^{6}*-lacZΩcat*	SP47	
pCH910	*amyE*::*mifM(I64A)-yidC2*^{6}*-lacZΩcat*	SP48	
pCH913	*amyE*::P_{mifM}*-rbsm1-gfp-mifM*$^{35-95}$*-yidC2*^{6}*-lacZΩcat*	SP8, SP10	SP9,
pCH917	*amyE*::*mifM(R75A)-yidC2*^{6}*-lacZΩcat*	SP49	
pCH924	*amyE*::*mifM(R59A)-yidC2*^{6}*-lacZΩcat*	SP50	
pCH925	*amyE*::*mifM(D89A)-yidC2*^{6}*-lacZΩcat*	SP51	
pCH929	*amyE*::P_{mifM}*-rbsm1-gfp-mifM*$^{35-95}$*-flag-yidC2*^{6}*-lacZΩcat*	SP11	
pCH985	*amyE*::P_{mifM}*-gfp-mifM*$^{35-95}$*-flagΩcat*	SP52	
pCH986	*amyE*::P_{mifM}*-gfp-mifM*$^{35-95}$*(R75A)-flagΩcat*	SP49	
pCH990	*amyE*::P_{mifM}*-gfp-mifM*$^{35-95}$*(I74A)-flagΩcat*	SP29	
pCH993	*amyE*::P_{mifM}*-gfp-mifM*$^{35-95}$*(R59A)-flagΩcat*	SP50	
pCH994	*amyE*::P_{mifM}*-gfp-mifM*$^{35-95}$*(T60A)-flagΩcat*	SP43	
pCH995	*amyE*::P_{mifM}*-gfp-mifM*$^{35-95}$*(D61A)-flagΩcat*	SP44	
pCH996	*amyE*::P_{mifM}*-gfp-mifM*$^{35-95}$*(F62A)-flagΩcat*	SP45	
pCH997	*amyE*::P_{mifM}*-gfp-mifM*$^{35-95}$*(L63A)-flagΩcat*	SP46	
pCH998	*amyE*::P_{mifM}*-gfp-mifM*$^{35-95}$*(I64A)-flagΩcat*	SP48	
pCH999	*amyE*::P_{mifM}*-gfp-mifM*$^{35-95}$*(I65A)-flagΩcat*	SP47	
pCH1000	*amyE*::P_{mifM}*-gfp-mifM*$^{35-95}$*(I66A)-flagΩcat*	SP21	
pCH1001	*amyE*::P_{mifM}*-gfp-mifM*$^{35-95}$*(Y67A)-flagΩcat*	SP22	
pCH1002	*amyE*::P_{mifM}*-gfp-mifM*$^{35-95}$*(H68A)-flagΩcat*	SP23	
pCH1003	*amyE*::P_{mifM}*-gfp-mifM*$^{35-95}$*(R69A)-flagΩcat*	SP24	
pCH1004	*amyE*::P_{mifM}*-gfp-mifM*$^{35-95}$*(I70A)-flagΩcat*	SP25	
pCH1006	*amyE*::P_{mifM}*-gfp-mifM*$^{35-95}$*(T72A)-flagΩcat*	SP27	
pCH1007	*amyE*::P_{mifM}*-gfp-mifM*$^{35-95}$*(W73A)-flagΩcat*	SP28	
pCH1009	*amyE*::P_{mifM}*-gfp-mifM*$^{35-95}$*(K76A)-flagΩcat*	SP30	
pCH1010	*amyE*::P_{mifM}*-gfp-mifM*$^{35-95}$*(V77A)-flagΩcat*	SP31	
pCH1011	*amyE*::P_{mifM}*-gfp-mifM*$^{35-95}$*(F78A)-flagΩcat*	SP32	
pCH1012	*amyE*::P_{mifM}*-gfp-mifM*$^{35-95}$*(R79A)-flagΩcat*	SP33	

pCH1013	*amyE*::P_{mifM}-*gfp-mifM*$^{35-95}$*(M80A)-flagΩcat*	SP34
pCH1014	*amyE*::P_{mifM}-*gfp-mifM*$^{35-95}$*(N81A)-flagΩcat*	SP42
pCH1015	*amyE*::P_{mifM}-*gfp-mifM*$^{35-95}$*(S82A)-flagΩcat*	SP35
pCH1016	*amyE*::P_{mifM}-*gfp-mifM*$^{35-95}$*(P83A)-flagΩcat*	SP36
pCH1017	*amyE*::P_{mifM}-*gfp-mifM*$^{35-95}$*(V84A)-flagΩcat*	SP37
pCH1018	*amyE*::P_{mifM}-*gfp-mifM*$^{35-95}$*(N85A)-flagΩcat*	SP38
pCH1019	*amyE*::P_{mifM}-*gfp-mifM*$^{35-95}$*(D86A)-flagΩcat*	SP39
pCH1020	*amyE*::P_{mifM}-*gfp-mifM*$^{35-95}$*(E87A)-flagΩcat*	SP40
pCH1021	*amyE*::P_{mifM}-*gfp-mifM*$^{35-95}$*(E88A)-flagΩcat*	SP41
pCH1060	*amyE*::P_{mifM}-*gfp-mifM*$^{35-95}$*(D89A)-flagΩcat*	SP51
pCH1061	*amyE*::P_{mifM}-*gfp-mifM*$^{35-95}$*(T71A)-flagΩcat*	SP26

Table S4: Oligonucleotides used in these studies

Name	Sequence
SP1	TGTCAAACATGAGAATTCGGGTCCCTGTATGGTGTATC
SP2	TGATGACAATGTTTGTGGGATCCGAATCGATAAATGACGT
SP3	GGATTGCATTCCTCTTAGGATCCCGGGAGTGCCGTGCGGG
SP4	CCGGTTCTCTTCTTTTAGGATCCTAAACCGCATTTATAAAAAG
SP5	AACGATGAGGAAGACGCCGGAAGCTTATTACTATGAACCGCATTTATAAAAA GGAG
SP6	ATGAATTCGCCTGTGAACTAAGAGGAAGACGCCGGTTCTC
SP7	GAACGATGAGGAAGACGCCGGTTCTCTTCTTTTATAAGGTTCTCTTCTTTTA TAAACCGC
SP8	ATAGTAAAATGAAGCTAGGAGGAGGATGTGATGACAATGT
SP9	AAGGATTTGAGCGTAGCGAAAA
SP10	GAAATAATGGATCCTGTTGCACCCCGCGGCCGTT
SP11	ACGCCGGTTCTCTTCTTTTAGACTATAAAGACGACGACGACAAACGGCCGT AAACCGCATTTATAAAAAG
SP12	GAATTCGCCTGTGAACGACGAGGAAGACGCCGGTTC
SP13	CTTCTTTTATAAACTAACGCATTTATAAAAAGGAGGAGAAC
SP14	GATACGTAAAGTCCTTCCGCATGAATTCGCCTG
SP15	GTGAACGATGAGGAAGACTAAGGTTCTCTTCTTTTATAA
SP16	CATCACTCTATGACAATAAATC
SP17	TCATAAATGGTTGCGTGCATGC
SP18	AATTCGCCTGTGAACGATTAAGAAGACGCCGGTTCTCTTCT
SP19	TCGCCTGTGAACGATGAGTAAGACGCCGGTTCTCTTCTTTT
SP20	CCTGTGAACGATGAGGAATAAGCCGGTTCTCTTCTTTTA
SP21	CGAACAGACTTTCTTATTATTGCGTATCATCGCATTACAA
SP22	ACAGACTTTCTTATTATTATAGCGCATCGCATTACAACTTG
SP23	GACTTTCTTATTATTATATATGCGCGCATTACAACTTGGAT
SP24	TTTCTTATTATTATATATCATGCGATTACAACTTGGATACG
SP25	CTTATTATTATATATCATCGCGCGACAACTTGGATACGTAA
SP26	ATTATTATATATCATCGCATTGCGACTTGGATACGTAAAGT
SP27	ATATATCATCGCATTACAGCGTGGATACGTAAAGTCTT
SP28	TATCATCGCATTACAACTGCGATACGTAAAGTCTTCCG
SP29	CATCGCATTACAACTTGGGCGCGTAAAGTCTTCCGCAT
SP30	ATTACAACTTGGATACGTGCGGTCTTCCGCATGAATTC
SP31	ACAACTTGGATACGTAAAGCGTTCCGCATGAATTCGCC
SP32	ACTTGGATACGTAAAGTCGCGCGCATGAATTCGCCTGT

SP33	TGGATACGTAAAGTCTTCGCGATGAATTCGCCTGTGAA
SP34	ATACGTAAAGTCTTCCGCGCGAATTCGCCTGTGAACGA
SP35	AAAGTCTTCCGCATGAATGCGCCTGTGAACGATGAGGA
SP36	CTTCCGCATGAATTCGGCGGTGAACGATGAGGAAGACG
SP37	CGCATGAATTCGCCTGCGAACGATGAGGAAGACGCC
SP38	ATGAATTCGCCTGTGGCGGATGAGGAAGACGCCGGTTC
SP39	AATTCGCCTGTGAACGCGGAGGAAGACGCCGGTTCTC
SP40	TCGCCTGTGAACGATGCGGAAGACGCCGGTTCTCTTCTTT
SP41	CCTGTGAACGATGAGGCGGACGCCGGTTCTCTTCTTTTAT
SP42	CGTAAAGTCTTCCGCATGGCGTCGCCTGTGAACGATGA
SP43	CGGTCTTTCACATTAACCGAGCGGACTTTCTTATTATTATATA
SP44	TCTTTCACATTAACCGAACAGCGTTTCTTATTATTATATATCA
SP45	TTCACATTAACCGAACAGACGCGCTTATTATTATATATCATCG
SP46	ACATTAACCGAACAGACTTTGCGATTATTATATATCATCGCAT
SP47	AACCGAACAGACTTTCTTATTGCGATATATCATCGCATTAC
SP48	TTAACCGAACAGACTTTCTTGCGATTATATATCATCGCATTAC
SP49	CGCATTACAACTTGGATAGCGAAAGTCTTCCGCATGAA
SP50	ACGGTCTTTCACATTAACGCGACAGACTTTCTTATTATTATA
SP51	GTGAACGATGAGGAAGCGGCCGGTTCTCTTCTTTTATAAA
SP52	GCATGGATGAACTATACAAAACTAGTGACTATAAAGACGACGACGACAAATA ACGGCCGTAATAGAGATCCGA
SP53	GGTTATGCTGTTATGCTGCCAAG
SP54	TTATTTGTCGTCGTCGTCTTTATAGTCCTTTTTCTTTCCTCCGGCTTTTTGCG

Table S5: Spore titers of mutations in the *spoIIIJ* Shine-Dalgarno sequence

Strain	relevent genotype	Spore titer[1]
SCB751	wild type	4 x 10^8 spores/ml
SCB757	*ΔspoIIIJ-jag*	2 x 10^3 spores/ml
ALB198	*spoIIIJ Shine-Dalgarno AGGAGG to AGGAAG*	3 x 10^7 spores/ml
ALB228	*spoIIIJ Shine-Dalgarno AGGAGG to AAGAGG*	8 x 10^7 spores/ml
ALB396	*spoIIIJ Shine-Dalgarno AGGAGG to AGAAGG*	1 x 10^8 spores/ml

[1]Spore titers reflect the number of cells that could survive 20 minutes of heating to 80°C after 24 hours of growth in DSM medium at 37°C.

References

Chiba, S., Coleman, K., and Pogliano, K. (2007). Impact of membrane fusion and proteolysis on SpoIIQ dynamics and interaction with SpoIIIAH. J Biol Chem *282*, 2576-2586.

Rubio, A., Jiang, X., and Pogliano, K. (2005). Localization of translocation complex components in *Bacillus subtilis:* enrichment of the signal recognition particle receptor at early sporulation septa. J Bacteriol *187*, 5000-5002.

Sawano, A., and Miyawaki, A. (2000). Directed evolution of green fluorescent protein by a new versatile PCR strategy for site-directed and semi-random mutagenesis. Nucleic Acids Res *28*, 78.

Youngman, P., Perkins, J.B., and Losick, R. (1984). A novel method for the rapid cloning in *Escherichia coli* of *Bacillus subtilis* chromosomal DNA adjacent to Tn917 insertions. Mol Gen Genet *195*, 424-433.

Chapter 5, in full, is a reprint of the material as it appears in *The European Molecular Biology Organization* 209 (Vol. 28 pp. 3461-3475). I was a secondary author and isolated and identified mutants from the random mutagenesis screen important for confirming the *mifM* regulation by the *mifM* stemloop, MifM transmembrane domain and *spoIIIJ*.

Chapter 6

Discussion

My thesis research has demonstrated that cytological profiling, a technique for mechanism of action (MOA) determination pioneered in eukaryotes (1, 2), can be adapted for use with bacteria. The effects of various antibiotics on cell architecture in *Bacillus subtilis* were easily distinguishable and cytological profiling was able to determine the MOA of two new compounds, SDP and a bromoalterochromide. The method I developed, and that Poochit Nonejuie is developing in *E. coli*, relies purely on fluorescence microscopy paired with viable cell counts to track changes in cell architecture and viability. Thus far, my analysis of fluorescence micrographs has been limited to visual comparison and, in the case of SDP, measurement of whole cell DNA intensity. This crude method sufficed to distinguish differences between all the compounds tested, but it certainly has limitations and introduces human bias. Indeed, I was unable to assign MOAs to three of the unknowns, spirohexenolide A, chlorothricin, and stenothricin. So far, I have only obtained cytological profiles from compounds with a handful of MOAs, and utilized only the crudest of image analysis techniques. A larger library of comparison compounds with known MOAs must be screened and quantitative analysis utilized if cytological profiling is to be improved. It is obvious that cytological profiling has great potential, but still requires much development before it becomes a fully formed MOA determining technique.

Although cytological profiling is still far from being a fully developed technique, it offers several advantages over current MOA determination methods, and so is worth the time and effort needed for development. In adapting cytological profiling, I was able to develop microculture techniques that reduced culture sizes to just 15 µl, vastly reducing the amount of compound used for testing compared to other

MOA determination techniques. This small sample size is already on the scale needed for samples in high-throughput screening. Adaptation to high-throughput methods should be possible, and large scale screening is what is required for effective characterization of the MOAs of the constantly growing pool of newly available natural products. Cytological profiling also works below the minimal inhibitory concentrations (MIC) of many molecules, so it is able to detect lower concentrations of antibacterial compounds than other methods. Another advantage cytological profiling has over other MOA determination techniques is the ability to visualize what is happening at the cellular level. This results in the ability to discriminate between MOAs at a much finer level than other semi-high-throughput screens, as closely related MOAs can result in physical differences. For example, during my studies on SDP, I was able to distinguish the effect of collapse of both components of the PMF from the effect of collapse of $\Delta\Psi$ or ΔpH alone. Another example is in the case of cell wall active antibiotics. Treatment with β-lactam antibiotics results in severe cell shape defects, whereas vancomycin does not, though both target the cell wall. Microarray approaches have lumped cell wall antibiotics into a single category (3, 4), but cytological profiling easily distinguishes between the two MOAs. Indeed, even when a novel MOA is detected, changes in cell architecture could provide clues as to the pathway targeted. Thus, cytological profiling has the potential to be high-throughput while retaining sensitivity and fine accuracy in MOA determination.

A. Improvement of cytological profiling MOA determination

The need for large data sets profiling as many compounds and MOAs as possible

This work is the first study utilizing cytological profiling for MOA determination in bacteria, and so it is unsurprising that I was unable to determine the MOA of most of the natural products I tested. I have only profiled a handful of control compounds thus far, and the number of MOAs tested needs to be greatly increased before I could expect to identify the MOA of most natural products. The prediction of MOA with any accuracy using comparative studies has only been achieved when large libraries of compounds have been screened as controls. Indeed, ongoing studies by graduate student Poochit Nonejuie to apply cytological profiling to *E. coli* cells utilize a larger range of control compounds and he is already able to quantitatively show differences between different translation inhibitors, DNA gyrase inhibitors, transcriptional inhibitors, lipid biosynthesis inhibitors and β-lactam antibiotics.

Microarray studies have found that a group of five or six compounds with the same MOA need to be profiled in order to obtain accurate clustering of new compounds (4). We do not know if a similar figure applies for cytological profiling, but we do need to test compounds with as many MOAs as possible to expand our dataset. This database must also include compounds that block the same pathway at multiple points to help us determine how finely we can assign MOA. Our preliminary studies are quite promising in this regard, as I was able to discriminate between collapsing either component of the PMF ($\Delta\Psi$, ΔpH) and both components and between compounds targeting different steps in cell wall biogenesis. Building a diverse library of cytological profiles is key to development of cytological profiling as an accurate determiner of the MOA of new natural products.

The need for automated image analysis

As previously mentioned, the cytological profiling I have done so far has relied on visual comparisons of fluorescence images, which is not a reliable measure. In order to differentiate accurately between a large number of MOAs, a quantitative approach must be taken that limits human bias. Automated data analysis would limit human bias and may pick up differences not apparent by eye. Poochit Nonejuie in Joe Pogliano's lab has been working on cytological profiling using *E. coli lptD* and has applied ImageJ and MATLAB threshold based programs to measure cell variables for quantitative comparison of different treatments. He has taken measurements of cell size and shape, DNA size, shape and intensity, and permeability of cells to SYTOX green. All of these parameters can be grouped based on similarity and simplified into three variables using principle component analysis (PCA). The PCA data can then be graphed three dimensionally to visually compare the data points. Treatments that have the same MOA appear on the graph as clusters, and assignment of MOA can be given for a new antibiotic based on this clustering. Mike has built up a large library of compounds covering major classes of MOA and he is able to easily differentiate between at least five MOA classes using a single PCA graph.

Choice of species – E. coli, B. subtilis or both?

All of Poochit's data was collected using images of *E. coli lptD* cells, and mine used *B. subtilis*. As can be seen in the cases of spirohexenolide A and chlorothricin, the results of the two species do not always agree. Whether this is due to a difference in the MOA of the compound on the two species or other factors remains to be seen. In some cases, this might be due to a compound having different MOAs in different species. However, the weaknesses in using cytological profiling for compounds of

certain MOAs might not overlap between species, thus multi-species profiling might compensate for the weakness of an individual species. It seems likely that a multi-species system will ultimately prove the most sensitive for determination of a specific MOA and generate the most confident identification.

There are several differences between *B. subtilis* and *E. coli lptD* that must be considered when choosing which strain to use. *E. coli lptD* exhibits a defect in outer membrane biogenesis which permeabilizes it to many molecules, such as Gram-positive specific antibiotics, that normally would not penetrate the outer membrane. This results in a strain that is sensitive to most, but not all, Gram-positive specific antibiotics. An advantage of using *E. coli* is that it is more tractable than *B. subtilis* for our current image analysis techniques. The cells are separated rather than chained, and they do not have the tendency to undergo autolysis as *B. subtilis* does, which makes cell measurements impossible. However, the MIC of a compound for the *E. coli* mutant is usually higher than for a Gram-positive species such as *B. subtilis,* and so if compound is extremely limited, experiments may be more manageable in *B. subtilis*.

The induction of autolysis can be a disadvantage, as it makes measurement of cell variables very difficult and determination of a cell outline impossible with current techniques, but it also offers another variable that can be included in the analysis. *B. subtilis* cells undergo autolysis when the PMF is collapsed, which can occur either through specific mechanisms, or because a compound has formed a non-specific pore in the membrane. There are a multitude of compounds that don't induce autolysis, such as RNA synthesis inhibitors and protein synthesis inhibitors, and thus do not present the discontinuous membranes that make cell measurements impossible.

Another tendency of *B. subtilis* is for membrane blobs to appear, frequently at septa. A disadvantage of these blobs is that they make recognition of cells difficult with our current image analysis techniques, the reasons for which are discussed below. However, the location and size of these blobs can be characteristic of a MOA. For example, vancomycin treatment results in large membrane blobs, which really are internal vesicles, at septa. The only other treatment that has exhibited a similar placement of internal vesicles is Triton X-100, but other variables, such as the total permeability of Triton X-100 treated cells, allow them to be easily discriminated. Treatment of *E. coli* cells does not usually result in membrane blobs, and so they are not available as a variable for use in the PCA analysis of *E. coli* cytological data.

Utilizing other factors to increase cytological profiling accuracy

Accuracy in cytological profiling all comes down to the measurement of information and utilization of that information. Increasing the number of variables used for input should allow finer differentiation between MOAs. One of the disadvantages of low-throughput methods is that they require a single timepoint or concentration to be utilized because otherwise, the method could not handle that many samples or it would become too expensive. One of the microarray studies emphasized that multiple timepoints were required to properly assign MOA. The later timepoint was necessary to broadly categorize the MOA, but an earlier timepoint was essential to complete MOA assignment (4). Cytological profiling studies in eukaryotes utilized a serial dilution method to capture multiple concentrations and allow determination of the correct concentration to use for their analysis in the same step (1). We have seen in our experiments that the morphological effects exerted on the cell are highly

dependent on concentration and timepoint. Early timepoints give additional variables, such as time to SYTOX green permeability, and sub-MIC effects can be characteristic for a compound. For example, cells treated at a sub-MIC concentration of stenothricin showed internal vesicles and SYTOX green permeability whereas above the MIC, the membrane appeared to fill the cytoplasm, apparently detaching from the peptidoglycan. Many compounds induce autolysis, and so using only a later timepoint could result in all cells being lysed. A pre-lysis timepoint would then been needed to see any architectural changes in the cell prior to lysis. Utilizing only one concentration or timepoint for each compound would result in missing information that could be essential for differentiating two MOAs and thus lead to incorrect identification of MOA.

Ultimately, having the ability to rapidly determine MOAs of uncharacterized natural products requires having the most information possible at your disposal. The first step is to generate cytological profiles of as diverse and complete a group of compounds as possible. Cytological profiling with *E. coli lptD,* including quantitative image analysis, paired with PCA is the single technique that will give the most information. However, not all compounds will affect the *E. coli* mutant, or at a low enough concentration to make the experiments feasible. In that case, *B. subtilis* can be used to generate a cytological profile. The most accurate MOA prediction will likely come from a combination of *E.coli* and *B. subtilis* data taken at multiple concentrations and timepoints. In this case, the more variables measured, the more accurate the predictions for MOA.

B. Quantitative analysis of cytological profiling images

We know that the key to developing cytological profiling as an accurate and simple method of MOA determination relies heavily on the quality of data analysis and the quantity of data in the reference library. Being able to detect and quantify subtle differences between cells treated with different compounds will allow specific MOA determination. Currently, there is still a lack of easy to use programs to accurately measure cells and nucleoids. Poochit has been utilizing simple thresholding in ImageJ, but it still takes 15 minutes per field of cells to conduct the analysis and requires a large amount of input. It also requires adjusting each image by eye and introduces human error that could lead to variability in results between users. Thresholding is very sensitive, and adjusting the images is a balance between identifying as many cells as possible and accuracy in size measurements. Cells that are not ideal are frequently not picked up by this technique, and it could skew the results. In the case of *B. subtilis* cells, membrane blobs can complicate the analysis. Thresholding is based on fluorescence intensity, and the membrane blobs are typically brighter that the rest of the cells, making it difficult to detect the rest of the membrane without completely blowing out the membrane blob, which makes it appear like a septum to the program, causing the cell to be counted as multiple cells. We've also been utilizing a MATLAB based thresholding program developed by Jangir Selimkhanov in Jeff Hasty's lab, but it does not offer much advantage over ImageJ as far as eliminating human bias and measuring cells with membrane blobs or discontinuous membranes.

Other options include a free software package MicrobeTracker which utilizes a MATLAB interface and IN Cell Investigator (Biacore), a commercial program used in

eukaryotic high content screening (5). MicrobeTracker was developed to analyze cell shape and protein localization from images gathered from high-throughput screening of *Caulobacter cresentus* (6, 7). It uses segmentation to measure cell shape with high accuracy and has also been used to look at protein localization within the cell. However, it was designed to use phase-contrast images to define cell outlines, not fluorescence images of cells with membrane stain, as is the case for our images. The program might need to be heavily adapted to accurately determine cell size and shape from our data. Even if we adapt this program for use with our images, it will still be unable to measure cells that have discontinuous membranes, such as those undergoing autolysis. In *B. subtilis*, the ability to measure these cells is key to complete data analysis. Likely we will have to collaborate on new software that can detect the presence of cells with discontinuous membranes and count them as a cell, to accurately identify cells in tightly packed confluent lawns and to detect and quantify the number and size of membrane blobs within a cell. It seems likely that the software used in high content screening for eukaryotic cells, that have internal membranes and that grow in tightly packed arrays, will have this ability. If not, additional effort must be made to create new software with higher functionality.

C. The need for high-throughput sample screening

In the introduction, I identified the lack of high-throughput methods for MOA determination in bacteria as a bottleneck in antibiotic discovery. Cytological profiling provides one answer to this issue and in eukaryotes it has already been used as a high-throughput screen (1, 2). Now that I've demonstrated that cytological profiling is

possible in bacteria, it can be adapted for high-throughput MOA determination. Unfortunately, the automated microscopy systems utilized for eukaryotic systems are based on an air immersion objective, which does not provide sufficiently high resolution or magnification for bacterial studies. However, the requirement for oil immersion objectives does not mean that the throughput of microscopy-based screening cannot be improved. In 2009, Zemer Gital's lab introduced a method for increasing throughput based on the use of agarose pedestals (8, 9). These pedestals allow for 48 samples to be imaged on a single slide, which makes the screening compatible with automated imaging. This method was used to screen almost 3000 strains of *C. crescentus* for localization of fluorescently tagged proteins (8), and demonstrates that many of the tools needed to make cytological profiling high-throughput already exist. We merely need to adapt them to our specific imaging system, and to strive to increase the capacity for image collection and analysis.

Another potentially high-throughput method for cytological profiling is the use of microfluidics to monitor the effect of different antibiotics over time. In collaboration with Jeff Hasty's lab, Poochit Nonejuie has just begun testing a 16 compartment microfluidics chip that only requires 10-20 μl of sample, comparable to our current cytological profiling experiments. This would theoretically allow timelapse microscopy to occur, as the cells would be in growth medium, and provide multiple timepoints from one sample. However, the chip currently does not support robust growth and is far from ready for deployment as a viable method. Additionally, the antibiotics must be dried down in the well prior to addition of cells. The addition of the culture rehydrates the antibiotic and diffusion mixes it, but diffusion also

ultimately results in cross contamination after an extended period of time, and the initial concentration of the antibiotic could vary depending on how well it solubilizes and mixes within the well, and where in the chamber the pictures are taken. Chips of this nature will likely find their primary use in hospital settings, where they can be used as a diagnostic for determining the resistance or sensitivity profiles of isolates, not as a precise tool for MOA determination. Other chips exist that allow for robust growth, but they are limited to only a few chambers per chip, require a much larger sample size, and cannot be moved during the experiment. Thus microfluidics chips are not ideal for high-throughput cytological profiling.

D. Utilizing cytological profiling for screening crude extracts

Once the method for cytological profiling has been adapted for high-throughput screening, it could be effectively utilized to screen crude extracts and subsequent fractions for the presence of antibacterial natural products. As we demonstrated for the crude extract containing the bromoalterochromide, cytological profiling can be utilized to determine the MOA of a natural product prior to purification. Indeed, other studies in the lab have demonstrated the ability to detect up to three distinct MOAs in a crude extract of *B. subtilis* strain 3610. This will allow extracts to be screened and cytological profiling can be used to determine which show promise for further purification and development. The fractions generated during purification can then be screened again for activity-guided purification. Cytological profiling of these fractions would require less than a microliter of the fraction per experiment, and thus provide valuable information on activity with a negligible

amount of sample required. For many natural products, the activity can be detected with sub-MIC levels of the molecule, as I have shown for stenothricin, the bromoalterochromide and nisin, making the method extremely sensitive. Cytological profiling represents a fast and effective means of screening for new natural products that will generate information about the MOA simultaneously with purification and allow dereplication without limiting the range of actions detected. This will also allow natural products to be prioritized based on MOA. Staying ahead of the microbes requires new molecules with a unique MOA. Cytological profiling will allow molecules with a unique MOA to be singled out early as promising lead candidates.

E. Concluding remarks

In this discussion I have reviewed why cytological profiling appears to be ideally suited to address the major bottlenecks of antibiotic discovery. It is adaptable to high-throughput screening, utilizes a minimal amount of compound, and offers the possibility of accurate MOA determination in a matter of hours. All that is required to make this a reality is the screening of a large library compounds with diverse MOAs and the development of new image analysis software to handle this new influx of imaging data. Both of these should be possible in the near future if effort is invested into development of cytological profiling. Once that is achieved, MOA determination should be a simple task that can be accomplished quickly and can be utilized directly in screens for new natural products, allowing the majority of time and effort to be spent in development of these molecules as antibiotics.

F. References

1. Perlman, Z.E., M.D. Slack, Y. Feng, T.J. Mitchison, L.F. Wu, and S.J. Altschuler, Multidimensional drug profiling by automated microscopy. Science, 2004. **306**(5699): p. 1194-8.

2. Tanaka, M., R. Bateman, D. Rauh, E. Vaisberg, S. Ramachandani, C. Zhang, K.C. Hansen, A.L. Burlingame, J.K. Trautman, K.M. Shokat, and C.L. Adams, An unbiased cell morphology-based screen for new, biologically active small molecules. PLoS Biol, 2005. **3**(5): p. e128.

3. Hutter, B., C. Schaab, S. Albrecht, M. Borgmann, N.A. Brunner, C. Freiberg, K. Ziegelbauer, C.O. Rock, I. Ivanov, and H. Loferer, Prediction of mechanisms of action of antibacterial compounds by gene expression profiling. Antimicrob Agents Chemother, 2004. **48**(8): p. 2838-44.

4. Freiberg, C., H.P. Fischer, and N.A. Brunner, Discovering the mechanism of action of novel antibacterial agents through transcriptional profiling of conditional mutants. Antimicrob Agents Chemother, 2005. **49**(2): p. 749-59.

5. Thomas, N., High-content screening: a decade of evolution. J Biomol Screen, 2010. **15**(1): p. 1-9.

6. Garner, E.C., MicrobeTracker: quantitative image analysis designed for the smallest organisms. Mol Microbiol, 2011. **80**(3): p. 577-9.

7. Sliusarenko, O., J. Heinritz, T. Emonet, and C. Jacobs-Wagner, High-throughput, subpixel precision analysis of bacterial morphogenesis and intracellular spatio-temporal dynamics. Mol Microbiol, 2011. **80**(3): p. 612-27.

8. Werner, J.N., E.Y. Chen, J.M. Guberman, A.R. Zippilli, J.J. Irgon, and Z. Gitai, Quantitative genome-scale analysis of protein localization in an asymmetric bacterium. Proc Natl Acad Sci U S A, 2009. **106**(19): p. 7858-63.

9. Gitai, Z., New fluorescence microscopy methods for microbiology: sharper, faster, and quantitative. Curr Opin Microbiol, 2009. **12**(3): p. 341-6.

Appendix A

Journal Cover

VOLUME 84 | NUMBER 3 | MAY 2012 | ISSN 0950-382X | www.mol-micro.com

molecular microbiology

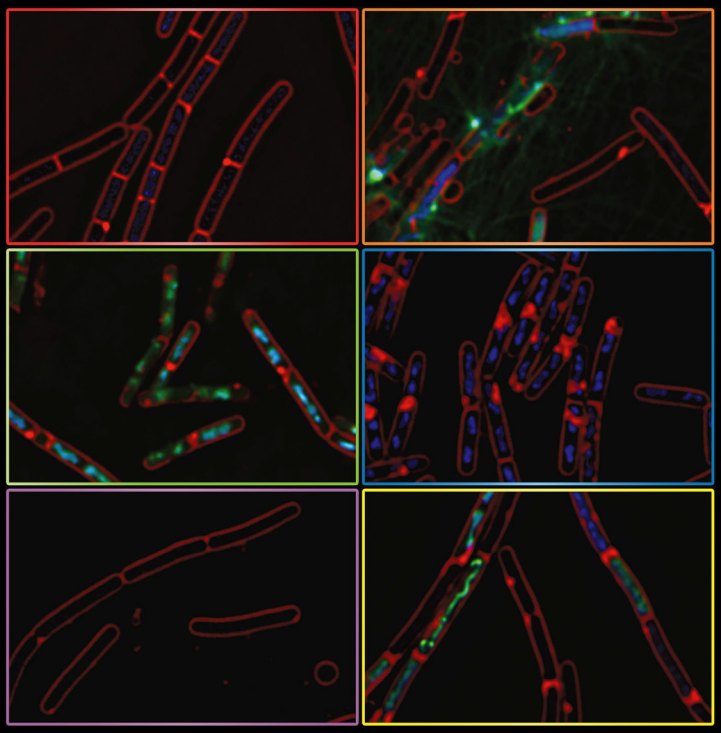

On the cover:
Visualizing cell envelope stress in *Bacillus subtilis*

Cactin is essential for G1 progression in *Toxoplasma gondii*

Contact-dependent growth inhibition in *Burkholderia pseudomallei*

The MicF sRNA controls Lrp translation

WILEY-BLACKWELL